Dynamics of motile forces and symmetry breaking in the migrating cell

Katharina Hennig

Communauté
UNIVERSITÉ Grenoble Alpes

THÈSE

Pour obtenir le grade de

DOCTEUR DE LA COMMUNAUTÉ UNIVERSITÉ GRENOBLE ALPES

Spécialité : Physique pour les Sciences du Vivant

Arrêté ministériel : 25 mai 2016

Présentée par

Katharina HENNIG

Thèse dirigée par **Martial BALLAND**, UGA

préparée au sein du **Laboratoire Laboratoire Interdisciplinaire de Physique**
dans **l'École Doctorale Physique**

Dynamique des forces motiles et brisure de symétrie chez la cellule migrante

Dynamics of motile forces and symmetry breaking in the migrating cell

Thèse soutenue publiquement le **17 octobre 2018**,
devant le jury composé de :

Madame ANA-MARIA LENNON-DUMENIL
DIRECTRICE DE RECHERCHE, INSERM DELEGATION PARIS, Rapporteur
Monsieur BENOIT LADOUX
DIRECTEUR DE RECHERCHE, CNRS DELEGATION PARIS-VILLEJUIF, Rapporteur
Monsieur ALDO LEAL-EGANA
CHERCHEUR, UNIV. ERLANGEN-NUREMBERG - ALLEMAGNE, Examinateur
Monsieur PAOLO MAIURI
PROFESSEUR ASSISTANT, IFOM - ITALIE, Examinateur
Monsieur FRANZ BRUCKERT
PROFESSEUR, GRENOBLE INP, Président

Acknowledgements

Dear Yoda, colleagues, friends and family,

I want to say thank you to all of you for your help and support during the course of my PhD thesis.

The biggest thank you goes out to my supervisor, colleague and friend Martial, who motivated me when research was frustrating, and inspired me when new ideas were needed, who introduced me to plenty of other researchers in the field, who took me to international conferences, who believed in me when I didn't do so myself, and who bought me beers when we went out together. Thank you for everything Yoda. You truly taught me how to use the force wisely, and over the years, I transitioned from being Padawan to becoming a real Jedi. I could have not wished for a better supervisor!

To all the people in my group (in the present and in the past), who I shared an amazing time with – either during cell culture room cleaning, lab meetings or apero times - I want to thank you all for always having an open ear and helping me when needed. It was so much fun working with all of you.

A very special thank you goes to Irene Wang and Philippe Moreau. My PhD would have been only half as successful if it wasn't for you. Whenever I needed your help (which happened a lot) you did not even hesitate for even a second to help me out. You are both amazing colleagues and wonderful people.

To Elisa, Vanni, and Tomas – my favorite office mates of all time. I had so much fun with you, laughing all the time, teasing each other, but also working together as a team. I love you all! However, a very warm thank you goes out to our cutipie Elisa. You were such a big help during all these years, and I think you don't even realize how much you supported me and my project.

To all my friends in the lab, many of who have already left. I spent such a great time working at Liphy mainly because of you guys. I enjoyed every coffee break, after work beer or gossip talk!

One big thank you to all the people from IAB, who welcomed me in their lab, and taught me how to do biology the proper way.

A very big thank you goes out to Kate and Sascho. My partners in crime – in and out of the lab. We had so much fun together. I really miss you guys.

And of course also to my favorite colleague and roomie of all time. Adele, we spent so many years working and then also living together. From the beginning on when you taught me optogenetics, to late night sessions drinking wine on the couch, talking about our frustrations, ideas and dreams, and to ending our PhDs together. I'll miss you when we both have to move on to other cities!

And last but far from being least – my family! Ich kann gar nicht sagen, wie sehr ich euch dankbar bin für eure jahrelange Unterstützung liebe Eltern. Ob finanziell oder mit Sekt, ihr ward immer für mich da und habt an mich geglaubt. Ich wusste, egal was auch passiert, ich kann immer auf euch zählen! Danke auch an meinen Bruder Peter, ich weiss, tief in dir drin bist du stolz auf deine kleine Schwester.

Und zum Schluss noch an grosses Danke an meine Freunde aus der Heimat. Vor allem an Charly, Stefan, Göppi und Holle – unsere Freundschaft hält schon seit Jahren, auch über Ländergrenzen hinweg!

Thank you all!!!

Table of content

Foreword **1**

1. Introduction to single cell migration **3**

1.1. The different modes of cell migration *3*

1.2. The migratory machinery of mesenchymal cells *6*

1.2.1. Cytoskeleton-based intracellular force generation 7

1.2.1.1. Intermediate filaments 10

1.2.1.2. Microtubules 11

1.2.1.3. Actin fibers 13

1.2.2. Adhesion-mediated force transmission 16

1.2.2.1. The extra cellular matrix 16

1.2.2.2. Cellular adhesions 17

1.2.2.3. The molecular clutch theory 20

1.2.3. Cell migration requires the establishment and maintenance of front-rear polarity 23

1.2.4. Symmetry and asymmetry principles in nature 23

1.2.5. Front-rear polarity of a migrating cell 26

1.2.5.1. Structural basis: cytoskeleton architecture and adhesion distribution 27

1.2.5.2. Dynamically regulation: RhoGTPases 30

1.2.6. Establishing polarity through symmetry breaking 34

1.2.6.1. The generally accepted model: integrating signals from the front to the back 34

1.2.6.2. Controversies in symmetry breaking: formation of the rear as a first step to initiate migration 36

1.2.6.3. Maintaining polarity 38

1.3. How to study single cell migration in vitro *40*

1.3.1. Experimental approaches based on microfabrication techniques 40

1.3.1.1. From planar 2D substrates to 3D matrices 41

1.3.1.2. 1D substrates mimic complex 3D fibrillar migration 44

1.3.2. Perturbing the mechanical activity of the cell 45

1.3.2.1. Why experimentally targeting cell adhesiveness and contractility? 46

1.3.2.2. Standard methods to tune adhesiveness and contractility 47

1.3.2.3. Optogenetics – a novel technique first used to study neurobiological processes 51

1.3.2.4. Optogenetics allows the spatio-temporal perturbation of single cell mechanics in a reversible manner 52

1.3.3. Quantitative traction force measurements 55

1.3.3.1. 2D traction force microscopy 56

1.3.3.2. Moving from 2D to 3D force measurements 59

1.3.3.3. Multipolar force analysis 61

2. Unraveling the force-motion relation: motivation and goals....63

3. Materials and Methods: experimental basis for unraveling the force-motion relation....66

3.1. Experimental strategy: Patterned Traction Cytometry....67

3.1.1. Soft micropatterning....68

3.1.1.1. Glass technique: printing adhesive lines on soft substrates....68

3.1.1.2. Quantification of relevant migratory parameters....70

3.1.2. Quantitative force measurements: Fourier Transform Traction Cytometry70

3.1.2.1. Step 1: Displacement field analysis....71

3.1.2.2. Step 2: Force field analysis....72

3.1.2.3. Step 3: Quantifying force parameters in 1D....74

3.2. Dynamic perturbation of cell mechanics....76

3.2.1.1. Pharmacological treatments....76

3.2.1.2. Optogenetics....77

4. Results....80

4.1. Study 1) Hennig et al. "Stick-slip dynamics of cell adhesion triggers spontaneous symmetry breaking and directional migration"....80

4.1.1. Introduction....80

4.1.2. Scientific article....82

4.1.3. Summary of major results....110

4.1.4. Open discussion: difficulties of quantifying a migrating cell....111

4.1.5. Future perspective: coupling actin retrograde flow speed measurements to traction force quantifications....113

4.2. Study 2) Monzo et al. "The formin FMN1 promotes directional changes of invasive GBM by increasing cell cytoskeleton's cohesion and traction forces on laminin linear substrate."....116

4.2.1. Introduction to glioblastoma, the most aggressive malignant brain tumor..116

4.2.2. Studying GBM migration *in vitro*....119

4.2.3. Experimental results....121

4.2.4. Discussion and conclusion....123

5. Final concluding words....127

6. Annex....130

6.1. Study 1) Supplementary data....130

6.2. Study 3) De Mets et al. "Fast and robust fabrication of reusable molds for hydrogel micro-patterning"....140

6.3. Study 4) Alkasalias et. al "RhoA knockout fibroblasts lose tumor-inhibitory capacity in vitro and promote tumor growth in vivo" *149*
6.4. List of references *159*

Foreword

Cellular migration is a fundamental process occurring throughout the lifespan of any multicellular organism – from fruit flies to humans: from the early development of an embryo, to tissue repair and immune surveillance during adult life, to the development of deadly diseases (Ridley 2003).

Various examples can be listed to emphasize the critical role of cell movement. Not long after fertilization, tissue rearrangements lead to the formation of a multilayer embryo. This process, termed gastrulation, relies on the coordinated collective movement of cells (McMahon 2008). Tissue repair (Zahm 1997) and immune response (Melchers 1999) are based on directed motion of epithelial or immune cells towards the damaged or infected tissue, respectively. Hence, cell migration plays an essential role in various physiological processes and, consequently, its tight regulation is crucial in order to develop and maintain a healthy organism (Reig 2014, Friedl 2009). However, if deregulated, diseases may arise. Malfunctions of cellular movement are often involved in cancer progression (Monzo 2016) and mental retardation (Zhang 2013) as well as pathological processes like osteoporosis (Ueland 2003, Fiedler 2006) or vascular disease (Raines 2000). It therefore comes as no surprise that research has focused intensively on obtaining a complete understanding of cell migration. Advances in the field have led to novel cancer treatments, transplantation techniques and artificial tissue preparations (Ridley 2003).

Although cell migration has been studied extensively, research in the field remains a challenging task due to the great complexity of cellular movement. The translocation of the cell involves shape changes that are regulated by various signaling processes, which need to be integrated and coordinated over space and time (Lauffenburger 1996). External mechanochemical cues of the surrounding environment influence those regulatory cascades and ultimately determine the mode of migration. While cells can move as isolated entities or collective sheets, they are also able to switch from one mode to another depending on the distinct properties of the surrounding tissue (Friedl 2009). Hence, the complexity of cellular movement comprises processes that occur at different spatio-temporal scales and are influenced by various internal and external factors.

The main focus of this thesis is on single cell migration. It is known that, independent of the mode of migration, a single cell needs to mechanically interact with its surrounding in an anisotropic way to propel itself forward. In order to do so, the cell needs to establish an asymmetric shape through a dynamic process termed symmetry breaking (Etienne-Manneville 2004). How the mechanical interaction between the cell and the substrate changes during the initiation of migration remains a central question in mechanobiology (Chen 2008, Tanimoto 2014). In order to answer this question, we need an experimental approach that allows us to directly address the evolution of cellular traction forces during the initiation of migration.

In this thesis, we will introduce the main features of cell migration by shining light on how the spatio-temporal control of the migratory machinery breaks force symmetry and ultimately drives the forward movement of a mesenchymal cell. We present the development of a one-dimensional single cell *in vitro* migration assay that mimics complex fibrillar *in vivo* movement. This approach is based on a combination of microfabrication and quantitative force imaging and it allowed us to identify a unique stick-slip slip scenario that shows that spontaneous symmetry breaking can occur due to mechanical instabilities. This stochastic mechanism highlights the crucial role of force-mediated adhesion detachment to initiate migration, where the critical controlling parameter is the adhesion turnover rate. Strikingly, this process can take place independent of any prior cytoskeletal polarity. Our findings were validated using optogenetics and pharmacological approaches that alter cellular contractility and adhesiveness. The stick-slip behavior was observed across many cell types from which we identified an inverse relation between cell length and migration speed. A theoretical model recapitulates the observed migration modes ranging from non-motile to stochastic stick-slip. Furthermore, we applied our quantitative *in vitro* migration assay to brain cancer cells directly derived from patients. In the light of our findings, we screened the ability of glioblastoma cells to migrate depending on their mechanical activity. We therefore show that by first understanding the force-motion relation of non-transformed cells from a fundamental point of view, we were able to transition into the more applied field of cancer cell biology.

1. Introduction to single cell migration

Cell migration is a fundamental process of high complexity that is regulated across different scales: from single molecules to whole tissue deformations. In this introductory chapter, we will discover a variety of molecular processes that all aim at facilitating one major cellular function: initiating and maintaining cellular movement.

We will first present common and distinct features of various migration modes that cells may possess while moving through complex tissues. After that, this thesis will mainly focus on a particular migratory behavior of single cells, which physically interact with their microenvironment: mesenchymal cell migration. The introduction chapter will present the two key features of cellular movement: (i) the migratory machinery and (ii) the establishment of cell polarity. We will elaborate both of those key aspects in great detail from molecular regulation principles to structural changes of the whole cell. We will further discuss how the chemical and mechanical properties the surrounding environment influence these processes. Once we have gained a broad understanding of cell migration, we will focus on how this complex process can be studied in simplified manner under *in vitro* laboratory conditions.

1.1. The different modes of cell migration

There are various ways cells can migrate: together as cohesive groups or independently as single cells. The morphological features that moving cells may exhibit allow us to categorize distinct modes of migration (**Figure 1**). The physical interaction with the surrounding environment is hereby critical.

When several cells move together, the established adhesion-mediated cell-substrate and cell-cell contacts are crucial in order to sense physical and chemical signals of the extracellular matrix (ECM) and coordinate the movement of the whole cell cluster accordingly (Ladoux 2017). We can here distinguish between cell streaming and collective migration depending on the time scale of cell-cell contacts. During cell streaming, also termed chain migration, cell-cell contacts are transiently formed and dissolved while moving

along one common track (Friedl 2009). For example, during metastasis, breast cancer cells linearly assemble to move together along ECM fibers to reach blood vessels and invade the body (Leung 2017). On the other, collective cell migration as sheets, strands or irregularly shaped masses arises when adhesions between neighboring cells are permanently present (Friedl 2009). This is, for instance, the case during wound healing, when epithelial cells move coherently towards the injury (Li 2013). In general, during movement as a group, cells are influenced by their neighbors. This adhesion-facilitated communication comprises an extra layer of complexity compared to the migration of isolated cells.

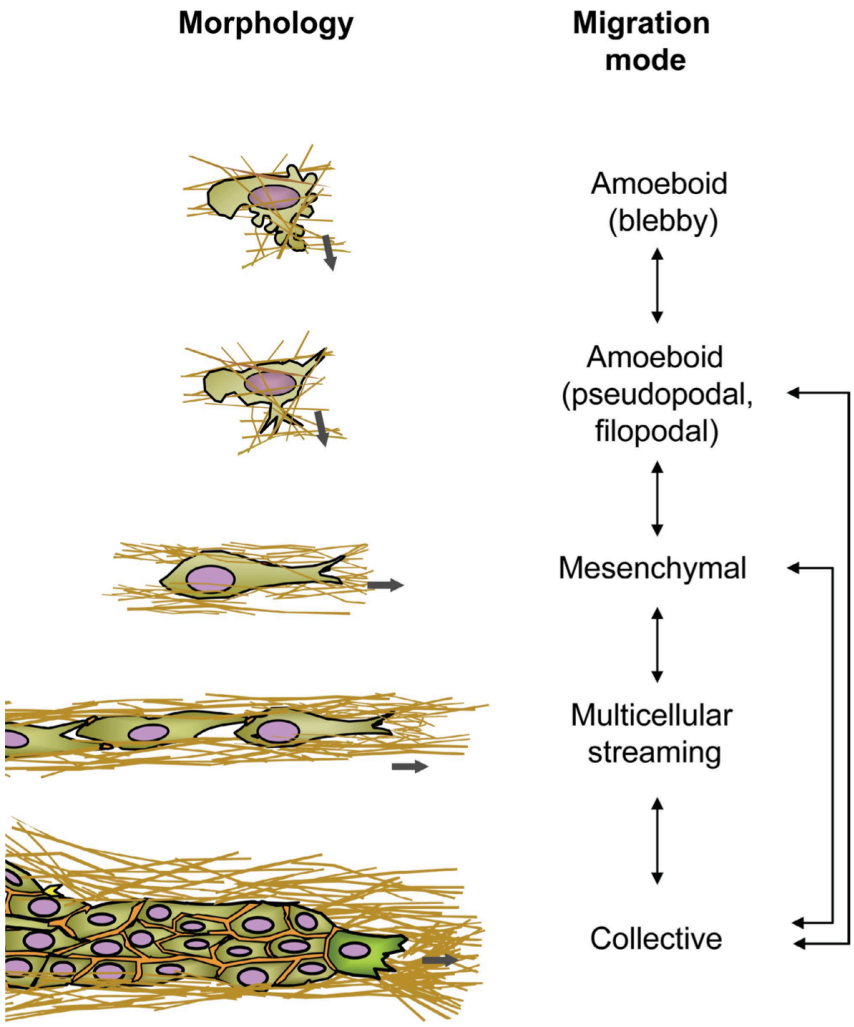

Figure 1 : Morphology-based modes of migration. *In vivo*, cells can move through tissues in various ways: together as groups or as single cells. Distinct modes of cell migration can be defined depending on morphological features that cells may possess. Additionally, cells are able to switch from one migratory behavior to another (indicated by arrows). [Figure taken from: (Friedl 2009)]

Single cell migration can be categorized depending on the mechanical interaction of the cell with its microenvironment. From that we can define two distinct modes of single cell migration: adhesion-independent amoeboid and adhesion-dependent mesenchymal migration (Case 2015, Friedl 2009). The most evident way to discriminate those two migratory phenotypes is by comparing cell shape and migration speed. Slower moving mesenchymal cells (e.g. fibroblast cells) are elongated and exhibit a distinct front-rear polarity. Amoeboid cells (e.g. immune cells), on the other hand, are faster moving cells that feature a more roundish, less polarized morphology (Friedl 2009). Both main phenotypes are based on the dynamic reorganization of the cytoskeleton. During adhesion-dependent movement, cells own an actin-rich, flat protrusive structure, called lamellipodium, as well as actin stress fibers. These structures are lacking in amoeboid cells, which can be further categorized into subgroup, depending on the kind of cellular protrusion the amoeboid cell possesses: actin polymerization driven pseudopods or pressure-driven blebs. During blebbing motility, the membrane locally detaches from the cell cortex, which creates a spherical actin protrusions due to a hydrostatic pressure created by the contraction of the actin cortex (Tyson 2014). Pseudopodia, on the other hand, are 3D, actin-filled protrusions that drive adhesion-independent cell crawling (Titus 2017). Hence, both main modes of single cell migration, mesenchymal and amoeboid, rely on actin-based protrusive structures. These structures generate intracellular, motile forces, which drive cellular migration.

However, in order to propel the forward movement of the cell, these intracellular forces need to be transmitted to the surrounding microenvironment. In order to do so, amoeboid and mesenchymal cells exhibit different mechanisms (Bergert 2015). Mesenchymal cells transmit their actin-generated forces via adhesion points to the substrate leading to an inward directed pulling force. Amoeboid cells lack mature adhesions. Instead, the extension of blebs applies a pushing force on the surrounding environment (Hawkins 2009, Friedl 2009). Therefore, one of the main characteristic differences between those two migratory modes is the mechanical cell-substrate interaction, which directly impacts cell shape and migration speed.

In general, the difference between the two motile phenotypes can be summarized as following: *in vivo* amoeboid cells deform their cell body to squeeze through narrow gabs of the complex fibrillar environment. Mesenchymal cells rather deform and remodel the surrounding matrix by applying pulling forces and by additionally releasing proteolytic

chemicals (**Figure 2** ; Pathak 2011). Interestingly, cells can even switch from one mode to the other (Liu 2015). Epithelial-mesenchymal transition (EMT) describes the phenomenon when static epithelial cell become motile. On the other hand, mesenchymal-amoeboid transition (MAT) and amoeboid-mesenchymal transition (AMT) describe a rapid switch in between the two migratory modes due to the suppression or enhancement of specific molecular pathways (Paňková 2010). Physiologically speaking, this transition is crucial especially for immune or cancer cells. For example, during the invasion of the human body, cell plasticity allows cancer cells to adapt their mode of locomotion to changes in the environment, leading to a high rate of metastasis (Paňková 2010, Friedl 2009).

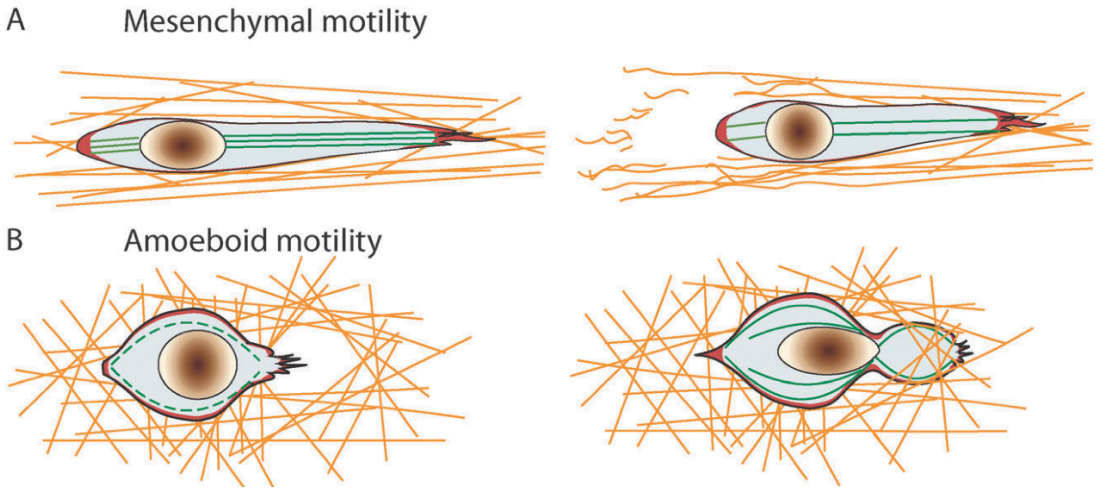

Figure 2: Two main modes of single cell migration. A) Mesenchymal cells exhibit an elongated shape, physically pull on the matrix via adhesions and exhibit stress fibers. During movement, mesenchymal cells degrade and remodel the fibrillar environment *in vivo*, while **B**) amoeboid cells adapt their shape to squeeze through pre-existing narrow gaps. Cells that possess this adhesion-independent migratory behavior are round and produce blebs. [Figure taken from: (Pathak 2011)]

1.2. The migratory machinery of mesenchymal cells

Cellular migration is a complicated process that involves morphological shape changes that are facilitated by the migratory machinery of the cell. From a general point of view, the migratory machinery has two main functions: (i) the intracellular generation of motile forces and (ii) the transmission of those motile forces to the surrounding environment (Renkawitz 2010). The main focus of this manuscript is on adhesion-facilitated mesenchymal migration. We therefore organized the following introduction chapters in two main sections: The first part will explain how the cytoskeleton generates intracellular forces

and the second part will elaborate how adhesive structures transmit these motile forces to the surrounding environment. Together, this adhesion-mediated contractile activity allows moving cells to actively respond to extracellular cues coming from the surrounding microenvironment (Lämmermann 2009).

1.2.1. Cytoskeleton-based intracellular force generation

Cell migration is a dynamic process that relies on the ability of cells to continuously change shape while moving through a complex environment (Lomakin 2015). The structural basis for maintaining mechanical integrity during these morphological changes is the cytoskeleton. It represents an intracellular scaffold, which exhibits a high degree of order. In general, the cytoskeleton consists of filamentous biopolymers and regulating proteins (Fletcher 2010). Each fiber is composed of individual building blocks (monomers or dimers). These components are highly dynamic allowing fibers to grow or shrink via addition or subtraction of building blocks, respectively (Huber 2015). The spatial organization and dynamic turnover within the cell is controlled via various fiber-associated proteins and relies on the consumption of energy, which is provided by the hydrolysis of adenosine triphosphate (ATP) or guanosine triphosphate (GTP). Overall, besides representing the structural backbone of the cell, dynamic cytoskeletal networks generate and transmit forces in response to intra- and extracellular cues that allow rapid cell shape adaptations during migration (Fletcher 2010).

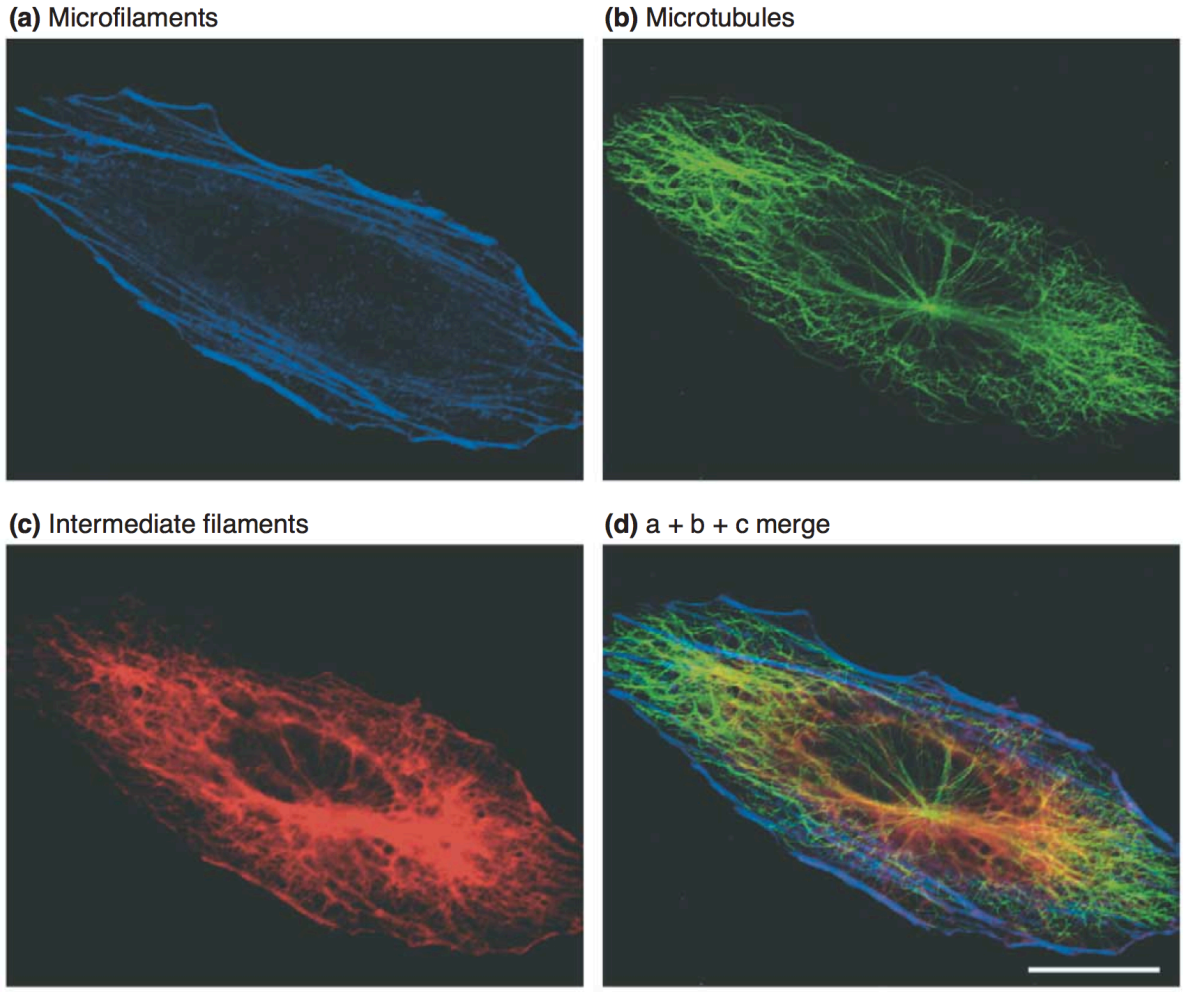

Figure 3: The three types of cytoskeletal polymer fibers. Microfilaments (**a**), microtubules (**b**) and intermediate filaments (**c**) vary in their molecular composition and network architecture and coexist within the eukaryotic cell (**d**). (Scale bar: 10 μm) [Figure taken from: (Omary 2006)]

The cytoskeleton is composed of distinct types of polymer fibers: microfilaments (also referred to as filamentous actin (FA)), microtubules (MT) and intermediate filaments (IF; **Figure 3**). These types of fibers vary in their molecular composition and can each interact with specific fiber-associated proteins (Omary 2006). Molecular motors are most striking class of proteins that interact with the cytoskeleton. Motor proteins convert chemical energy (e.g. ATP) into mechanical energy in order to transport cargo along fibers or produce cellular forces (Vale 2003). Other fiber-associated proteins regulate the network's architecture and polymerization/depolymerization rate. Taken all together, each subsystem possesses specific mechanical properties and turnover dynamics in order to facilitate distinct intracellular functions. However, actin fibers, microtublues and intermediate filaments cannot be described as completely isolated entities of the cytoskeleton, as the three

subsystems also interact with each other in a direct or indirect manner (**Figure 4**). This filament crosstalk may occur through direct or cross-linker-mediated binding as well as steric effects. On the other end, biochemical pathways mediate an indirect communication between distinct filament types (Huber 2015).

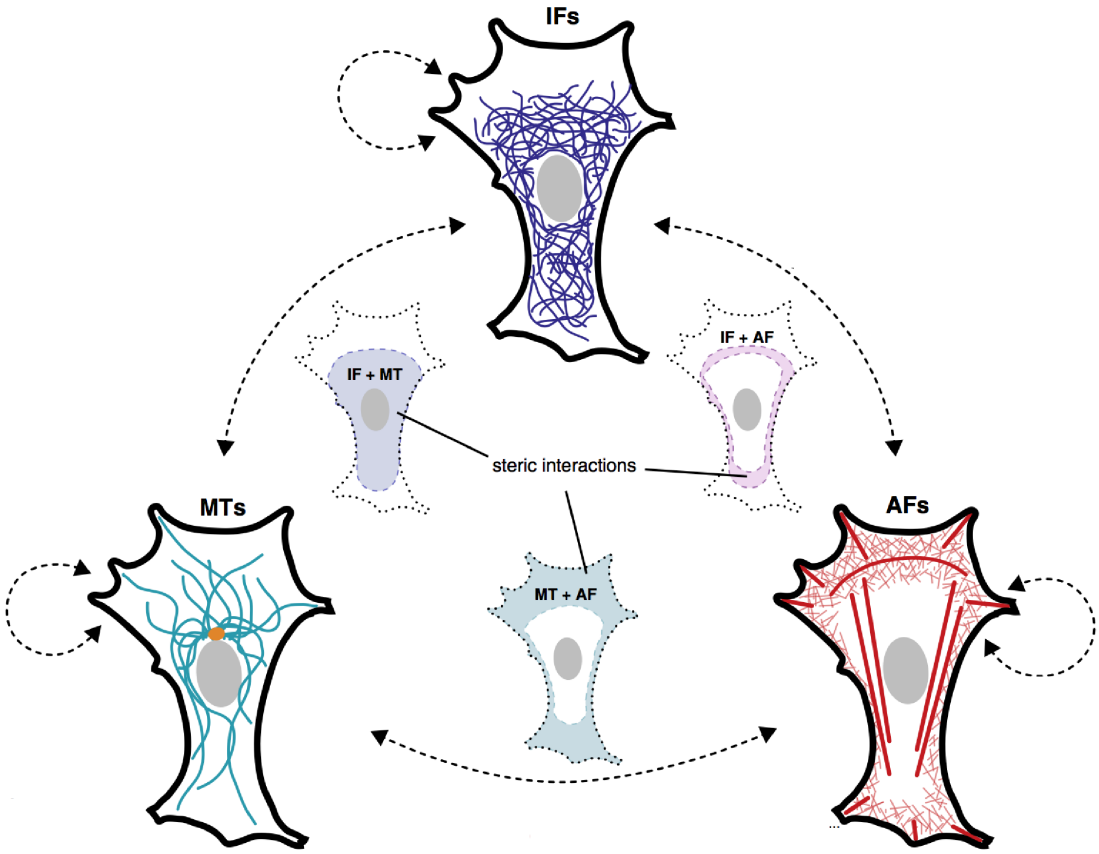

Figure 4: The three main filament types of the cytoskeleton, their specific fiber-associated proteins and the crosstalk with each other. Intermediate filaments (IFs), microtubules (MT) and actin fibers (AF) within the eukaryotic cell exhibit distinct molecular structures and compositions. Specific fiber-associated proteins regulate the spatio-temporal reorganization of each individual network. While AF and MT possess specific motor proteins and cross-linkers, IF are only connected via cross-linkers. Besides that, cross-linkers and molecular motors as well s steric hindrance facilitate the interaction in between cytoskeleton subsystems (indicated via dashed black arrows). [Figure adapted from: (Huber 2015)]

In the upcoming subchapters, we will explain the different fiber structures and network architectures that determine distinct mechanical properties of actin filaments, microtubules and intermediate filaments. In addition to that, we will elaborate molecular regulation mechanisms that control the dynamic filament reorganization and turnover. Finally, we will explain how each network performs specific mechanical functions that are crucial during cell migration.

1.2.1.1. Intermediate filaments

In general, intermediate filaments possess extraordinary mechanical and dynamic properties and connect the external microenvironment to intracellular organelles, which together contribute to key steps that lead to migration. IFs are 10 nm-wide, non-polar homo- or heteropolymers that may consist of at diverse intermediate filament proteins (e.g. keratin, nestin, vimentin; Leduc 2015). Depending on the genetic substructure or sequence homology of these proteins we can distinguish six subgroups, which vary in their cell-type specificity. Independent of their heterogeneity, the primary structure of those fibers is well persevered: Non-helical head and tail domains with varying length and composition at the N- and C-termini, respectively, flank a central helical rod domain that consists of α-helical coils connected via linkers (Chung 2013, Loschke 2015).

The molecular compositions as well as the structural architectures determine the mechanical fiber properties. In general, intermediate filaments are soft viscoelastic materials with non-linear elasticity. Astonishingly, IFs can withstand large deformations, making them unique among other cytoskeleton filaments. The single filament can extend above three times its original length before breaking, while a fiber network can withstand huge strains (above 100%) and even recover its elastic modulus after being damaged (Wagner 2007).

During cell migration, those semi-flexible polymers perform essential mechanical functions (Wagner 2007). Intermediate filaments have been found to facilitate mechanical interactions with the surrounding environment (**Figure 5**). For example, keratine colocalizes with desmosomes and hemidesmosomes to facilitate cadherin-based cell-cell and cell-substrate contacts, respectively (Chung 2013). Upon the initiation of collective migration, keratine decreases in order to enhance desmosome turnover leading to weakened cell-cell contacts that enable collective movement (Roberts 2011). Disrupting plaque-mediated connection of hemidesmosomes to intermediate filaments (e.g. via knockout of the adhesion junction protein Bullous pemphigoid antigen 1 (BPAG1)) has shown to impair cell migration in mice (Guo 1995). Additionally, intermediate filaments play a role during force transmission to the nucleus via the LINC-complex (Linker of Nucleoskeleton and Cytoskeleton; Chung 2013). Upon the disruption of the nucleo-cytoskeletal coupling, cells possess less organized intermediate filaments and actin networks, which reduce cell speed and directionality (Lombardi 2011).

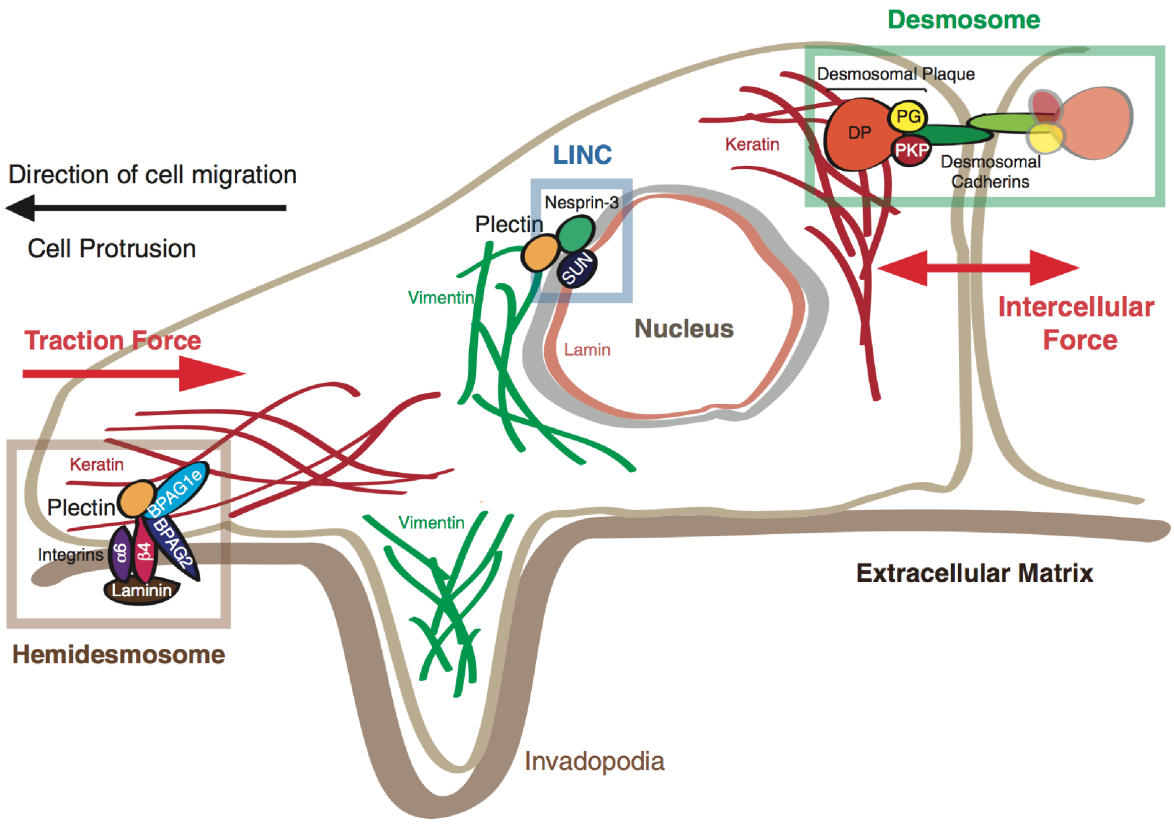

Figure 5: The role of intermediate filaments during cell migration. The schematic representation shows how intermediate filaments and distinct signaling and structural proteins colocalize within desmosome and hemidesmosome. Hence, IFs are involved in facilitating mechanical cell-cell and cell-substrate interactions in order to transmit intercellular or traction forces, respectively. [Figure taken from: (Chung 2013)]

1.2.1.2. Microtubules

Microtubules are structural components of the cytoskeleton, responsible for maintaining an asymmetric cell shape and positioning organelles during migration (Gundersen 1988). MTs are the largest type of cytoskeletal filaments with a diameter of about 25 nm. Filaments are composed of heterodimers of α- and β-tubulin. The heterodimers align in a polar head to tail-fashion forming a protofilament. Finally, thirteen protofilaments arrange parallel to each other and form a hollow rod-like cylinder: the microtubule filament (**Figure 6a and 6b**; Akhmanova 2008).

MTs nucleate at the microtubule-organizing center (MTOC), e.g. the centrosome in close proximity to the nucleus, and extend towards the cell periphery. While microtubule (-)-ends are associated with the MTOC, assembly and disassembly occurs on the filament (+)-ends. These highly dynamic polymers can rapidly switch between growth and shrinkage via the addition or subtraction of tubulin on its free ends, respectively (Gundersen 1988,

Akhmanova 2008). This dynamic behavior of MTs, termed dynamic instability (Mitchison 1984), relies on phases of filament elongation that are interrupted by rapid shrinking periods (catastrophe). During shortening, dynamics may stochastically switch back to a polymerization state (rescue; **Figure 6c**; Gardner 2013).

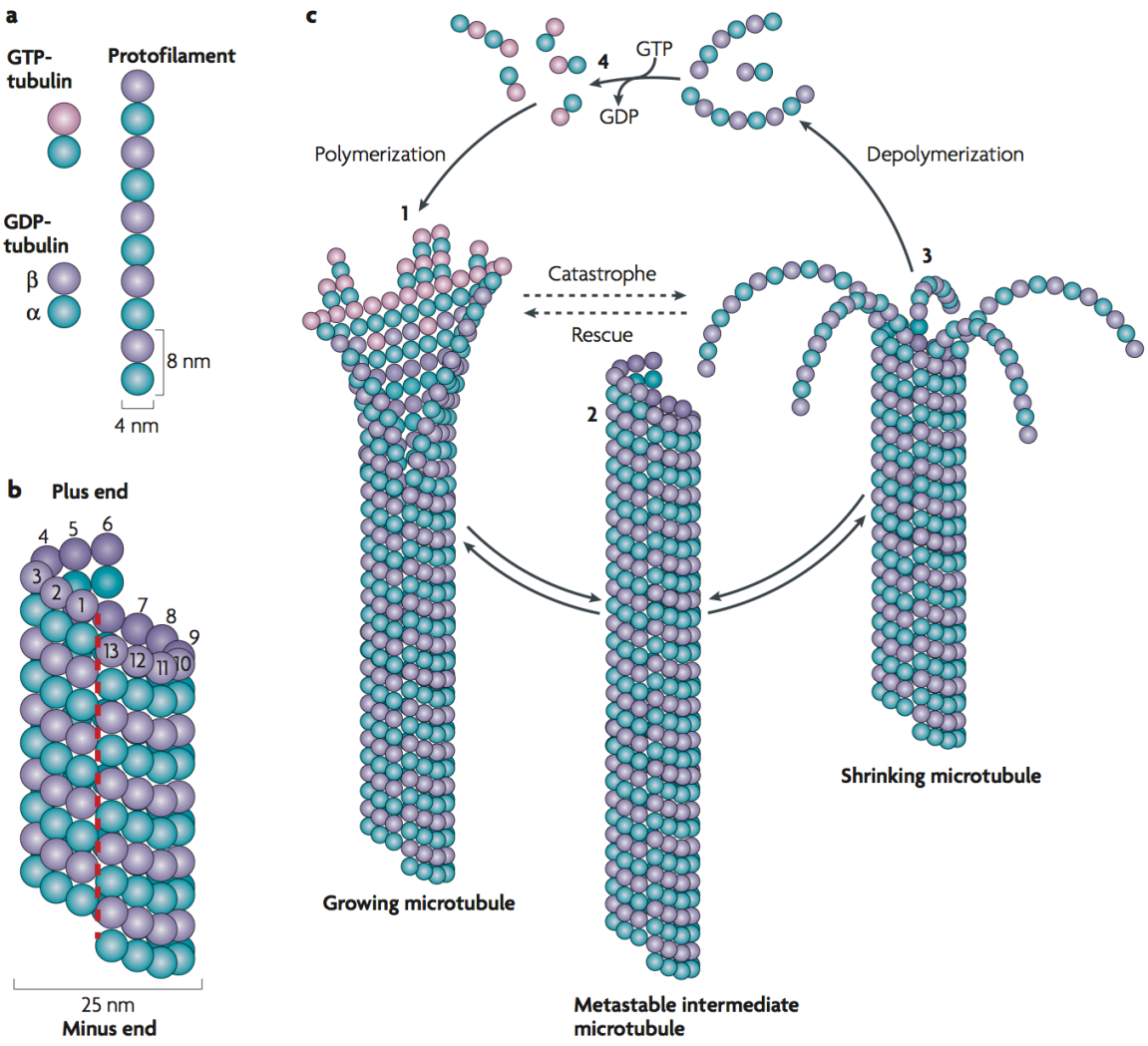

Figure 6: Microtubule structure and dynamics. a) α- and β-tubulin heterodimers assemble into protofilaments. **b**) Thirteen protofilaments form a cylindrical, polar microtubule filament. **c**) The dynamic instability describes the filament's polymerization and depolymerization and its ability to rapidly switch in between the two states (catastrophe or rescue, respectively). [Figure taken from: (Akhmanova 2008)]

The dynamic instability of microtubules depends on the nucleotide state of tubulin and is controlled by microtubule-associated proteins (MAPs) and plus-end tracking proteins (+TIPs). The assembly and disassembly is driven by guanine nucleotide binding, hydrolysis and exchange on the β- tubulin subunit. During polymerization α- and β-tubulin are bound to GTP. GTP-hydrolysis to GDP occurs only at β-tubulin, which, if faster than the rate of

assembly, leads to filament depolymerization (Gardner 2013). In addition to that, MAPs and +TIPs are molecular motor and non-motor proteins that organize the microtubule network. Those MT-associated proteins can pull, slide, anchor or guide as well as stabilize or destabilize the filaments in space and time (Mimori-Kiyosue 2011, Akhmanova 2008). On average, microtubules possess a rapid turnover with a half-life time of 10 min, though a more stable subset of filaments exists, which allows stabilization of local cellular structures (Gundersen 1988).

The MT associated motor and non-motor proteins play an essential role in maintaining polarity during cell migration. Motor proteins of the dynein or kinesin superfamily hydrolyse ATP to transport cargo (e.g. organelles, ribonucleoprotein complexes, or proteins) along microtubule filaments towards the (-)- or (+)-end, respectively (Vale 2003). In response to external cues, dynein-facilitated Golgi positioning towards the stimulus defines the front of the cell (Yadav 2012). Within the leading edge, selective filament stabilization maintains an asymmetric cell shape (Gundersen 1988, Aumeier 2016). However, the cell looses its anisotropy and therefore its ability to persistently migrate if the filament network is disrupted (Zhang 2014, Yadav 2009). These examples emphasize the crucial role of MTs in maintaining a polarized cell shape during migration.

1.2.1.3. Actin fibers

Actin fibers together with their main molecular motor, non-muscle myosin II, have been described as the main actor during cell migration (Wehrle-Haller 2003). Under consumption of ATP, monomeric globular actin (g-actin) assembles into a double stranded, right-handed, 7 nm-thin helix. The rate-limiting step is the prior nucleation of actin dimers/trimers. The subsequent fiber formation is rapid and dependent on the cytoplasmic g-actin concentration (Blanchoin 2014). If the monomer concentration drops below a certain threshold, f-actin disassembly may occur (**Figure 7**; Revenu 2004). The assembled actin fibers are intrinsically polarized possessing two ends with distinct kinetics: fast growing barded and slow growing pointed ends. Pointed ends exhibit a higher critical monomer concentration below which depolymerization occurs than barbed ends. At intermediate concentration of monomers (when g-actin and f-actin are at equilibrium), barbed ends grow while pointed ends shorten simultaneously (treadmilling). Intriguingly, barbed ends can assemble with a

speed of up to 3000 subunits per second, spanning a distance of several micron within one second (Blanchoin 2014). Additionally, there are several actin-binding proteins that control the rate of assembly and disassembly as well as diverse fiber network architectures (Ridley 2003).

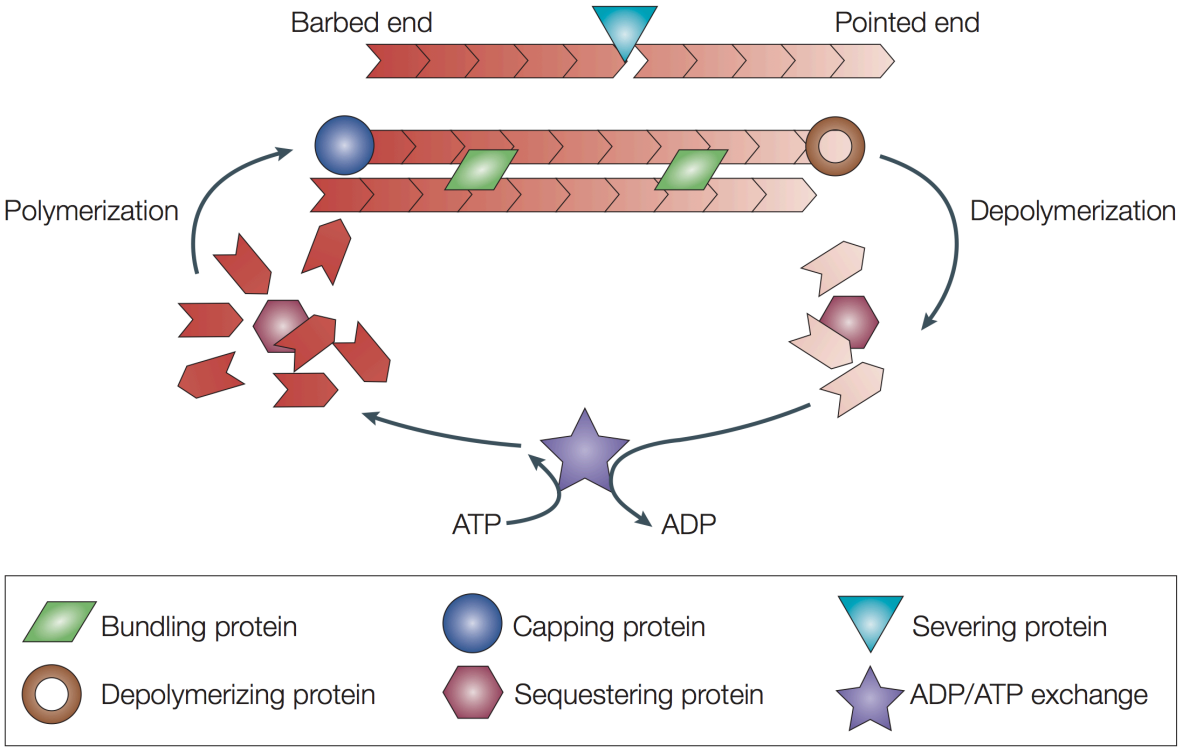

Figure 7: Structure and dynamics of actin filaments. Actin fibers are double stranded helices possessing two ends with distinct kinetics (barbed and pointed ends). Fiber formation occurs after nucleation through the assembly of monomeric units of g-actin under consumption of ATP. Several actin-associated proteins control the fiber polymerization, fiber depolymerization and network architecture. [Figure taken from: (Revenu 2004)]

Within the migrating cell, distinct filament organizations can be found: branched f-actin networks, cross-linked meshworks, parallel f-actin bundles, and anti-parallel stress fiber bundles (Revenu 2004, Blanchoin 2014). The Arp2/3 complex (Actin related protein 2/actin related protein 3) mediates the formation of branched actin fibers that are characteristic for membrane protrusions like lamellipodia. Additional cross-linking proteins (e.g. spectrin, filamin or α-actinin) might physically connect already assembled actin filaments. For example, a cross-linked actin network is characteristic for the cell cortex. Cross-linked fibers that are oriented in parallel with their barbed ends towards to membrane can be found in membrane protrusions like filopodia. Antiparallel actin filaments associated with myosin II form stress fibers that induce contraction within the cell (Blanchoin 2014).

The actin cytoskeleton, together with its associated proteins, constitutes the major component of the contractile machinery within a moving eukaryotic cell. Actin-based intracellular force generation may occur via actin polymerization or acto-myosin contractility (Murrell 2015). During migration, actin nucleators (e.g. Arp2/3) and elongators (e.g. formin) trigger the formation of a branched network (Krause 2014). The filament growth at the barbed ends is oriented towards the cell membrane, generating a protrusive pushing force in the leading edge (Murrell 2015, Wehrle-Haller 2003).

Actin-generated contractility, on the other hand, relies on the interaction of stress fibers with non-muscle myosin II. Structurally, myosin II consists of two head domains with an actin-binding and an ATPase motor domain. The heads are connected to a coiled-coil rod domain via the essential light chain and the regulatory light chain (Vicente-Manzanares 2009). The rod-domains self-associate to form bipolar myosin II filaments of anti-parallel oriented myosin molecules, which present a high number of actin-binding heads (**Figure 8a**; Vicente-Manzanares 2009, Murrell 2015). Upon the binding of polarized f-actin, an ATP-dependent conformational change of myosin II heads translocates actin filaments towards barbed ends. The power stroke-mediated sliding of two cross-linked actin filaments can lead to a local contraction or extension depending on the localization of myosin II (**Figure 8b**; Murrell 2015). But, over the whole cell scale, acto-myosin networks are usually contractile, as actin is a flexible filament that can also buckle (Lenz 2012). Hence, particular actin organizations together with their associated proteins drive distinct force generation mechanisms relevant during cell migration. How particular actin modules further coordinate the front and the rear movement of a polarized cell will be further discussed in **Chapter 1.3.2**.

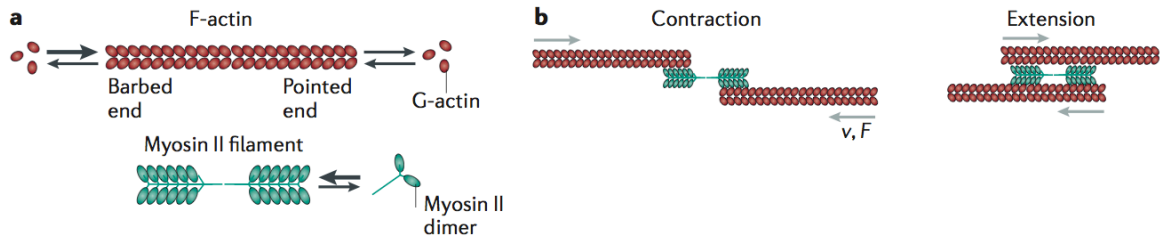

Figure 8: Myosin II-mediated translocation of actin-filaments. a) Polar f-actin filaments (red) are connected via myosin II filaments (green). **b**) Upon ATP-mediated power stroke of myosin heads actin fibers slide towards their barbed ends with a certain velocity (***v***) and a characteristic force (***F***). Depending on the position of the motor filament with respect to the middle of actin filaments local contraction or extension may occur. [Figure taken from: (Murrell 2015)]

1.2.2. Adhesion-mediated force transmission

The migrating cell is continuously submitted to forces. As described in the previous sections, the cytoskeleton generates intracellular forces based on the expansion (polymerization) and shrinkage (contraction) of the cytoskeleton network (Lämmermann 2009). In addition to those internal forces, the cell is also submitted to external forces like shear from the surrounding fluid or tensile forces from the surrounding matrix. These external forces depend on the mechanical properties of the surrounding environment, which need to be sensed by the cell in order to adapt its migratory behavior accordingly. The fact that those external cues influence migration has long been underestimated. But, since a few years, research in the field of mechanobiology has emphasized the actual crucial role of the external matrix (Chen 2008). Moreover, the mechanical interaction between the cell and its environment is essential for the cell in order to move. As shortly introduced before, mesenchymal and amoeboid cells pull or push themselves forward by directly or indirectly interacting with their surrounding, respectively.

To conclude, the transmission of intracellular forces is crucial in order to (i) generate a friction that propels the forward movement of the cell and (ii) simultaneously sense biochemical information of the extracellular space. The focus of this thesis is on the adhesion-mediated force transmission of mesenchymal cells. In the following subchapters, we will discuss the role of the microenvironment and further elaborate how cells exert forces to their surrounding in order to move. At last, we will elaborate how cells regulate their adhesion strength and contractile activity to adapt their migratory behavior to the properties of the external matrix.

1.2.2.1. The extra cellular matrix

In vivo, cells within organs and tissues are embedded in a complex three-dimensional (3D) macromolecular network (Theocharis 2016). The ECM consists of various cell-secreted macromolecules that can be categorized into two classes: proteoglycans and fibrous proteins (e.g. collagen, fibronectin, laminin, elastin). Those non-cellular components bind each other forming a hydrated gel. Depending on the tissue, matrix composition and topology vary and therefore determine the mechanical and biochemical properties of the

network (Frantz 2010). The cell can sense and adapt to those tissue-specific properties due to its receptor-facilitated binding of specific attachment sites within the matrix. For instance, certain transmembrane proteins (integrins) recognize extracellular proteins, like fibronectin, as they contain an Arg-Gly-Asp (RGD) amino acid sequence (Pierschbacher 1984). The physical adhesion-mediated binding exerts a force on the surrounding environment, which enables the cell to sense external cues. In addition to these pulling forces, the mesenchymal cell also releases enzymes with proteolytic activity (Pathak 2011). Both processes lead to a constant remodeling and degradation of the surrounding matrix. Hence, the ECM is a highly dynamic structure, which acts a physical scaffold for cells within all tissues and presents external mechanochemical cues that regulate various cellular processes including cell migration.

Advances in microfabrication techniques (further discussed in **Chapter 1.4.1**) allow studying the impact of ECM structure and composition on the migratory behavior of cells. For example, the direction of cellular movement can be guided by a stiffness gradient (durotaxis; Lo 2000, Aubry 2015) and integrin-mediated binding of collagen facilitates the attachment of T-cells during an immune response (Ray 2004). However, abnormalities in ECM structure and composition can lead to the development and progression of pathological conditions including fibrosis and cancer (Theocharis 2016, Frantz 2010). For instance, during the progression of breast cancer, collagen cross-linking stiffens the matrix, which induces cellular adhesion assembly and promotes tissue invasion and metastasis (Levental 2009). One explanation could be the increasing nuclear localization of YAP1, a mechanosensitive signaling protein involved in cancer metastasis, with increasing stiffness of the external matrix, which has been shown experimentally by modulating the young modulus of the *in vitro* substrate (McKenzie 2018). Hence, the function of the ECM extends beyond providing a physical scaffold, as its biochemical composition and architecture regulate cellular processes in healthy and pathological conditions.

1.2.2.2. Cellular adhesions

The cell needs to physically interact with its surrounding in order to survive. In the specific case of mesenchymal cells, the physical coupling between the internal cytoskeleton and the external microenvironment is facilitated by adhesions (Lomakin 2015, Gardel 2008).

Those cellular anchoring points are sensitive to external adhesive cues, substrate stiffness, and confinement (Ladoux 2016). At the adhesion sites, internal and external forces are balanced resulting in a stress that allows cellular adhesions to act as mechanosensors (**Figure 9**; Chen 2008). Those nano-scale force sensors transmit physical information of the ECM into biochemical signals (mechanotransduction), and *vise versa*. They thereby represent an organizing center of the migratory machinery by localizing biochemical signals that control the arrangement of the cytoskeleton (Barnhart 2011).

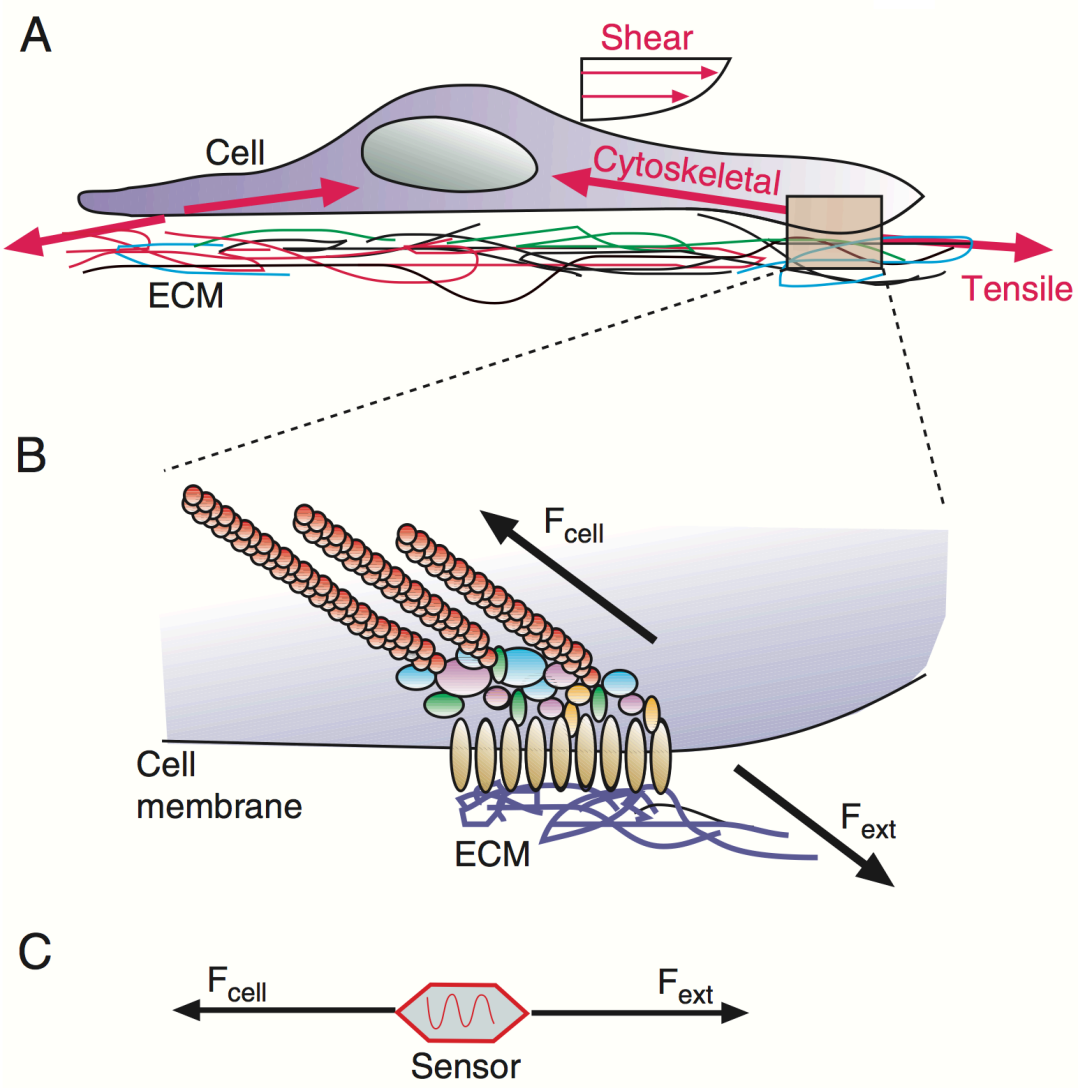

Figure 9: Mechanosensitivity of cellular adhesions. A) The cell in constantly submitted to internal and external forces. **B**) Adhesions are composed of transmembrane proteins (brown) and a variety of signaling and structural proteins (blue, green, yellow and purple). Those adhesive clusters physically link the contractile machinery of the cell (f-actin in red) to the extracellular matrix (dark blue) and are therefore submitted the cellular (F_{cell}) and external (F_{ext}) forces. **C**) The created stress at the adhesion site allows the cell to sense the mechanical properties of the cell. [Figure taken from: (Chen 2008)]

Adhesions are complex, hierarchical structures that are composed of over 50 different proteins including transmembrane receptors, structural proteins and signaling molecules (Barnhart 2011, Wang 2007). Integrins are transmembrane proteins that are composed of heterodimeric α- and β-subunits. Those receptor proteins recognize and bind ECM proteins on the outside, and interact with signaling proteins like kinases or phosphatases as well as actin binding proteins (e.g. vinculin, paxillin, talin) on the intracellular side. The signaling of integrins is bi-directional, facilitating cell binding to the surrounding matrix (inside-out) or transmitting outside signals to the cell (outside-in signaling) (**Figure 10**). During integrin activation, internal signaling proteins (e.g. talin) trigger a conformational change of integrins, which increases their affinity towards extracellular ligands. During outside-in signaling, integrins act as receptors sensing external matrix cues that in return alter the biochemical response of the cell. Both processes are linked, enabling the migrating cell to establish a mechanical cell-substrate interaction required for force transmission while simultaneously sense and adapt to mechanical properties of the microenvironment (Shattil 2010, Huttenlocher 2011).

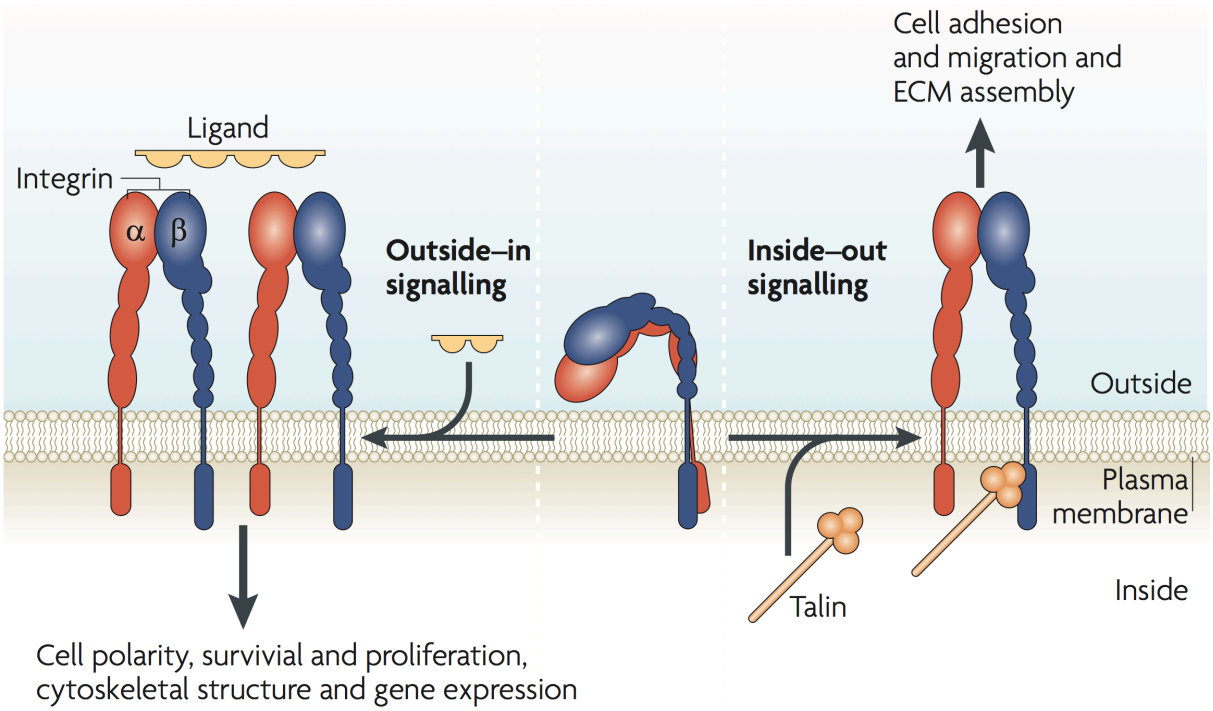

Figure 10: Integrins mediate a bi-directional signaling between the inter- and intracellular space. Integrins are composed of α- (red) and β- (blue) subunits. Inactivated integrins (middle) can be activated through external ligand binding (outside-in signaling; left) or via internal signaling proteins like talin (inside-out signaling; right), which both trigger a conformational change of integrin heterodimers. [Figure taken from: (Shattil 2010)]

Both signaling processes rely on the dynamic assembly and disassembly of adhesive structures (turnover). There are various types of adhesions that are categorized into different classes depending on their state of maturation and molecular compositions (Webb 2002): nascent adhesions, focal complexes, focal adhesions and fibrillar adhesion (**Figure 11**; Gardel 2010). During cell migration, the Rac-mediated formation of small, dynamic adhesions like focal complexes in the front of the cell allows a fast forward motion. Under Rho-generated tension, focal complexes can mature into large, stable adhesion points (focal adhesions) that are associated with stress fibers and are involved in the transmission of contractile traction forces to the ECM.

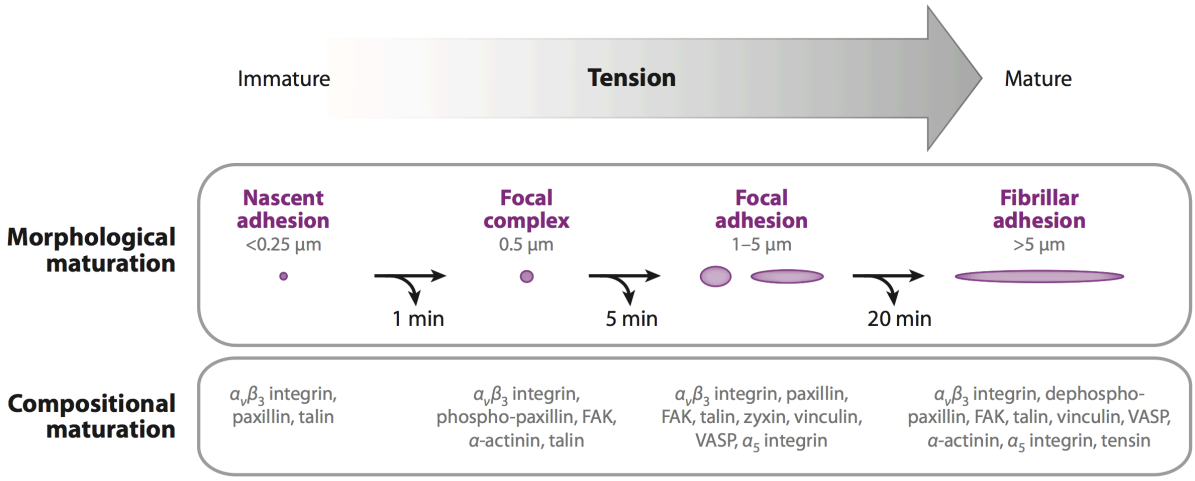

Figure 11: Adhesions can be categorized depending on their state of maturation. Under increasing tension, adhesions increase their size. During this morphological maturation, the molecular composition of adhesions changes. [Figure taken from: (Gardel 2010)]

1.2.2.3. The molecular clutch theory

How is it possible that a car drives along a road? From a physical point of view, the mechanism relies on an engaged clutch, which connects the gear to the engine and transmits power to the wheels. For a migrating cell, the same principle applies: motile forces need to be generated and transmitted to the microenvironment. The “molecular clutch theory” is a mechanical metaphor that explains the involved molecular mechanisms (Case 2015, Gardel 2008).

In general, the transmission of intracellular actin-based forces through the membrane to the ECM generates a friction between the cell and the substrate. In fact, the previously described two main modes of migration vary in their transmission principles and therefore in their generated friction: amoeboid cells generate a non-specific friction during bleb-based motion, while mesenchymal cells generate a specific friction due to the integrin-mediated cell-substrate interaction (Case 2015). Due to the focus of this thesis, we will here describe the molecular clutch hypothesis for adhesion-mediated locomotion.

During mesenchymal cell migration, polymerization of a branched actin network in the lamellipodium pushes against the membrane, which causes the continuous forward movement of the leading edge. The membrane however imposes a constraint for the growing network. This creates a counterforce, which consequently pushes the whole f-actin structure backwards until it disassembles (**Figure 12a**; Case 2015). In the back of the cell, the acto-myosin network generates a contractile force needed for the retraction of the rear (Cramer 2010). Together, actin treadmilling and local force-generation processes create a retrograde flow of f-actin within the motile cell.

This retrograde actin flow represents the driving force of migration as it is coupled to the surrounding environment via transmembrane adhesions (Maiuri 2015). Local mechanosensitve protein-protein interactions at adhesion sites (molecular clutch; **Figure 12b and c**) mediate a transient indirect interaction between the backwards-flowing actin fibers and the ECM bound integrins. Adhesions locally slow down the reward actin flow and create traction on the substratum, which is converted into a forward movement (Gardel 2008). Hence, the spatio-temporal coordination of actin-based forces and their adhesion-dependent coupling to the substrate are crucial for cellular migration (Cramer 2010).

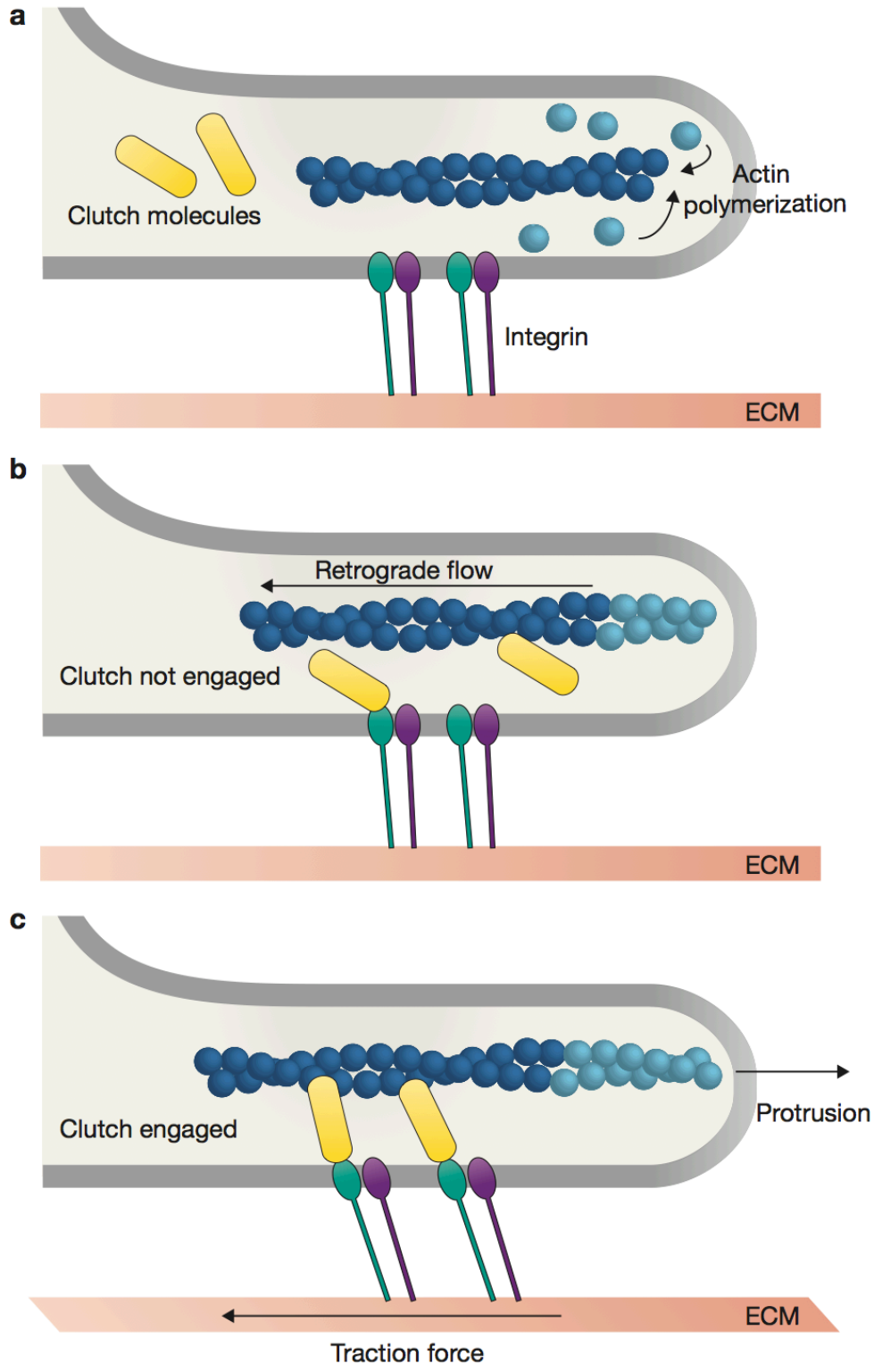

Figure 12: The molecular clutch theory. **a**) Actin polymerization at the leading edge creates a (**b**) retrograde flow of f-actin (**c**) that is coupled to the ECM via mechanosensitive protein-protein interactions when the clutch is engaged. The transmitted intracellular forces generate a traction force on the surrounding environment, which drives the forward movement of a mesenchymal cell. [Figure taken from: (Case 2015)]

1.2.3. Cell migration requires the establishment and maintenance of front-rear polarity

1.2.4. Symmetry and asymmetry principles in nature

Symmetry is an abundant concept in nature that occurs at distinct domains of life bridging across all scales. It governs laws of nature in biology, chemistry and physics, determines human behavior and can be found in areas of life like art and architecture. As humans respond pleasantly to the aesthetics of certain shapes it comes as no surprise that symmetrical objects were long at the center of our attention. Already Leonardo da Vinci or Ernst Häckle studied the proportions of the human body or investigated symmetrical features of plants and animals (**Figure 13**).

Figure 13: Da Vinci's "The Vitruvian Man" and Ernst Häckel's "Studies of different life forms" representing the early focus of humans on symmetry principles occurring in nature. [Figures taken from: Google images]

In 1972, P.W. Anderson defined symmetry as a system that possesses different viewpoints from which the system looks the same (Anderson 1972, Li 2010). And, according to Nobel laureate Richard Feynman, if a symmetric object is subjected to a certain operation it will remain exactly the same afterwards (Feynman 1971, Genz 1999). Due to this uniformity, symmetry can guide us to understand complex systems. For example, studying one honeycomb allows us to understand the whole structure of the hive. However, various

phenomena in our universe occur when symmetry is broken, as an increased level of asymmetry correlates with a higher level of complexity and functional specialization (Li 2010).

The event of symmetry breaking may occur through self-organization or by placing intrinsically polar objects inside a symmetric entity (Li 2008). As a consequence, the object becomes polar: the asymmetrical and ordered distribution of structures along an axis leads to a system that possesses two poles with distinct and opposite properties (Wolpert 2013). Just like a magnet exhibits a negative and positive magnetic pole (**Figure 14**).

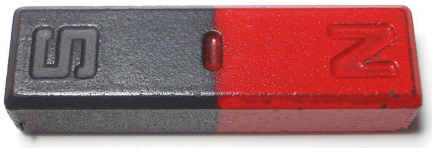

Figure 14: A magnet depicting the concept of polarity: a system with two opposite poles. [Figure taken from: Google images]

While the concept above describes polarity from a physical point of view, its definition might vary depending on the domain. In biology, polarity is rather related to an asymmetry spanning from the molecular to the whole tissue scale (Li 2010, Iden 2008) occurring in all kinds of organisms, from bacteria to mammals (Etienne-Manneville 2004, Wolpert 2013).

The survival of cellular organisms depends on the ability of cells to establish an asymmetry (Li 2010) that is related to structural components like the organization of the cytoskeleton, distribution of signaling proteins, positioning of the membrane or mechanical cell-substrate/cell-cell interactions (**Figure 15**). The formation of those well-defined structures translates into specific functions (Li 2008) like proliferation, differentiation, morphogenesis and cell migration (Etienne-Manneville 2004). Hence, symmetry breaking is fundamental to every physiological process, as it is at the basis of all cellular transitions and decision-making processes (Li 2010).

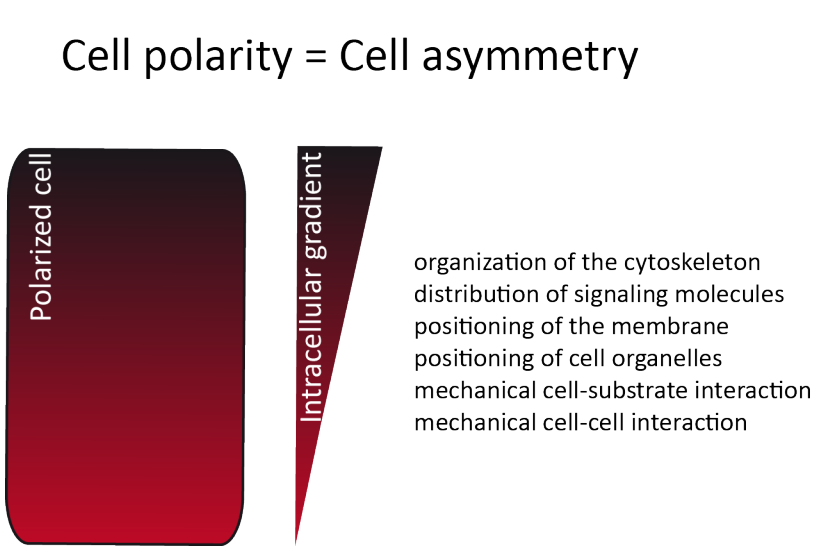

Figure 15: Schematic representation of cell polarity. A polar cell (schematically represented at the left) is characterized by the asymmetric distribution (gradient) of various intracellular components.

How organisms optimize their morphology depending on their function has been intensively studied using various model systems: multicellular assemblies like drosophila and *C. Elegans* as well as single cell organisms like yeast and mammalian cells like neurons and epithelial cells (Li 2010, Etienne-Manneville 2002). We will here focus on the latter: how defined structures at the single cell level determine functional diversification.

In vivo, cells may establish a polar structure depending on their functions and in response to their surrounding microenvironment (**Figure 16**). For example, specialized immune cells, called T-cells, establish a polar structure to facilitate cell-cell contacts with their target cell by orienting the microtubule network and the secretory pathway towards the invading cell. The polar apical-basal structure of epithelial cells allow the regulation of membrane trafficking involved in endocytic and secretory pathways. And cellular forces mediate the asymmetric positioning of the microspindle and reorganization of microtubules in order to trigger asymmetric division in *C. Elegans* resulting in two non-equivalent daughter cells (Etienne-Manneville 2004).

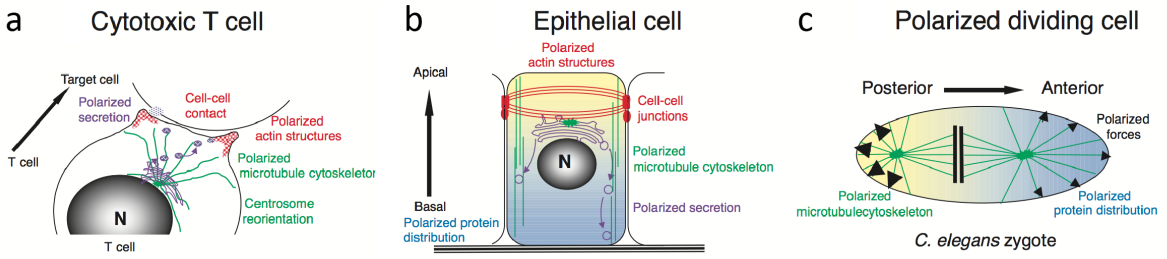

Figure 16: Polar cellular structures allow cell-specific functions *in vivo*. T-cells, epithelial cells and *C. Elegans* need to distribute their cellular components in an anisotropic way in order to function properly. (red : actin, green : microtubules, purple : secretion pathways, blue : signaling proteins, polarity axis : arrow) [Figure adapted from: (Etienne-Manneville 2004)]

1.2.5. Front-rear polarity of a migrating cell

Cell polarity is a crucial key requirement for cell migration (Ridley 2015). The associated asymmetry is termed front-rear polarity: a morphology where we can clearly distinguish front and back of the cell. In general, protrusive activity may arise on several cell edges, but only if one protrusion becomes dominant, polarity builds up (**Figure 17**; Reig 2014). Hence, the lamellipodium needs to be restricted to one part of the plasma membrane in order to contribute effectively to cell migration (Ridley 2015).

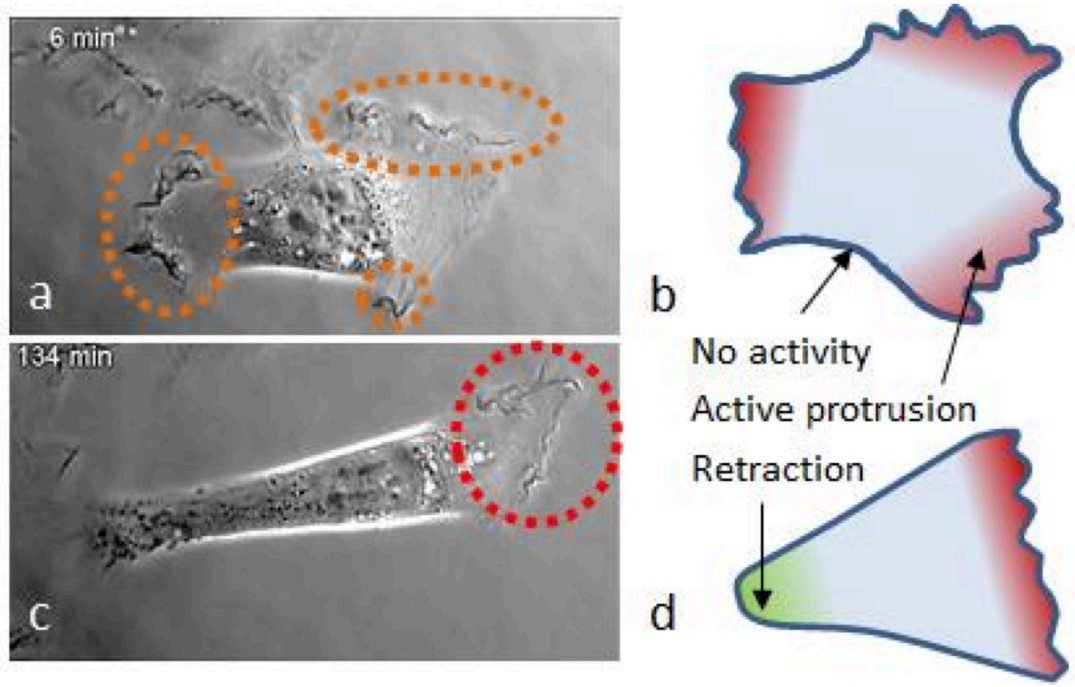

Figure 17: The concept of front-rear polarity. a, b) The cell can possess protrusive activity at various membrane regions. **c, d**) However, polarity can only arise if the protrusion is localized in one area. [Figure taken from: (Valon 2014)]

In the following chapters, we will discuss how distinct spatial distributions of signaling and structural molecules within the cell lead to an architectural, and therefore functional, difference within the cell front and rear: a protrusive leading edge and contractile tail within the migrating cell. Though, plenty of polarity principles exist, our main focus will be on the actin cytoskeleton and cellular adhesions - the two main actors of the migratory machinery (Wehrle-Haller 2003).

1.2.5.1. Structural basis: cytoskeleton architecture and adhesion distribution

As for other cellular functions, the contractile machinery is key in establishing a front-rear polarity specific for cell migration. The polar migrating cell is characterized by distinct actin cytoskeleton architectures, adhesion turnover dynamics, and consequently force generation mechanisms within the front and rear (Lawson 2018, Reig 2014). This subchapter will focus on the structural polarity, while the next subchapter (**1.3.2.2**) explains the involved molecular regulation mechanisms.

The protruding front of a mesenchymal cell is characterized by two distinct actin-based modules, which spatially overlap but are only weakly coupled: a protrusive (lamellipodium or filopodia) and a contractile module (lamella). The thin and broad lamellipodium assembles at the leading edge and subsequently disassembles at a distance of about 1 – 3 μm (Ponti 2004). Actin polymerization creates a cross-linked, dendritic network within the lamellipodium. As fiber polymerization occurs on barbed ends of f-actin, the membrane is pushed forward, which simultaneously generates a retrograde actin flow. At the basis of the lamellipodium, depolymerization of branched actin filaments occurs, leading to a sufficient treadmilling. On the other hand, the assembly of fingerlike protrusions in the front, which locally sense ECM properties, is structurally based on bundled parallel actin fibers. Generally, both explained protrusive modules, lamellipodia and filopodia, exhibit actin-based filament elongation, retrograde flow as well as treadmilling at the cell edge (Gardel 2010).

The contractile lamella is localized a few micron from the leading edge, containing actin, myosin II, and adhesion components. There are three contractile actin architectures within the lamella: transverse actin arcs, dorsal stress fibers and ventral stress fibers

(Burnette 2014). Dorsal stress fibers and transverse arcs are formed via polymerization from small actin-rich spots or assembly of pre-existing short actin bundles, respectively. Both actin architectures undergo continuous formation and disassembly and may convert into ventral stress fibers when associated with adhesions on both ends (Hotulainen 2006).

Dorsal stress fibers are anchored to the substrate via focal adhesions on one side and extend vertically, while myosin II-enriched transverse arcs, which do not bind to adhesion patches, are oriented parallel to the leading edge. Myosin II located within the transverse actin arcs allows the network to contract. Upon contraction of the actin meshwork, non-contractile dorsal fibers are pulled away from the substrate, causing the lamella to flatten. Both actin structures disappear at the beginning of the cell body, while ventral stress fibers originate within the lamella and span through the whole posterior of the cell to promote the retraction of the rear (**Figure 18**; Burnette 2014).

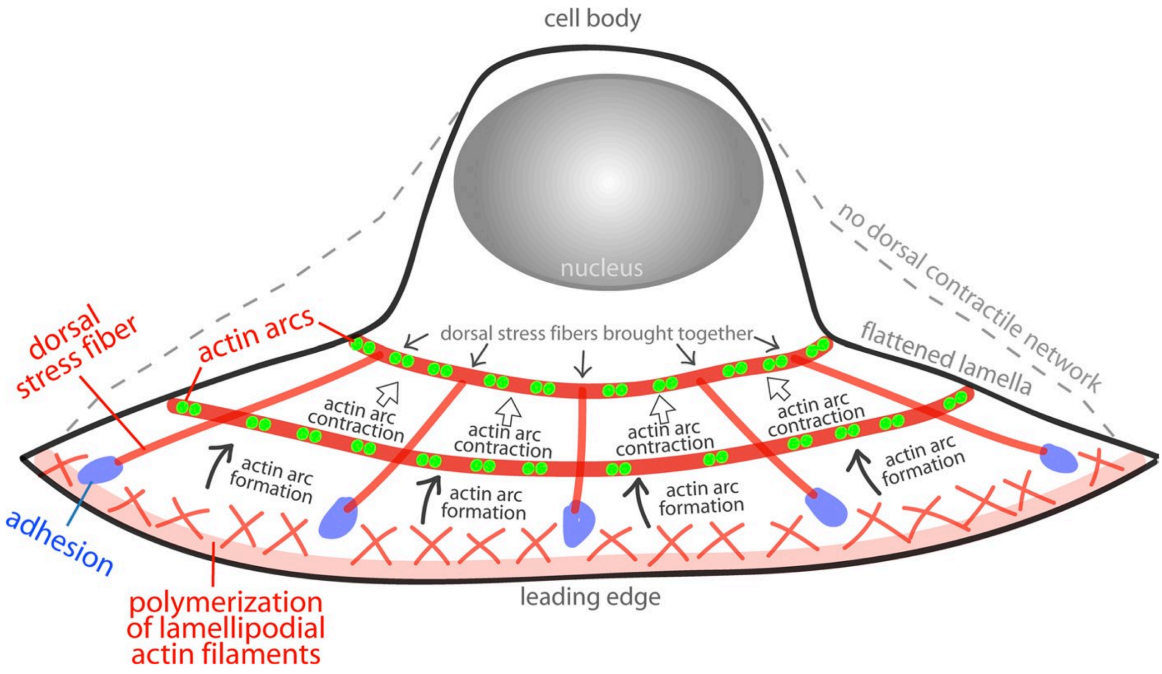

Figure 18: Diverse actin architectures within the leading edge cause the lamella to flatten. The lamellipodium is characterized by a cross-linked, dendritic network of actin fibers (actin in red) at the leading edge of the cell. Myosin II (two green dots represent the two motor domains of myosin II filaments) activity causes transvers actin arcs to contract and shorten in length. The induced contractility exerts a force the non-contractile dorsal stress fibers, which is counterbalanced by adhesions (purple), and causes the whole lamella to flatten (dashed grey line shows cell body without actin arc contraction). [Figure taken from: (Burnette 2014)]

The actin-generated contractility relies on the physical anchoring of the cell to the substrate. Within a migrating cell, diverse adhesion types can be found which differ in their

state of maturation and, hence, in their molecular composition (Gardel 2010). In the front, cell protrusion is to be anchored to the ECM via nascent adhesions or focal complexes. From a molecular point of view, talin facilitates this mechanical link between actin fibers and the ECM by activating integrins, which ultimately leads to the assembly of those small (< 0.25 µm), highly dynamic adhesions in the front of the cell (Shattil 2010, Ciobanasu 2012).

Nascent adhesions can either disassemble or mature into bigger adhesion clusters. The latter one is initiated by acto-myosin forces. Under tension, nascent adhesions grow into focal complexes (< 1 µm) and further maturate into big focal adhesions (1 - 5 µm). The maturation into focal adhesions is accompanied by the recruitment of other adhesion proteins, like vinculin, VASP and α-actinin, triggering also the formation of stress fibers (**Figure 19**). Together, actin stress fibers anchored the ECM via focal adhesions induce contractility within the cell body, triggering adhesive clusters in the tail to dissemble and slide, while the rear retracts (Ciobanasu 2012). To conclude, the migrating cell is characterized by distinct actin architectures and adhesion distributions that are localized within the front, body, and rear of the cell.

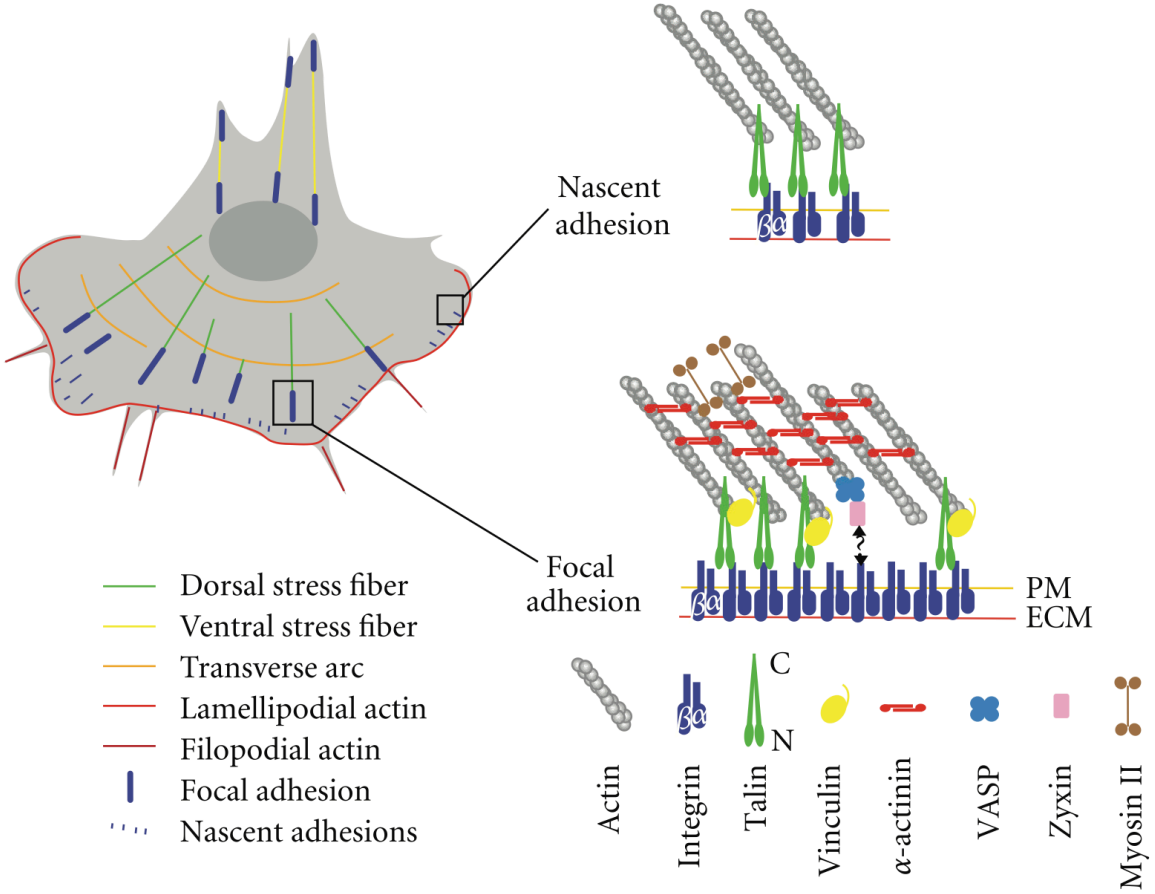

Figure 19: Front-rear polarity of a migrating cell. During cellular movement, distinct cytoskeleton and adhesion structures can be found in the front, body and rear of the cell. [Figure taken from: (Ciobanasu 2012)]

1.2.5.2. Dynamically regulation: RhoGTPases

As mentioned above, directed movement is based on the continuous reorganization of the cytoskeleton and turnover of adhesive contacts. Those dynamic processes need to be regulated in time and space by specialized signaling proteins allowing the cell to rapidly adapt to ECM signals. The major class of signaling molecules, which is present in all cell types (Lawson 2018), is called small RhoGTPases. By acting as dynamic molecular switches, RhoGTPases can activate or inactivate downstream signaling cascades in order to trigger morphological shape changes. In the following section, we will elaborate how small RhoGTPases communicate polarity information to the migratory machinery (Barnhart 2011, Ridley 2015, Lomakin 2015).

From a molecular point of view, the ON or OFF state of RhoGTPases depends on the state of phosphorylation and the localization within the cell (**Figure 20**). The main molecular regulators of RhoGTPases are activating guanine nucleotide exchange factors (GEFs) and inhibiting GTPase activating proteins (GAPs): GEFs facilitate the exchange of GDP for GTP (activation), while GAPs catalyze the hydrolysis of GTP (inactivation; Lawson 2018). If in their inactive form, RhoGTPases are located within the cytoplasm and blocked in their GDP-bound state due to their association with guanine nucleotide exchange inhibitor (GDI). Upon receiving upstream signaling (e.g. from upstream membrane receptors that were activated by external cues), RhoGTPases are released from GDIs. The release of RhoGTPases allows their localization at the cell membrane via a CAAX-domain and specific GEFs to facilitate the GDP to GTP exchange. Subsequently, activated RhoGTPases trigger specific downstream signaling cascades of various effectors (e.g. kinases, lipid-modifying enzymes, or activators of actin polymerization) that are involved in shape changes (Ridley 2003). Finally, GTPase activating proteins (GAPs) mediate the deactivation of RhoGTPases by controlling the dephosphorylation of GTP (Etienne-Manneville 2002).

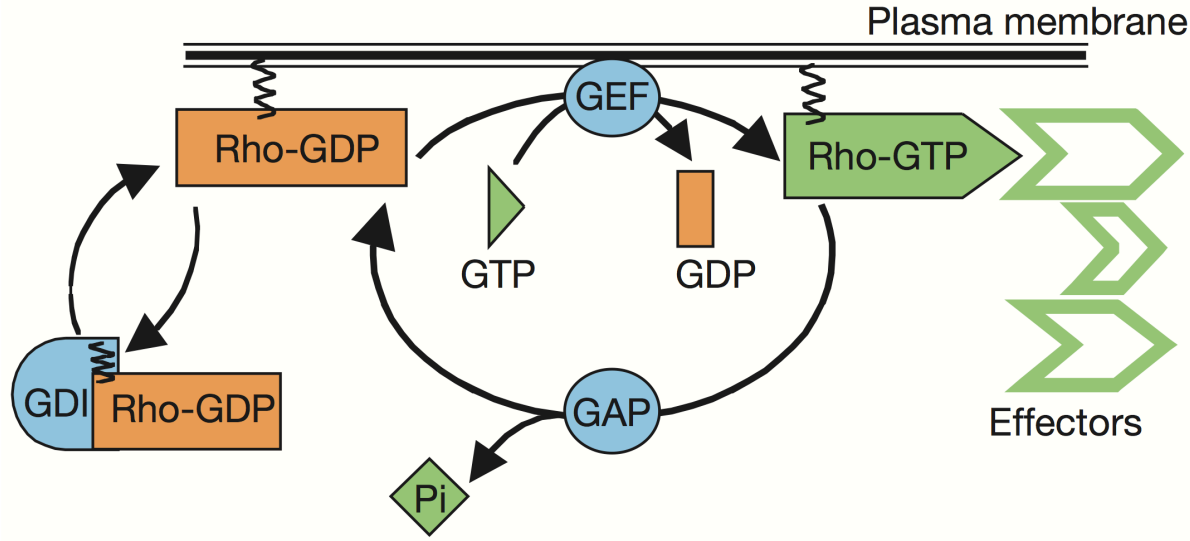

Figure 20: RhoGTPase activation cycle. Inactive RhoGTPases are bound to GDP (Rho-GDP) and associated with guanine nucleotide exchange inhibitor (GDI), which localize Rho-GDP within the cytoplasm. After GDI dissociation and subsequent membrane anchoring, guanine nucleotide exchange factors (GEFs) exchange GDP for GTP, activating the RhoGTPases (Rho-GTP). In their active form, Rho-GTP further trigger downstream signaling cascades of various effectors involved in cytoskeleton rearrangements and adhesion dynamics. Upon GTP-hydrolysis via GTPase activating proteins (GAP), RhoGTPases are deactivated again. [Figure taken from: (Etienne-Manneville 2002)]

There are 20 different RhoGTPases that all follow this cyclic activation-inactivation mechanism. We will focus here on the most intensively studied RhoGTPases that were found to regulate cell migration in all tested animal models: Rac, Rho and Cdc42 (Ridley 2015, Lawson 2018). Those small RhoGTPases interact with distinct signaling molecules that control different actin architectures. Cdc42 and Rac are responsible for stimulating actin polymerization, cell-cell and cell-matrix contact in the front of the cell, while Rho is involved in the regulation of acto-myosin contraction in the cell rear (**Figure 21**; Ridley 2003). Therefore, the molecular regulation of migration relies on the temporal activation of RhoGTPases at distinct locations and their formation of complexes with other regulating proteins (Lawson 2018).

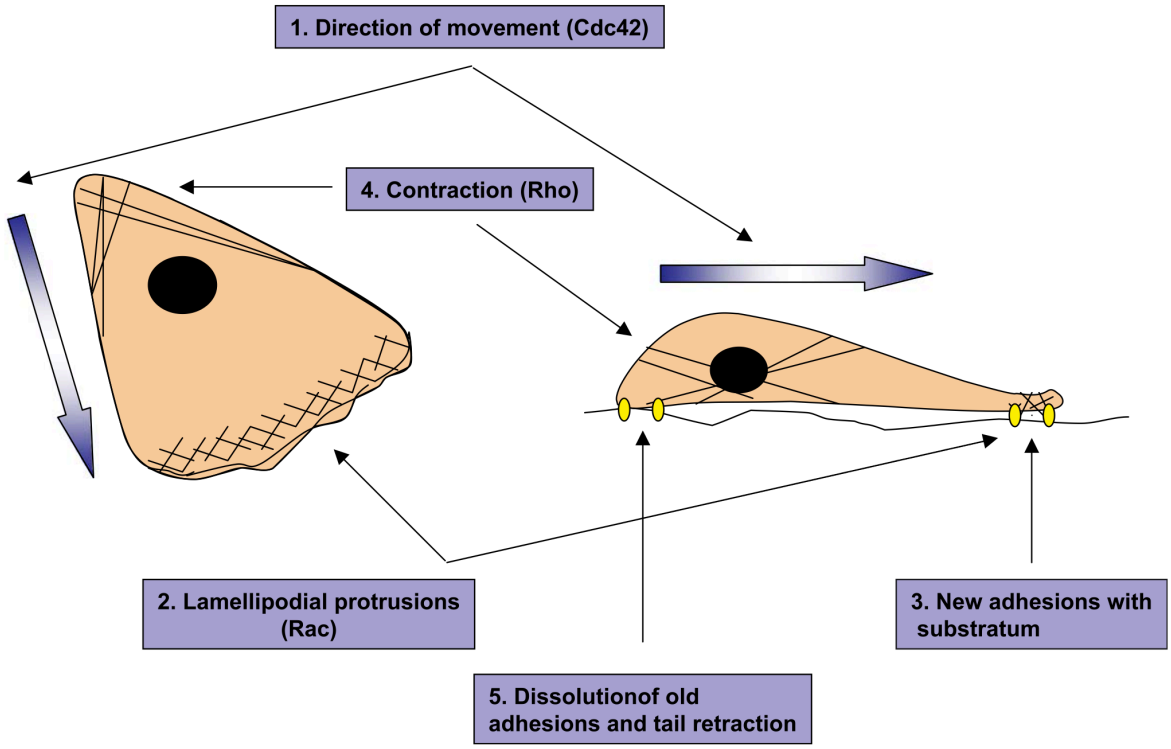

Figure 21: The spatio-temporal regulation of cell migration via RhoGTPases. Rac and Cdc42 are activated in the front of the cell controlling actin-polymerization in the lamellipodium and directing migration, respectively. Rho is activated in the rear of the moving cell, inducing acto-myosin contractility and adhesion disassembly. [Figure taken from: (Raftopoulou 2004)]

How RhoGTPases and their downstream effectors control distinct actin organizations within the moving cell can be seen **Figure 22**. In the front of the cell, Cdc42 and Rac drive the polymerization of actin filaments by activating Arp2/3 through the WASP/Scar/WAVE signaling family. As a result, both RhoGPTases, Cdc42 and Rac, lead to the formation of

distinct actin-based protrusions at the leading edge: filopodia and lamellipodia, respectively. In order to facilitate efficient actin treadmilling in the front, both small RhoGTPases act through the serine/threonine kinase p65PAK to trigger cofilin-mediate depolymerization at the pointed ends of f-actin. In general, Cdc42 is responsible for the directionality of a moving cell. During directed cell migration, the Rac-controlled extension of the lamellipodium needs to be locally restricted in order to form a polarity axis. This local activity arises due to two factors: (i) the Cdc42-mediated localization of Rac in the front of the cell and (ii) the antagonist activity of Rho, which expels Rac from the rear (Raftopoulou 2004, Etienne-Manneville 2002).

Rho activity is mainly restricted to the back of the cell, leading to the formation of a contractile acto-myosin network. Rho stimulates actin polymerization through activation of formin (mDia; Lawson 2018, Ridley 2015). Its other downstream effector p160ROCK promotes the phosphorylation of myosin light chain (MLC) via inhibition of MLC phosphatase. Besides that, inactivation of cofilin leads to a stabilization of actin fibers (Raftopoulou 2004). To conclude, RhoGTPases play a critical role during cell migration, by controlling the crucial balance of lamellipodium formation in the front and contractility generation in the rear of a moving cell (Ridley 2015).

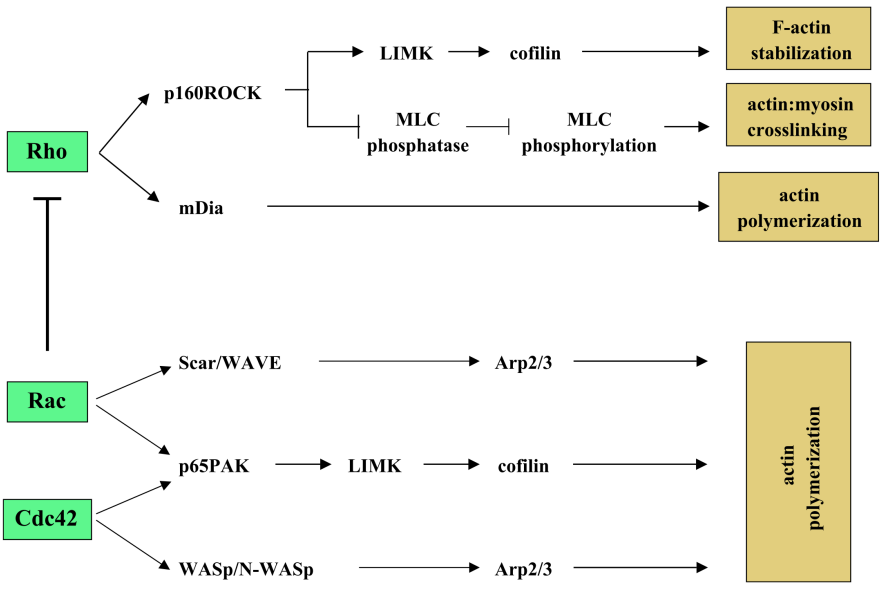

Figure 22: The spatio-temporal activation of RhoGTPases triggers distinct actin network structures and dynamics within the migrating cell. In the front of the cell, Rac and Cdc42 both activate Arp2/3 and cofilin to trigger actin polymerization and depolymerization, respectively. On the other hand, Rho and its downstream effectors create a contractile acto-myosin network in the back of the cell. [Figure taken from: (Raftopoulou 2004)]

1.2.6. Establishing polarity through symmetry breaking

Cells can establish cell polarity in response to intrinsic or extrinsic cues, but also possess an intrinsic ability to spontaneously break their symmetry via self-organization (Wedlich-Soldner 2003). Hence, the internal biochemical state or the recognition of pre-existing external spatial asymmetries leads to the initiation of cell migration.

In general, there are two main properties of symmetry breaking (Li 2008): (i) asymmetric accumulation of mobile components (regulatory molecules) and (ii) oriented organization of cytoskeleton filaments (Ridley 2003). The interaction of those two components is crucial in order to establish and maintain polarity. The communication of signaling and structural proteins is based on local positive feedback loops and global inhibitors, which lead to the assembly of multiprotein complexes that induce downstream signaling in order to achieve asymmetry (Wedlich-Soldner 2003, Iden 2008).

In the following paragraphs, we will explain the dynamics of symmetry breaking and the on-going debate of experts in the field concerning the spatio-temporal sequence of events occurring during the initiation of migration.

1.2.6.1. The generally accepted model: integrating signals from the front to the back

Many models have been proposed that describe the dynamics of symmetry breaking. It is generally accepted that cellular polarization arises do to a signal integration from the front to the back of the cell (Ridley 2003, Cramer 2010). In general, the initiation of cell migration occurs in subsequent steps: 1) front extension, 2) adhesion formation, 3) contractility increase within the rear, and 4) tail retraction (**Figure 23**).

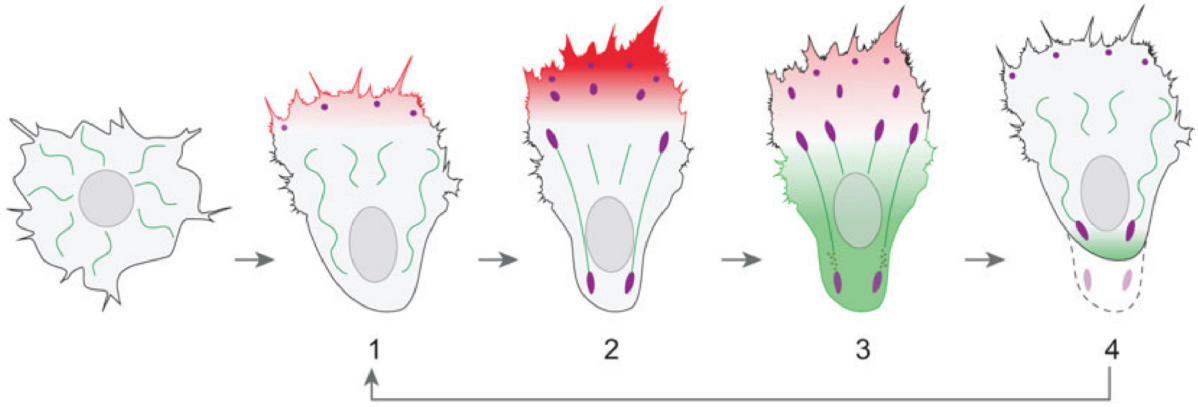

Figure 23: The migration cycle. Symmetry breaking occurs in four subsequent steps by integrating signals from the front to the back. This generally accepted scenario identifies the formation of the front as the first step to initiate movement: 1) Extension of the lamellipodium (red), 2) cell adhesion (purple), 3) contractility (green) and 4) rear retraction (dashed line). [Figure taken from: (Reig 2014)]

The starting point of symmetry breaking is the sensing of extracellular signals like chemokines, growth factors or ECM molecules via membrane receptors. The activation of, for example, G proteins or tyrosine kinases trigger a cascade of events: (1) Specific GEFs activate and locally recruit Cdc42 as well as Rac, which trigger Arp2/3-mediated formation of the protrusive front. (2) Additionally, the activation of Cdc42 facilitates to the local activation of PI3K (a lipid kinase), which leads to talin-mediated activation of integrins and other adhesion molecules. Besides that, Rac recruits integrin molecules. Together, Rac and Cdc42 drive the formation of adhesions, which function as anchoring points of the leading edge and stabilize the protrusion. In a positive feedback loop, new adhesions reinforce the activity of Rac, Cdc42 and PI3K. (3) As a consequence of the locally activated Rac and Cdc42, Rho activity is decreased at the leading edge. This leads to a gradient of Rho activity towards to rear of the cell, which in turn reinforces polarity by restricting Rac activity to the front of the cell. Together, actin polymerization in the front and acto-myosin contractility in the back, generate a propulsive driving force, which gets transmitted to the substrate via adhesions. (4) As a last step, adhesions in the rear of the cell disassemble due to the activity of several signaling proteins (e.g. focal adhesion kinase, extracellular-signal-regulated kinase, Src and microtubule dynamics). This disassembly leads to the retraction of the rear mediated by Rho kinase and acto-myosin contractility (Ridley 2003). To conclude, symmetry breaking is often presented in four distinct steps, which involve the integration of signals from the front to the rear.

1.2.6.2. Controversies in symmetry breaking: formation of the rear as a first step to initiate migration

Just as the symmetry breaking mechanism described in the previous section, cellular migration has mainly been presented as a cyclic, multi-step process, which identified the formation of the front as the first step. However, those observations were made while examining cells that initiate migration in response to pre-existing external cues – and those external cues were usually attracting the cell chemically. This migration mode is termed chemotaxis. It describes how a chemogradient induces migration with high directionality. The process is based on local Cdc42 activation in the front of the cell, which directs the turning of the cell towards to chemoattractant cue (Yam 2007, Yang 2015).

However, polarization can also occur under homogenous chemical conditions (chemokinesis), which results in random walk migration that lacks directionality (Yang 2015). Due to this, one can conclude that a gradient of chemical signals mainly controls the direction, but not the general ability of cells to migrate. Moreover, cell migration can also be mechanically stimulated. For example, a stream of medium can be locally applied to the cell using a micropipette. This mechanical stimulation leads first to the retraction of the rear and a subsequent movement away from the externally applied cue (Yam 2007). Hence, one could reason, that depending on the cue, attracting or repelling, the front or rear forms first, respectively.

However, the understanding grew that there are amplification systems (positive feedback loops between structural and regulating molecules) present within the cell. Those positive feedback loops can amplify transient and local signals and asymmetries or even stochastic fluctuations (noise) and turn them into stable asymmetries that are maintained throughout cellular movement. A cell can therefore, in absence of any external cue, spontaneously break its symmetry (Li 2010, Yam 2007).

And indeed, various studies of neutrophils, fibroblasts and keratocytes have been performed showing the ability of cells to spontaneously polarize (Barnhart 2015, Yam 2007). As keratocytes do not respond to chemical attractants, they are great candidates to study this intrinsic ability of cells to initiate movement. In contradiction with other studies using chemoattractant cues, Yam et al. have identified the formation of the rear as a first step of spontaneous symmetry breaking. Their study shows that tail retraction is initiated due to a

local increase of the centripetal actin flow in the perspective rear of the cell (Yam 2007). The local increase of actin retrograde flow reduces local protrusion, cell-substrate adhesions and weakens cellular traction forces. This leads to a destabilization of the perspective rear. It occurs before acto-myosin contractility initiates the retraction of the rear and ultimately triggers persistent migration (Barnhart 2015, Cramer 2010).

To conclude, many studies of symmetry breaking have been performed using mainly chemoattractant cues, towards which cells move. As an inevitable consequence, molecular models on cellular movement have been conceptualized as a cycle describing the extension of the lamellipodium as the first step (Ridley 2003)**.** However, if cells move away from repellent cues or in absence of any external stimulus, the formation of the rear was often observed first (Barnhart 2015, Yam 2007). Hence, the nature of the external or internal cue seems to determine the temporal sequence of events during symmetry breaking. Moreover, the cell type might also play an important role, as their physiological function differs from one cell type to the other. Due to this, distinct cell migration models have been proposed, which vary in their spatio-temporal order of activation of cytoskeleton forces (**Figure 24**). Consequently, this has triggered a debate of experts in the field of cell migration, which is still ongoing (Cramer 2010).

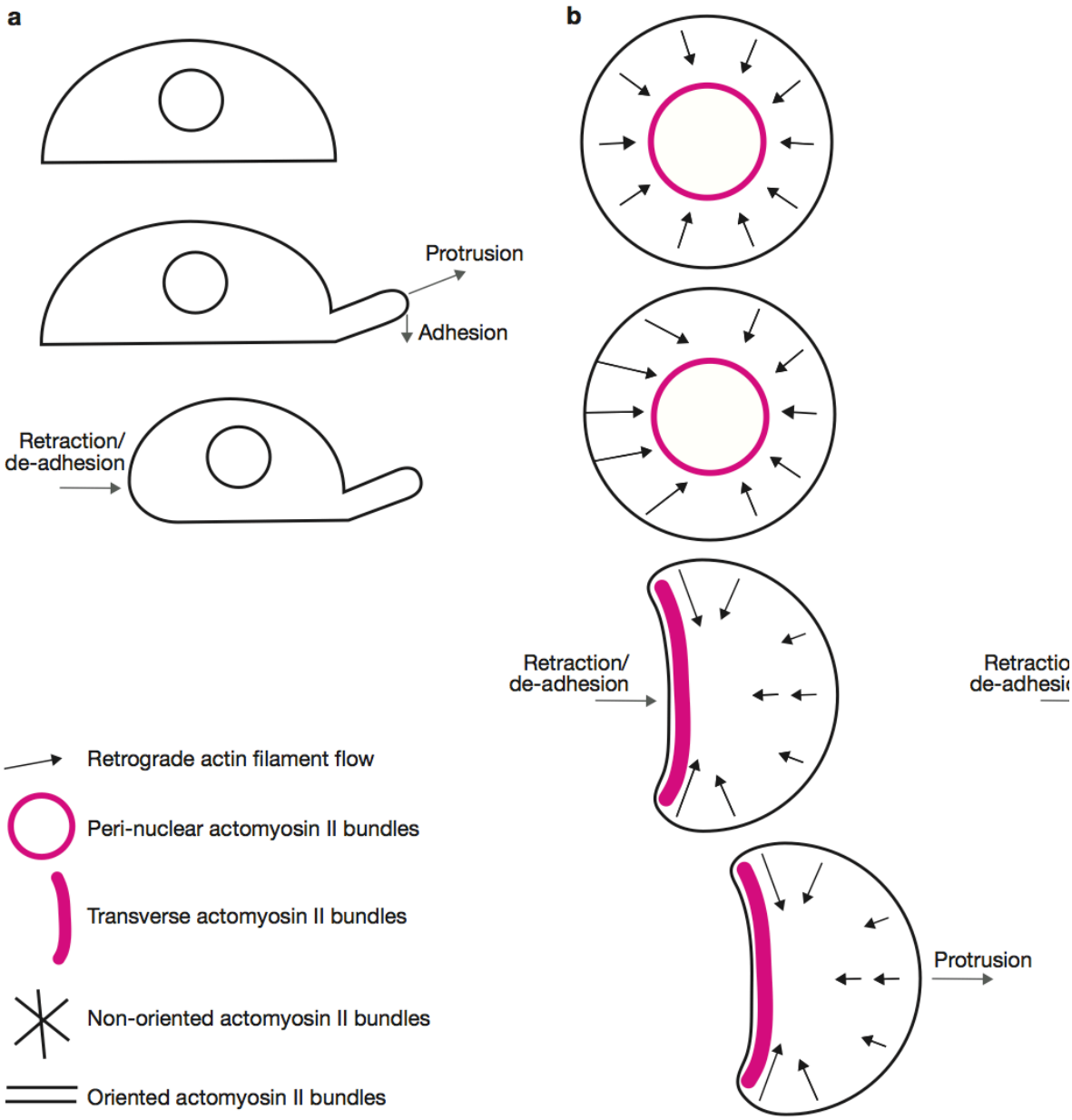

Figure 24: The debate about the first step of symmetry breaking. a) Top view of a cell that first extends its protrusion and **b**) side view of cell that first retracts its rear during the initiation of migration. [Figure taken from: (Cramer 2010)]

1.2.6.3. Maintaining polarity

Until now, this chapter on cell polarity has underlined the crucial step of symmetry breaking during the initiation of cellular migration. However, the established asymmetry needs to be maintained in order for a cell to move over a longer period of time. It has been shown that the maintenance of polarity is due to cytoskeletal transport of polarity cues (i.e. regulatory or structural molecules), which concentrates these polarity factors at the rear

while depleting them from the front (Maiuri 2015). Various positive feedback loops that maintain cell polarity have been proposed, which are based on microtubule (Zhang 2014) and/or actin network dynamics (Maiuri 2015). We will here focus again on the latter.

The retrograde actin flow has shown to impact migration speed and persistence time (a measure of how cells maintain their direction during movement). For instance, Maiuri et al. have identified the reward actin flow as a main regulator in maintaining directed cell migration. The retrograde flow enhances the asymmetric distribution of polarity cues (e.g. myosin, actin polymerization regulators, or microtubule dynamics regulators) for both amoeboid and mesenchymal cells. Upon actin binding, advection of polarity factors leads to an asymmetric distribution profile, which is stabilized by the retrograde actin flow (**Figure 25**). Hence, increasing actin flow speed reinforces cell polarity, finally leading to a universal coupling between cell persistence and speed (UCSP; Maiuri 2015).

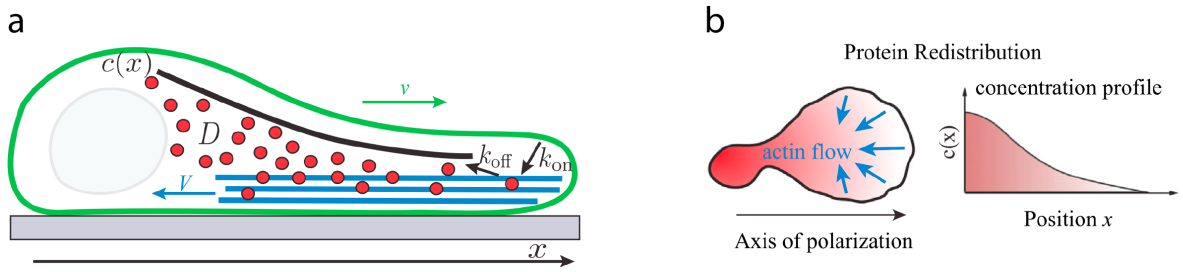

Figure 25: Maintaining front-rear-polarity due to the asymmetric distribution of intracellular polarity cues. a) The retrograde flow of f-actin (blue) with a certain velocity (*V*) triggers the advection of polarity cues (red) to the rear of the migration cell (green arrow indicates direction of migration with a certain velocity *v*). Depending on the interaction strength with the filaments (koff and kon), a gradient of polarity cues is created from the front to the back. **b**) The concentration profile shows the spatial distribution of polarity proteins within the polarized cell. [Figure taken from: (Maiuri 2015)]

1.3. How to study single cell migration *in vitro*

Cell migration has been intensively studied due to its importance in development, immune response and diseases. So far, we have covered essential features of cell migration, mainly from a biomechanical point of view. But, how have scientists revealed those detailed information on migratory behaviors and molecular mechanisms? Methods to examine cell migration have been very useful tools in cell biology, immunology, cancer research, or other related fields (Justus 2014). This last introductory chapter aims at giving an overview on different approaches used to study cell migration, while explaining their use on representative example studies. We will focus on the *in vitro* migration assays based on microfabrication techniques, describe pharmacological and genetic methods to interfere with regulating signaling cascades and explain quantitative force measurement techniques.

1.3.1. Experimental approaches based on microfabrication techniques

In vivo, cells migrate through several types of extracellular matrices: dense connective tissue, loose connective tissue, or tightly packed basement membranes (Even-Ram 2005). As a consequence, cells encounter distinct pore sizes, rigidities, protein compositions, and ligand densities. Depending on those properties of the surrounding 3D microenvironment, cells adapt their shape, organization, and migration behavior (A. D. Doyle 2009, Guetta-Terrier 2015). The direct impact of ECM properties on cell physiology challenges to study cellular migration, especially *in vivo*.

In vitro approaches based on microfabrication techniques allow to examine the effect of specific mechanical and biochemical cues on migratory behavior in a straightforward manner (Tseng 2011). Various artificial substrates exist, which can be fabricated in a controlled and reproducible manner. The following subchapters will introduce a variety of *in vitro* substrates with distinct spatial dimensions and controlled architectures (1D, 2D or *3D* migration assays).

1.3.1.1. From planar 2D substrates to 3D matrices

Historically, cellular processes have been studied *in vitro* on 2D substrates, often made out of glass. Those studies have obtained excessive information concerning general signaling pathways, the crucial role of adhesions, the dynamics of the cytoskeleton, and the generation of cellular traction forces involved in cell migration (Calero-Cuenca 2018, Burkel 2016). For example, the molecular clutch theory, which is universal to all migratory cells, has first been observed and explained on flat surfaces (Thiam 2016). The extensive use of 2D assays has been experimentally convenient and crucial in gaining a broad understanding of cellular migration (Guetta-Terrier 2015).

However, hard substrates like glass are non-physiological, as cells within tissues encounter much softer microenvironments (10-10000 Pa; Yeung 2005). In addition to that, 2D substrates neglect structural and mechanical properties that cells receive *in vivo* (Burkel 2016). To elaborate this crucial point, let us consider the following example. Within tissues, cells are confined and need to overcome certain barriers like epithelial sheets, the ECM as well as neighboring cells and pass through pores below the size of the cell. The ability of cells to pass through tight, micrometric gaps (Calero-Cuenca 2018) strongly depends on their deformability: actin and microtubule cytoskeleton are dynamically remodeled, while the plasma membrane and internal membranous organelles do not limit deformation (Thiam 2016). However, the nucleus has a certain size and stiffness and therefore represents the rate limiting step in cell migration. Its rigidity and viscosity needs to be controlled in order to allow the nucleus to be pushed, pulled and deformed (Calero-Cuenca 2018, Guetta-Terrier 2015). This 3D interaction of cells with their physiological ECM does not occur in 2D cultures. However, the use of 3D assays has identified novel mechanisms (e.g. nucleus deformation and rapture) in the regulation of cell migration *in vivo* (Burkel 2016, Calero-Cuenca 2018). There are two *in vitro* 3D substrates that can be used to mimic the porous nature of *in vivo* tissues: 3D gels and microchannels (A. Doyle 2016, Thiam 2016).

3D gels are based on matrices that are cell-derived or reconstituted from purified ECM proteins (Burkel 2016). One example is collagen 1, the most abundant fibrillar component of physiological ECMs (Di Lullo 2002). 3D collagen gels with defined architectures (aligned or randomly organized fibers of distinct length) can be created by controlling several factors (e.g. ECM concentration, pH, ionic concentration, and temperature) during gel

polymerization (Even-Ram 2005, Burkel 2016). For instance, by changing the collagen concentration, a spectrum of defined pore sizes within the fiber network can be produced to study nuclear deformation during fibrillar migration (Raab 2016). Besides that, the degree of cross-linking as well as the origin of the fabricated 3D matrix determines the mode of migration (**Figure 26**) (Even-Ram 2005). Other example studies have investigated collective cell migration, spheroid formation and the remodeling of collagen during tumor progression and chronic inflammation using 3D gels (Burkel 2016, A. Doyle 2016).

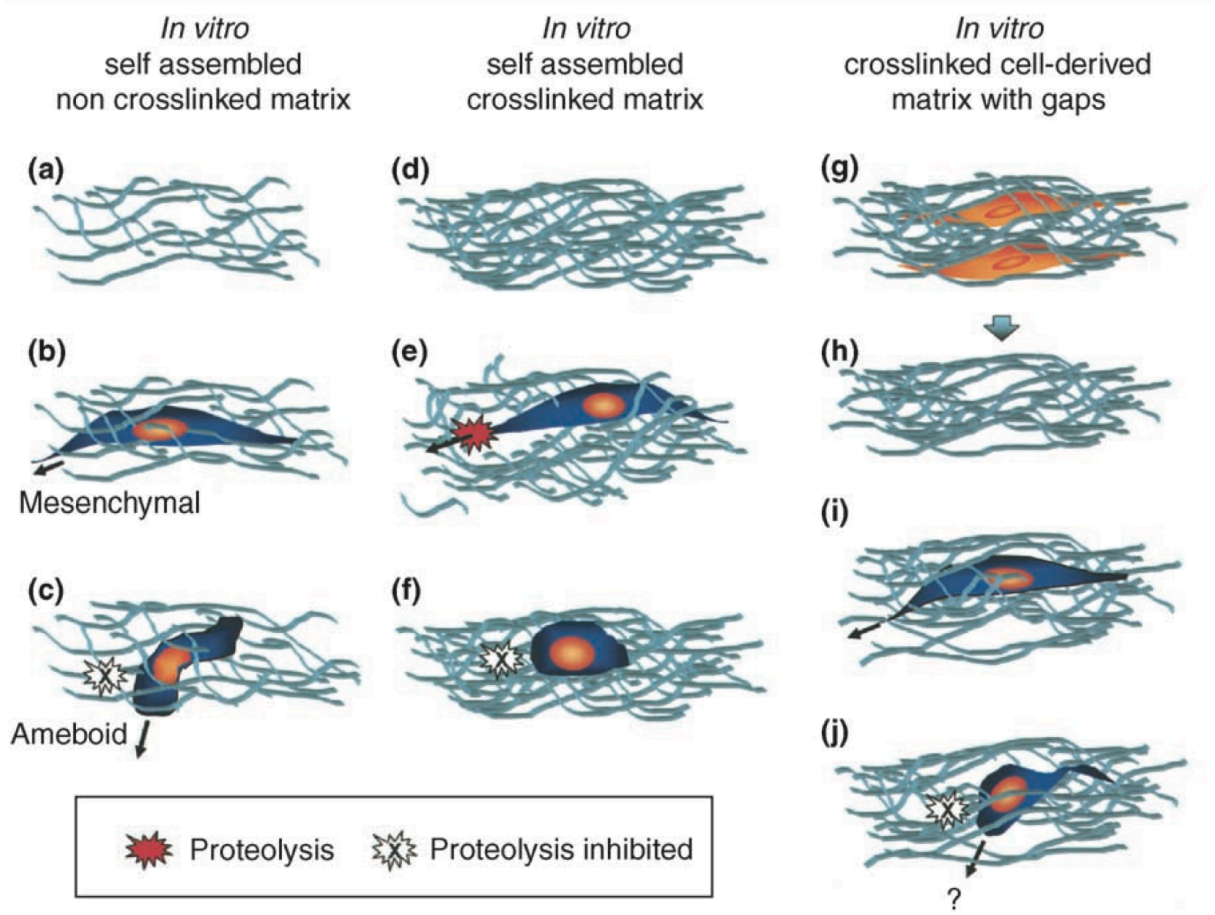

Figure 26: The fabrication of 3D matrix architectures with distinct properties controls the mode of cell migration. a) Within non-cross-linked collagen gels cell employ (**b**) a mesenchymal migration mode or (**c**) switch to amoeboid motility if proteases are inhibited. **d**) Cross-linked matrices with very small pore sizes limit migration, hence (**e**) cell need to locally degrade the matrix, otherwise (**f**) cell migration cannot occur. **g, h**) Cell-derived matrices are characterized by gaps within the meshwork that before accommodated cells. **i**) Mesenchymal cells migrate along the fibers by passing through those gaps. So far, it is not known if (**j**) cells might switch to integrin-independent movement if protease inhibitors are used. [Figure taken from: (Even-Ram 2005)]

Compared to 3D gels, microfabricated microchannels possess an even higher degree of control concerning pore size, while simultaneous enabling the observation of moving cells with high spatial and temporal resolution (Raab 2016). The precise control over the pore size

is essential when investigating the threshold below which the nucleus can no longer sustain deformation and consequently raptures (Thiam 2016). In order for the moving cell to survive, the nuclear rapture needs to be repaired (Calero-Cuenca 2018, Raab 2016). Using 3D microchannels, survival mechanisms of dendritic, RPE-1 and HeLa cells during 3D fibrillar migration were studied (Raab 2016). For example, Thiam et al. identified the crucial role of Arp2/3 in creating an actin network around the nucleus, which supports its deformation even in presence of a stiff nuclear lamina shell (**Figure 27**) (Thiam 2016). To sum up, the mechanism of nuclear deformation and rapture depicts a representative example of a newly identified scenario in cell migration that was discovered by moving from 2D planar substrates to 3D migration assays.

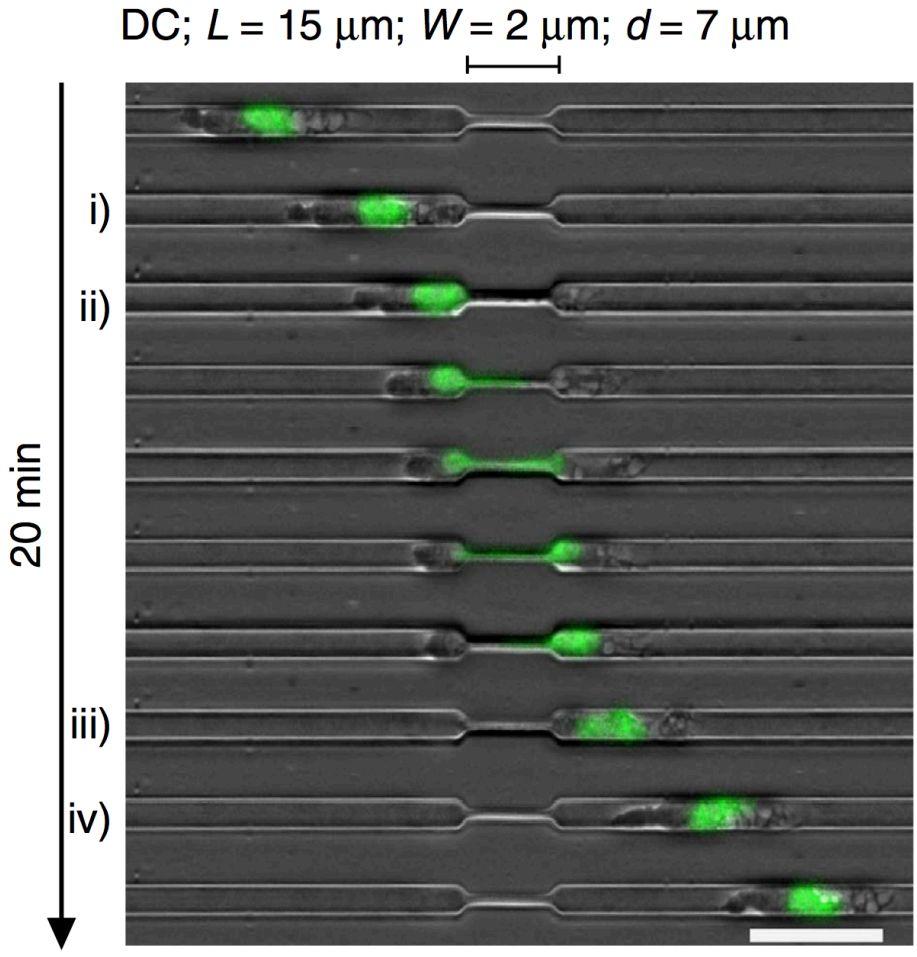

Figure 27: 3D migration study of nuclear rapture using microchannels. The dendritic cell migrates through the microchannel of a defined width. Narrow gaps allow to study survival mechanisms, like nuclear rapture and repair (nucleus in green), when passing through a pores below a certain size. (Scale bar: 30 µm) [Figure taken from: (Thiam 2016)]

1.3.1.2. 1D substrates mimic complex 3D fibrillar migration

3D *in vitro* substrates can mimic certain structural and mechanical features important to fully understand *in vivo* migration. However, quantitative imaging is challenging when cells are free to move in all directions within a complex fibrous networks. A promising alternative approach is the use of 1D systems. It has been shown that 1D topography can mimic certain characteristics of complex 3D migration: morphology, cytoskeleton organization, speed, and microtubule position are alike in 1D and 3D settings, but vary in 2D (A. D. Doyle 2009). Hence, 1D substrates can partially mimic complex fibrillar migration**,** while allowing time-resolved high-resolution imaging. Techniques like micropatterning of adhesive lines (Schuster 2016)and electrospinning of coated nanofibers (Guetta-Terrier 2015) have been used to create spatially confined microenvironments.

Thin electrospun fibronectin-coated nanofibers of controlled fiber size, ligand density, and orientation were used to study novel aspects of fibrillar migration. For example, the study of Guetta-Terrier et al. shows the formation and propagation of wave-like protrusions for various cell types (fibroblasts, epithelial, endothelial and brain-derived cell lines). Those fin-like structures are essential to promote movement along fibers. The actin wave nucleation and size is controlled by the interplay of Rac/Arp2/3-mediated actin polymerization and Rho/formin-generated contractility (Guetta-Terrier 2015).

Micropatterning techniques on the other hand, are based on local deposition of ECM proteins like fibronectin or collagen on top of hard substrates like glass, soft gels, or arrays of micropillars (Tseng 2011). Distinct adhesive islands can be created via techniques like microcontact printing or deep UV exposure through a photomask. In order to create a true 1D system, the width of micropatterned adhesive lines should be below 5 μm (Schuster 2016, A. D. Doyle 2009). In fact, 1D topography recovers specific features (like fast cell speed, elongated phenotype, and centrosome positioning in the rear) of cells moving along ligand-dense fibers during 3D cell migration (**Figure 28**). For example, the observed biphasic relation between migration speed and ligand density on planar substrates (with maximum speed at intermediate density) is valid in 2D, but absent in 1D and 3D condition (A. D. Doyle 2009). Due to that, 1D systems depict a simpler, more accurate alternative to mimic and study complex 3D fibrillar migration and their involved cytoskeleton, adhesion and force dynamics than 2D systems.

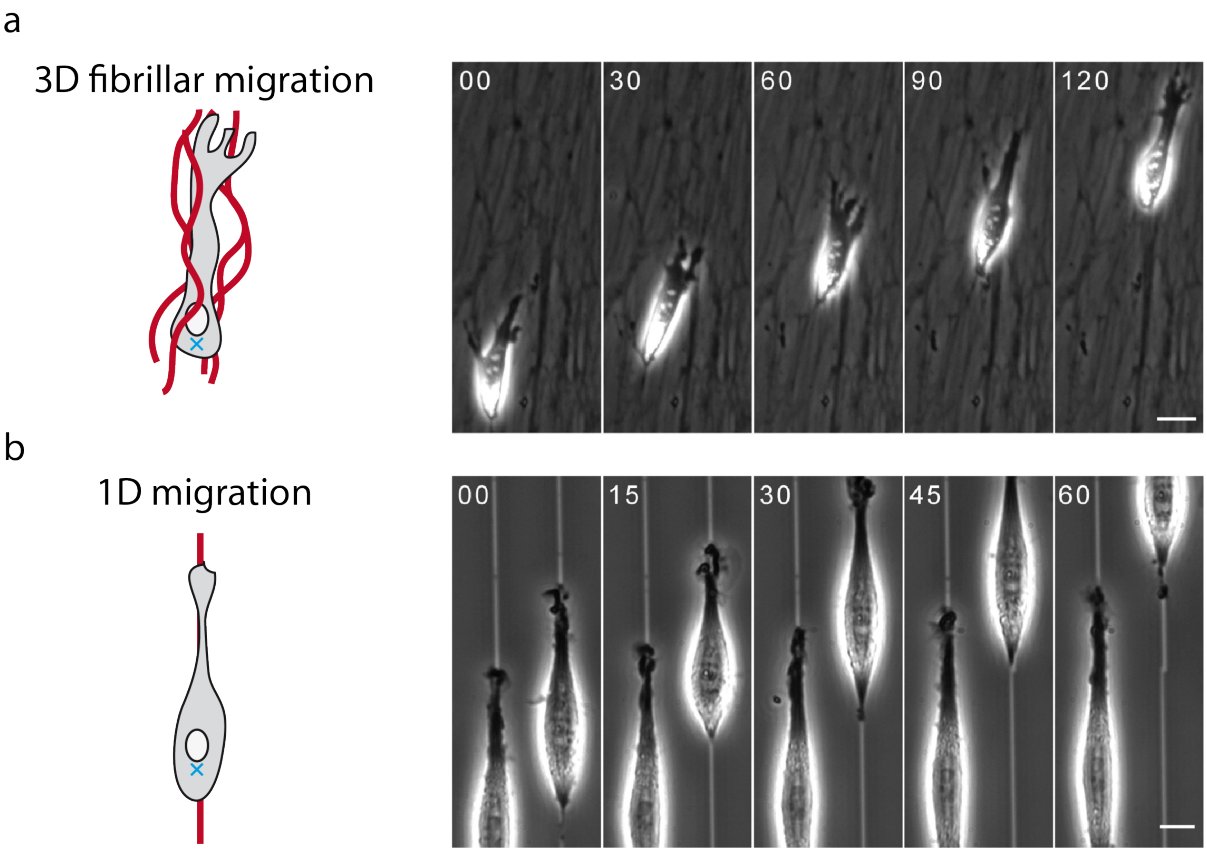

Figure 28: Mimicking complex 3D fibrillar migration *in vitro* using 1D topography. Schematic representation and brightfield images of NIH 3T3 fibroblast migrating rapidly **a**) through a 3D cell-deprived matrix and **b**) on top of microfabricated thin adhesive fibronectin lines (width 1.5 µm; Scale bar : **a**) 20 µm **b**) 10 µm). [Figure adapted from: (A. D. Doyle 2009)]

1.3.2. Perturbing the mechanical activity of the cell

As introduced in **Chapter 1.2 "The migratory machinery"**, cell adhesion connect the contractile cytoskeleton of the cell to the extracellular matrix and transduce external mechanical cues into biochemical signals, and *vise versa*. Hence, the propagation of biomechanical signals throughout a single cell depends on the dynamic interplay of adhesiveness and contractility. A vast amount of experimental techniques exist that enable the perturbation of a cell's mechanical behavior by controlling external cues of the surrounding microenvironment or interrogating intracellular signaling pathways. For example, standard techniques like microfabrication, pharmacological or genetic approaches, as well as novel alternative strategies like optogenetics have been used to study the mechanics of cell migration (Barnhart 2011, Valon 2017, Liu 2015).

In the following chapters, we will first introduce how mechanochemical ECM cues influence cell polarity, and subsequently focus on experimental methods that interfere with the coupling of cell adhesion and contractility.

1.3.2.1. Why experimentally targeting cell adhesiveness and contractility?

The central role of mechanochemical cues in controlling cell migration as well as other physiological processes became obvious over the last few decades. In general, sensing ECM properties lead to a preferential orientation of the cell's cytoskeleton and to adaptation in cellular adhesion size and distribution, which consequently control the level of applied traction forces (Yeung 2005). With increasing, the cell possesses a higher state of polarization characterized by aligned actin fibers and mature adhesion sites that generate higher traction forces (**Figure 29**). In addition to that, biochemical cues (e.g. substrate coating with cadherin or fibronectin) directly impact cell polarity, too. However in absence of any external cue, cells are able to self-polarize. When spreading on hard substrates, a fibroblast cell, for example, transitions from a non-polarized, round morphology to a polarized state by spontaneously breaking its symmetry. Independent of the polarity cue, extrinsic or intrinsic, during polarization cell adhesion and contractility evolve simultaneously (Ladoux 2016). Hence, the coupling of those two key factors determines the efficiency of cell migration on distinct substrates (Barnhart 2011).

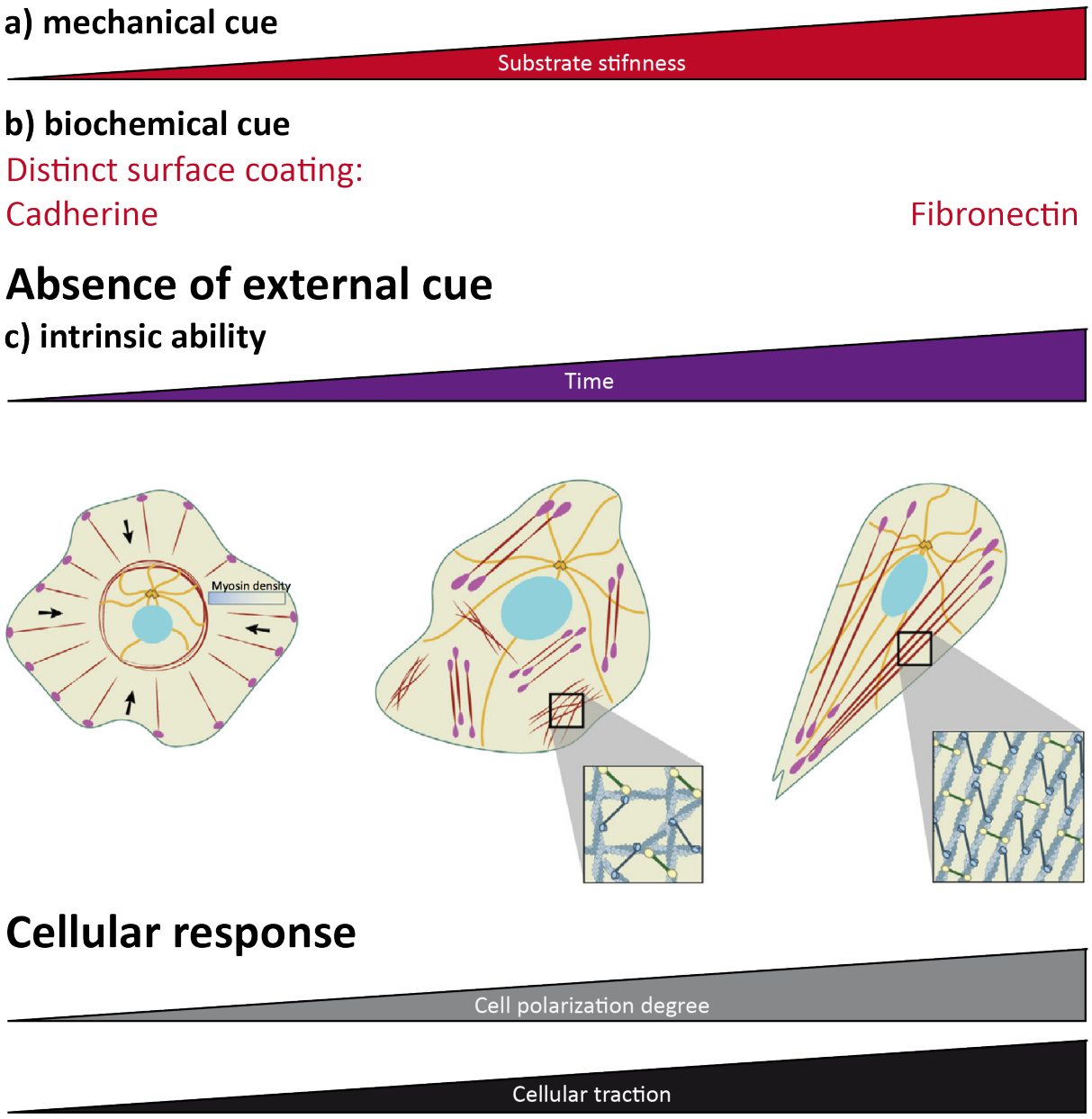

Figure 29: Cell polarization occurs in response to biochemical cues or spontaneously. The degree of polarity increases (from left to right) with increasing substrate stiffness, is determined by ECM proteins, or arises with time. **Left**: A non-polarized, round cell exhibits non-contractile actin fibers at the cell edge and transverse arcs (actin fibers in red) in the center, which confine microtubules (orange). Actin retrograde flow is directed inwards (black arrow) and the cell is anchored to the substrate via focal adhesions (purple dots). **Middle**: Domains of locally aligned actin stress fibers induce an intermediate state of order. **Right**: A high polarization state is characterized by aligned actin fibers. [Figure adapted from: (Ladoux 2016)]

1.3.2.2. Standard methods to tune adhesiveness and contractility

The surrounding microenvironment present several external stimuli to the cell that ultimately influence cell adhesion and contractility: (i) chemical ECM cues, which depend of

ligand density, integrin expression level and integrin-ECM binding affinity, and (ii) mechanical factors, like substrate stiffness, topography and confinement (Gupton 2006). As discussed previously, advances in microfabrication techniques have allowed to control the biophysical properties of the substrate and therefore to study their impact on migratory behaviors *in vitro*.

One approach is to vary the coating of *in vitro* substrates to control ECM ligand density, which is sensed by the cell, and therefore alter the strength cellular adhesion. For instance, Barnhart et al. used the copolymer poly-L-lysine-graft-polyethylene glycol (PLL-PEG) that can be functionalized with RGD peptides. By diluting PLL-PEG-RGD with non-functionalized PLL-PEG, the strength adhesion-facilitated cell-matrix interaction can be controlled. The study shows that cell morphology and migration speed of keratocytes exhibit a biphasic dependency on substrate adhesiveness: at intermediate adhesion strength fan-like keratocytes move fast, while at low or high adhesiveness, keratocytes are round and slow moving. At the basis of the adhesion-dependent motile behavior are distinct actin organizations and myosin II distributions (**Figure 30**) (Barnhart 2011). Other migration studies, which based their experimental strategy on microfabrication techniques, have confirmed this bi-phasic response of motile behavior to adhesion strength/ligand density for mesenchymal as well as amoeboid cell types migrating on top of ECM protein-coated substrates, within 3D gels or through microchannels (Bergert 2015, A. D. Doyle 2009, Gupton 2006).

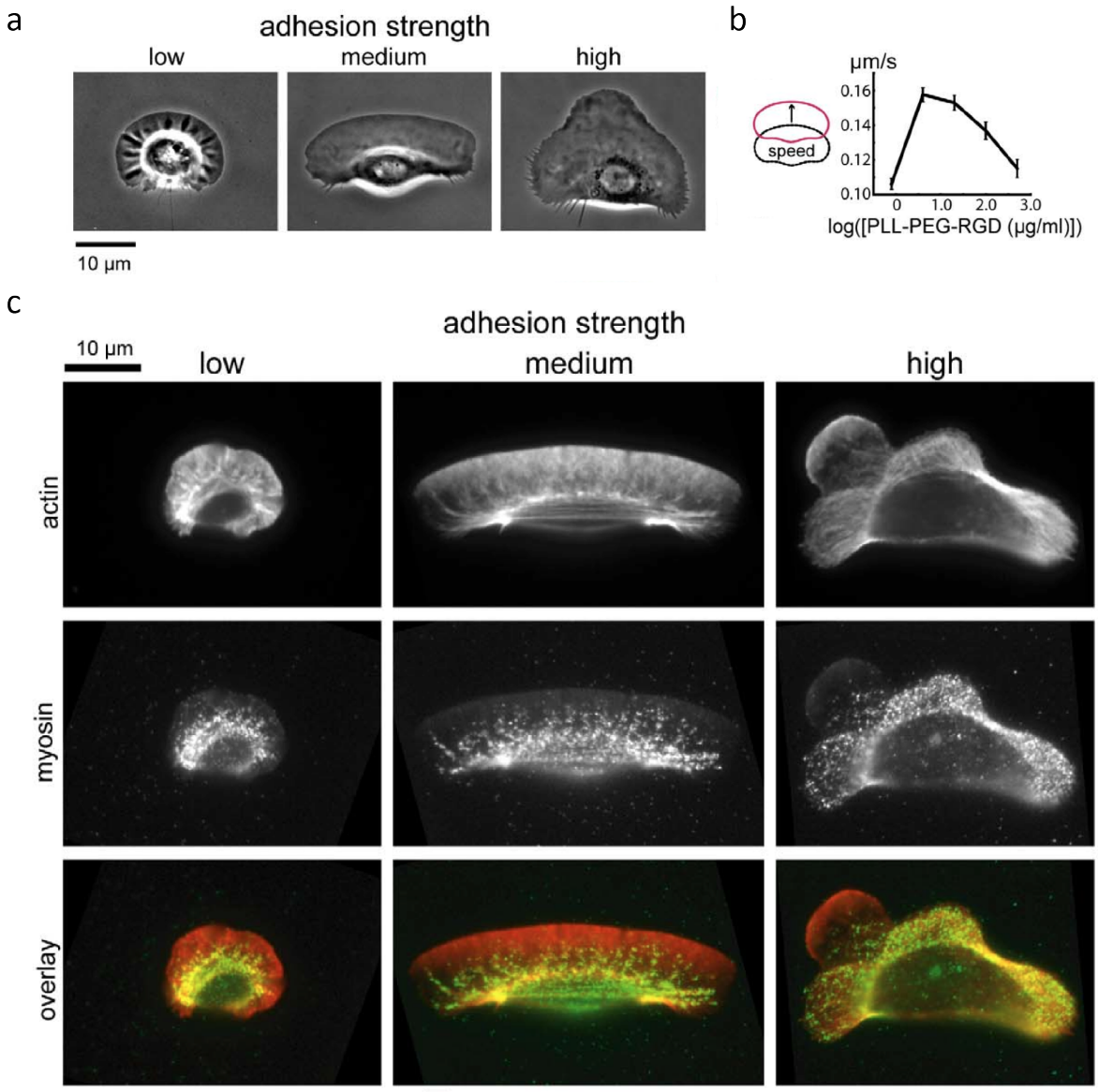

Figure 30: Adhesion strength determines cell shape and migration speed in keratocytes. The surface coating was varied to adapt the adhesion strength, which had a direct impact on **a**) shape, **b**) speed of migration and **c**) myosin II and actin distribution pattern in keratocytes. [Figure adapted from: (Barnhart 2011)**]**

Other studies have investigated the direct impact of contractility or adhesiveness on cell migration using specific drugs, which inhibit distinct intracellular signaling cascades. Those pharmacological methods are used to target specific molecules involved in the regulation of intracellular force generation and transmission mechanisms (Toettcher 2011). Various inhibiting drugs exist that alter cell contractility and adhesion dynamics. For instance, Lomakin et al. have triggered migration by lowering cell contractility using blebbistatin (an myosin II ATPase activity inhibitor (Kovács 2004)). Keratocytes and endothelial cells that were treated with the myosin inhibitor trigger migration and maintain

a polarized cell shape over long trajectories (**Figure 31**) (Lomakin 2015). In general, pharmacological approaches have been extremely useful tools to investigate the role of various intracellular signaling proteins involved in cell migration (Barnhart 2011, Schuster 2016).

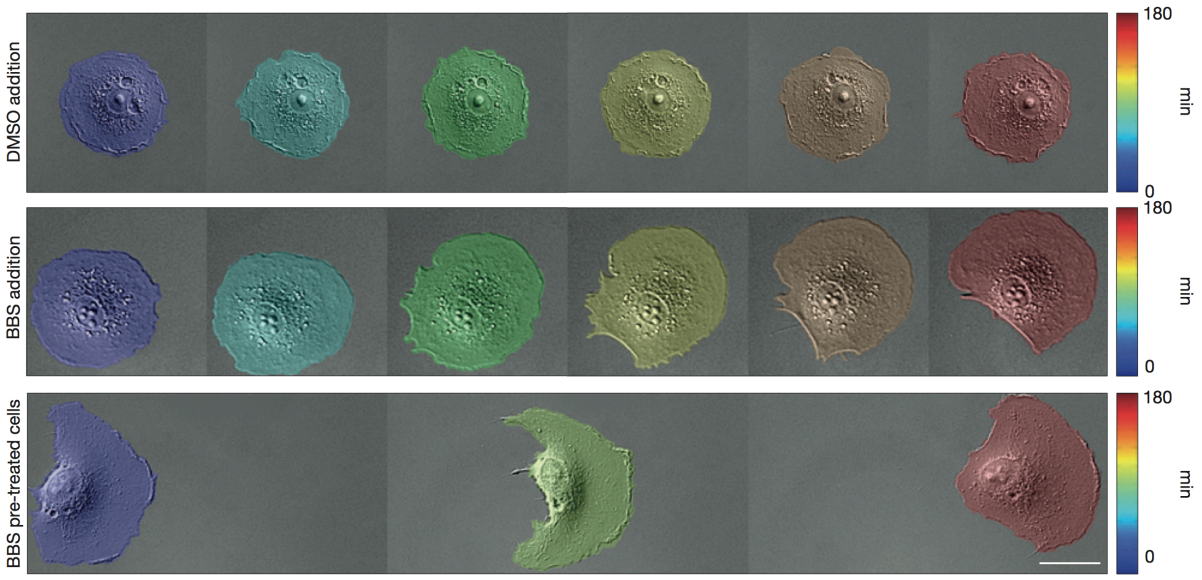

Figure 31: Effect of lowering cell contractility on the migration efficiency of keratocytes. The addition of blebbistatin triggered an asymmetric cell shape, which enabled a continuous migration of the polarized cell. (Scale bar: 20 µm) [Figure taken from: (Lomakin 2015)]

In addition to pharmacological approaches, genetic perturbation methods are used in order to investigate mechanisms that underlie certain motile behaviors. Standard methods include knockdown, overexpression, or mutation of specific signaling molecules or structural proteins (Toettcher 2011). For example, the precise genetic-based depletion of certain integrins (e.g. αvβ3 or α5β1 integrins) has led to an increase or decrease (respectively) of cellular traction forces (Milloud 2017). Another study demonstrates the crucial role of RhoGTPases in fibroblast cells that possess the capacity to suppress tumor growth *in vivo*. Alkasalias et al. have knocked down RhoA in cancer-associated fibroblasts, which triggers the reorganization of cytoskeleton filaments and causes a decrease in contractility. As a consequence, RhoA depleted fibroblasts loose their capacity to impede the progression of cancer (Alkasalias 2017).

To conclude, the discussed standard methods have enabled biologists to investigate cellular motion and other processes by controlling and/or perturbing the mechanical activity

of the cell. These studies show that the cell's migratory machinery adapts to mechanochemical ECM properties or pharmacologic/genetic perturbations by altering cell adhesion and contractility. As both of those key factors are bi-directionally coupled, it is their fine balance that ultimately controls cell migration (Liu 2015, Gupton 2006).

1.3.2.3. Optogenetics – a novel technique first used to study neurobiological processes

Substrate coating, standard genetic perturbation methods and pharmacological approaches have enabled scientists to gain a mechanistic insight into cell migration. However, mechanotransduction principles rely on the tight interplay of mechanical and biochemical processes that are highly dynamics (Chen 2008). To address the spatio-temporal coordination of the three key players of migration (molecular regulators, cell adhesions, cytoskeleton filaments) interrogation techniques need to offer high temporal and spatial control in manipulating the cell's mechanical behavior. However, the previously discussed standard methods lack spatial precision, temporal resolution and/or reversibility and are therefore not suited to address the dynamic coordination of cellular movement (Toettcher 2011).

Optogenetics is a rather novel technique that overcomes these disadvantages by dynamically controlling the activation and localization of specific target proteins within living systems by using light (Peron 2011). This genetically-based approach ultimately allows to directly link molecular activities to specific cellular functions (Toettcher 2011).

The first genetically encoded protein was Channelrhodopsin-2, an ion channel with sensory photoreceptors that transports cations across a plasma membrane in response to light. In nature, channelrhodopsins optimize the efficiency of photosynthesis by guiding microalgae towards or away from light (phototaxis) (Hegemann 2011). As an optogenetic probe, it allows the direct spatial activation of cells on the millisecond time scale (Peron 2011).

Historically, optogenetics was first used in the field of neurobiology. Over the years, new variants of channelrhodopsin as well as other optogenetic tools have been developed to manipulate the activity of neurons (Hegemann 2011). Several outstanding studies have investigated the link between local neuronal activity and animal behavior. The

photostimulation of specific neuronal circuits is based on sophisticated optical systems that deliver light to the brain of living organisms. For example, the optogenetic activation of local sensorimotor neurons triggers whisker movement in head-restraint rodents (Auffret 2018). Another study has induced a cyclic movement of behaving mice with light, by using an implantable wireless optogenetic device (Montgomery 2015). Over the years, this selective manipulation of neuronal systems has led to new insights into the field of neurobiology.

1.3.2.4. Optogenetics allows the spatio-temporal perturbation of single cell mechanics in a reversible manner

Nowadays, optogenetics has moved from neuroscience to other biological fields. The development of new probes has allowed the interrogation of biological processes at different scales: from collective multicellular activities to subcellular signaling pathways. We will here focus on optogenetic tools that allow local interference with mechanical and biochemical mechanisms within a single cell (Kennedy 2010). The outstanding spatial precision and temporal resolution of optogenetics matches the time scale of mechanosensitive processes involved in cell migration, and enables their investigation (Toettcher 2011).

Various light-controllable tools are available. These optogenetic probes are based on genetically encoded light-sensitive proteins that are usually taken from organisms that possess light-sensing systems. The photoactivation of these photoisomeriable chromophores is based on a conformational change upon wavelength specific illumination. In general, there are two main optogenetic principles that control the localization and activity of a specific target protein: (i) light-switchable allostery and (ii) light-controlled protein-protein interactions. In the first case, the protein of interest is fused to the optogenetic probe, which sterically blocks its function. Upon a photo-induced conformational change, the steric inhibition is removed and the protein of interest is active. On the other hand, the second approach is based on light-triggered dimerization of either two single proteins or two split portions of one single protein. This allows to dynamically activate the target protein by recombining two dimers (e.g. recruiting two partners of a signaling cascade together) or to control the location of the light-sensitive fusion protein at specific sites and further activate the target protein/deplete it from its site of action, respectively (**Figure 32**) (Toettcher 2011).

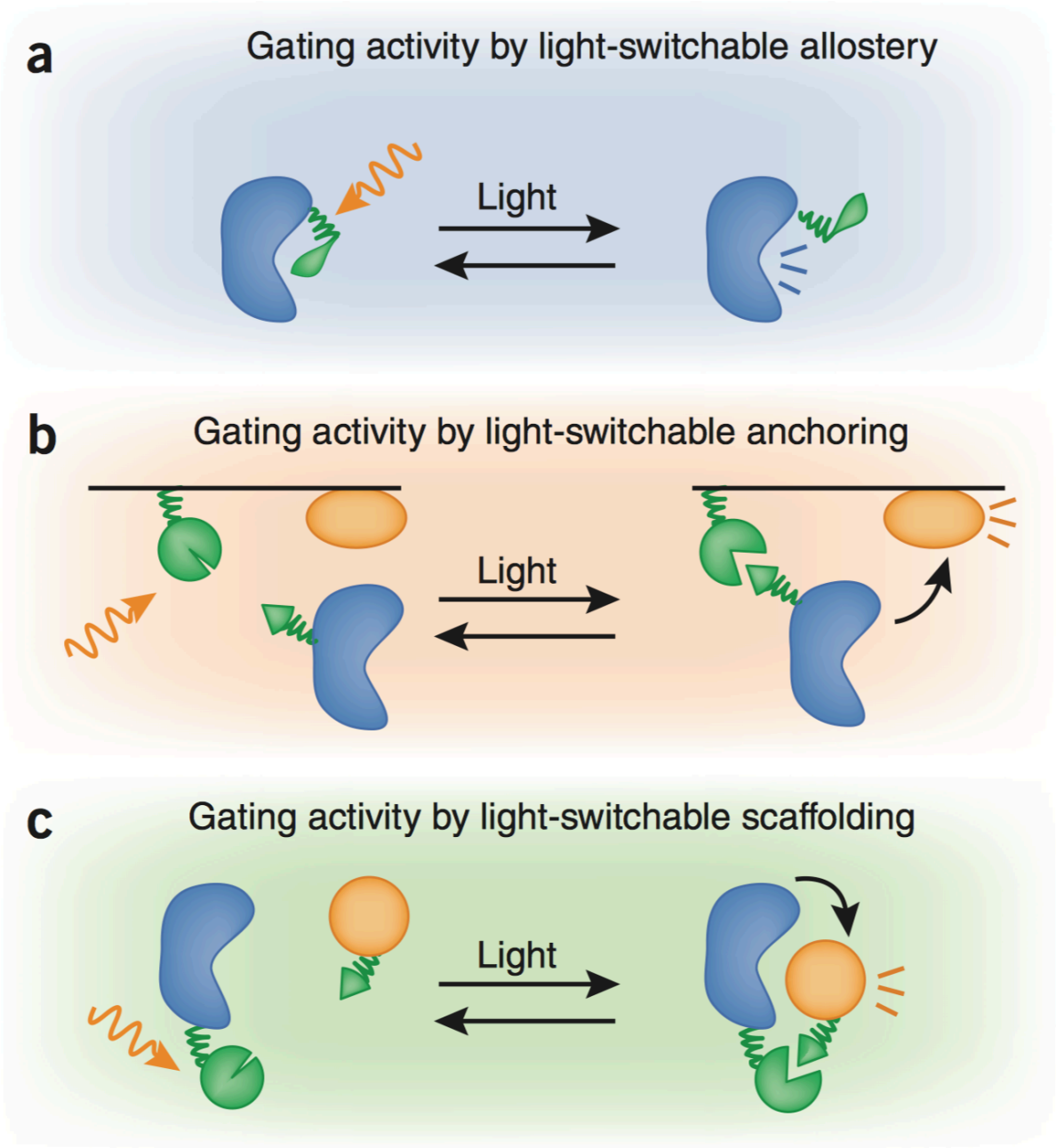

Figure 32: Main optogenetic principles. a) Allosteric hindrance of the protein of interest can be released by triggering a conformational change with light. On the other hand, a light induced dimerization can (**b**) locate the protein of interest at a specific intracellular location (e.g. the membrane) or (**c**) combine two signaling partners. [Figure taken from: (Toettcher 2011)]

The described activation principles represent the basis for the dynamic interference with signaling cascades. Interestingly, by changing the light dose and frequency of the photoactivation, the rate of perturbation can be modulated (Toettcher 2011). Various photosensitive protein families, with distinct dynamic characteristics, exist that are used as optogenetic systems: Light-Oxygen-Voltage (LOV), Cryptochrome (CRYs), and Phytochrome

(PHY) proteins (Pudasaini 2015, Bugaj 2013). The properties of these photoregulated protein modules can vary in their dimerization kinetics, reversibility and dependence on other molecular cofactors (Kennedy 2010). However, a detailed discussion of all available optogenetic probes is beyond the focus of this thesis. We will rather concentrate on exemplary studies, which have used optogenetics to interrogate mechanosensitive components involved in cell migration.

RhoGTPases and G-protein coupled receptors are upstream regulators of the migratory machinery of the cell. Their dynamic control in space and time using optogenetics has enabled to trigger symmetry breaking and/or direct cell migration. For example, a photoreactive LOV-domain can be fused to Rac1, which sterically blocks its activity. Upon light stimulation, the steric hindrance is removed and the target protein Rac1 is activated within the region of illumination. This local photoactivation induces cell protrusion and membrane ruffling in prostate cancer cells, which is sufficient to initiate and direct cell movement (Wu 2009). O'Neill et al. have studied the local activation of Cdc42 in immune cells (macrophages) using the LOV-domain-based localization of a specific GEF (an upstream regulator of Cdc42). The light-triggered Cdc42 activation subsequently activates Rac and hence defines the photoactivated region as the protrusive front. At the opposite side of the cell, Rho signaling increases causing acto-myosin contractility in the generated rear (**Figure 33**) (O'Neill 2016). Hence, the subcellular activation of a specific signaling protein using optogenetics can establish front-rear polarity and trigger directed cellular movement.

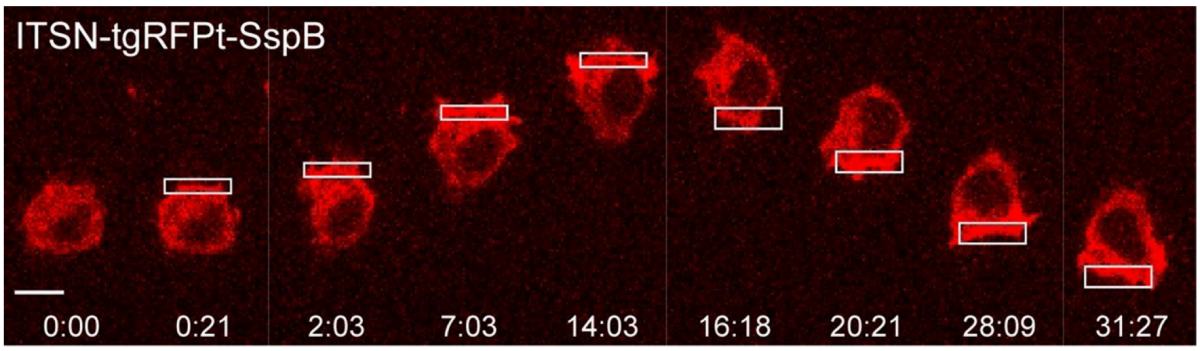

Figure 33: Optogenetics allows to trigger front-rear polarity and to induce migration through local photoactivation of distinct target proteins. The optogenetic construct (ITSN-tgRFPt-SspB and iLID-CaaX) locally activated Cdc42 with light and hence created the front of the cell and induced movement. (Scale bar: 10 µm) [Figure taken from: (O'Neill 2016)]

1.3.3. Quantitative traction force measurements

Mesenchymal cells need to apply traction forces to their surrounding environment in order to move forward. Hence, since decades, scientists have aimed at quantifying the magnitude and spatial distribution of cellular forces. However, directly measuring cellular traction forces has been challenging, as the forces are very weak (pN – nN) and applied over small lengths scales (nm – µm) (Harris 1980, Polacheck 2016, Style 2014).

One of the first qualitative measurements of cellular traction forces were performed by Harris and coworkers in 1980, who cultured cells on top of an elastic substrate that could be distorted by weak mechanical interactions of the cells with the substrate (Burton 1997) (Harris 1980). Wrinkles within the used thin silicone membranes were created due to the crawling motion of single fibroblast cells (**Figure 34**) - the first evidence of exerted, inward-directed cellular traction forces (Harris 1980).

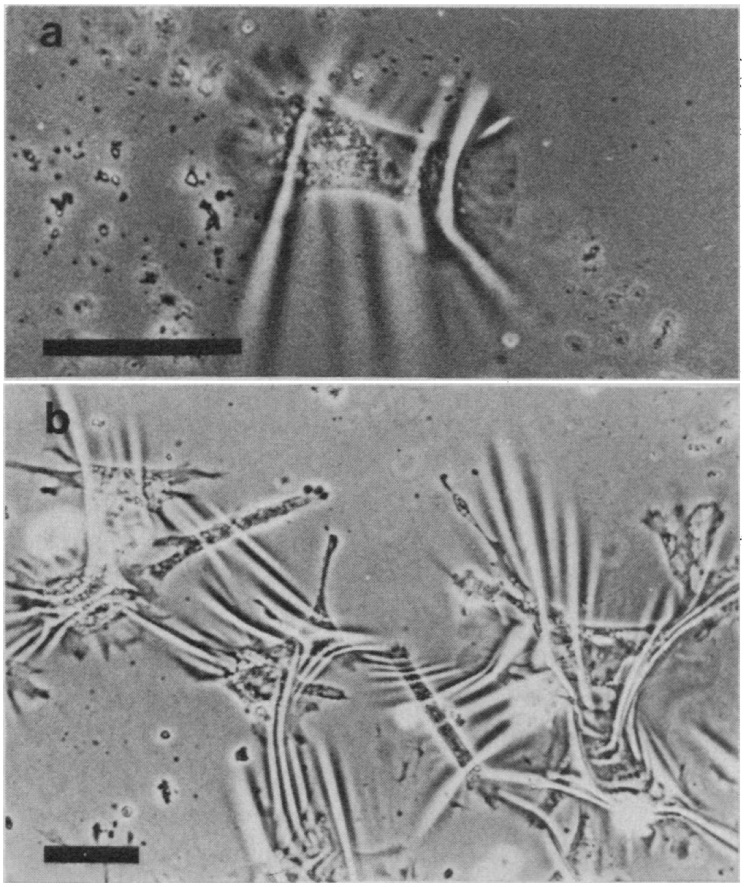

Figure 34: The first qualitative measurement of inward directed, cellular traction forces. Migrating fibroblasts induce wrinkles within a soft silicone membrane. (Scale bar: upper image 50 µm, lower image 100 µm) [Figure taken from: (Harris 1980)]

Since then, various methods of measuring the mechanical interaction of cells with their surrounding environment have been developed, which differ in their assumptions, ease of use and experimental set-up. In general, force measurements are based on displacement calculations, which may extend to compute actual traction force magnitudes from the substrate deformation. Deformation based techniques (e.g. laser ablation of cell-cell junctions) are the simplest way to prove the presence of cellular forces, while not computing the actual force (Polacheck 2016). However, advances in the field have led to quantitative techniques that perform spatially resolved measurements of interfacial cell-matrix forces with high temporal resolution (Style 2014).

The following paragraphs aim at introducing the basis of quantitative force measurements at the single cell level. We will explain the general principle on the example of 2D force microscopy, without going into complex computational details. We will further elaborate technical advances in the field that have allowed scientist to extract the full force field in three dimensions.

1.3.3.1. 2D traction force microscopy

Traction force microscopy has become a standard procedure in many laboratories to investigate mechanical cellular processes (Sabass 2008). The principle is comparable to Hooke's law: $\boldsymbol{F} = k\boldsymbol{X}$. The force (***F***) of a spring can be calculated from its extension (***X***) when knowing the mechanical properties (i.e. stiffness) of the spring (k) (Style 2014). For TFM, a similar principle, where cellular tractions are calculated from the deformation of the substrate, applies.

In order to extract cellular traction forces, microscopic experiments need to be performed first. For 2D TFM, a standard wide-field microscope is sufficient as the displacement and traction fields are calculated within the 2D imaging plane, neglecting the out-of-plane forces. In order to extract the deformation map, we need a material with well-defined mechanical properties that behaves like a linear elastic solid under deformation. In addition to that, the substrate needs to be inert to any cellular degradation in order to maintain its mechanical properties (Polacheck 2016). The soft materials of choice are usually polyacrylamide (PAA) or polydimethylsiloxane (PDMS), which can be functionalized with adhesion-stimulating proteins like fibronectin or collagen (Sabass 2008). The substrate

deformation can be followed by tracking either (i) the deflection of micropillars or (ii) the position of tracers (fluorescent beads) embedded within a 2D planar hydrogel (**Figure 35**). We will here briefly introduce both approaches, but then focus on 2D traction force microscopy, which we routinely use in our laboratory.

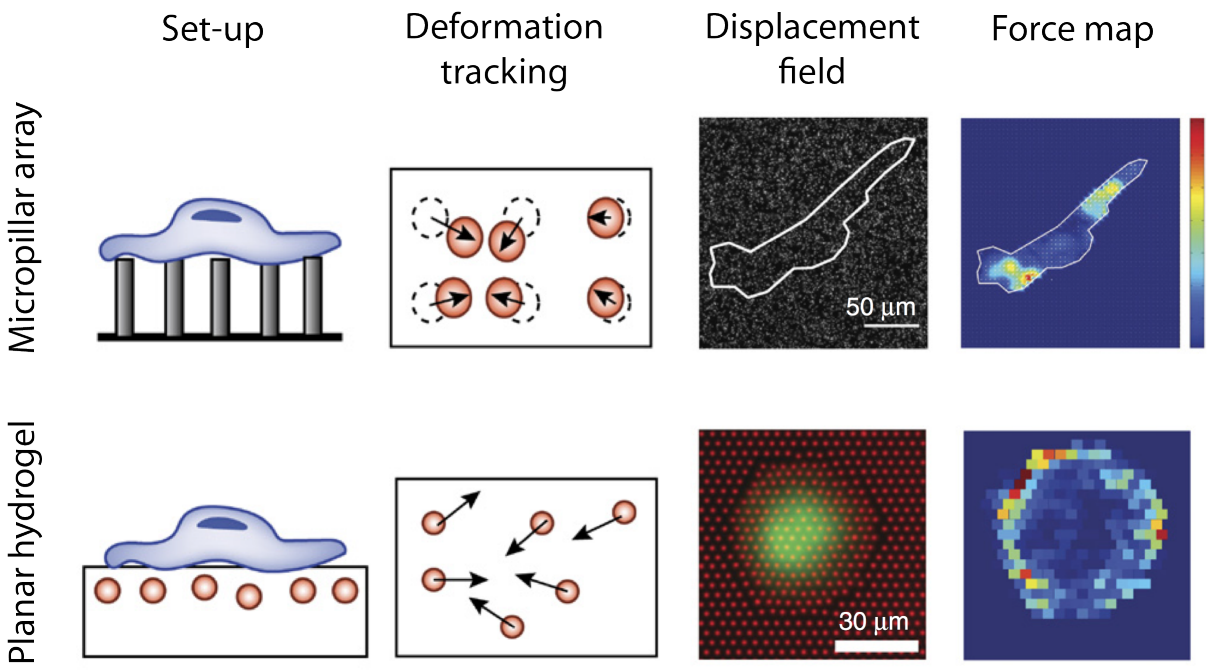

Figure 35 2D TFM approaches using micropillar arrays or planar substrates. Schematic representation shows the experimental set-up and the method for tracking substrate deformations. Micropillars deflection and bead displacement allow to calculate the force map of the cell. [Figure adapted from: (Polacheck 2016)]

An array of elastic pillars coated on top with ECM proteins allows adhesion-mediated cell attachment. The cell spans over several pillars, which get deflected due to the mechanical interaction between the cell and the substrate (Coppola 2017). The elastic pillars possess a controlled geometry (length and width) as well as defined mechanical properties (stiffness). In addition to that, each pillar can move independently of the other. This enabled the direct computation of cellular traction forces in accordance with Hooke's law, which dramatically simplifies the analysis (Polacheck 2016). However, adhesive micropillar arrays represent a unique surface to the cell and limit the spatial resolution of the quantitative force measurement.

An alternative approach is to track to displacement of fluorescent tracers embedded in 2D planar substrates. As fluorescent beads are much smaller than the cell, force measurements can be performed at the subcellular scale. However, due to the elastic nature

of the substrate, a single point force locally applied to the substrate causes displacements of several beads. Those long-range interactions between the tracers within the continuous substrate challenge the computational analysis (Polacheck 2016).

The analysis of performed TFM experiments involves two subsequent steps: (i) displacement field calculation and (ii) force field computation. To compute the displacement field, we need to experimentally acquire images of the stressed (i.e. with the attached cell on top) and relaxed substrate (when the cell is detached) (Sabass 2008). Various algorithms exist, which determine the particle displacement within the gel over a given time interval. In general, those methods extract the trajectories of single particles (particle tracking velocimetry, PTV) or the mean displacement of multiple particles within a given window (particle image velocimetry, PIV) (Sabass 2008, Stitou 2001).

Subsequently, the force field can be calculated from the displacement field using a variety of computational methods. Most algorithms are based on the assumption that the cell-generated material strains are small enough to be analyzed within a linear elastic theory framework (Toyjanova 2014). The calculation of the force field can be done using distinct methods: the boundary element method (BEM), Fourier transform traction cytometry (FTTC), or traction reconstruction with point forces (TRPF) (Sabass 2008). The final result is a quantitative force field at subcellular resolution, which has enabled scientists to address mechanical processes at the single cell level. Overall, 2D TFM is based on a relatively straightforward experimental work. Besides that, algorithms with reduced computational cost have been implemented. Due to this, it is now a standard procedure used in many laboratories (K. W. Mandal 2014, Tseng 2011, Polacheck 2016).

For example, Bergert et al. used 2D TFM in order to determine the difference in forces involved in amoeboid and mesenchymal cell migration. The study shows a significantly lower average stress level for non-adherent blebbing cells (approximately 1 Pa) than for adhesion-dependent cells (range of kPa). The low non-specific friction was then sufficient to propel movement of amoeboid cells while no physical adhesion-facilitated connection to the ECM was needed (Bergert 2015).

1.3.3.2. Moving from 2D to 3D force measurements

Conventional 2D TFM only takes in-plane forces into account. However, cellular tractions are composed of two components: in-plane and out-of-plane tractions. In order to characterize the full 3D force field, scientists needed to extend 2D approaches. 2.5D methods are based on high-resolution imaging techniques, like confocal microscopy, that give access to parallel and perpendicular bead displacements within a 2D hydrogel. However, the computational effort to calculate out-of-plane tractions is higher than for standard 2D TFM (Polacheck 2016).

A multidimensional stress profile showing the 3D nature of cellular forces on planar substrates has been shown by Chen and coworkers (**Figure 36**). In-plane tractions are exerted in the center of elongated adhesions, whereas normal tractions are either upward or downwards oriented at distal (towards cell edge) or proximal (towards cell center) ends of adhesions, respectively. The normal forces may function as pivots to exert a torque on the surrounding environment. Therefore, by taking 3D substrate deformations into account, Chen et al. demonstrate that cells exert out-of-plane rotational moments just beneath focal adhesions (Legant 2013).

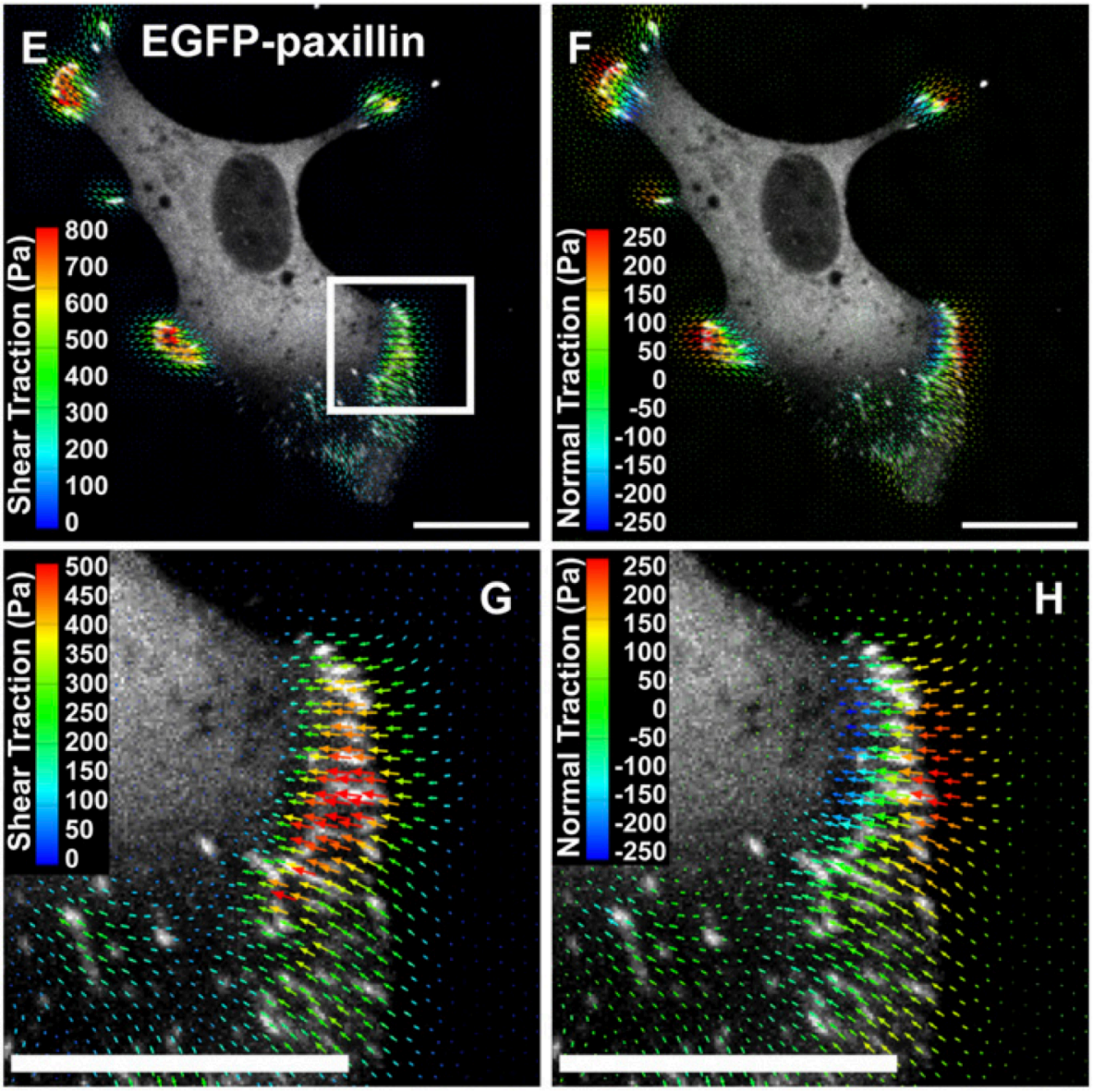

Figure 36: 2.5D TFM reveals 3D rotational moments at focal adhesions. Cells fluorescently labeled for their adhesions (via expression of EGFP-paxillin) exert in-plane (E, zoom in G) and out-of-plane forces (F, zoom in H) just beneath their adhesions. In-plane forces were detected in the middle of the adhesions, whereas normal up- or downwards directed forces are located at the adhesion ends. (Scale bar: 20 µm) [taken from: (Legant 2013)]

2.5D approaches give access to a 3D force field of cells plated on top of planar 2D hydrogels. However, *in vivo* cells migrate through complex fibrillar networks. 3D force quantification techniques exist, which quantify the mechanical interaction between cells and their 3D matrix. Unfortunately, the tracking of fluorescent markers through optically dense fibers complicates the observation of substrate deformations. Additionally, the anisotropic and non-linear mechanical properties of artificial 3D fiber networks challenge the quantification of traction forces compared to 2D TFM (**Figure 37**) (Polacheck 2016).

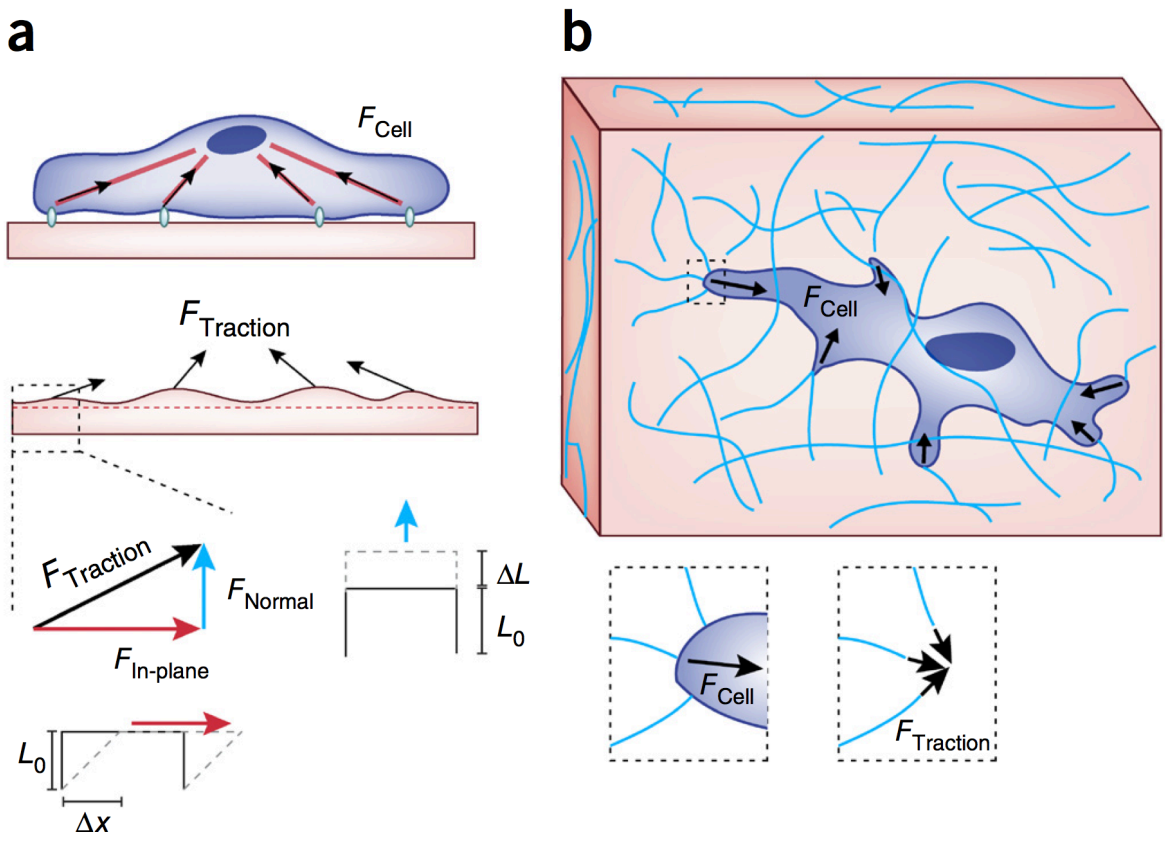

Figure 37: The mechanical interaction of cells with their 2D or 3D microenvironment can be measured via TFM. a) Adhesions transmit cellular forces that deform the surrounding matrix. Those applied tractions are composed of in-plane and out-of-plane forces. Conventionally used 2D TFM only considers in-plane forces, while 2.5D TFM also measures normal forces. **b**) In 3D, cellular tractions can propagate throughout the fibers, which ultimately renders the mechanical properties of the fibrous network. [Figure taken from: (Polacheck 2016)]

All together, various methods exist to access the mechanical interaction between the cell and the substrate in a quantitative way. While conventional 2D TFM measures the tractions exerted parallel to the observation plane, 2.5D and 3D techniques also consider out-of-plane forces, but therefore increase the computational effort. Recent advances in TFM techniques have highlighted the significance of extracting a full force field in all dimensions and gained a deeper understanding of how cells interact with the external matrix.

1.3.3.3. Multipolar force analysis

During cell migration, several forces act on mobile cells: internal forces f_{int}^{i}, inertial forces $m^i v^i$, forces from the fluid f_{fluid}^{i} and forces from the substrate f_{sub}^{i}.

$$\sum_i m^i \frac{dv^i}{dt} - \left(\sum_i f_{int}^i + \sum_i f_{fluid}^i + \sum_i f_{sub}^i \right) = 0 \tag{1.1}$$

In accordance with Newton's laws of motion internal forces need to cancel each other out. On the other hand, due to the small spatial scale at which cell migration occurs, inertial forces and viscous forces (i.e. from the fluid acting on the cell surface) are negligible (pN) compared to higher substrate forces (nN), which counterbalance cell traction at adhesion sides (Chen 2008). The summation of all active forces therefore adds up to zero:

$$-\sum_i f_{sub}^i = 0 \tag{1.2}$$

Due to this, the quantitative analysis of cellular traction needs to extend beyond a simple summation of forces and also consider their spatial distribution (Tanimoto 2014).

In order to due so, a multipolar analysis, which extends beyond measuring the magnitude of mechanical cell-substrate interaction, needs to be performed. Tanimoto et al. have performed multipolar analysis of cellular tractions (i.e. the rotational and front-rear asymmetries of the stress field) to characterize the spatial distribution of forces during cell migration. As shown before, the zero-*th* order moment defined the net force, which is equal to zero. The force dipole corresponds to the first order moment, and allows to identify the cell orientation, and hence the axis of migration (K. W. Mandal 2014). The second order moment, the force quadrupole, determines the direction of migration (Tanimoto 2014). To conclude, migrating cells exert anisotropic pinching forces on their surrounding environment, which can be further quantified in their spatial distribution. We can therefore address the dynamics of the force-motion relation in a quantitative manner.

2. Unraveling the force-motion relation: motivation and goals

Cellular migration is a fundamental process at the heart of many biological functions that are involved in the development and maintenance of healthy organisms. Aberrations in cell motility can lead to pathological situations like cancer metastasis and invasion (Friedl 2009). At the single cell level, two main modes of migration exist: integrin-based mesenchymal and non-adherent amoeboid migration (Friedl 2009). Independently of how fundamentally different those two main modes are, they have one major criterion in common, which determines a cell's ability to move forward: the breaking of symmetry (Ridley 2003).

The process of symmetry breaking leads to distinct architectural, and therefore functional, differences between the front and rear within a moving cell. During movement the polarized cell possesses a forward moving protrusive leading edge and a retracting contractile tail (Wehrle-Haller 2003). This established front-rear polarity is essential for a cell to move (Cramer 2010). The involved dynamic processes, which lead to the initiation of migration, have mostly been presented as a four-step cycle: formation of the front, followed by adhesion attachment, increase in contractility, and finally retraction of the rear (Ridley 2003). The identification of the front formation as a first step may be an unavoidable consequence of migration studies that have been performed using chemoattractant cues (Yang 2015). Complementary studies using repellent or no external cues at all (Yam 2007) have emphasized a different scenario, where the rear formation occurs first. The debate of the sequence of events during the establishment of front-rear polarity is still ongoing. So far, distinct cell migration models have been proposed that vary in their temporal sequence of the molecular activation of cytoskeleton forces (Cramer 2010).

Many studies have intensively focused on obtaining a full mechanistic insight of cell migration. The development of molecular, genetic or microscopic tools as well as microfabrication techniques has led to a broad molecular understanding of symmetry breaking. Key signaling cascades, adhesion turnover, and cytoskeleton dynamics have been linked together (Barnhart 2011, Etienne-Manneville 2002). However, over the last few years,

mechanobiology has emerged as a new field of research (Chen 2008). It emphasizes the crucial role of the mechanical properties of cells and their surrounding environment on physiological processes (Ladoux 2016). Indeed, locomotion relies on the generation of intracellular forces and their transmission to the surrounding matrix. In addition to those internal forces, moving cells are continuously subjected to external forces exerted by the surrounding microenvironment (Chen 2008). In mesenchymal cells, both processes are bi-directionally coupled through an adhesion-mediated link between the contractile machinery of the cell and the ECM. This allows the migrating cell to perform two processes simultaneously: (i) transmit motile forces to the surrounding (Case 2015) and (ii) sense biochemical cues of the surrounding microenvironment (Shattil 2010).

This indicates a strong interplay between cellular traction forces and movement. However, until today, a full understanding of how these forces drive cell migration is lacking. One reason might be that the central role of cell mechanics, in addition to genetics, has just recently been accepted. Besides that, special techniques, needed to address the evolution of cellular forces during the event of symmetry breaking, are not implemented in many laboratories yet. Due to that, several questions remain unanswered and prevent us from obtaining a full understanding of cell migration (Eyckmans 2011). At the beginning of my PhD thesis, we therefore decided to tackle this problem by unraveling one major question of the force-motion relation of mesenchymal cells:

What is the temporal sequence of events occurring during spontaneous symmetry breaking?

In order to address this question, which extends beyond molecular mechanisms, we defined three major goals for my PhD project. The first objective was to design an experimental set-up and create a standardized protocol for high-throughput quantification of cellular traction forces, while following the trajectory of single moving cells over a long period of time (**aim1**). After having developed a suitable *in vitro* migration assay, our goal was to investigate cell migratory and force parameters during the initiation of migration in order to unravel how/if cytoskeletal forces determine a cell's ability to break symmetry (**aim2**). Our final goal was then to extend our study beyond fundamental research. In collaboration with Dr. Nils Gauthier and Dr. Pascale Monzo, we aimed at screening the

motile potential of invasive cancer cells (glioblastoma) according to their mechanical behavior (**aim3**). In order to achieve these ambitious goals, we based our experimental strategies on a combination of various techniques and an original theoretical framework, which ultimately enabled us to identify a novel contractility-driven and adhesion-dependent scenario of spontaneous symmetry breaking.

3. Materials and Methods: experimental basis for unraveling the force-motion relation

The general goal of this thesis was to unravel a temporal sequence of events by following the evolution of the mechanical cell-substrate interaction during spontaneous symmetry breaking. In order to do so, we needed to the design an *in vitro* cell migration assay. Ideally, our *in vitro* approach should allow us to extract morphometric and mechanical parameters with high temporal and spatial resolution. To do so, our experimental set-up was based on a mixture of different techniques: the migration assay combined microfabrication of thin adhesive linear tracks on soft substrates with time-resolved traction force microscopy (output). This bottom-up approach, called patterned traction cytometry (K. W. Mandal 2014), was supposed to identify key regulating parameters of the force-motion relation. Additionally, we wanted to further validate and challenge our prospective findings by using pharmacological treatments and optogenetic approaches (input; **Figure 38**).

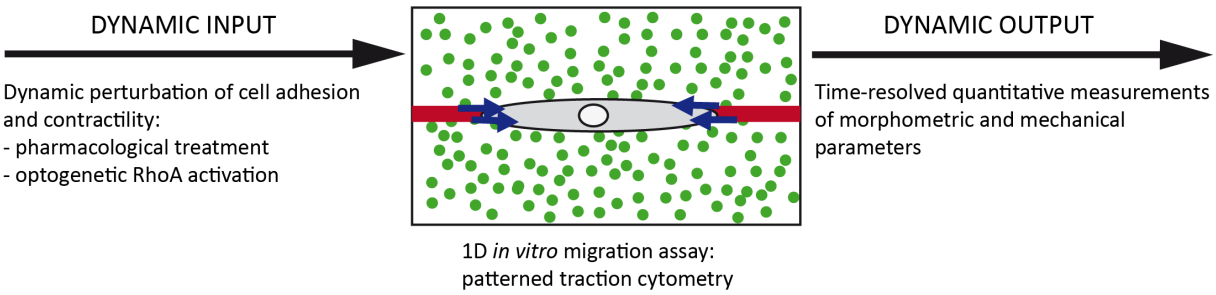

Figure 38: Schematic representation of our experimental strategy. A combination of different techniques allows the dynamic perturbation of cell mechanics and the simultaneous dynamic read-out of the cellular response.

The following subchapters of this **"Material and Methods"** section aims at explaining the techniques that we used to study the relation between cell migration and adhesion-based contractility. We will discuss the experimental strategies behind key methods, general experimental procedures and their advantages, as well as the quantification of relevant migratory parameters. Additional protocols and further details of all methods can be found

in the "Methods and Materials" part of our scientific publication (see **Annex Chapter 6.1**). The final results that we obtained using a combination of the here introduced techniques will be presented in the subsequent **Chapter 4**.

3.1. Experimental strategy: Patterned Traction Cytometry

Traction force microscopy has been a very powerful tool to access weak cellular traction forces at the subcellular scale. Due to Newton's law of motion, the vector sum of all forces is zero at the single cell scale. Therefore, a multipolar analysis is needed to address the spatial distribution (and therefore the asymmetry) of cellular tractions (Tanimoto 2014). However, freely moving cells facilitate frequent morphological and directional changes and possess complex spatial force patterns, which challenge the interpretation of the evolution of cellular forces during symmetry breaking.

Innovative tools based on microfabrication methods have allowed scientists to standardize cellular behavior and to precisely control mechanochemical properties of the *in vitro* substrate, which enabled to reproduce physiological conditions that cells encounter *in vivo* (K. Mandal 2012). We based our migration assay on microfabrication techniques to confine migratory cells to thin adhesive lines. This 1D topography possessed several advantages over performing TFM experiments on homogenously coated 2D planar substrates (**Figure 39**). The most practical advantage for data analysis and comparison with theoretical predictions was the characteristic spatial force profile that cells exhibited in 1D, from which we could extract and interpret multipolar force parameters in a simplified manner (Leal-Egaña 2017). Besides that, the movement of adhesive cells along lines was restricted in direction. Due to that, quantitative position tracking of the front, rear and nucleus was straightforward. In addition to that, latest research has proven that 1D topography can partially mimic complex 3D fibrillar migration (A. D. Doyle 2009, Schuster 2016). To sum up, our 1D migration assay allowed to extract and interpret migratory and force parameters in simplified and straightforward manner, while, at the same time, mimicking relevant physiological conditions absent in 2D migration studies. The next chapters will further elaborate technical details of the two combined experimental techniques: (i) soft micropatterning and (ii) quantitative force measurements.

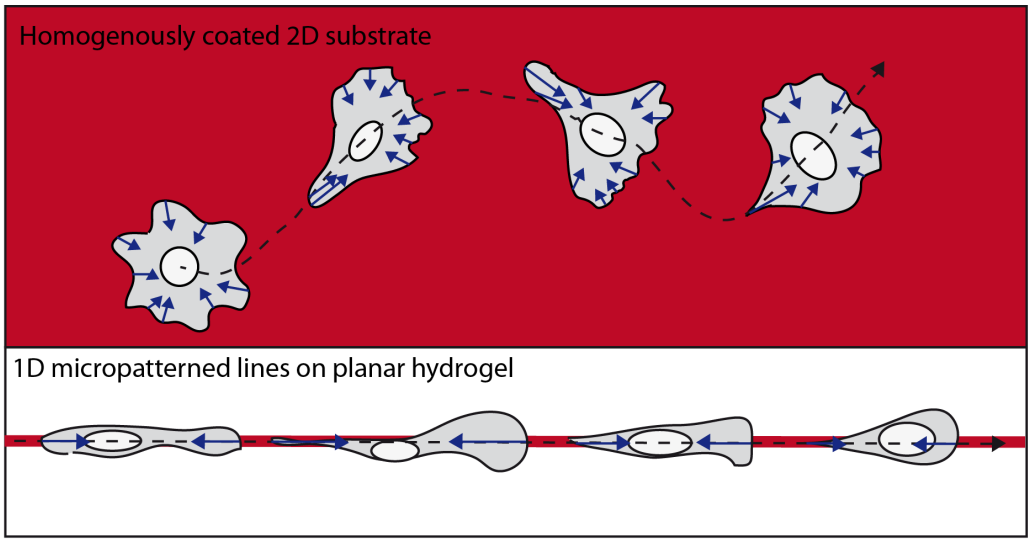

Figure 39: Schematic representation of 2D vs. 1D migration assays. A soft hydrogel can be coated homogenously with fibronectin (red), allowing the cell (grey) to randomly migrate in any direction. The traction forces (blue arrows) are inward directed and mainly located at the cell periphery. Creating a thin line of fibronectin on top of a hydrogel allows the cell to attach. As a consequence, the cell is elongated and restricted in its movement. Besides that, the forces are aligned with the micropattern/migration axis.

3.1.1. Soft micropatterning

In this subchapter, we will focus on the micropatterning technique that we used to produce adhesive fibronectin lines of defined width on top of a soft polyacrylamide hydrogels. Surface patterning allowed us to control and modulate mechanical substrate properties like stiffness (within the physiological range of several kPa) and confinement (line width below 5 μm) to mimic conditions of the physiological microenvironment of cells.

3.1.1.1. Glass technique: printing adhesive lines on soft substrates

The used microfabrication approach was called “glass technique” (Vignaud 2014) and consisted out of two steps: (i) producing micropatterned lines on glass and (ii) transferring the micropattern onto soft polyacrylamide substrates. The experimental procedure is schematically shown in **Figure 40**. First, a cleaned and activated glass coverslip was coated with pLL-PEG. The polymer brush self-assembled due to its positively charged pLL chain that bound to the negative glass surface. The coated coverslip was then transferred onto a commercially available photomask (Toppan). The photomask consisted out of quartz crystal and was patterned with light-impermeable chrome. Upon exposure to deep UV light (190

nm), the polymer brush was locally burned, leaving patterned lines within the pLL-PEG coating. Subsequently, the coverslip was incubated with a fibronectin solution (20 µl/mg) containing fluorescent Alexa546-conjugated fibrinogen (20 µl/mg), which enabled the imaging of the micropatterned areas on top of the hydrogel later on. At this stage, we had created micropatterned lines on a glass coverslip, which then needed to be transferred onto a soft hydrogel. The polyacrylamide solution was sandwiched in between the patterned glass coverslip and a silanized coverslip. In order to perform TFM experiments, fluorescent microbeads were added to the PAA solution. After polymerization, the silanized coverslip was removed with a scalpel, containing the PAA gel with embedded microbeads and patterned fibronectin lines.

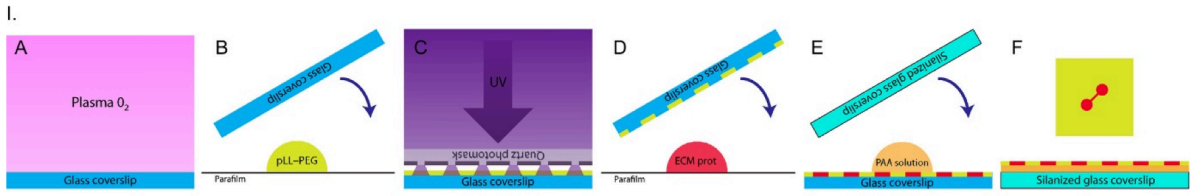

Figure 40: Schematic representation of creating micropatterns on top of soft hydrogels using the glass technique. A) Activation of a glass coverslip with plasma. **B**) Coating the activated glass coverslip with pLL-PEG. **C**) Burning of the polymer brush via local UV exposure through a photomask. **D**) Incubation with ECM protein solution (in our case fibronectin and fibrinogen). E) Polymerization of acrylamide solution in between the patterned glass coverslip and a silanized coverslip. F) After the peal-off, the final result is an adhesive micropattern of defined geometry on top of a soft polyacrylamide gel, which is attached to the silanized glass coverslip. [Figure taken from: (Vignaud 2014)]

The technique had several advantages. Compared to other micropatterning techniques, no chemical cross-linkers were used, which usually challenge the reproducibility of the hydrogels. The procedure was fast (2.5 hours) and allowed us to create patterned lines with submicron resolution in a reproducible manner. Besides that, polyacrylamide was optically transparent and the chemical compounds were available at low cost. It was inert to chemical degradation and prohibited the non-specific attachment of cells outside the micropattern (Vignaud 2014). In addition to that, the mechanical properties could be tuned within a physiologically relevant range (Sabass 2008). By controlling the ratio of monomer cross-linkers, the mesh size of polymerized hydrogel could be varied, which ultimately determined substrate stiffness (Tse 2010). All together, the glass technique enabled us to create, in a reproducible manner, an *in vitro* microenvironment with defined mechanical and chemical properties suitable for cell migration studies.

3.1.1.2. Quantification of relevant migratory parameters

Microscopic imaging of single cells attached to adhesive lines was performed over long periods. We used a homemade Matlab routine, written by our colleague Dr. Irene Wang, to manually extract morphometric parameters (positions of front, rear and nucleus; **Figure 41**). Please note, we computed these morphometric parameters from our own time-lapse brightfield images (one frame every 1 or 5 minutes) and from the cell race data (1 frame every 15 minutes) (Maiuri 2012). Taking the difference in temporal resolution into account, we calculated the migratory parameters as following. We analyzed the time traces by first extracting the center of mass (middle of the front and rear position), smoothed the trajectory by convolution (over a 15 minute time window), and computed the instantaneous velocity and instantaneous speed over a small time window of 30 minutes. Subsequently, the extracted instantaneous values were averaged over the whole cell trajectory. A further discussion of why we chose to analyze cell migration this way can be found in **Chapter 4.1.4**.

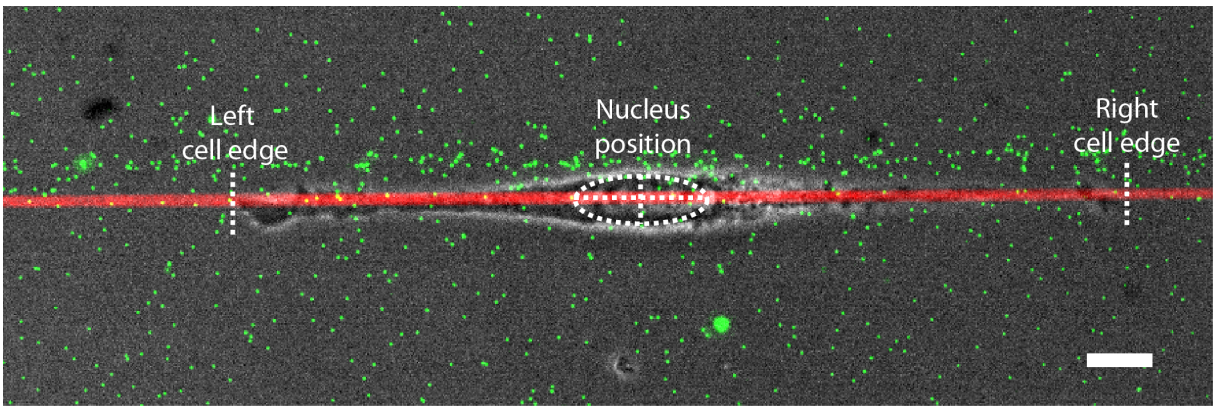

Figure 41: Manual position tracking of single cells attached to 1D adhesive lines. Brightfield image of RPE-1 cell merged with fluorescent images: fibronectin line pattern (stained with Alexa546-conjugated fibrinogen; red) on top of a soft PAA hydrogel with embedded fluorescent beads (green). We tracked the positions of the left and right cell edge (white, dashed lines) and the nucleus (white, dashed circle). (Scale bar: 10 µm)

3.1.2. Quantitative force measurements: Fourier Transform Traction Cytometry

As mentioned before in **Chapter 1.4.3**, numerous techniques exist to quantify cellular traction forces at the subcellular scale. In this section, we will explain the used 2D TFM technique, termed Fourier transform traction cytometry (FTTC), which was implemented in our laboratory a few years ago. Our homemade algorithm (written by Dr. Irene Wang) was

computationally inexpensive and allowed the rapid analysis of dynamic force modulations. We will describe our quantitative force imaging technique in three steps: (i) the TFM experiment and subsequent image analysis to extract the displacement field, (ii) the computational approach to calculate the force field and (iii) the multipolar analysis to extract relevant force parameters.

3.1.2.1. Step 1: Displacement field analysis

The resolution of TFM critically depends on the displacement field analysis. Small errors in the displacement field analysis can lead to big errors in the force calculation (Polacheck 2016). In addition to that, deformations can be in the range of nm to μm depending on the substrate stiffness and contractile activity of the cell (Sabass 2008). In order to capture these small displacements, we needed a suitable experimental set-up and computational method.

We employed a standard inverted epifluorescence microscope (Nikon Eclipse Ti) coupled with Zyla sCMOS camera (Andor), which allowed imaging at high spatio-temporal resolution. To control the microscope, we utilized the software iQ3 from Andor. The focus plane for bead imaging was just below the uppermost layer of the hydrogel. Time-lapse imaging of the stressed gel (fluorescent tracers in far red) and the cell (brightfield channel) were performed (1 frame per minute or faster). After the experiment, cells were detached using trypsin, and the relaxed bead image was taken (Tseng 2011).

The displacement and force field analysis was performed in Matlab. Various strategies exist that either track the displacement of individual beads or multiple beads within a certain area. In order to combine robustness and spatial resolution, we combined both approaches, particle image velocimetry (PIV) and single particle tracking (SPT) (Tseng 2011, K. W. Mandal 2014).

First, a global drift correction was achieved via a global cross-correlation of the stressed and relaxed bead images. The translation was determined by the position of the peak value in the correlation image and subsequently corrected, while the bead images were resized to possess the same dimension. Once corrected, the tracked bead displacements were only due to deformations of the gel, induced by the cell.

Subsequently, PIV analysis was performed. The stressed and relaxed bead images were subdivided into smaller interrogation windows, which could overlap to a certain extend to avoid missing beads at the boundaries. The maximum of the cross-correlation of each corresponding window determined the mean displacement in each PIV window. Afterwards, the relaxed bead image was shifted by the amount of the computed mean displacement. During the subsequent SPT analysis, ambiguity between neighboring beads was therefore eliminated, as large displacements were already corrected. The final displacement field was then interpolated on a regular grid. This two-step procedure (**Figure 42**) enabled us to compute the displacement field with high spatial resolution (Tseng 2011, K. W. Mandal 2014).

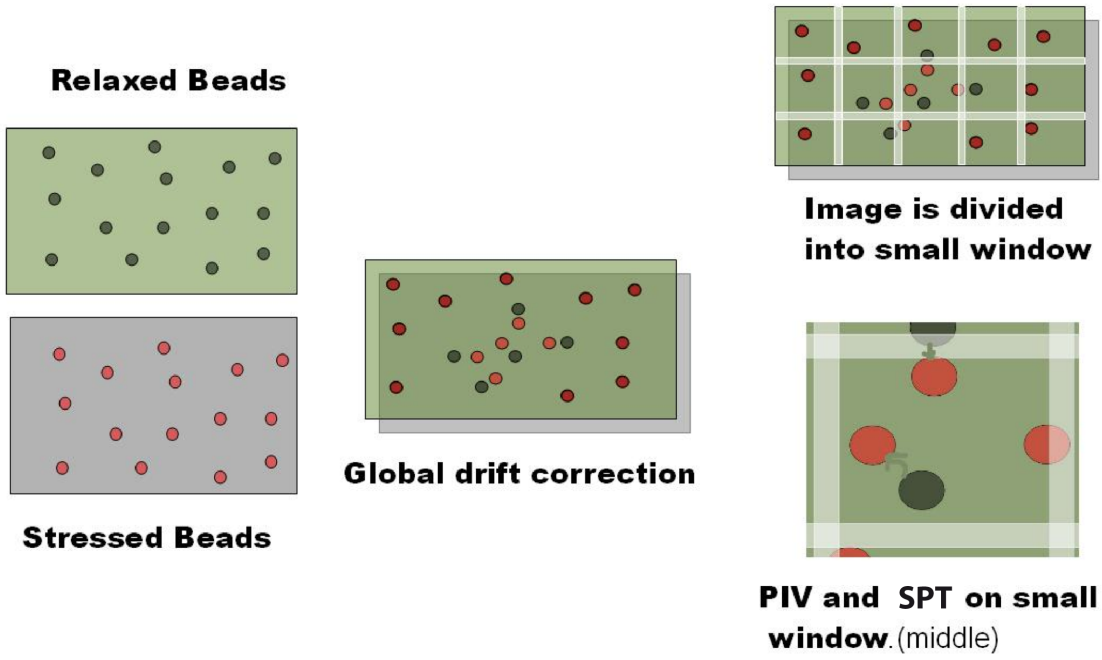

Figure 42: Schematic representation of the displacement field analysis. First, the experimental drift is corrected via a global auto correlation. Afterwards, the images were divided into smaller interrogation window, on which PIV and afterwards SPT was performed. [Figure taken from: (K. Mandal 2012)]

3.1.2.2. Step 2: Force field analysis

The final step of our 2D TFM analysis was to compute cellular tractions from the deformation of the continuous soft substrate. The elastic behavior of polyacrylamide is

homogenous, isotropic and linear. The mathematical problem is defined as the following convolution (Butler 2002, Sabass 2008, Martiel 2015):

$$\boldsymbol{u}_i(\boldsymbol{x}) = \int \sum_n \boldsymbol{G}_{ij}\,(\boldsymbol{x}-\boldsymbol{x}')\,\boldsymbol{f}_j(\boldsymbol{x}')d\boldsymbol{x}' \tag{3.1}$$

This equation describes the linear relation between displacement $\boldsymbol{u}(\boldsymbol{x})$ and the traction field $\boldsymbol{f}(\boldsymbol{x})$, where $\boldsymbol{x} = (x_1, x_2)$ (as normal displacements, and hence tractions, are neglected). As the substrate is approximated as an elastic half space, we can use the Boussinesq Green function ***G***, which describes the mechanical gel properties (Martiel 2015):

$$\boldsymbol{G}(\boldsymbol{x}) = \frac{(1+v)}{\pi E r^3}\begin{pmatrix}(1-v)\,r^2 + vx^2 & vxy \\ vxy & (1-v)\,r^2 + vx^2\end{pmatrix} \tag{3.2}$$

with $r = |\mathbf{x}|$ as the distance from the force application point, E the Young modulus (a measure of the material stiffness), and v the Poisson ratio (an elastic parameter describing the substrate deformability) of the hydrogel.

To calculate the traction field **f**(**x**) from the displacement field $\boldsymbol{u}(\boldsymbol{x})$, the convolution needs to be inverted, which is in general computationally expensive as ***G*** is not diagonal in real space. This problem however does not arise in Fourier space. We therefore employed the FTTC method, originally proposed by Butler et al. (Butler 2002). In frequency space, the convolution becomes a simple product, and the Green tensor becomes diagonal:

$$\tilde{u}(k) = \tilde{G}(k) * \tilde{f}(k) \tag{3.3}$$

As a consequence, FTTC computation was easy and less time consuming, as:

$$\tilde{f}(k) = \tilde{G}^{-1}(k) * \tilde{u}(k) \tag{3.4}$$

with

$$\tilde{G}_{ijk} = \frac{2\,(1+v)}{Yk^3}\begin{bmatrix}(1-v)k^2 + vk_y^2 & vk_xk_y \\ vk_xk_y & (1-v)k^2 + vk_y^2\end{bmatrix} \tag{3.5}$$

.

Afterwards, the displacement field, which was before interpolated on a regular grid, was calculated in Fourier space. Now the force field could be calculated in Fourier space by multiplying the displacement field (at each *k* value) with the inverse of G. We imposed a 0^{th} order regularization parameter to the Fourier transform equation (Sabass 2008). Finally, the calculated force field was transformed into real space.

To sum up, we used a home made Matlab script to compute the traction force field of a single cell by first tracking and determining the displacement field of fluorescent beads using PIV and SPT. Subsequently we computed the force field by employing FTTC on a regular grid in Fourier space. From this, the stress map, hence the distribution of cellular forces over the whole cell area could be displayed (**Figure 43**).

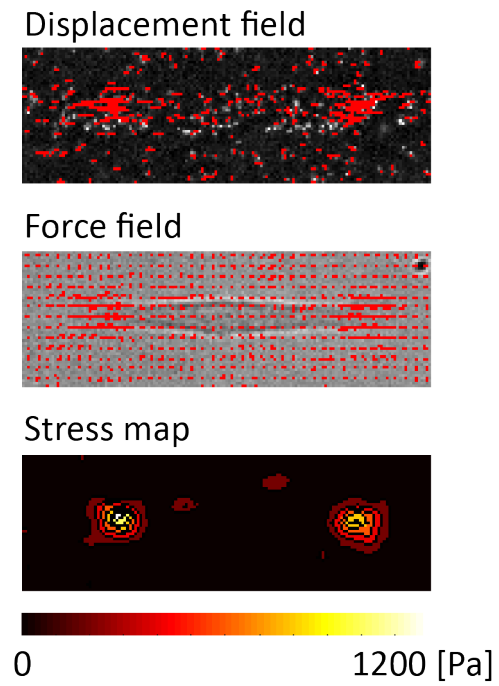

Figure 43: Home-made algorithm based on FTTC allows to extract cellular forces from substrate deformations. First, the bead displacement (red arrows) is computed. From that, the cellular force field (on a regular grid) as well as the stress map can be calculated.

3.1.2.3. Step 3: Quantifying force parameters in 1D

The purpose behind TFM was to follow the force evolution of a migrating cell. In order to do so, the strength of the mechanical interaction between the cell and the substrate was computed. A mask (corresponding to the outline of the cell) was applied to

compute force parameters. To access the total force, the magnitude of every point force was summed up over the whole cell:

$$F_{tot} = \int_{cell} \|\boldsymbol{T}(\boldsymbol{r})\| \, d^2\boldsymbol{r} \tag{3.6}$$

with ***T*** as the traction stress.

According to Newton's law of motion, the sum of all vector forces cancels out at the cell level, as the acceleration of the cell is negligible (Tanimoto 2014). Due to this, the characterization of spatial stress profile, which extended beyond the summation of the point forces, was crucial. A multipolar analysis was performed to define the spatio-temporal dynamics of traction stresses. The force asymmetry factor was computed as following.

First, the stress profile (presented before in **figure 43**) was dissected depending on the orientation of forces (inward directed forces in (+) and (-) direction with respect to the micropatterned line). Then the stress map was projected in one-dimension, by reducing the traction to the sum of the projected T_x along the micropattern axis ($T_{1D}(x)$). Then, the 2nd order moment of each pole (D+ and D-), which represented the spatial extend of each force compartment, was computed:

$$D+ = \sqrt{\frac{\int_{T1D>0}(x-x_{G+})^2 T_{1D}(x)dx}{\int_{T1D>0} T_{1D}(x)dx}} \; ; \; D- = \sqrt{\frac{\int_{T1D<0}(x-x_{G-})^2 \, |T_{1D}(x)|dx}{\int_{T1D<0} |T_{1D}(x)|dx}} \tag{3.7}$$

(3.8)

with G+ and G- being defined as the center of (+) and (–)-oriented tractions:

$$G+ = \sqrt{\frac{\int_{T1D>0} x T_{1D}(x)dx}{\int_{T1D>0} T_{1D}(x)dx}} \; ; \; G- = \sqrt{\frac{\int_{T1D<0} x|T_{1D}(x)|dx}{\int_{T1D<0} |T_{1D}(x)|dx}} \tag{3.9}$$

(3.10)

Finally, the normalized ratio $\frac{D--D+}{D-+D+}$ (equivalent to the force quadrupole) was defined as the force asymmetry parameter (**Figure 44**).

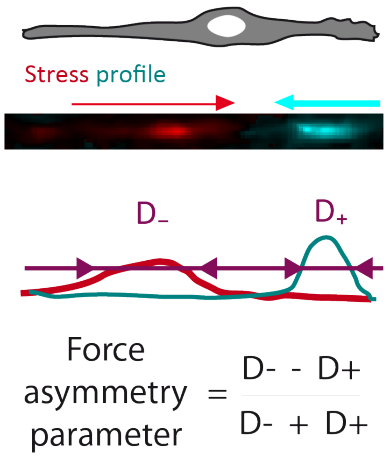

Figure 44: Schematic representation of analyzing the force asymmetry of a single cell. The adherent cell applies a stress to its substrate, which is located at each cell edge and only varies in its direction (color-coded stress map and arrows: red: (+)-directed forces; blue: (-)-minus directed forces). The 1D projection of the stress profile gives access to the spatial distribution of each force pole. The normalized ratio of the spatial extend of each force compartment defines a force asymmetry factor.

3.2. Dynamic perturbation of cell mechanics

Chapter 3.1 explained both techniques, micropatterning and TFM, which were combined in order to create a 1D migration assay and to extract morphometric and mechanical parameters during single cell migration. The assay was further compatible with other methods used to perturb cell mechanics: pharmacological treatments and optogenetics. The next subchapters will describe the general effect of used inhibiting drugs and the optogenetic probe. The obtained findings, hence to cellular response to the interference with cell contractility and adhesiveness, will be presented in **Chapter 4 Results**.

3.2.1.1. Pharmacological treatments

Small molecular inhibitors can penetrate the cell and directly interfere with specific signaling cascades. Usually, the effect is reversible when the drug is washed-out. Two inhibitors, which block the activity of specific intracellular signaling proteins, were used to identify and validate molecular key players of cell migration: blebbistatin and pF573,228.

As discussed previously, myosin II is a non-muscle motor protein responsible for generating contractility in interplay with the actin-cytoskeleton. Blebbistatin is a commonly

used drug possessing high affinity and selectivity for myosin II. It blocks the ATPase activity of myosin II by binding to the myosin-ADP-P_i complex and interfering with the phosphate release. As a consequence, myosin heads are blocked in a low affinity state towards actin. It therefore remains in its actin-detached state, which ultimately interferes with acto-myosin driven cell motility (Kovács 2004, Limouze 2004). The cellular response to blebbistatin is highly concentration dependent. The drug is used within the μM-range, presenting a hyperbolic decrease in ATPase activity with increased inhibitor concentration and possessing a half-maximal inhibition at ~2 μM (Straight 2003). Due to its specificity, blebbistatin was our drug of choice to investigate how contractile forces drive cell migration. Cells were treated with a low working concentration (3 μM) in order to decrease (but not fully block) acto-myosin contractility.

On the other hand, cells were treated with a different drug to interfere with cell adhesiveness. Focal adhesion kinase (FAK) is a cytoplasmic tyrosine kinase involved in integrin signaling during cell migration. Integrin clustering stimulates FAK phosphorylation, which further phosphorylates downstream signaling molecules involved in adhesion disassembly (Mabeta 2016). In order to target cell adhesion dynamics, we utilized the FAK inhibitor pF573,228. The inhibitor blocks the phosphorylation of FAK by binding to its ATP-binding pocket. The blocked enzymatic activity of FAK reduces the phosphorylation of its downstream effector paxillin, which inhibits adhesion turnover (Slack-Davis 2007).

Though blebbistatin and pF572,228 are inhibitors with high target specificity, contractility and adhesiveness are bi-directionally coupled through feedback loops. Therefore, using pharmacological approaches did not allow us to decouple the effect of interfering with either of the two factors separately. We rather aimed at perturbing the balance between adhesiveness and contractility with our pharmacological interference strategy.

3.2.1.2. Optogenetics

We employed an optogenetic system developed by Dr. Leo Valon during his PhD thesis in the group of Dr. Mathieu Coppey at the Curie Institute in Paris. We chose his particular probe as it has been shown to enable the optogenetic up-regulation of cellular forces by controlling the localization of an upstream regulator for RhoA with blue light.

Valon et al. demonstrated a relative increase of cellular traction forces of up to 50% in MDCK cells, which expressed the optogenetic probe. Photostimulation could be performed over long time periods, while contractility and relaxation cycles could be alternated, which triggered a mechanical cellular response that was highly reproducible (Valon 2014).

The optogenetic system was based on two genetically encoded dimerization partners: membrane-anchored CIBN and light-sensitive Cry2. Protein-protein dimerization could be induced with blue light and did not require any exogenous ligands. The system possessed high temporal and spatial resolution at the subsecond and submicron scale, respectively (Kennedy 2010). Valon's optogenetic probe allowed to locally and dynamically activate RhoA, our protein of interest. It was based on controlling an upstream regulator of RhoA, instead of RhoA itself. This approach had the advantage that changes in the mechanical activity of the cell were due to an endogenous level of RhoA, hence placing the system close to its physiological mechanical state.

Our optogenetic cell line of NIH3T3 fibroblasts expressed the catalytic domain of a RhoA-specific GEF (DHPH domain of ARHGEF11), which was fused to light-sensitive Cry2 and the fluorophore mCherry (further referred to as optoGEF-RhoA). CIBN was localized at the cell membrane by a CAAX domain and was fluorescently labeled with GFP. Upon blue light stimulation, optoGEF-RhoA translocated from the cytoplasm to the membrane, where it specifically activated RhoA (**Figure 45**) (Valon 2017).

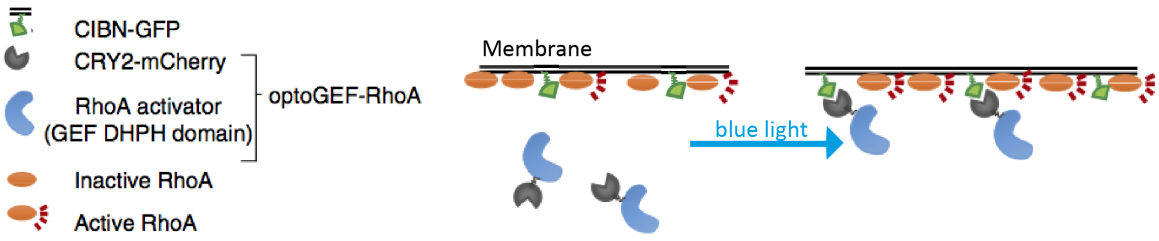

Figure 45: Optogenetics allows the dynamic activation of RhoA. The optogenetic probe was based on the Cry2-CIBN and allowed the dynamic activation of RhoA through its upstream regulator ArhGEF11 (RhoA activator). [Figure adapted from: (Valon 2017)]

As discussed in the introduction chapters, RhoA is known to be a main regulator of cell contractility in the tail of a moving cell. We reasoned that its anisotropic distribution could be artificially triggered by locally activating the optogenetic system. The created

gradient of RhoA activity within the cell was intended to mimic intrinsic symmetry breaking and trigger the movement of the cell away from the photoactivation region (**Figure 46**).

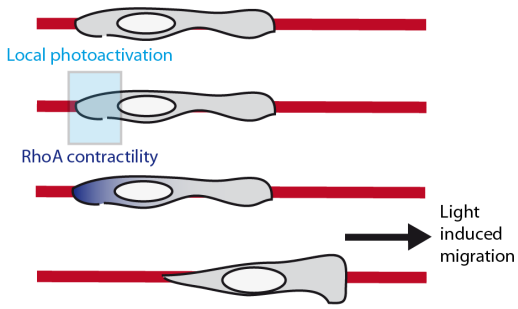

Figure 46: Working hypothesis: triggering spontaneous symmetry breaking using optogenetics. The local photoactivation of optoGEF-RhoA should induce a local increase in cell contractility. This should further allow us to control the formation of the rear and hence trigger migration away from the photoactivation area.

4. Results

The first part of this results chapter is dedicated to our scientific publication (Hennig et al. "Stick-slip dynamics of cell adhesion triggers spontaneous symmetry breaking and directional migration"), which is currently in submission at *Science Advances*. The preprint was uploaded to the online server Biorxiv and can be found under the following link: https://www.biorxiv.org/content/early/2018/06/25/354696. The second part will be dedicated to a fruitful collaboration with Dr. Nils Gauthier and Dr. Pascale Monzo (IFOM, Milan, Italy), which aimed at studying invasive properties of cancer cells (Their publication, which is currently in preparation, will be referred to as (Monzo 2018 unpublished)).

4.1. Study 1) Hennig et al. "Stick-slip dynamics of cell adhesion triggers spontaneous symmetry breaking and directional migration"

4.1.1. Introduction

Over the last few decades, research in the field of cell migration has led to enormous advances in understanding its complex nature. Key discoveries identified the spatio-temporal regulation of the migratory machinery and the establishment of a front-rear polarity as the fundamental basis of cell movement (Ridley 2003), with actin cytoskeleton as the key player in the process (Wehrle-Haller 2003). Intriguingly, actin-polymerization is known to push cellular leading edge forward, while acto-myosin contractility triggers the retraction of the rear. This implies a crucial role of cellular traction forces in controlling cell movement, however the temporal axis of cytoskeleton force induction during spontaneous symmetry breaking remains elusive (Cramer 2010).

Importantly, to date, the vast majority of quantitative studies examining the force-motion relation has been performed under static conditions and are thus limiting as actin dynamics occur on minute scales (Blanchoin 2014). In fact, only few studies investigated the evolution of traction force development during migration in a time-resolved manner (Han 2016, Leal-Egaña 2017, Jiang 2015), but without addressing the spatio-temporal evolution of cellular forces during spontaneous symmetry breaking. At the cellular scale, traction forces

between the cell and the substrate must be balanced, resulting in a force dipole for both stationary and migrating cells (K. W. Mandal 2014). Hence, a complete understanding of breaking force symmetry requires going beyond total magnitude and dipolar moment measurements by using multipolar analysis coupled to real-time morphometric quantification (Tanimoto 2014).

We thus developed a single cell, one-dimensional migration assay based on real-time force measurements, quantitative microscopy, and soft micropatterning. This bottom-up approach mimicked complex *in vivo* fibrillar migration (A. D. Doyle 2009) and was used to simultaneously quantify mechanical and morphological parameters during spontaneous symmetry breaking. Our multipolar analysis showed that spontaneous symmetry breaking was triggered by coupled dynamics of the acto-myosin generated contractility and cell-substrate adhesion strength. More precisely, cell migration could be trigger by a force-mediated detachment of adhesions in the rear of the cell, which could occur in absence of any pre-established cytoskeleton polarity. A theoretical model based on the experimentally observed stick-slip motion recapitulated this scenario and demonstrated an inverse relation between cell length and migration speed. Indeed, we validated this relation by analyzing single cell trajectories of various cell types that possessed distinct migratory behaviors, which confirmed the robustness of the proposed stick-slip behavior.

4.1.2. Scientific article

Title: "Stick-slip dynamics of cell adhesion triggers spontaneous symmetry breaking and directional migration"

One sentence summary: Cells can autonomously break their symmetry through traction force oscillations (mechanical instabilities) that lead to stochastic detachment of adhesion patches on one side of the cell and the subsequent initiation of migration.

Authors: Hennig K.[1], Wang I.[1], Moreau P.[1], Valon L.[2], DeBeco S.[3], Coppey M.[3], Miroshnikova, Y. A.[4], Albiges-Rizo, C.[4], Favard C.[5], Voituriez R.[6]*, Balland M.[1]*

Affiliation:

[1] *Laboratoire Interdisciplinaire de Physique, Grenoble Alpes University, Saint Martin d Heres, France*

[2] *Institut Pasteur, Department of Developmental and Stem Cell Biology, 25 rue du Dr. Roux, 75015 Paris, France*

[3] *Laboratoire Physico-Chimie, Institut Curie, Centre National de la Recherche Scientifique UMR168*

[4] *DYSAD, Institut for Advanced Biosciences (IAB), Centre de Recherche UGA / Inserm U 1209 / CNRS UMR 5309, France*

[5] *Membrane Domains and Viral Assembly, IRIM, UMR9004 CNRS/Université de Montpellier, 1919, route de Mende, 34293 Montpellier Cedex.*

[6] *Laboratoire de Physique Théorique de la Matière Condensée, Universite Pierre et Marie Curie, Tour 13-12, 5eme etage, 4 place Jussieu, 75252 PARIS Cedex 05, France*

* Corresponding authors:

Martial Balland, martial.balland@univ-grenoble-alpes.fr

ORCID #: orcid.org/0000-0002-6585-9735

Mailing address: Laboratoire Interdisciplinaire de Physique, UMR 5588 , 140 avenue de la physique 38402 Saint Martin d Heres, France

Raphaël Voituriez, voituriez@lptmc.jussieu.fr

Mailing address : Laboratoire de Physique Théorique de la Matière Condensée, Universite Pierre et Marie Curie, Tour 13-12, 5eme etage, 4 place Jussieu, 75252 PARIS Cedex 05, France

Abstract:

Directional cell motility during organism and tissue development, homeostasis and disease requires symmetry breaking. This process relies on the ability of single cells to establish a front-rear polarity, and can occur in absence of external cues. The initiation of migration has been attributed to the spontaneous polarization of cytoskeleton components, while the spatio-temporal evolution of cytoskeletal forces arising from continuous mechanical cell-substrate interaction has yet to be resolved. Here, we establish a one-dimensional microfabricated migration assay that mimics complex *in vivo* fibrillar environment while being compatible with high-resolution force measurements, quantitative microscopy, and optogenetics. Quantification of morphometric and mechanical parameters reveals a generic stick-slip behavior initiated by contractility-dependent stochastic detachment of adhesive contacts at one side of the cell, which is sufficient to drive directional cell motility in absence of pre-established cytoskeleton polarity or morphogen gradients. A theoretical model validates the crucial role of adhesion dynamics during spontaneous symmetry breaking, proposing that the examined phenomenon can emerge independently of a complex self-polarizing system.

Main text:

Directional motility is a plastic process*(* 1 *)* that is the fundamental basis of key biological processes in eukaryotes, such as embryonic morphogenesis, leukocyte trafficking in immune surveillance, and tissue regeneration and repair *(* 2*,* 3*,* 4*)*. Furthermore, aberrations in signaling pathways regulating cell migration contribute to

tumor invasion *(5)* and metastasis *(6).* Over the last decades, two main modes of migration have been identified: adhesion-dependent mesenchymal *(7)* and adhesion-independent amoeboid migration *(8).* These migration modes differ in the way forces are generated and transduced within the cell. Importantly however, the breaking of cell symmetry is a fundamental process at the basis of any migration event (9, 10 *).*

In the absence of external polarity cues, several mechanisms of spontaneous symmetry breaking have been proposed and are based on polarization of cytoskeleton components *(* 11). For instance, gradients or patterns of morphogens can arise due to specific reaction-diffusion patterns within the cell, leading to its polarization *(12).* More recently, several mechanisms of spontaneous symmetry breaking of the actin myosin system itself have been proposed, based either on actin polymerization *(* 13, 14 *)* or acto-myosin contractility *(* 15, 16, 17 *).* However, relating such symmetry breaking events of the various components of the cellular cytoskeleton to both cell-substrate forces and cell locomotion remains largely unexplored.

In the specific case of mesenchymal migration, the spatio-temporal sequence of mechanical symmetry breaking remains controversial. Different models are distinguished by the temporal order in which distinct cytoskeleton forces are activated to trigger directional movement *(* 18 *).* Most studies emphasize force generation due to actin polymerization in the cell front as a first step to initiate migration *(* 3, 19 *).* On the contrary, acto-myosin II-mediated contractility within the cell rear has been identified as a first step to break cell symmetry in keratocytes *(20).* Thus,

determining the spatio-temporal dynamics of cellular forces and morphological events at the initiation of a migration is still an open and major question in biology.

To investigate quantitatively the dynamics of spontaneous symmetry breaking events in cells at the level of both morphological parameters and distribution of interaction forces with the environment, we developed a one-dimensional migration assay (**Fig. 1A)** that combined time-resolved traction force microscopy (TFM) *(* 21*,* 22*,* 23 *)* and soft micro patterning *(* 24 *)* (Materials and methods can be found in supplementary materials).

Using this bottom-up approach, we followed single epithelial cells (hTERT-immortalized retinal pigment epithelial cell line [RPE1]) during the initiation of spontaneous migration and extracted morphometric and mechanical parameters. As expected *(* 25*,* 26 *)*, RPE1 cells plated on patterned 40kPa polyacrylamide hydrogels adhered to one-dimensional fibronectin lines (2 or 5 μm width) within 1-2 hours. The cells displayed elongated shapes with long actin fibers oriented parallel to the micropattern and cell axis (**Fig. 1B**).

In the absence of any external cue, we observed a biphasic motile behavior: symmetric elongation of a static cell (spreading phase) prior to spontaneously initiated directional movement (migration phase) (**Fig. 1C**). In parallel, tangential stress measurements revealed defined stress compartments at both cell edges due to contractile forces oriented towards the center of the cells (**Fig. 1D**). Hence, cells behaved as force dipoles, as described previously *(* 14*,* 27*,* 28*,* 29 *).* During the spreading phase, both cell elongation dynamics and force distribution patterns were fully symmetric with respect to the cell center of mass. At the onset of motility,

morphological polarization and simultaneous asymmetrical redistribution of forces occurred, characterized by a single defined local stress compartment at the cell front and a significantly widened stress distribution with lower traction stress at the rear (**Fig. 1D**). This was accompanied by rapid retraction of the cell rear (**Fig. 1D**).

Current models emphasize the formation of a distinct cell front as the first event when cell migration is initiated *(* 10*,* 30 *).* In contrast, we observed that cell spreading was qualitatively symmetric on both sides and that symmetry breaking occurred with the sudden retraction of the rear. This led us to hypothesize that contractility builds up in a non-polarized cell, resulting in a local stress increase at both extremities.

To challenge the hypothesis that symmetry breaking does not require pre-established rear-front polarity as previously thought *(* 31*,* 20 *),* we quantified the coordination between mechanical polarization and morphological events. To first confirm the qualitative observation of anisotropic redistribution of traction forces, we adapted multipole analyses, classically used in the field of micro-swimmers*(* 32 *),* to quantify the asymmetry of the force distribution. We first projected the stress profile along the micropattern axis to obtain a 1D stress profile, a mechanical footprint of the cell. From that, we computed the variance of (+)- and (-)-directed traction stress profiles (D+, D-), which quantified the spatial distribution of each stress compartment at opposite poles of the cell. The normalized ratio, (D+ - D-)/(D+ + D-), (analogous to the normalized quadrupole) quantifies the symmetry of the spatial stress distribution and will be referred to as force asymmetry parameter (**Fig. 2A**).

Non-migrating cells exhibited a force asymmetry parameter fluctuating around zero, indicating a non-polarized static phase (**Fig. 2A**). Consistently, fluctuations in the

actin profiles were also observed in static phases (**Fig. S1**). Importantly, no significant polarization of actin distribution was observed prior to migration initiation. Nevertheless, upon initiation of each migration step, the force asymmetry parameter displayed a sharp transient peak. This sudden increase corresponded to a widening of the spatial stress distribution in the rear of the cell while the stress pattern at the cell front remained localized to the cell edge. This asymmetry subsequently relaxed leading to another static phase. Several iterations of such phases were typically observed. Consistently, we found larger values in the amplitude of the asymmetry parameter in moving phases in comparison to the static ones for multiple analyzed cells. Thus, initiation of migration is characterized by a sharp increase of the force asymmetry parameter and can occur in absence of prior polarization of the actin cytoskeleton.

We subsequently hypothesized that stress builds up and fluctuates during the spreading phase until one end randomly detaches producing a cell rear. This hypothesis was supported by the evolution of the total traction force, a measure of the strength of the mechanical interaction of the cell with the substrate, quantified via TFM. We observed that, in static phases, cell spreading was associated with an increase of the total traction force. Upon the initiation of migration, the force level dropped approximately by 50% (**Fig. S2**). Strikingly, this decrease in mechanical interaction was directly correlated with a shortening in cell length due to the sudden retraction of the rear (**Fig. 2B, Fig. S3**). To confirm the role of adhesion detachment, we fluorescently labeled cell-substrate anchor points using vinculin-eGFP to follow the time evolution of adhesion patches during migration. Adhesion sites at the front of the cell were continuously contacting the substrate while adhesion sites at the rear

followed two distinct phases: attachment (cluster growth) and switching abruptly to detachment (disassembly and sliding of smaller adhesion patches) (Fig. 2C). Cell morphology and its polarity features showed similar behavior as after the initial symmetric spreading phase, abrupt retraction of the rear triggered subsequent nuclear translocation**.** Furthermore, throughout the migration cycle the trailing edge displayed two distinct phases of motion, while the front continuously moved forward (**Fig. 2C**). This destabilization of the trailing edge demonstrated the critical role of adhesion detachment in the back of the cell. The observed discontinuous migration is known in physics as a stick-slip mechanism (**Fig. 2D).** During the initial spreading phase, cells elongated symmetrically while increasing their contractile stress (stick). Upon reaching a level of stress that adhesion complexes could no longer sustain, adhesions on one cell edge stochastically detached from the substrate. This led to cell shortening due to retraction of the rear and a decrease in cell-substrate interaction (slip). Recovery of the initial cell length and contractility level occurred during the subsequent stick phase. As a consequence of this stick slip migration, the propensity of cells to enter migratory phases appeared to crucially depend on (i) contractility and (ii) adhesion properties.

In order to substantiate this observed stochastic stick-slip behavior, we devised a physical model based on minimal ingredients. The actin cytoskeleton was described as an active, homogeneous 1D viscoelastic gel *(* 33 *).* We assumed that the cell's cytoskeleton was fully unpolarized, and that the cell body could be mechanically characterized by an effective stiffness *k*. This elastic behavior encompasses active (i.e. due to motor activity) and passive contributions of both cytoskeleton and membrane. Adhesion sites were described in the framework of the active gel theory

as localized regions at both cell extremities carrying outward pointing actin polarity ***p***, and subjected to an active force $\boldsymbol{F_a}=\chi\,\boldsymbol{p}$, where χ is a phenomenological coupling constant, which induced cell expansion. The key ingredient of the model relies on the dynamics of adhesion sites, which was written phenomenologically as $\dot{p} = g(v_p) - \lambda p$. Here λ models the rate of actin turnover, and *g* the dynamics of adhesion sites assembly that depends on the local velocity $v_p = v \cdot u_p$ over the substrate. Importantly, *g* is a priori very asymmetric (**Fig. 2E**). This accounts for the fact that adhesion assembly is drastically reduced upon edge retraction, and mildly affected by edge expansion. The analysis of the model revealed that the actin turnover rate critically controls the dynamics. In particular at slow turnover rate (as defined in SI), the system was found to display a stochastic stick-slip behavior, (which notably differs from classical stick-slip behaviors characterized by deterministic oscillations). Cells were predicted to slowly expand and reach the fixed point of the dynamics where any fluctuation leading to infinitesimal retraction is unstable: one end of the cell therefore retracts before spreading symmetrically again. Finally, the model successfully predicts that it is critically controlled by adhesion turnover rate λ and maximal contractile force, as summarized in the phase diagram of **Fig. 2F**, and reproduces the observed stochastic stick-slip dynamics (**Fig. 2G**).

To challenge the proposed stochastic stick-slip mechanism, we used optogenetics to disrupt its predicted spatio-temporal sequence. We used NIH3T3 cells stably expressing a Cry2-CIBN optogenetic probe to dynamically control the localization of ArhGEF11, an upstream regulator of the master regulator of cell rear retraction, RhoA (from now on referred to as optoGEF-RhoA) *(34)*. Upon stimulation with blue light, optoGEF-RhoA dimerizes with the CAAX-anchored protein CIBN, leading to its

immediate translocation from the cytoplasm to the membrane where it activates RhoA, triggering asymmetric recruitment of actin and subsequent cell migration away from the photo-activation spot. The initiated movement was characterized by a distinct front-rear polarity that was maintained throughout the whole stimulation cycle. Interestingly, by switching the side of stimulation, actin polarity and direction of movement were inverted (**Fig. 3A**).

This optogenetic approach combined with quantitative force measurements revealed a RhoA-mediated instantaneous and local increase of traction forces in the zone of activation. This transient and spatially confined force increase was followed by a global decrease of the mechanical interaction of the moving cell with its substrate, as seen on the total traction force (**Fig. 3B**). This drop was similar to the one observed during spontaneous migration (**Fig. 2C**), which was attributed to adhesion detachment at the cell rear. To confirm that the same process was at play here we imaged adhesions by transiently transfecting vin-iRFP. Upon light-induced RhoA activation, we observed first reinforcement, then detachment and sliding of adhesions (**Fig. 3C**). Indeed, as acto-myosin contractility was stimulated, adhesions were submitted to an increasing level of stress that first led to vinculin recruitment (positive feedback) *(* 35 *),* but ultimately caused the adhesion to dissociate. Hence, local stimulation artificially created the cell rear, triggering the first steps of cell translocation (adhesion detachment) as in the case of spontaneous migration.

A key prediction of the stick-slip model is that spontaneous symmetry breaking strongly depends on contractility and adhesiveness. To challenge this prediction and to further investigate the stick-slip migration mechanism illustrated in **Fig. 2**, we systematically analyzed the main parameters of our theoretical model (cell length,

adhesion size, and total traction forces) and correlated them with the migratory behavior of single cells of two distinct cell types exhibiting different migratory behavior. The instantaneous speed of the cell centroid averaged over the whole cell trajectory was used as a parameter to represent the migration capacity of single cells. To test the broader applicability of the model, fast-migrating RPE1 *(36)* cells were compared to fibroblast cells (NIH3T3) that exhibit slow mesenchymal migration *(37).*

RPE1 cells exhibited a higher speed compared to NIH3T3 that mostly remained in a static spreading phase with less frequent retraction phases. Comparing cell morphology and traction force level of both cell types, we observed that NIH3T3 cells exhibited a longer spreading length associated with a larger mechanical interaction of the cells with their microenvironment (**Fig. 4A**). This result may appear counter-intuitive as larger traction forces should facilitate detachment of adhesions and thus cellular movement. However, in the classical catch-bond model, an increase of force would also induce a stabilization and reinforcement of adhesion sites *(38).* Consistent with this, NIH3T3 cells had larger adhesion patches compared to RPE1 cells.

To analyze adhesion strength in more detail, we quantified adhesion dynamics in both cell types. First, total internal reflection fluorescence microscopy (TIRF) of vin-eGFP adhesions revealed faster adhesion turnover in RPE1 cells compared to NIH3T3 fibroblasts (**Movie S1**). Fluorescence recovery after photobleaching (FRAP) experiments over single adhesion patches localized at the cell edges of each cell type revealed two time components: a fast one that was related to the diffusion of vinculin molecules within the cytosol and a slow one corresponding to the residence time of immobilized vinculin within the adhesion sites (**Fig. 4B**). The measured slow

and fast component ratios revealed that RPE1 cells displayed a lower fraction of bound vinculin compared to NIH3T3. Since vinculin binding promotes adhesion stability, our data indicated that RPE1 cells exhibited more labile adhesions, while NIH3T3 adhesions were expected to sustain higher tension without breaking. These findings are in agreement with the stick-slip model since faster RPE1 cells would undergo fast spreading/retraction cycles (large λ), while less motile NIH3T3 relaxed more slowly to the unstable fixed point (small λ). Therefore, the migratory behavior of these two cell types could be explained, in the framework of a stick-slip model, by cells having different levels of adhesiveness and contractility.

To further confirm the validity of this model, we used pharmacological treatments to perturb the balance between adhesiveness and contractility. We used a low dose of blebbistatin (3µM) to decrease contractility *(39)* in NIH3T3 fibroblasts and 1µM pF573,228 to stabilize adhesions *(40)* in RPE1 cells. As both parameters (contractility and adhesion strength) are bi-directionally coupled through positive feedback loops *(38, 41, 42)*, one could not be modulated without affecting the other. Blebbistatin-treated NIH3T3 cells were able to initiate migration more readily, as shown by the increase of their migration speed (**Fig. 4C**). They exhibited a decrease of total traction force as expected, but also a shortening of the average cell length, which suggested that these cells can more easily detach their adhesions. Indeed, the size of adhesion patches decreased significantly upon blebbistatin treatment (**Fig. 4C**). Hence, by inhibiting contractility, cell adhesiveness was lowered, which facilitated the rear detachment and led to cell shortening and increased motility. In agreement with the stick-slip model, low maximal contractile force corresponded with low cell/substrate interactions, giving rise to reduced cell spreading and therefore

smaller cell length and potentially larger speeds, provided that the cytoskeleton is polarized.

On the contrary, stabilizing focal adhesions on RPE1 cells decreased their average velocity. It also induced a lengthening of the cells and larger adhesion patches (**Fig. 4D**) as predicted by our model: diminishing the turnover rate λ induces a marked stick-slip behavior, with long spreading phases, and therefore large cell length, and slow speed. Remarkably, the dependence of the stick-slip behavior on the turnover rate and contractility results in inverse correlation between average cell length and migration velocity (**Fig. 5**A), which was consistently observed in both NIH3T3 and RPE1 cells. More elongated cells, such as NIH3T3, were associated with stronger adhesions, as they could spread more without detaching, and hence a lower velocity. When this detachment occurred at an early stage of spreading, corresponding to low stress levels, cells were shorter and exhibited higher migration speeds, as in the case of RPE1.

Finally, we asked if the stick-slip paradigm would operate also in the presence of other polarization mechanisms. We utilized deposited data of single cell trajectories of various cell types on patterned adhesive one-dimensional lines (World Cell Race *(* 37 *)*). For each cell line, both instantaneous cell speed and cell length were extracted and correlated with each other (**Fig. 5B**). Strikingly, the negative correlation between cell length and cell speed, consistent with the stick-slip regime, was confirmed for most of cell lines.

Our findings demonstrate that a stochastic stick-slip mechanism, which is intrinsically based on the properties of adhesion dynamics, is a very robust feature of adherent

cell migration. In particular, while this mechanism provides a simple scenario of spontaneous symmetry breaking and cell polarization, our results suggest that stick-slip behavior occurs also in the presence of other polarization mechanisms.

Using a one-dimensional approach based on soft micropatterning, force imaging and optogenetics in combination with theoretical approaches, we have uncovered a generic, stick-slip mechanism that can initiate cell migration. This mechanism allows cells to spontaneously break their symmetry by stochastically detaching adhesive contacts on one side, resulting in a migratory step in the opposite direction. This work shows that cell symmetry breaking can emerge independently of a prior polarity of the actin cytoskeleton, due to instabilities of the mechanochemical coupling of the cell to its environment via adhesion sites. This process is found to be controlled by the interplay of contractile forces and focal adhesion dynamics. Hence, by modifying contractility and adhesiveness of the cell, the rate of such stochastic steps (i.e. the instantaneous speed of cell motion) can be controlled. Interestingly, we found that stochastic stick slip is responsible for a negative correlation between cell length and cell speed, which we observed across many cell types, thereby further emphasizing the relevance and robustness of this mechanism. In the light of our findings, cell length represents a direct readout of cell adhesiveness and thus appears as straightforward parameter to predict cell migratory behavior.

We observed for several cells of different cell types that the first stochastic step can lead to the emergence of a more persistent polarity within the moving cell, as some cells tend to take several migration steps in the same direction. Stochastic stick slip therefore appears as a basic mechanism of symmetry breaking conserved across

adherent mammalian cell types, which can coexist with other polarization mechanisms, based e.g. on cytoskeleton instabilities or reaction diffusion patterns.

References:

Materials and methods are available as supplementary materials at the Science website.

1. Renkawitz, J. and Sixt, M., Mechanisms of force generation and force transmission during interstitial leukocyte migration. *EMBO reports* **11** (10), 744-750 (2010).
2. Webb, D.J., Parsons, J.T. and Horwitz, A.F., Adhesion assembly, disassembly and turnover in migrating cells–over and over and over again. *Nature Cell Biology* **4** (4), E97 (2002).
3. Ridley, A.J., Schwartz, M.A., Burridge, K., Firtel, R.A., Ginsberg, M.H., Borisy, G., Parsons, J.T. and Horwitz, A.R., Cell migration: integrating signals from front to back. **302** (5651), 1704-1709 (2003).
4. Friedl, P. and Wolf, K., Plasticity of cell migration: a multiscale tuning model. *The Journal of cell biology*, jcb-200909003 (2009).
5. Monzo, P., Chong, Y.K., Guetta-Terrier, C., Krishnasamy, A., Sathe, S.R., Yim, E.K., Ng, W.H., Ang, B.T., Tang, C., Ladoux, B. and Gauthier, N.C., Mechanical confinement triggers glioma linear migration dependent on formin FHOD3. *Molecular biology of the cell* **27** (8), 1246-1261 (2016).
6. van Zijl, F., Krupitza, G. and Mikulits, W., Initial steps of metastasis: Cell invasion and endothelial transmigration. *Mutation Research/Reviews in Mutation Research* **728** (1), 23-34 (2011).
7. Huttenlocher, A. and Horwitz, A.R., Integrins in cell migration. *Cold Spring Harbor perspectives in biology* **3** (9), a005074 (2011).
8. Fackler, O.T. and Grosse, R., Cell motility through plasma membrane blebbing. *The Journal of cell biology* **181** (6), 879-884 (2008).
9. Lomakin, A. J., Lee, K. C., Han, S. J., Bui, D. A., Davidson, M., Mogilner, A., & Danuser, G., Competition for actin between two distinct F-actin networks defines a bistable switch for cell polarization. *Nature Cell Biology* **17** (11), 1435 (2015).

10. Lauffenburger, D. A., & Horwitz, A. F., Cell migration: a physically integrated molecular process. *Cell* **84** (3), 359-369 (1996).

11. Tee, Y.H., Shemesh, T., Thiagarajan, V., Hariadi, R.F., Anderson, K.L., Page, C., Volkmann, N., Hanein, D., Sivaramakrishnan, S., Kozlov, M.M. and Bershadsky, A.D., Cellular chirality arising from the self-organization of the actin cytoskeleton. *Nature cell biology* **17** (4), 445 (2015).

12. Turing, A. M., The chemical basis of morphogenesis. *Philosophical Transactions of the Royal Society of London* **237** (641), 37-72 (1952).

13. Callan Jones, A.C., Joanny, J.F. and Prost, J., Viscous-fingering-like instability of cell fragments. *Physical review letters* **100** (25), 258106 (2008).

14. Blanch-Mercader, C. and Casademunt, J., Spontaneous Motility of Actin Lamellar Fragments. *Physical review letters* **110** (7), 078102 (2013).

15. Hawkins, R.J., Piel, M., Faure-Andre, G., Lennon-Dumenil, A.M., Joanny, J.F., Prost, J. and Voituriez, R., Pushing off the walls: a mechanism of cell motility in confinement. *Physical review letters* **102** (5), 058103 (2009).

16. Callan Jones, A.C. and Voituriez, R., Active gel model of amoeboid cell motility. *New Journal of Physics* **15** (2), 025022 (2013).

17. Ruprecht, V., Wieser, S., Callan-Jones, A., Smutny, M., Morita, H., Sako, K., Barone, V., Ritsch-Marte, M., Sixt, M., Voituriez, R. and Heisenberg, C.P., Cortical contractility triggers a stochastic switch to fast amoeboid cell motility. *Cell* **160** (4), 673-685 (2015).

18. Cramer, L. P., Forming the cell rear first: breaking cell symmetry to trigger directed cell migration. *Nature Cell Biology* **12** (7), 628 (2010).

19. Pollard, T.D. and Borisy, G.G., Cellular Motility Driven by Assembly and Disassembly of Actin Filaments. *Cell* **112** (4), 453-465 (2003).

20. Yam, P.T., Wilson, C.A., Ji, L., Hebert, B., Barnhart, E.L., Dye, N.A., Wiseman, P.W., Danuser, G. and Theriot, J.A., Actin–myosin network reorganization breaks symmetry at the cell rear to spontaneously initiate polarized cell motility. *Journal of Cell Biology* **178** (7), 1207-1221 (2007).

21. Butler, J.P., Tolic-Nørrelykke, I.M., Fabry, B. and Fredberg, J.J., Traction fields, moments, and strain energy that cells exert on their surroundings. *American Journal of Physiology-Cell Physiology* **282** (3), C595-C605 (2002).

22. Dembo, M. and Wang, Y.L., Stresses at the cell-to-substrate interface during locomotion of fibroblasts. *Biophysical journal* **76** (4), 2307-2316 (1999).

23. Lafaurie-Janvore, J., Maiuri, P., Wang, I., Pinot, M., Manneville, J.B., Betz, T., Balland, M. and Piel, M., ESCRT-III assembly and cytokinetic abscission are induced by tension release in the intercellular bridge. *Science* **339** (6127), 1625-1629 (2013).

24. Tseng, Q., Wang, I., Duchemin-Pelletier, E., Azioune, A., Carpi, N., Gao, J., Filhol, O., Piel, M., Théry, M. and Balland, M., A new micropatterning method of soft substrates reveals that different tumorigenic signals can promote or reduce cell contraction levels. *Lab on a Chip* **11** (13), 2231-2240 (2011).

25. Doyle, A. D., Wang, F. W., Matsumoto, K., & Yamada, K. M., One-dimensional topography underlies three-dimensional fibrillar cell migration. *The Journal of cell biology* **184** (4), 481-490 (2009).

26. Schuster, S.L., Segerer, F.J., Gegenfurtner, F.A., Kick, K., Schreiber, C., Albert, M., Vollmar, A.M., Rädler, J.O. and Zahler, S., Contractility as a global regulator of cellular morphology, velocity, and directionality in low-adhesive fibrillary micro-environments. *Biomaterials* **102**, 137-147 (2016).

27. Mandal, K., Wang, I., Vitiello, E., Orellana, L.A.C. and Balland, M., Cell dipole behaviour revealed by ECM sub-cellular geometry. *Nature communications* **5**, 5749 (2014).

28. Stéphanou, A., Le Floc'h, S. and Chauvière, A., A hybrid model to test the importance of mechanical cues driving cell migration in angiogenesis. *Mathematical Modelling of Natural Phenomena* **10** (1), 142-166 (2015).

29. Bergert, M., Erzberger, A., Desai, R.A., Aspalter, I.M., Oates, A.C., Charras, G., Salbreux, G. and Paluch, E.K., Force transmission during adhesion-independent migration. *Nature cell biology* **17** (4), 524-529 (2015).

30. Mitchison, T.J. and Cramer, L.P., Actin-based cell motility and cell locomotion. *Cell* **84** (3), 371-379 (1996).

31. Ladoux, B., Mège, R.M. and Trepat, X., Front–rear polarization by mechanical cues: From single cells to tissues. *Trends in Cell Biology* **26** (6), 420-433 (2016).

32. Wu, H., Thiébaud, M., Hu, W.F., Farutin, A., Rafaï, S., Lai, M.C., Peyla, P. and Misbah, C., Amoeboid motion in confined geometry. *Physical Review E* **92** (5), 050701 (2015).

33. Kruse, K., Joanny, J.F., Jülicher, F., Prost, J. and Sekimoto, K., Generic theory of active polar gels: a paradigm for cytoskeletal dynamics. *The European Physical Journal E* **16** (1), 5-16 (2005).

34. Valon, L., Etoc, F., Remorino, A., di Pietro, F., Morin, X., Dahan, M. and Coppey, M., Predictive spatiotemporal manipulation of signaling perturbations using optogenetics. *Biophysical journal* **109** (9), 1785-1797 (2015).

35. Galbraith, C.G., Yamada, K.M. and Sheetz, M.P., The relationship between force and focal complex development. *Journal of Cell Biology* **159** (4), 695-705 (2002).

36. Maiuri, P., Rupprecht, J.F., Wieser, S., Ruprecht, V., Bénichou, O., Carpi, N., Coppey, M., De Beco, S., Gov, N., Heisenberg, C.P. and Crespo, C.L., Actin flows mediate a universal coupling between cell speed and cell persistence. *Cell* **161** (2), 374-386 (2015).

37. Maiuri, P., Terriac, E., Paul-Gilloteaux, P., Vignaud, T., McNally, K., Onuffer, J., Thorn, K., Nguyen, P.A., Georgoulia, N., Soong, D. and Jayo, A., The first world cell race. **22** (17) (2012).

38. Liu, Z., Bun, P., Audugé, N., Coppey-Moisan, M. and Borghi, N.,, Vinculin head–tail interaction defines multiple early mechanisms for cell substrate rigidity sensing. *Integrative Biology* **8** (6), 693-703 (2016).

39. Kovács, M., Tóth, J., Hetényi, C., Málnási-Csizmadia, A. and Sellers, J.R., Mechanism of Blebbistatin Inhibition of Myosin II. *Journal of Biological Chemistry* **279** (34), 35557-35563 (2004).

40. Slack-Davis, J.K., Martin, K.H., Tilghman, R.W., Iwanicki, M., Ung, E.J., Autry, C., Luzzio, M.J., Cooper, B., Kath, J.C., Roberts, W.G. and Parsons, J.T., Cellular characterization of a novel focal adhesion kinase inhibitor. *Journal of Biological Chemistry* **282** (20), 14845-14852 (2007).

41. Renkawitz, J., Schumann, K., Weber, M., Lämmermann, T., Pflicke, H., Piel, M., Polleux, J., Spatz, J.P. and Sixt, M., Adaptive force transmission in amoeboid cell migration. *Nature cell biology* **11** (12), 1438 (2009).

42. Liu, Y.J., Le Berre, M., Lautenschlaeger, F., Maiuri, P., Callan-Jones, A., Heuzé, M., Takaki, T., Voituriez, R. and Piel, M., Confinement and low adhesion induce fast amoeboid migration of slow mesenchymal cells. *Cell* **160** (4), 659-672 (2015).

43. Tse, J.R. and Engler, A.J., Preparation of hydrogel substrates with tunable

mechanical properties. *Current protocols in cell biology*, 10-16 (2010).

44. Sabass, B., Gardel, M.L., Waterman, C.M. and Schwarz, U.S., High Resolution Traction Force Microscopy Based on Experimental and Computational Advances. *Biophysical journal* **94** (1), 207-220 (2008).

45. Vignaud, T., Ennomani, H. and Théry, M., Polyacrylamide hydrogel micropatterning.. *Methods in cell biology* **120**, 93-116 (2014).

46. Horzum, U., Ozdil, B. and Pesen-Okvur, D., Step-by-step quantitative analysis of focal adhesions. *MethodsX* **1**, 56-59 (2014).

Acknowledgements:

We thank Matthieu Piel and Paolo Maiuri for valuable discussions and sharing the cell race data with us. We also thank Thomas Boudou and Manuel Théry for critical discussions, Jean Bernard for technical assistance, and members of the MOTIV team at LiPhy for support. We thank Laurent Blanchoin's Cytomorpholab in Grenoble for providing us RPE1 cells and Helder Maiato from the University of Porto for providing us with NIH3T3 cells. Furthermore, we want to thank Alexander Kyumurkov at the Institute of Advanced Biology in Grenoble for assisting with adhesion imaging. **Funding:** This work was supported by Nanoscience fondation (MB), and the ARC fondation (MB). **Author contributions**: K.H. performed experiments and analyzed the data. S.dB. performed optogenetic experiments on vinculin-iRFP transfected cells. L.V. designed the optogenetic cell line in M.C.'s laboratory. Y.A.M. designed the vinculin-eGFP RPE1 and NIH3T3 cells in C.A.R.'s laboratory. C.F. provided insights on the FRAP experiments and performed the related data analysis. R.V. developed the theoretical framework. M.B. supervised the research. All authors contributed to write the paper. **Competing interests:** No authors have competing interests.

List of Supplementary Materials:

Materials and Methods

Figure S1 – S3

Movie S1

References 24, 27, 43 – 46

Figures:

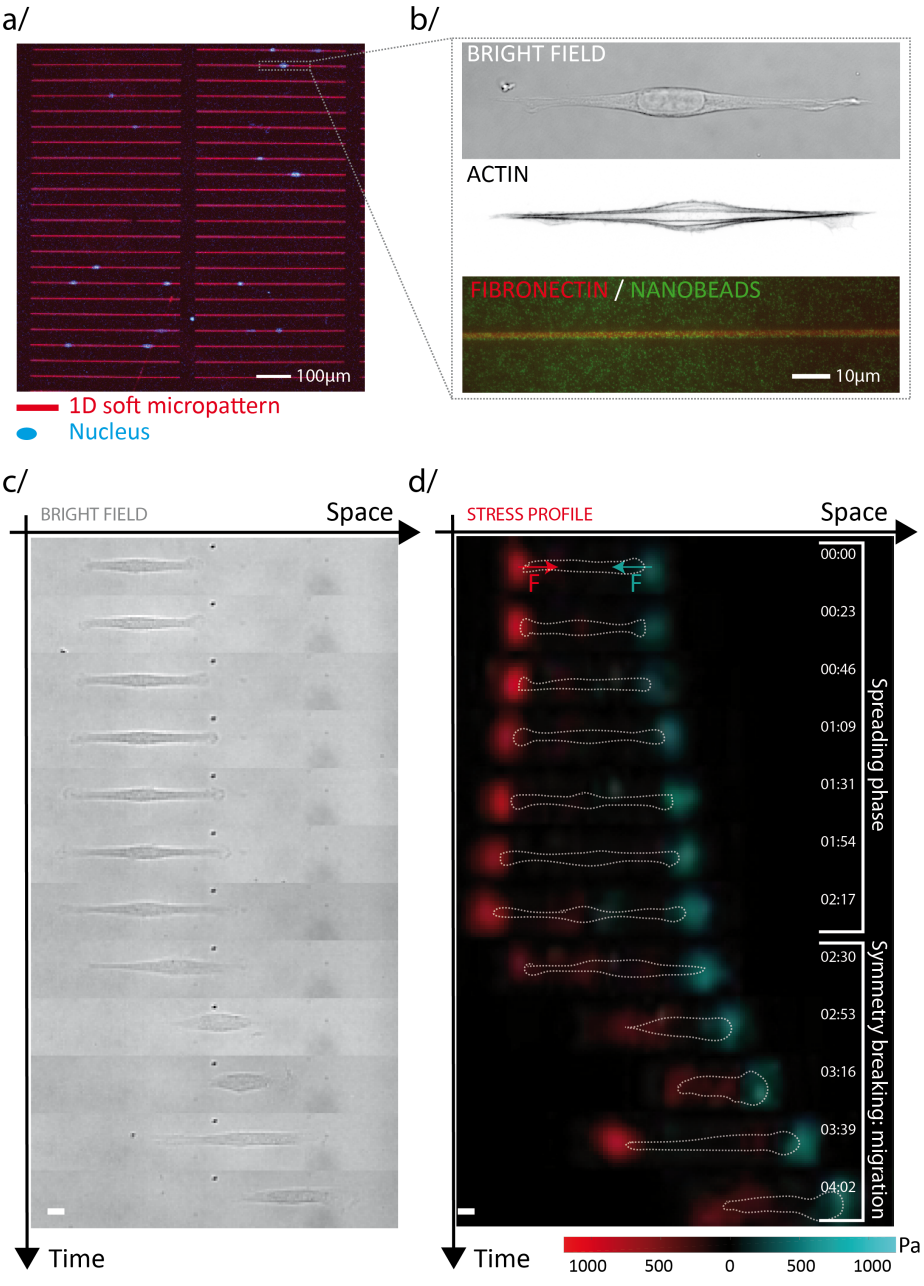

Fig. 1 | One-dimensional single cell migration assay based on soft micropatterning and traction force microscopy mimics complex 3D fibrillar *in vivo* migration. (a) 40 kPa polyacrylamide gel with RPE1 cells (blue: nucleus staining) on top of 2 μm micro-patterned fibronectin lines (red). **(b)** Brightfield, actin cytoskeleton and bead imaging of RPE1 on 2 μm line allowed extracting morphometric and mechanical parameters simultaneously. **(c)** Time sequence of RPE1 cell migrating on fibronectin lines and **(d)** its associated stress profile extracted via TFM (dotted white line: cell outline; color coded stress profile depending on the direction of applied traction forces $\vec{F}$: red in and blue against the direction of migration; Scale bars: 10 µm).

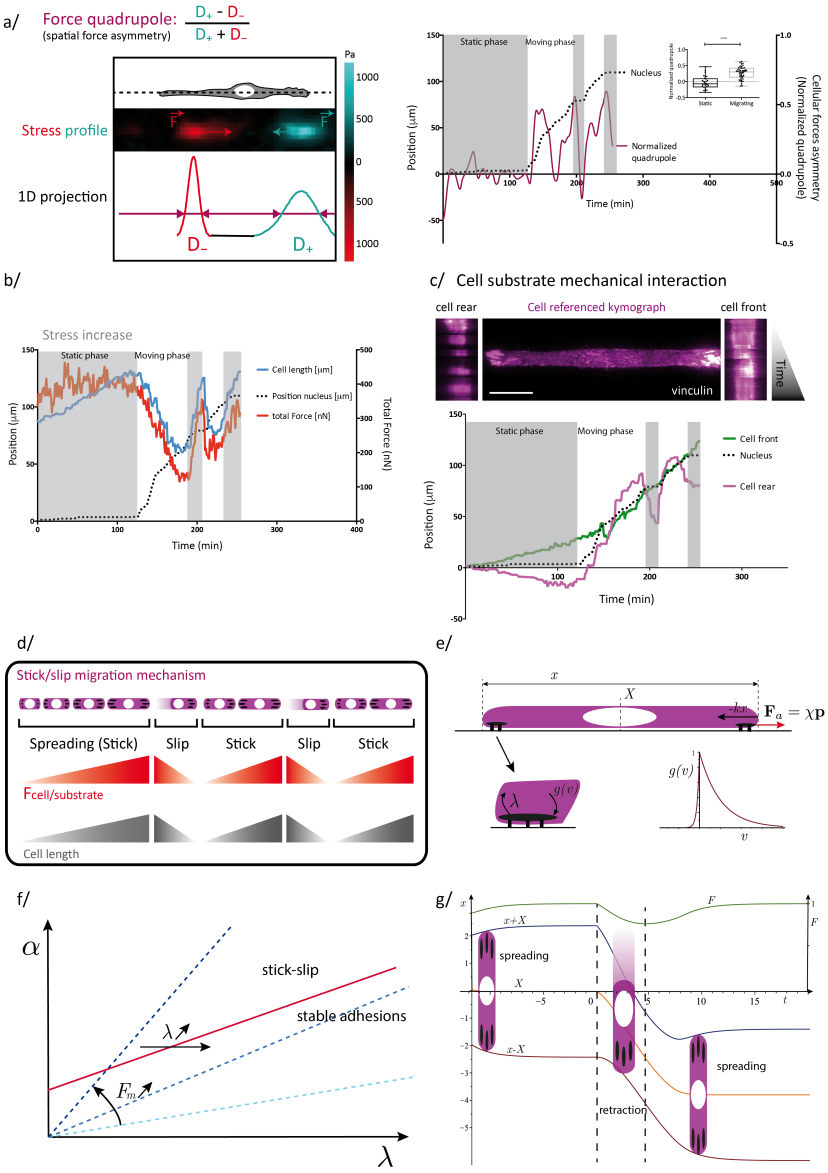

Fig. 2 I RPE1 cells exhibit intermittent migration following a stick-slip motion. **(a)** Scheme of the force asymmetry analysis: the normalized quadrupole was extracted from the 1D projection of the stress profile of an adherent cell (color coded stress map and 1D profile depending on the direction of applied traction forces $\vec{F}$ exerted: red in and blue against the direction of migration). Dynamic measurements revealed a symmetric spatial force profile during static spreading and an asymmetric distribution during migration phases. Inset: average force asymmetry during static

and mobile phases of several cells (n = 10). **(b)** Cell length and total force correlation: increase during spreading phase and decrease during migration. **(c)** Referenced kymograph of RPE1 cells stably expressing vinculin-eGFP showing a continuous attachment of the front while adhesions in the rear detached and reattached during one migration cycle (Scale bar: 10 µm). Tracking the front, rear and nucleus position over time could further represent this destabilization of the rear. **(d)** Deduced scheme of the proposed stick-slip migration mechanism: during non-motile spreading (stick) the cell builds up a high traction force that eventually will overcome adhesion strength in the perspective rear of the cell. Upon the retraction of the rear, the cell shortens and lowers its mechanical interaction with the substrate to initiate migration (slip). **e,** Schematic of the model and parameters as defined in the text. **(f)** Example of stick slip dynamics predicted by the model. Dynamical equations 2-3 are solved numerically with $vm = 0.5$, $v_p = 0.5$, $\lambda = 1$, $\mu = 1$, $\alpha = 1$ (arbitrary units). Blue, orange and brown line show rear, nucleus and front position over time, respectively. Green line depicts the relative traction force level F. **(g)** Phase diagram of dynamic behaviors predicted by the model, as a function of the actin turn-over rate λ and phenomenological parameter α (arbitrary units). Dashed-lines show different values of the maximal contractile force $Fmax = \frac{\chi\alpha}{\lambda}$.

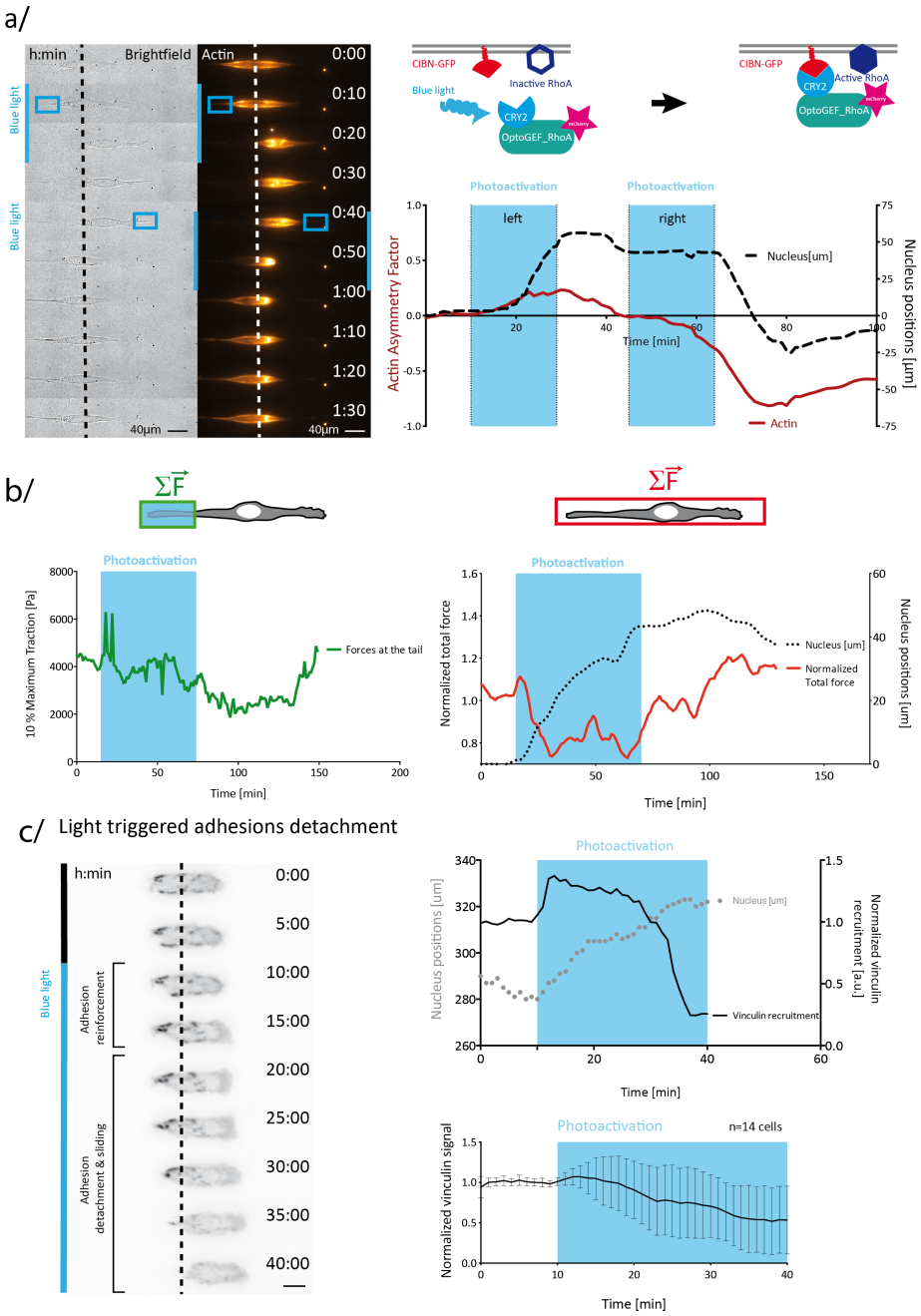

Fig. 3 | RhoA optogenetic control of cellular force symmetry breaking. (a) Schematic representation of light-induced Cry2-CIBN dimerization and local RhoA

activation due to its close proximity to its upstream regulator opto_GEFRhoA. Brightfield and actin imaging and quantification showed the light induced migration away from the photoactivation area (blue square), which is characterized by a transient front-rear polarity and actin asymmetry (dashed line: nucleus position at t0). **(b)** Local and global force response of the light-induced rear and of the whole cell, respectively, showed a transient local contractility increase at the perspective rear followed by a global decrease of the mechanical cell-substrate interaction. **(c)** stably expressing vinculin-iRFP revealed local adhesion reinforcement within the photostimulated area followed by a subsequent adhesion detachment. Dashed line indicates nucleus position at t0. Scale bar: 10 µm.

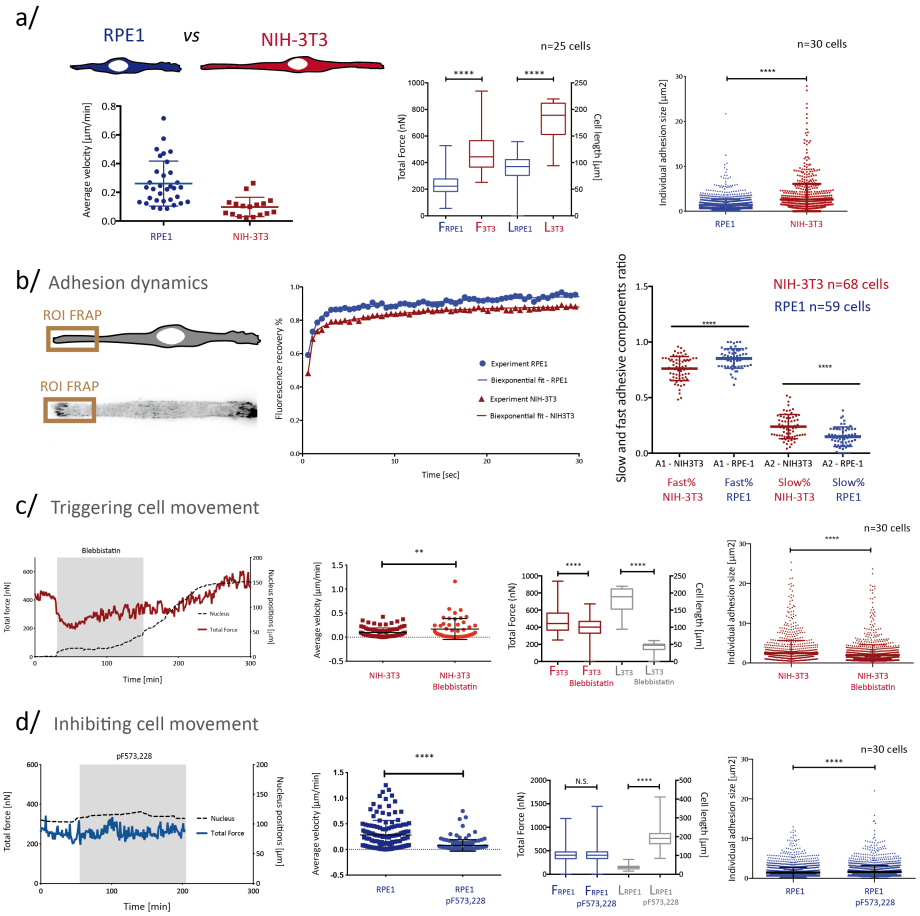

Fig. 4 | Adhesiveness and contractility control the migratory behavior of NIH3T3 and RPE1 cells. (a) Comparison of instantaneous migration speed, total force, cell length and individual adhesion size of RPE1 and NIH3T3 cells. **(b)** FRAP experiments of adhesions located at one cell edge were modeled with a bi-exponential fit to extract a fast and slow component representing mobile vinculin within the cytoplasm and slow vinculin bound to adhesions. **(c) and (d)** Altering the migratory behavior of RPE1 and NIH3T3 using 1 μM pF573,228 to inhibit and 3 μM blebbistatin to trigger migration, respectively. Shown are measured parameters relevant for stick-slip migration: average migration speed, total force, cell length and individual adhesion size. Statistical significance tested with unpaired t-test ($P < 0.05$). Scatter plots with mean and standard deviation. Box plots from minimum and maximum values with the mean and standard deviation. Number *n* of analyzed cells per condition indicated on the respective graph figures.

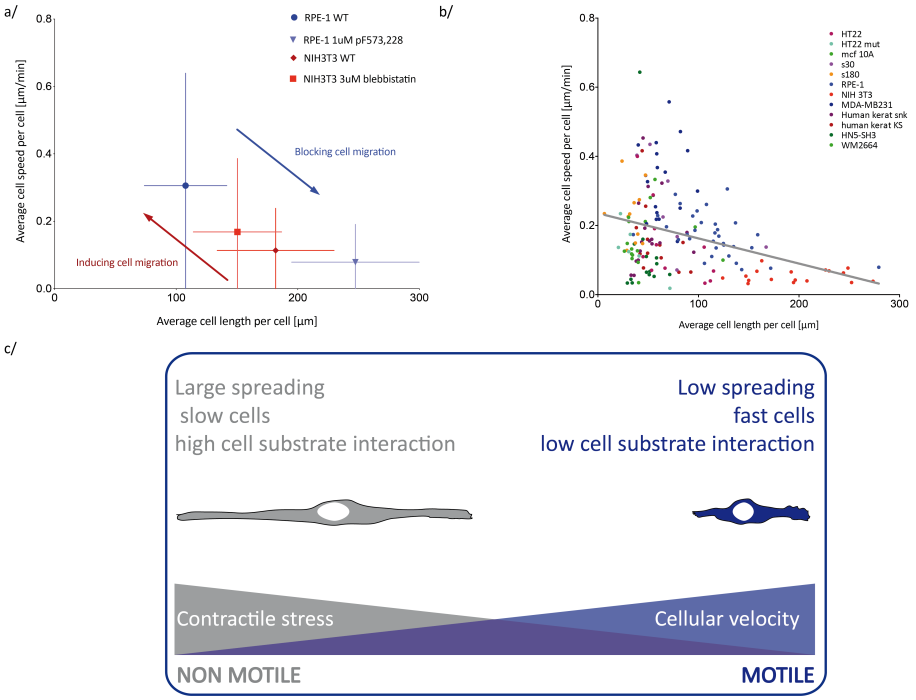

Fig. 5 I The inverse relation between cell length and speed. (a) Experimentally deduced phase diagram using a pharmacological approach to alter the migratory behavior of RPE1 and NIH3T3 cell (error bars show the standard deviation from the mean). **(b)** Length-speed relation validated by analyzing several cell types coming from the cell race data (one color used per cell type; black line: linear fit of all data points). **(c)** Summary showing how cell contractility, and therefore adhesiveness and cell length, control cellular migration.

4.1.3. Summary of major results

Our experimental and theoretical work identified a stick-slip migration mode that led us to the following two main findings: (i) spontaneous symmetry breaking can occur via stochastic retraction of cell rear, without any pre-existing cytoskeleton polarity, and (ii) cellular traction forces/adhesiveness/cell length are inversely correlated to migration speed.

Indeed, our non-trivial stick-slip model provides strong evidence that spontaneous symmetry breaking can occur independently of any prior cytoskeleton polarity, due to mechanical instabilities. At its stable point, before the initiation of migration, a non-migrating cell does not exhibit any signatures of asymmetry, but rather displays symmetric edge dynamics and isotropic force and actin cytoskeletal distributions. In order to transition to the migratory phase, a threshold in force generation must be overcome. This occurred during the spreading phase due to the presence of internal and/or external noise: As cell length increased, intracellular tension increased, which in turn induced a dynamically unstable state of the system. Noise-induced fluctuations in the intracellular force level then led to the stochastic detachment of adhesion sites at one cell edge, as adhesions could no longer sustain the increased tension. Hence, mesenchymal cells, in absence of any external stimulus, broke their symmetry, due to the stochastic retraction of one cell edge, which defined the rear and triggered migration in the opposite direction. This mechanism highlights the crucial role of force-mediated adhesion detachment in initiating migration. Thus, we demonstrated that adhesion turnover is critical for symmetry breaking and defining cellular front and rear. Furthermore, once in motion, cells decreased the level of mechanical cell-substrate interaction and a shortened total cell length. Importantly, this mechanism of switching from non-motile to stochastic stick-slip migration was validated *in silico* using the data from our empirical findings.

To further validate our hypothesis and challenge the theoretical framework, we utilized optogenetic and pharmacological approaches to dynamically induce symmetry breaking by altering the balance between contractility and adhesiveness, respectively. For instance, we employed two cell types with opposite migratory behaviors (slow migrating NIH3T3 compared to fast migrating RPE-1 cells (Maiuri 2012, Maiuri 2015)) and inverted their cell-type dependent ability to initiate migration using specific inhibitors that perturb

cell mechanics. Specifically, NIH3T3 cells treated with a low concentration (3 µM) of blebbistatin (a myosin II ATPase inhibitor (Kovács 2004)), decreased their cell length, became less contractile, and formed smaller adhesion patches, which is indicative of faster adhesion turnover. This ultimately enabled NIH3T3 cells to enter into mobile phases and move more rapidly. On the other hand, inhibition of FAK in RPE-1 cells (using 1 µM pF573,228 (Mabeta 2016)) decreased cell movement. FAK inhibitor-treated cells were more elongated, possessing bigger (hence, more stable) adhesions with increased vinculin content, and thus incapable of decreasing their mechanical interaction with the substrate.

Intriguingly, we found an inverse relationship between cell length/adhesiveness/ traction forces and the cell's ability to migrate. Cell length was the most easily accessible migratory parameter, as it did not rely on fluorescent imaging of cellular structures or substrate deformation tracers, and therefore represented a straightforward readout of cell adhesiveness/contractility. And indeed, we validated this inverse relation between cell length and cell migration across many cell types utilizing already existing video date from the previously published "cell race" experiments (Maiuri 2012).

4.1.4. Open discussion: difficulties of quantifying a migrating cell

One of our major obstacles during my PhD work was to extract quantitative information that represented the complexity of different migratory behaviors. This paragraph will briefly conclude major key points of the field's ongoing debate, which might facilitate an open discussion in the future.

My major questions were: What defines a migrating cell? More precisely, what is the most accurate way to calculate migration speed? The most straightforward approach is to calculate the average velocity of a single cell over its whole trajectory (Diz-Muñoz 2016, Monzo 2016, Meijering 2012). However, averaged data might be misleading since cells alternate between mobile and static periods during their lifetimes. Thus, in order to differentiate between the two distinct migration regimes, a threshold needs to be applied (Diz-Muñoz 2016, Schuster 2016). A minimum velocity can be set, however, instantaneous velocity is subject to noise due to small fluctuations in the position of the cell, which are not related to an actual translocation. Hence, the data needs to be smoothened to a certain

extent. As an alternative, a threshold in persistence time could be set. However, defining the direction of movement by precisely following the cell edge in 2D remains challenging. In addition and independent of the chosen threshold parameter, cellular variability prohibits one to set a constant threshold value for all distinct cell types.

We finally decided to extracted the instantaneous speed (and instantaneous cell length) and averaged it over the whole migration trajectory for the following three reasons: (i) to avoid setting any threshold, (ii) to extract migration speed independent of the direction of movement, which at the same time (iii) represents the propensity of the cell to enter into a moving phase. To decrease noise, we smoothed the data over a small time window that was below the persistence time. Here, the major limitation in my approach was the low temporal resolution of the cell race data (one image every 15 minutes (Maiuri 2012)). Yet, by averaging the instantaneous speed and instantaneous length over many successive migratory steps, we were able to extract an inverse length-motion relation valid across many mesenchymal cell types.

As the instantaneous cell length represents a straightforward read-out of adhesiveness/contractility, and therefore migratory behavior, one could image to apply this knowledge in the future to develop diagnostic tools, which identify for example metastatic cancer cells. And indeed, our findings are in agreement with other studies that have shown an inverse length-speed relation for cancer cells (Leal-Egaña 2017, Guetta-Terrier 2015). Leal-Egaña et al. identified two size-based cancer cell subpopulations that exhibit distinct mechanistic properties (metastatic and proliferative). Smaller cells possessed higher motile potential and lower cellular traction forces (Leal-Egaña 2017). Future efforts to analyze and validate whether the inverse length-speed relationship is a universal phenomenon require further quantification of single cell trajectories at high spatial and temporal resolution. Form that, robust alternative migration parameters, beyond average cell speed, need to be identified that take into account the complexity of cellular movement.

4.1.5. Future perspective: coupling actin retrograde flow speed measurements to traction force quantifications

Our work has already revealed a major role for adhesion dynamics in determining cellular ability to polarize spontaneously by adapting to changes in cellular forces. However, we cannot exclude the possibility that other polarity mechanisms might also be at play to bias the direction of movement. Hence, future perspectives include the observation of cellular components that might also be involved in (i) breaking of symmetry and (ii) maintenance of polarity during persistent movement. Various polarity mechanisms have been identified in the past that might occur in parallel to our stochastic symmetry breaking scenario: anisotropic membrane trafficking, secretory pathways, cytoskeletal rearrangements, organelle positioning, and/or cell-cell contacts (Etienne-Manneville 2004). We believe that one key process that should to be examined in the future is actin retrograde flow for the following reasons.

The major finding of our work was the force-dependent stochastic detachment of adhesions that triggered migration in absence of any pre-established cytoskeleton asymmetry. We validated this hypothesis by defining an asymmetry factor for actin cytoskeleton, which quantified its spatial distribution, but did not take into account its retrograde flow. Previous studies that investigated spontaneous symmetry breaking demonstrated increased actin flow speed in the rear of the cell prior to the initiation of movement (Yam 2007, Barnhart 2015). Furthermore, others have correlated the migration speed with the f-actin flow speed: fast-migrating cells were associated with faster retrograde flow and more persistent migration in a universal fashion (Renkawitz 2009, Maiuri 2015, Liu 2015). This led us to hypothesize that there are two coupled timescales that are crucial for controlling the establishment and maintenance of cell polarity during cell migration: the speed of cellular force build-up and the rate of adhesion turnover.

Given this, we believe that during the initiation of migration actin retrograde flow directly impacts the rate of cell spreading and therefore determines the timescale of force increase experienced by adhesive contacts. We further speculate that if this force increase is faster than the rate at which adhesions build up, adhesive contacts would not be able to adapt to this mechanical alteration and consequently detach triggering cellular movement. Hence, in the perspective of the classical molecular clutch model, the tight coupling between

those two timescales might fix the critical point at which cells efficiently transmit forces to the substrate to transit from a non-moving to a moving state.

Additionally, what remain unknown are the mechanisms that maintain a front-rear polarity once cellular symmetry is stochastically broken. Our stick-slip model explains adhesion-dependent initiation of migration with an equal probability to move in either one of the two possible directions. Yet, we observed that some cells take several migration steps in the same direction after symmetry breaking, leading to a highly persistent movement. While others exhibit oscillatory movement with rapid and directional changes occurring during stick phases. Therefore, the first stochastic step leads to the emergence of stabilized polarity in some migrating cells. However, the mechanisms that reinforce front-rear polarity and lead to high persistence need further investigation.

In that respect, as mentioned previously, several studies have emphasized the central role of retrograde actin flow on the anisotropic distribution of polarity cues within the cell (Maiuri 2015). An exciting future perspective is to measure the actin retrograde flow speed and motile forces during cell migration at the same time. However, this is experimentally difficult, as both processes, retrograde flow and cell migration, occur at different time scales: while cytoskeletal f-actin flows rapidly backwards (0-30 nm/sec) (Gardel 2008), cell migration is orders of magnitude slower (µm/h) (Schuster 2016, Maiuri 2015, A. D. Doyle 2009). Conventionally, actin cytoskeleton needs to be imaged at high temporal and spatial resolution (several images per second) in order to extract its flow. Cell migration on the other hand can to be observed with a lower frame rate, but over a longer time period (in the range of hours). Hence, imaging over several hours at very high frame rate could not just lead to phototoxicity and also generate an immense amount of data. To tackle those problems, we suggest to combine fast and slow sampling rates as following: microscopic imaging of cellular movement (combined with quantitative force measurements) every few minutes and rapid actin flow speed imaging (e.g. using fluorescent or even photoconvertible actin (A. K. Doyle 2012)) over short time periods only at defined time intervals.

Taken all together, future experiments should be based on new strategies dedicated to synchronized quantitative measurements of both actin flow and motile traction forces during cell migration. This would potentially give rise to new insights into the mechanical cell-substrate coupling that is mediated by clutch molecules that link actin flow to integrins

and generate a friction that ultimately drives force symmetry breaking and directed migration.

4.2. Study 2) Monzo et al. "The formin FMN1 promotes directional changes of invasive GBM by increasing cell cytoskeleton's cohesion and traction forces on laminin linear substrate."

After creating an elegant and novel *in vitro* migration assay (aim1) and screening migratory potential of non-cancerous cells (aim2) we applied our knowledge to the field of mechano-oncology. Our aim was to study how cell mechanics determines migration of non-normal, cancerous cells (aim3). This final thesis section will elaborate on our exciting collaborative work with Dr. Nils Gauthier and Dr. Pascale Monzo from IFOM (the FIRC Institute of Molecular Oncology) in Milan, Italy. This side project highlights how fundamental research can extend beyond establishing basic principles and move towards a more applied field of cancer biology. In this respect, we utilized our findings on the force-motion relation of non-transformed cells as a guideline to screen how mechanical cellular activity determines the migratory potential of malignant cells.

The scientific publication concerning this project is currently in preparation and we will refer to the unpublished results as (Monzo 2018 unpublished).

4.2.1. Introduction to glioblastoma, the most aggressive malignant brain tumor

In the 1920, neurosurgeon by the name of Dr. Walter Dandy was attempting to cure invasive brain tumors by removing huge parts of the patient's brain. Even though some patients survived this invasive procedure, death was unavoidable and occurred within a few months due to the recurrence of cancer (Dandy 1928). Although, therapeutic methods have improved since then, the battle with the inevitable mortality has not been won (Reifenberger 2017).

Glioma is the most common primary malignant brain tumor in humans (Dunn 2012). It involves various cancers of the central nervous system (CNS), including glioblastoma multiforme (GBM). GBM is the most aggressive form (grade IV) of glioma, which accounts for 55% of this brain tumor, and has a dismal 5-years survival rate of <5% (**Figure 47**) (Lim 2018) (Umans 2017). Headaches, nausea, motor deficiency, and/or seizures are just a few of the possible symptoms characteristic for GBM. Treatment involves a combination of surgery, chemotherapy and radiotherapy (Stupp 2005). However, GBM development invariably leads

to the patient death 3-15 months post diagnosis even with the most intensive medical care (Umans 2017, Louis 2016).

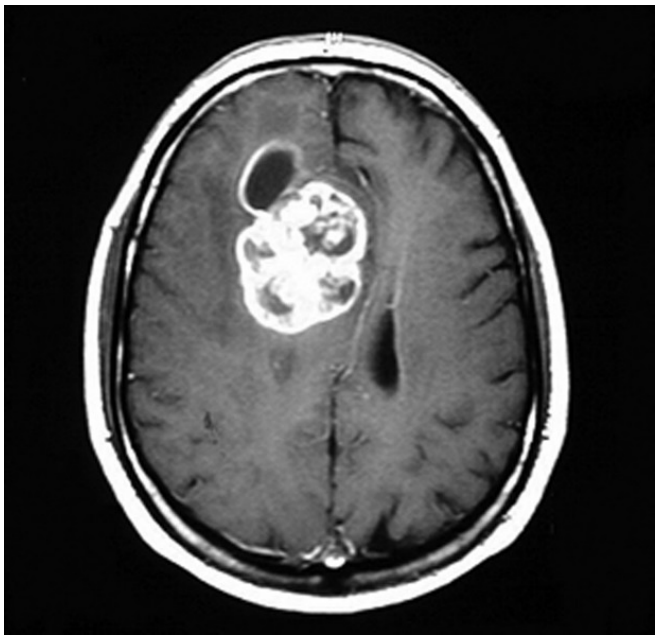

Figure 47: Magnetic resonance imaging (MRI) of glioblastoma. The glioblastoma tumor is fast growing and highly invasive. (Duncan 2013)

One major difficulty with GBM is that they are highly heterogeneous tumors, which are composed of proliferative cells located within the bulk tumor and migratory cells capable of leaving the primary tumor site. The proliferative cells cause hemorrhage and necrosis and the migratory cells cause invasion at distal brain sites (Monzo 2018 unpublished, Farin 2006). The highly invasive potential of a subset of tumor cells increases the disease's resistance to chemotherapy, which only targets proliferating cells and does not affect non-proliferating, migrating cells (Beadle 2008). In addition, given the invasive nature of GBMs and their location within the brain, invading tumor cells are likely left behind after surgical removal of the bulk tumor. This eventually leads to cancer relapse, typically within 3 months, due to the formation of secondary tumors in distal brain regions (Demuth 2004). In addition, the extensive remodeling of the ECM during cancer cell movement and tumor formation locally destroys the brain (Monzo 2018 unpublished, Farin 2006). The central therapeutic goal of present research is therefore to suppress GBM cell motility to prevent invasion, and thus stop patient relapse. In order to do so, research has started to focus on identifying key regulating proteins involved in GBM migration. The inhibition of cancer invasion would allow

to locally treat brain tumors using focal therapies and reduce the chance of recurrence (Beadle 2008, Ulrich 2009, Monzo 2016).

Within the brain, GBM can migrate through brain cells like neuronal axons and dendrites (Beadle 2008) or along the blood vessel walls (Farin 2006, Monzo 2016, Hirata 2012). The migratory behavior differs depending on the physiological environment that cells encounter. Within the brain parenchyma, glioma randomly move through tight pores in a contractility dependent manner, while possessing a faster, directed cell streaming motility along blood vessels (Farin 2006, Monzo 2016, Hirata 2012).

In vivo, migration of glioma cells has been described on rat brain slices with C6 rat glioma cells (Farin 2006, Hirata 2012) and more recently in mice brain with human glioblastoma stem cells (Griveau 2018). Glioma cells that move as single cells in the parenchyma are usually compared to neuroprogenitor cells moving through tightly packed white matter (Beadle 2008). The cell possesses a broad, often branched, lamellipodium in the front, which continuously penetrates and dilates gaps within the extracellular space. The cell squeezes through the dilation by producing a pulling force in the front, which is generated via intersecting actin fibers cross-linked by myosin II. Acto-myosin contractility in the rear pushes the nucleus through narrow pores and retracts the tail of the cell (Beadle 2008). This neuronal movement within the brain parenchyma is random and based on high levels of Cdc42 and Rac activity (Hirata 2012).

However, *in vivo* studies show that GBM cells are mainly located around blood vessels (Jones 1982). The brain is one of the most vascularized tissues with vessels, ranging from small micron-wide capillaries to millimeter-wide arteries, that create a network of hundreds of kilometers, which glioma cells can exploit to direct their migration. Indeed, GBM cells can move along blood vessel walls by switching to a faster, Rho-based neuronal motility mode (Monzo 2016). In contrast to the migratory behavior described in the previous section, GBM cells exhibit a unipolar, elongated morphology and move in a saltatory manner (comparable to fibroblast migration on linear tracks). This guided movement is characterized by fast speed and high directionality (Monzo 2016, Hirata 2012). Additionally, these cells can also be highly proliferative, often resulting in high tumor cell densities around the blood vessel (Zagzag 2000). Due to this, *in vivo* movement along linear tracks increases the invasive potential of GBM cells and is therefore the focus of this study.

Dr. Monzo's and Dr. Gauthier's research investigates the progression of GBM from a cell-mechanics' point of view. Their aim is to decipher mechanical pathways that contribute to the invasiveness of glioblastoma. Thus, our collaboration focuses on identifying how cell mechanics is linked to the invasive potential of GBM cells.

4.2.2. Studying GBM migration *in vitro*

The aim of this study was to compare specific invasive and proliferative behaviors of three distinct GBM cell lines isolated directly from patients: NNi11, NNi21 and NNi24 (**Figure 48**). NNi11–based tumors are fast growing and hemorrhagic (i.e. cells destroy blood vessels) but non-invasive in mouse xenografts. The differences between the other two GBM cell lines, which both possess high migratory activity, is that NNi21 tumors are fast growing and hemorrhagic compared to slower growing, non-hemorrhagic NNi24-based brain cancer phenotypes when xenografted into mice.

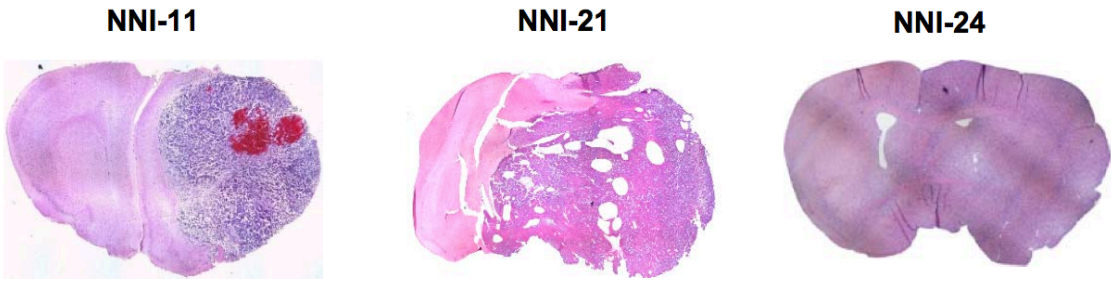

Figure 48: Heterogeneity of glioblastoma. Xenografted mouse brain injected with distinct glioblastoma cell lines and sectioned after 3 (NNi11), 2 (NNi21) and 4.5 months (NNi24) demonstrate their distinct proliferative and invasive behaviors (from left to right): non-invasive, highly invasive and damaging, and slowly invasive without being damaging. [Figure received from: (Monzo 2018 unpublished)].

Our goal was to extract force parameters and link the mechanical activity of these cells to their investigated migratory behaviors. Within the brain, blood vessels are covered with ECM proteins like fibronectin, collagen and laminin and confine cellular movement (Jones 1982). Especially laminin plays a crucial role during tumor development and GBM cell migration (Monzo 2016). All blood vessels are lined with a basement membrane composed mainly of laminin. Laminin on brain blood vessels is provided by surrounding astrocytes and endothelial cells, or secreted by glioma cells themselves (Cuddapah 2014).

In vitro studies of glioma migration on flat 2D substrates have shown a myosin II-independent mesenchymal migration mode comparable to moving epithelial cells, which is fundamentally different than the neuronal motility in 3D or along linear tracks (Monzo 2016). Other *in vitro* studies have observed a different migration on fibronectin coated soft substrates, which is characterized by a round morphology and impaired movement (Ulrich 2009). Monzo et al. have observed a saltatory movement of elongated GBM cells along 1D tracks on hard substrates (**Figure 49;** Monzo 2016) as well as on electrospun nanofibers (Monzo 2018 unpublished), mimicking *in vivo* glioma movement.

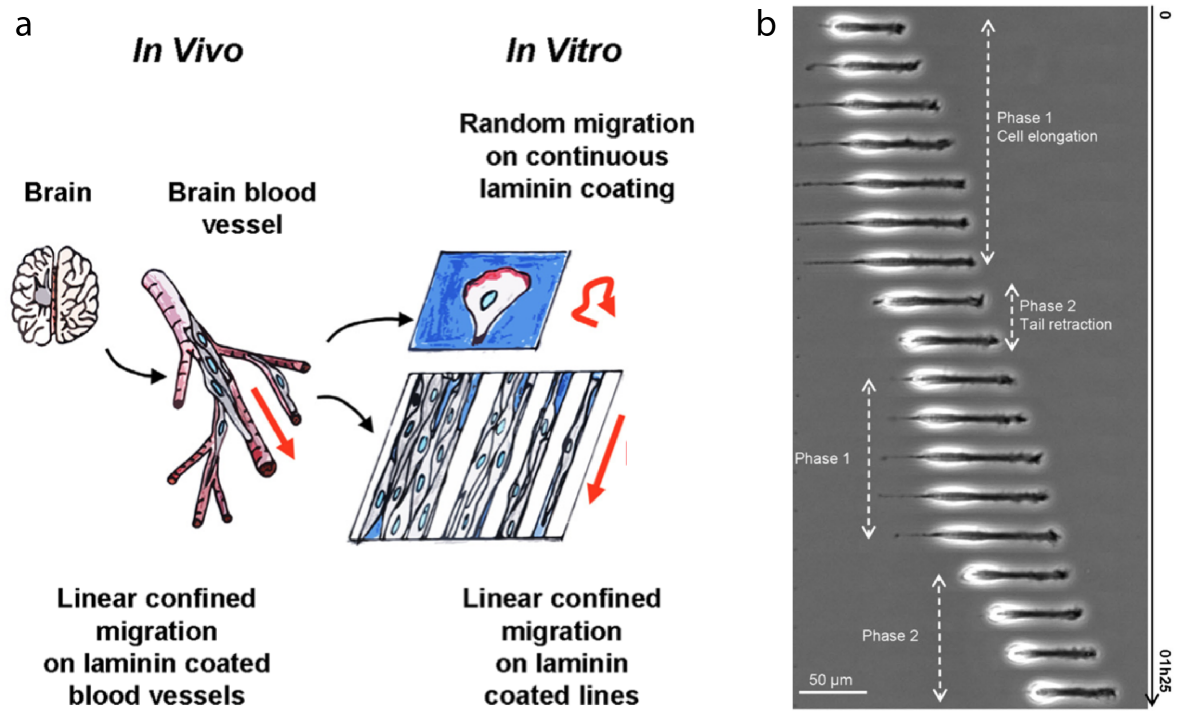

Figure 49: Mimicking *in vivo* migration along blood vessels using linear migration tracks *in vitro*. A) Schematic scheme comparing different migration modes depending on the environment. Within the brain, glioma cells move along vessel walls, mainly composed of laminin, in a directed, saltatory manner. On *in vitro* 2D substrates cells move randomly, but can switch to a persistent formin-based movement under confined conditions. B) Two-phase neuronal movement of GBM on 3 µm-wide laminin lines on glass. [Figure adapted from: (Monzo 2016)]

We therefore set up to modify our 1D migration system to match specific physiological conditions of the brain. Our strategy was to create thin adhesive laminin lines on top of soft polyacrylamide substrates, thus mimicking *in vivo* linear blood vessel tracks and allowing to simultaneously access migratory and force parameters of single GBM cells.

4.2.3. Experimental results

Monzo et al. have observed neuronal migration of glioma cells on linear tracks microprinted on hard substrates (glass and plastic) (Monzo 2016). In order to perform TFM experiments at the single cell level, we needed to create 1D lines on top of a deformable PAA substrate, and first observe how the mechanical substrate properties influence cellular migratory behavior.

To set-up our experimental approach, we created 50 µg/ml laminin patterned lines of 2 µm width on top of soft PAA hydrogels. We used rat C6 cells, a frequently used experimental glioma cell model (Grobben 2002, Monzo 2016). C6 cells were able to adhere to the micropatterned lines, adopt an elongated shape, proliferate and migrate. The migration was qualitatively comparable with prior observed *in vivo* and *in vitro* two-phase saltatory neuronal motility: continuously forward moving leading edge, destabilized tail (**Figure 50**). We used a hydrogel stiffness of 5kPa in order to allow sufficient substrate deformation induced by the low traction forces of glioma cells, while simultaneously being closer to the physiological stiffness of the brain (~2 kPa in white matter (Budday 2015)).

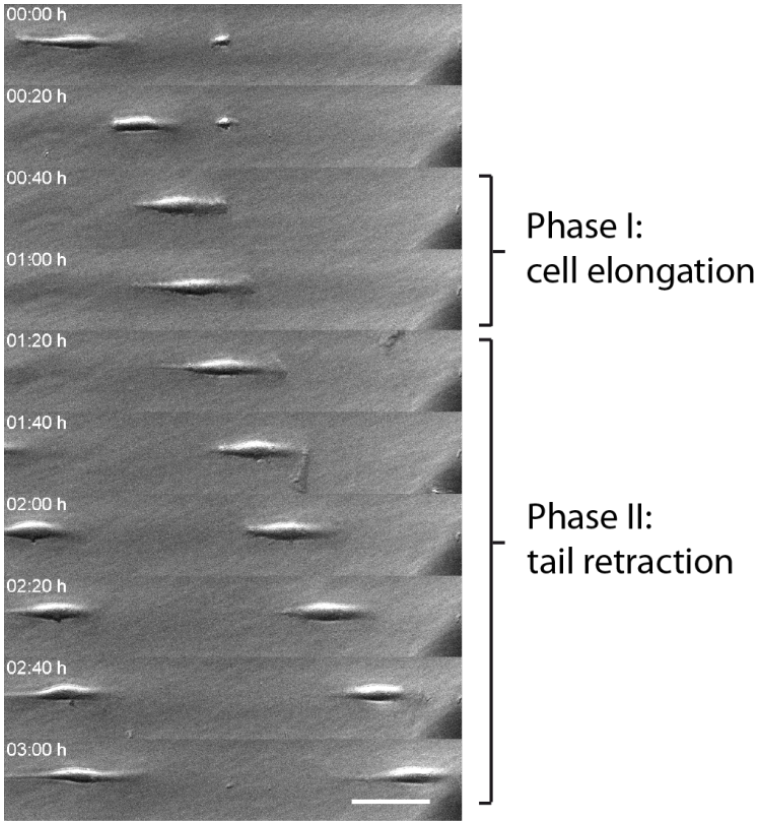

Figure 50: 1D topography mimics neuronal migration on soft *in vitro* substrates. C6 rat cells plated on thin adhesive laminin lines exhibit a two-phase motility characteristic for *in vivo* glioma migration. (Scale bar: 50 µm)

In the next step, we confirmed the previously observed neuronal migration characteristics of NNi11, NNi21 and NNi24 cell lines. On hard substrates, Monzo et al. observed static NNi11, while motile NNi21 and NNi24 displayed a fast movement with lower or higher persistence, respectively (Monzo 2018 unpublished). Indeed, we recovered the same migratory behavior on soft PAA hydrogels. Subsequently, we performed static force measurements to screen the mechanical activity of single cells of all three GBM cell lines (**Figure 51**). All cells spatially exerted forces on their cell edges, behaving as a force dipole (Mandal 2014). The traction force magnitude of non-motile NNi11 (3,57 nN) was significantly lower compared to highly motile NNi21 (11,41 nN) and NNi24 (11,98 nN).

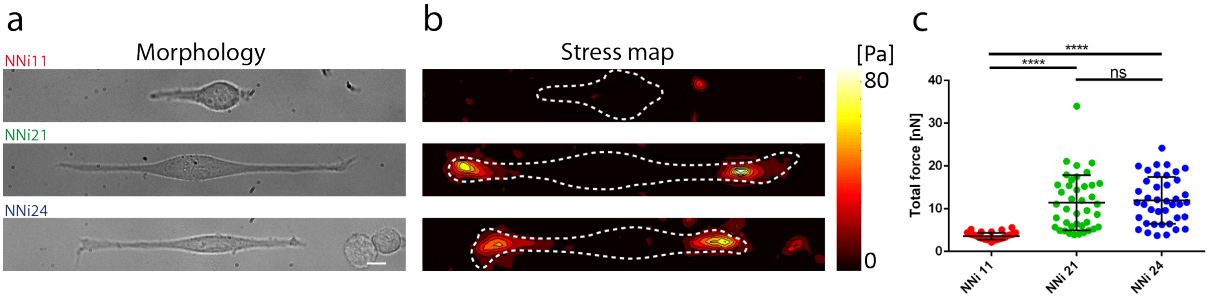

Figure 51: Mechanical interaction between the glioma cells and *in vitro* substrate. A) NNi11, NNi21, and NNi24 adhered to 1D laminin lines on top of 5kPa PAA hydrogels. b) Locally exerted traction stresses show dipole behavior of GBM in 1D. C) Quantitative force measurements show a significantly lower force level for non-invasive NNi11. (Scale bar: 10 µm; Graphs shows mean with standard deviation, statistical comparison: two-tailed p-test)

Monzo et al. have demonstrated that formin 1 (FMN1), a rarely studied regulating protein involved in promoting actin nucleation and cell adhesion (Campellone 2010), was only expressed in fast, stochastic moving NNi21 that formed faster growing, hemorrhagic tumors, compared to NNi24. To test weather FMN1 determines the high invasiveness and/or support hemorrhage, NNi21 FMN1 knockdown cells (FMN1 Kd) were used (Monzo 2018 unpublished). On 1D laminin lines, these knockdown cells possessed a slower motility with decreased persistence characterized by a decreased mechanical cell-substrate interaction (7,25 nN; **Figure 52**).

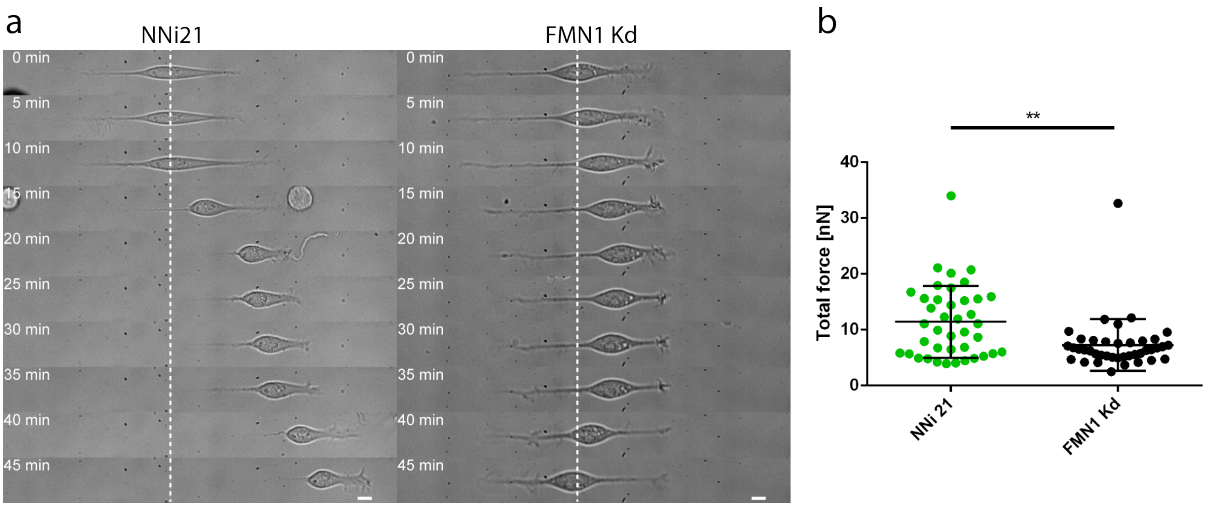

Figure 52: FMN1 knockdown in NNi21 affects its invasiveness. A) NNi21 possess a fast migration on patterned laminin lines, which is impaired when FMN1 is depleted. B) FMN1 promotes the generation of traction forces. (Scale bar: 10 µm; Graphs show mean with standard deviation, Statistics: two-tailed p-test)

4.2.4. Discussion and conclusion

Our collaboration with the Gauthier's laboratory aimed to assist in quantifying the mechanical activity of distinct patient-derived GBM cell lines exhibiting particular invasive and proliferative properties. The collaborative work was part of a bigger project aiming at identifying the crucial role of FMN1 in regulating mechanical pathways involved in cancer progression and invasion. The associated scientific article is currently in preparation. We will give a brief overview of the latest, unpublished results obtained by Monzo et al., which are needed to further discuss the results of this collaboration in the light of our findings on the force-motion relation of mesenchymal cells.

As mentioned previously, Monzo et al. have used three distinct glioma cell lines, and characterized the following migratory parameters (that we have identified to be crucial during stick-slip migration): cell length, migration speed, and adhesion size/dynamics. Static NNi11 were small, while fast migrating NNi21 and NNi24 possessed an elongated cell shape. Cell adhesion of NNi21 and NNi24 were large compared to small clusters of NNi11, which displayed almost no adhesion (**Figure 53**; Monzo 2018 unpublished).

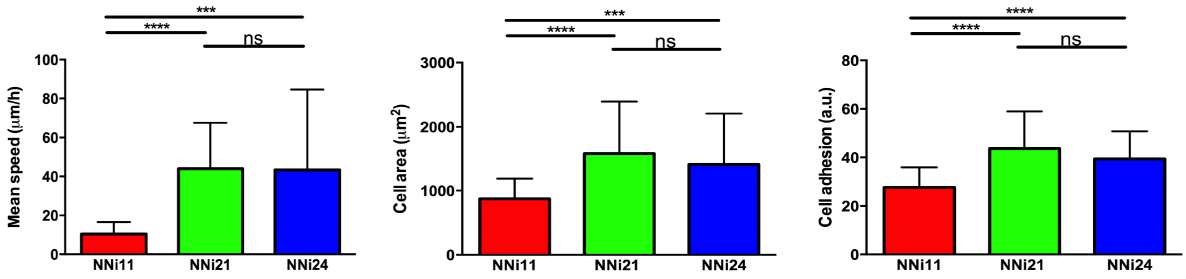

Figure 53: Quantifying cellular parameters that determine cell migration. In comparison the static NNi11, NNi21 and NNi24 both possess a (A) higher migration speed, (B) larger cell area, and (C) an increased cell adhesion (defined by the vinculin signal normalized by the cell area). (Graphs show mean with standard deviation; statistical analysis: two-tailed t-test). [Unpublished data received from (Monzo 2018 unpublished)]

The results of Monzo et al. complemented the observations of the force-motion relation on mesenchymal cell migration. Let us first focus on motile NNi21 and NNi24 cells. Both cell types possessed sufficient cell adhesion to transmit motile forces to the substrate and propel cellular movement. However, the major difference is the hemorrhagic activity of NNi21, which triggers a more rapid death of animals (1.5 months) compared to non-hemorrhagic, slower growing NNi24-based tumors. Our investigation could not explain the hemorrhagic tumor property of NNi21, which we hypothesized might be due to an increased mechanical cell-substrate interaction that locally destroys the blood vessel wall. However, we did not observe any significant difference in force level between the two invasive glioblastoma cell lines. We therefore hypothesize that other biological cell processes, like secretion of soluble factors, might be at play. Another explanation could be due to the distinct migration behaviors of NNi21 and NNi24. NNi21 migrate faster but less persistent, therefore moving back and forth on the blood vessel wall, eventually covering a greater surface area than NNi24, destroying blood vessel faster, while applying the same amount of forces.

Static NNi11 cells, on the other hand, exhibited very low traction forces and smaller cell areas, which was counterintuitive to our proposed stick-slip model, which emphasized that contractility-dependent stabilization of adhesions impairs migration. Our force-motion relation was observed and validated across various cell lines, which adhered to fibronectin and facilitated a mesenchymal migration. Additionally our findings were in accordance with other cell migration studies (Leal-Egaña 2017, Guetta-Terrier 2015). One therefore has to consider that GBM cells moved along laminin tracks in a neuronal cell migration mode

(Monzo 2016), therefore exhibiting a different, additional mode of motility compared to amoeboid or mesenchymal locomotion.

Besides that, studies complementary to our force-motion relation have shown that intracellular forces need to be transmitted to the surrounding ECM in order to propel the forward movement of the cell (Case 2015). This caused the force-motion relation to be non-linear, with two extreme situations: no movement if cell adhesion is too low or two high (Bergert 2015, Barnhart 2011). Indeed, even though vinculin expression was confirmed, NNi11 formed almost no adhesion on either the laminin-based ECM, where cell spreading was lowered, or electrospun nanofibers, from which cells even fell off (Monzo 2018 unpublished). Hence, in the light of the general molecular clutch model, insufficient cell adhesion (clutch disengaged) decouples the intracellular force generation from the ECM (Case 2015), rendering the NNi11 cells unable to move.

The second aim of Monzo's study was to identify key regulating proteins involved in cell mechanics of glioma migration. Their target proteins were formins, which have been shown to be involved in neuronal migration (Monzo 2016). Both motile cell lines, NNi21 and NNi24, were arrested by using a generic formin inhibitor (SMIFH2 (Isogai 2015)). The further screening of formins identified FMN1 as a potential key regulating protein that is supporting invasion, as it was only expressed in stochastic, fast moving NNi21 (Monzo 2018 unpublished).

FMN1 kd decreased the size of cellular adhesions and increased the speed of their turnover (measured via Fluorescence Recovery After Photobleaching). The decrease in cell adhesion ultimately decreased traction forces and inhibited cell migration in FMN1 Kd, as adhesions were unstable and failed to transmit motile forces. Wild type NNi21 expressed FMN1, which led to stable adhesions, facilitated traction forces and promoted neuronal movement on 1D laminin tracks. Though, Monzo et al. observed the opposite than our proposed force-motion mechanism in non-malignant cells (**Chapter 4.1** Hennig et al.; in submission), these results indicate the crucial role of FMN1 in facilitating cell adhesion in order to effectively transfer actin-generated forces to the ECM. All together, these findings led to the conclusion that FMN1 facilitates a robust cytoskeleton cohesion needed to trigger the highly invasive potential of NNi21.

To conclude, the *in vitro* analysis of linear neuronal motility using microfabricated migration assays can help to gain a full understanding of complex GBM motility along blood vessels within the brain. New insights in how the disregulation of cell mechanics contributes to the progression of cancer can identify specific mechanical markers involved in invasiveness and therefore offer novel therapeutic perspectives.

5. Final concluding words

Symmetry principles as well as spontaneous polarization mechanisms are at the core of modern theoretical physics, ranging from high energy to condensed matter physics (Gross 1996). In biology, symmetry breaking is a major key process, giving rise, during development for example, to the emergence of functional structures and patterns that ultimately define organismal fates (van der Gucht 2009). It has been known for decades that biochemical networks control symmetry breaking at the cellular and multicellular level, whereas the importance of the mechanical properties of cells and their environment has been demonstrated only recently. In this context, directional single cell motility is a striking example for which symmetry breaking has generally been attributed to polarization of cytoskeletal components. Different models have in fact been proposed that show the intrinsic capacity of the acto-myosin network to self-polarize symmetry (Li 2010, Yam 2007). Our work however shows that font-rear polarization can even emerge in absence of any prior polarity of the migratory machinery. Astonishingly, instabilities of the mechanochemical link of the cell to its environment via focal adhesion sites are sufficient to trigger migration.

The stick-slip model that we described in this thesis provides strong evidence that spontaneous symmetry breaking occurs firstly via formation of the rear. We therefore entered into the long-lasting debate of unraveling the sequence of events occurring during the initiation of migration (Cramer 2010). Indeed, cells have a variety of ways to move either towards an attracting cue (Yang 2015), away from a repellent stimulus (Yam 2007), or even spontaneously in a random manner (Li 2010). Interestingly, in all three cases the same molecular processes seem to be involved, but differ in their temporal sequence of activation (Cramer 2010). Given the extensive focus on the formation of the front of the cell, we suggest that future studies must place a greater emphasis into understanding the formation of the rear of the migrating cell. Further careful investigation of both, front and rear, for a broad range of cell types at high spatio-temporal resolution using novel approaches based on a combination of experimental techniques will help to settle this continuing discussion.

In addition, holistic understanding of cellular movement, in terms of physics, is still unclear, yet the molecular details are intensively studied. Scientists have uncovered multiple relations concerning cellular shape changes and motion, cytoskeleton rearrangements and shape changes, cytoskeleton dynamics and intracellular forces, while barely addressing the force-motion relation (Tanimoto 2014). Recent research suggests an essential role of cellular forces in driving cell migration by regulating cell adhesion, molecular signaling, and cellular shape changes (Chen 2008). So far, mainly static (Tanimoto 2014) and only a few dynamic (Leal-Egaña 2017) multipolar force analyses have been performed, which do not address the on-set of a migration event. This work is, to our knowledge, the first attempt to examine simultaneously morphometric and force parameters during spontaneous symmetry breaking, by integrating mechanical measurements into a biochemical migration assay. So far, the evolution of traction forces has been a missing piece to gain a full understanding of cellular motility from a physical point of view. Important questions remain about other polarity mechanisms like actin retrograde flow and MTOC positioning that might bias the outcome of our stick-slip scenario.

During the last few decades, both communities, biologists and physicists, have worked together in order to gain a greater qualitative understanding of the complex process of cell migration. Interdisciplinary studies like ours have revealed fundamental key mechanisms in cell motility, which might lead to novel therapeutic or diagnostic approaches of motility-based diseases (Caballero 2015). A valuable example of such is the second study presented in this thesis and performed in collaboration with Dr. Gauthier and Dr. Monzo. The molecularly focused work has identified FMN1 as a potential target protein involved in invasive glioblastoma migration. This is a crucial result, regardless of the identity of this molecule, as, within the last few decades, the survival rate of brain tumor patients has not increased, which is due to the invasive and proliferative nature of glioma that leads to extensive tumor growth and destroys large regions of the brain (Lim 2018, Umans 2017). If migration is limited, localized treatments like surgical resection, chemotherapy and radiotherapy would effectively reduce the tumor, while the risk of cancer relapse at secondary tumor sites would be minimized (Grobben 2002). In general, addressing single cell mechanics in a quantitative manner using newly developed model systems will be essential

in developing anti-migration strategies to fight the progression of brain or any other invasive/metastatic cancer (Guck 2010).

6. Annex

6.1. Study 1) Supplementary data

Supplementary information

Methods and Materials:

Cell culture

RPE1 WT (kindly provided by Laurent Blanchoin, Cytomorpholab Grenoble, France, and stably transfected with vinculin-eGFP by Yekaterina A. Miroshnikova, Institute of Advanced Biology, France), NIH3T3 WT (gift by Helder Maiato, University of Porto, Portugal, and stably transfected with vinculin-eGFP by Yekaterina A. Miroshnikova, Institute of Advanced Biology, France) and NIH3T3 optoGEF_RhoA (given by Mathieu Coppey, Institute Curie, France) were cultured under standard cell culture conditions (37 °C, 5 % CO_2) in Gibco DMEM/F-12 GlutaMAX and Gibco DMEM GlutaMAX (Life technologies), respectively, containing 10 % heat-inactivated FBS (Life Technologies) and 100 ug/ml penicillin/streptomycin (Sigma-Aldrich).

Cells were plated on patterned polyacrylamide (PAA) hydrogels at a low density of 6 x 10^3 cm^{-2} and allowed to spread for 2 to 4 h. For life imaging, the medium of NIH3T3 WT / vin-eGFP / optoGEF_RhoA was replaced by Leibovitz's L-15 medium (Life technologies).

Soft micropatterning

Fibronectin line patterned PAA hydrogels were micro fabricated using the glass technique described by Vignaud et al. *(45)*. In short, 32 mm glass coverslips (VWR) were plasma treated for 30 sec and incubated for 30 min at room temperature (RT) with 0,1 mg/ml poly-L-lysine-grafted-polyethylene glycol (pLL-PEG, SuSoS) diluted in HEPES (10 mM, pH 7,4, Sigma). After washing in deionized phosphate-buffered saline (dPBS, Life technologies), the pLL-PEG covered coverslip was placed with the polymer brush facing downwards onto the chrome side of a quartz photomask (Toppan) for photolithography treatment (5 min UV-light exposure, UVO Cleaner Jelight). Subsequently, the coverslip was removed from the mask and coated with 20 µl/ml fibronectin (Sigma) and 20 µl/ml Alexa546-conjugated fibrinogen (Invitrogen) diluted in dPBS for 30 min at RT. In the meantime, a premix of acrylamide (Sigma), N,N-Methylenebis(acrylamide) (Sigma) and dPBS was mixed (ratio for a final young modulus of 40 kPa described in *(43)* and degased for 20 min. After, fluorescent nanobeads (dark red: F-8807 PS Invitrogen; dragon green: FCDG003 Bangs Laboratories) were added to the premix and the dispersion was sonicated for 5 min (Bandelin Sonorex). To initiate polymerization, 1 µl ammonium persulfate (APS) and 1 µl tetramethylethylenediamine (TEMED) were added to 165 µl premix and vortexed. A drop of 47 µl was immediately places onto the protein-coated glass coverslip and covered with a previously silanized glass coverslip. Salinization was facilitated beforehand by treating the glass surface with 100 % ethanol (Fluka Analytical) containing 0,0035 % (v/v) PlusOne Bind-Silane (GE Healthcare Life Science) and 0,0035 % (v/v) acetic acid (Sigma). After 30 min of polymerization at RT the sandwiched coverslips were emerged in ddH20 and separated with a scalpel. The PAA hydrogel patterned with fibronectin attached to the silanized coverslip and were stored in dPBS at 4 °C for up to 1 week.

Drug treatment

After at least 3 h of cell spreading either one of the following inhibitors was added: 3 µM blebbistatin (Sigma) or 1 µM pF573,288 (Sigma). Control samples were treated with 0,025 % Dimethyl sulfoxide (DMSO, Sigma).

For static imaging, cells were fixed after 2 subsequent hours of incubation with the inhibitor. For live imaging, cells were exposed to the inhibitor for up to 16 h.

Pre-permeabilization and fixation

RPE1 vin-eGFP and NIH3T3 vin-eGFP cells were fixed after 5 hours of spreading. First, cells were pre-permeabilized using 0,25 % Triton X-100 (Sigma) diluted in cytoskeleton buffer (10mM 2-ethanesulfonic acid (MES, Sigma), 100 mM potassium chloride (KCl, Sigma), 3.6 mM Magnesium Chloride Hexahydrate (MgCl $6H_20$, Sigma) and 1.9 mM aminopolycarboxylic acid (EGTA, Sigma) in ddH_2O). The sample was quickly rinsed with the pre-polymerization solution and immediately placed into the fixation buffer (4 % paraformaldehyde, 10 % (w/v) sucrose (Sigma) in cytoskeleton buffer). After 15 min fixation at RT, samples were washed ones with cytoskeleton buffer and blocked for 30 min at RT with blocking buffer (0.5 % bovine serum albumin (BSA, Sigma-Aldrich), 0.1 % sodium azide (NaN_3, Sigma-Aldrich) and 20 mM Glycine (Sigma-Aldrich) in dPBS). For additional staining of filamentous actin (F-actin), samples could be incubated for 30 min at RT with Alexa Fluor® 647 phalloidin (Sigma) diluted in blocking buffer (1:1000). The fixed sample was mounted onto a glass slide using Fluoromount-G (Electron Microscopy Sciences) and stored at 4 °C.

Adhesion imaging and analysis

Static adhesion imaging was performed on fixed samples using an inverted confocal microscope (Leica TCS-SP8) using a 40X objective (oil immersion, numerical aperture 1.3). Individual adhesion sizes of different conditions were extracted with Fiji using an approach described previously *(46).*

For dynamic adhesion imaging, NIH3T3 vin-eGFP, RPE1 vin-eGFP or NIH3T3 optoGEF_RhoA cells were plated on fibronectin line patterned glass substrates to enable Total Internal Reflection Fluorescence microscopy (TIRFm). We used an inverted microscope (AxioVert 200M, Zeiss) equipped with a CCD camera (Clara CCD, Andor) and a 488nm argon laser. Cells were kept at 37 °C and imaged every minute for at least 1 hour. Adhesion dynamics were quantitatively analyzed plotting a kymograph using Fiji. Blue light induced adhesion modification was quantified by measuring the vinculin-iRFP recruitment within the photoactivation area. To do so, the integrated fluorescence intensity was measured per image frame using Fiji.

Fluorescence recovery after photobleaching (FRAP) experiments were performed on NIH3T3 vin-eGFP and RPE1 vin-eGFP plated on patterned 40 kPa hydrogels using an inverted confocal spinning disk microscope (Andromeda, TILL-FEI). Each FRAP experiment was performed as following: prebleach, bleach and recovery. Images were acquired every 500 ms. First, the signal was monitored over 50 time before photobleaching (prebleach). Per cell, two adhesive cluster located at the edge of the cell were bleached within two rectangular regions of interest (ROI) of 7.5 μm^2 using a

488 nm laser at full power (bleach). Afterwards, we followed the fluorescence signal over 100 time points (recovery). After waiting 5 min, the experiment was repeated twice for the same ROIs within the same cell. The extracted fluorescence signal was fit with a bi-exponential curve to extract a slow and fast component ratio equivalent to the free vinculin within the cytosol and the vinculin engaged within adhesions, respectively.

Traction force microscopy

Experimentally, force measurements were conducted on cells after 2-4 hours of spreading using an inverted microscope (Nikon Ti-E) with a Zyla sCMOS camera (Andor) and a temperature control system set at 37 °C.

Single cell force measurements were performed using a method described previously *(24).* Images of fluorescent beads within the stressed and relaxed polyacrylamide substrate were taken before and after detachment of the adherent cell, respectively. The displacement field analysis was done using a homemade algorithm based on the combination of particle image velocimetry and single particle tracking. After drift correction, bead images were divided into smaller sub-images (9.22 μm). Cross-correlating corresponding sub-images in the stressed and reference images yields the mean displacement over each considered region. After correcting this mean displacement, single particle tracking was performed in each sub-image, leading to displacement measurements of high accuracy and spatial resolution of 20 nm. The final displacement field was interpolated on a regular grid with 1.15 μm spacing. From that cellular traction forces were computed using Fourier Transform Traction Cytometry with zero-order regularization *(27, 44)*, under the assumption that the substrate is a linear elastic half space and considering only in-plane displacement and stress (tangential to the substrate). The final traction stress was obtained on a grid with 1.15 μm spacing. To estimate the total force exerted by a cell, local stress values multiplied by the unit grid area are summed over the whole cell area. All calculations and image processing were performed with Matlab.

1D dipole and quadrupole analysis

Cells on lines are analyzed in 1D by projecting and summing all cell-exerted traction on the axis of the line. Typically, the 1D traction exhibit two peaks, one at each cell edge, that are respectively oriented toward the positive and negative directions, forming a contractile dipole. First, small stress values corresponding to noise (less than 10 % of the stress peak value) were filtered out. Then, plus- and minus-oriented tractions were considered separately. The first order moment of each traction peak was used to derive the center of mass for each traction peak: $x_s = (\int x T_s dx)/(\int T_s dx)$, where the sign s is either + or – referring to the considered traction direction. Then, the width of each stress peak was evaluated by computing its second-order moment centered on each center of mass, x_s, by: $D_s = \int (x - x_s)^2 T_s dx/(\int T_s dx)$. Finally the asymmetry factor is obtained from the normalized difference between the width of + and – oriented traction, $(D_+ - D_-)/(D_+ + D_-)$. This factor is closely related to the 'force quadrupole' used in other works. It has values between -1 and 1. Its amplitude quantifies the degree of force asymmetry (0 corresponding to a symmetric stress distribution) and its sign indicates the direction of this asymmetry.

In this way, the force asymmetry is evaluated at each time point (one point every minute) on TFM movies of cells on lines. To statistically investigate the force-motion relation, we divided the 4 to 5-hour movies into 30-minute intervals. For each time interval, the cell was deemed to be either in a static or a moving phase based on the average velocity of its nucleus. Static phases correspond to velocity slower than 0.1 μm/min, while moving phases correspond to velocity higher than 0.3 μm/min. The mean asymmetry amplitude was calculated by averaging the force asymmetry factor over each 30-minute-interval. Since cells motion have equal probability to be directed toward the right or the left, raw asymmetry values are centered around zero. To distinguish noise from motion induced asymmetry, the final asymmetry amplitude was defined as the raw asymmetry values multiplied by the sign of the cell velocity (averaged over the same interval).

F-actin staining and asymmetry analysis

SiR-actin (Spirochrome) was used to stain F-actin within life cells. Cells were incubated over night with 100 nM SiR-actin and 10 μM verapamil. A Nikon Ti-E inverted microscope was used to image the cytoskeleton structure over several hours.

Actin fluorescence images were analyzed to quantify actin asymmetry using the following procedure: after smoothing, the image was divided at the position of the cell nucleus into two sub-images, corresponding to the left and right edges of the cell. The transverse actin distribution width each extremity, W_{left} and W_{right}, were estimated by projecting each sub-image onto a line orthogonal to the migration axis and by calculating the centered second order moment of the resulting profile. Comparing these two widths enabled us to quantify asymmetries in the shape of the actin distribution. The asymmetry factor was defined as: $\frac{W_{right}-W_{left}}{W_{right}+W_{left}}$

Optogenetic experiments

Our Nikon Ti-E inverted, fluorescent microscope was equipped with a digital mirror device (DMD, Nikon) to locally control area of illumination with a 460 nm LED. NIH3T3 optoGEF_RhoA cells were plated as described on patterned hydrogels and kept at 37 °C during all optogenetic experiments. Images were acquired every 15 or 60 seconds. First, cells were observed before photo-stimulation for at least 10 min. During the subsequent photo-activation cycle, one side of the cell was locally exposed to 150 ms blue light pulses every minute over a period of at least 15 min. A relaxation period of at least 15 min was done in between two subsequent photo-activation cycles. We were able to perform bead imaging for TFM and/or actin imaging in parallel with the optogenetic stimulation.

Position tracking and cell length/velocity measurements

Single cell tracking and extraction of morphometric parameters (front, rear and nucleus positions) was performed on time-lapse brightfield images of cells migrating on lines by manually clicking on those structures on each frame. Images acquired in the present work (RPE and NIH cells) have been recorded every 5 minutes, while data originating from the cell race have an interval of 15 minutes between frames.

The time traces of the morphometric parameters were analyzed in Matlab. First, the cell center position (middle of the front and rear positions) was smoothed by convolution with a 15 min flat window. The migration velocity and cell length were calculated over an interval of 30 min. We chose this short interval to capture the instantaneous velocity (knowing that the cell race videos have a temporal resolution of 15 min). Then these instantaneous velocities (in absolute value) and the cell length were averaged over one time-trace corresponding to one cell. Each cell was represented by one data point in the velocity versus length graph depicting different cell types. Videos of PRE1 and NIH3T3 (with or without inhibitor) had a higher time resolution (1 frame every 5 minutes) but were smoothed and migration parameters were calculated over the same time interval used for the cell race data.

Statistical analysis

All data was plotted and statistically analyzed in GraphPad Prism (GraphPad Software, San Diego, CA, USA). To test the significance in between data, we performed two-tailed Student's T-tests. Error bars on graphs represent the standard deviation. If a linear fit was applied, GraphPad Prism computed it with a confidence interval of 95 %.

Supplementary figures:

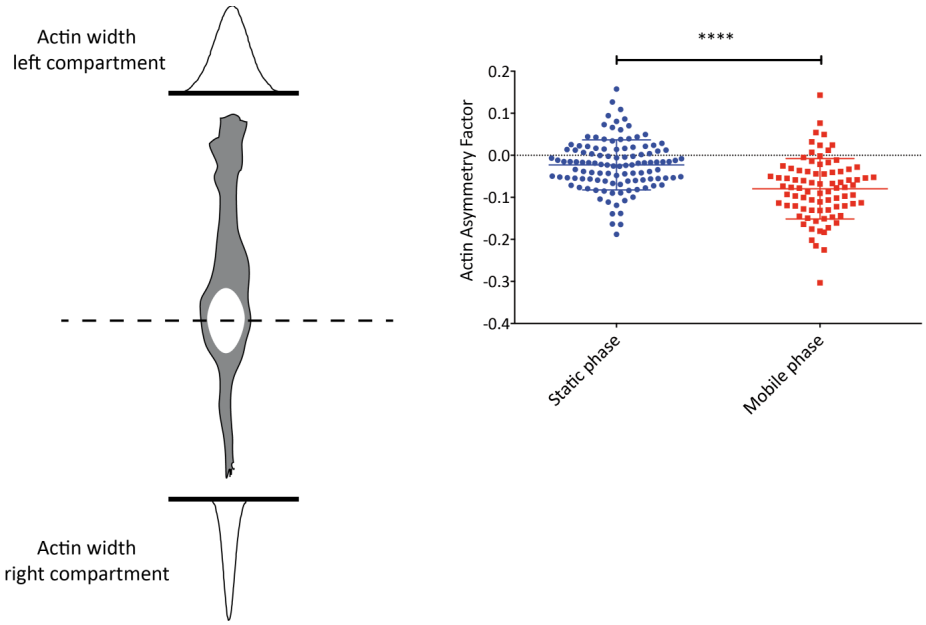

Fig. S1 | Polarization of the actin cytoskeleton. Schematic representation depicts the actin asymmetry factor calculation, which was based on the comparison of the actin distribution of either cell side. The quantification reveals a symmetric distribution during static phases. This symmetry is broken when cells moves. Statistical significance tested with unpaired t-test ($P < 0.05$), error bars on graphs show standard deviation from the mean ($n = 10$ cells).

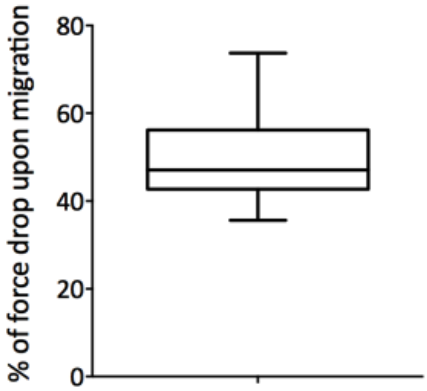

Fig. S2 | Mechanical interaction between the cell and its environment decreases upon the initiation of migration. Relative drop of the total traction forces of single cells. (*n* = 10 cells)

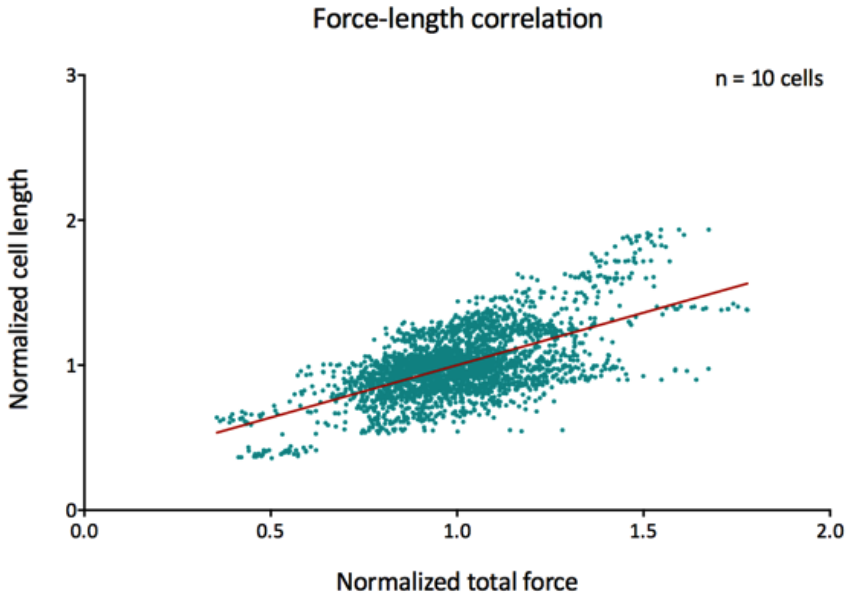

Fig. S3 | Force-length correlation during stick-slip migration. Cells during stick phases elongate while increasing their mechanical interaction with the substrate. Upon initiation of migration (slip phase), both cell length and total force level drop due to the detachment of the rear. Blue: normalized instantaneous cell length and total force during a single cell's migration trajectory. Red: Linear fit.

Movie S1 | **Adhesion dynamics of RPE1 and NIH3T3 cells.** TIRF imaging of stably expressed vin-eGFP quantitatively revealed a fast adhesion turnover for fast migrating RPE1 cells compared to slow migrating NIH3T3 cells. Adhesion patches for RPE1 slide and disassemble with the retracting rear, while NIH3T3 cells rapidly reattach their back adhesions.

References supplementary information:

45. Vignaud, T., Ennomani, H. and Théry, M., Polyacrylamide hydrogel micropatterning. *Methods in cell biology* **120**, 93-116 (2014).

43. Tse, J.R. and Engler, A.J., Preparation of hydrogel substrates with tunable mechanical properties. *Current protocols in cell biology*, 10-16 (2010).

46. Horzum, U., Ozdil, B. and Pesen-Okvur, D., Step-by-step quantitative analysis of focal adhesions. *MethodsX* **1**, 56-59 (2014).

24. Tseng, Q., Wang, I., Duchemin-Pelletier, E., Azioune, A., Carpi, N., Gao, J., Filhol, O., Piel, M., Théry, M. and Balland, M., A new micropatterning method of soft substrates reveals that different tumorigenic signals can promote or reduce cell contraction levels. *Lab on a Chip* **11** (13), 2231-2240 (2011).

27. Mandal, K., Wang, I., Vitiello, E., Orellana, L.A.C. and Balland, M., Cell dipole behaviour revealed by ECM sub-cellular geometry. *Nature communications* **5**, 5749 (2014).

44. Sabass, B., Gardel, M.L., Waterman, C.M. and Schwarz, U.S., High Resolution Traction Force Microscopy Based on Experimental and Computational Advances. *Biophysical journal* **94** (1), 207-220 (2008).

6.2. Study 3) De Mets et al. "Fast and robust fabrication of reusable molds for hydrogel micro-patterning"

One of our expertises in Dr. Balland's group is microfabrication of defined adhesive islands of ECM proteins on top of soft hydrogels. During the course of my thesis, I was involved in a side project together with a PhD student at that time, Dr. Richard De Mets, who worked on the microfabrication of re-usable molds to micropattern soft PAA substrates in a fast and robust manner. The technique relied on patterned polymer brushes that were grafted on top of a glass substrate. The patterned glass functioned as a template to transfer patterns of fibronectin to PAA gels. My contribution to this project can be seen in **Figure 4** of the scientific article, which was published *Biomaterials Science* in 2016.

Biomaterials Science

PAPER

View Article Online
View Journal

Cite this: DOI: 10.1039/c6bm00364h

Fast and robust fabrication of reusable molds for hydrogel micro-patterning

Richard De Mets,[a,b,c] Katharina Hennig,[a,b] Lionel Bureau*[a,b] and Martial Balland*[a,b]

Received 27th May 2016,
Accepted 16th September 2016
DOI: 10.1039/c6bm00364h
www.rsc.org/biomaterialsscience

Mechanical interactions between cells and their microenvironment are crucial for fundamental biological processes ranging from migration to differentiation. This has led, over the last decades, to the development of new ways to culture cells. Living cells are now grown not only on glass coverslips, where they completely lose the mechanical and geometrical constraints coming from their microenvironment, but also on soft patterned substrates that mimic the rigidity and spatial information of their *in vivo* niches. Microfabrication processes have thus logically emerged has new tools to create model environments to probe the behavior of biological objects. Here, we present a method for fast and robust protein micro-pattern transfer onto polyacrylamide hydrogels that can be used for traction force microscopy. The technique relies on the elaboration of glass templates bearing patterned polymer brushes, which can be re-employed several times for the production of patterned gels without the need to repeat the critical microfabrication steps.

1 Introduction

Surface micropatterning is a powerful tool for the design of cell-based assays and sensors, or for fundamental studies of cellular response to environmental cues. Surface chemistry and microfabrication techniques allow creating substrates onto which adhesion can be tuned so as to obtain regular 2D arrays of cells immobilized under a defined geometrical constraint. Such patterns have proven to be highly valuable for *e.g.* statistical analysis of the response of cells cultured in a well-controlled microenvironment.[1] In this context, a recent focus has been put on the development of micropatterned hydrogels for their interest in mimicking the mechanical properties of the physiological cell environment,[2,3] but also for their use in the measurement of cellular traction forces as a mechanical readout of cell phenotypic behavior (cancer cell diagnosis).[4]

Typically, surface patterning strategies of soft hydrogels fall into two classes:[2] (i) direct patterning of adhesion proteins or peptide fragments from the extracellular matrix (ECM) onto the surface of an elastic and crosslinked gel,[4–10] and (ii) pattern transfer upon gelation.[11–14] Methods of type (i) combine physical deposition of protein patterns with chemical immobilization at the gel surface, achieved *e.g. via* photochemical[4,5,9] or activated ester[10] coupling, hydrogen-bonding,[6] or redox activation/coupling.[7] Strategies of type (ii) are nominally simpler, as they rely on the fact that ECM proteins, pre-patterned on a counter-surface, get encased in the vicinity of the gel surface during its polymerization and crosslinking, and subsequently displayed at the cell/gel interface after removal of the casting counter-surface.

All these techniques, based on microcontact printing or photo-lithography/chemistry, have led to the successful elaboration of patterned hydrogels. Yet, they may exhibit drawbacks in terms of ease of use (*e.g.* needed equipments or large number of fabrication steps), spatial resolution, large scale homogeneity of the patterns, or stability of the produced surfaces. Most noticeably, these well-established techniques require that the whole series of elaboration steps, and in particular those associated with micropatterning, be repeated each time a new gel is produced. In the hands of non-expert users, this may lead to cumbersome reproducibility issues from one gel to the next.

Here, we describe a method that combines the simplicity of pattern transfer strategies with the superior protein-templating properties of polymer brushes.[15,16] We show that high density brushes of poly(*N*-isopropylacrylamide) (PNIPAM), grafted to flat substrates *via* the so-called "grafting-from" method and patterned by direct photo-ablation, represent a reliable, fast and cost-effective means to design micro-patterned molds that can be repeatedly used for the transfer of proteins onto

[a]Univ. Grenoble Alpes, LIPHY, F-38000 Grenoble, France.
E-mail: lionel.bureau@univ-grenoble-alpes.fr, martial.balland@univ-grenoble-alpes.fr
[b]CNRS, LIPHY, F-38000 Grenoble, France
[c]Mechanobiology Institute, National University of Singapore, Singapore 117411

polyacrylamide (PAA) gels. The method we report combines several important features from other existing techniques: (i) the ease of use of transfer methods (no need for gel/proteins chemical coupling), (ii) the large scale homogeneity (up to centimeters square) and sub-cellular spatial resolution (micrometer range) of the patterned gels obtained with photo-patterning techniques.[2] Moreover, we show that the brush-based micro-molds can be straightforwardly reused, and thereby allow for the production of several tens of gel samples without noticeable loss of cell adhesion confinement. This feature greatly improves the reproducibility of the prepared gels, and considerably reduces the number of steps required for batch sample preparation.

2 Experimental procedure

The protocol to fabricate micropatterns on soft hydrogels with a subcellular resolution relies on the following successive steps:

(1) Elaboration of a master mold made of patterned PNIPAM brush grafted on a glass surface,

(2) Coating of the mold *via* non-specific adsorption of ECM proteins,

(3) Casting of a pre-gel solution on the coated master,

(4) After gelation, lifting off the hydrogel layer bearing the transferred protein patterns.

Owing to the covalent grafting of the polymer brush on its substrate, the master mold is not degraded at the lift-off step, can be readily cleaned with usual solvents, and reused directly from step 2.

2.1 Materials

N-Isopropylacrylamide (NIPAM, 99%), 3-aminopropyltriethoxysilane (APTES, 99%), triethylamine (TEA, 99.7% pure), copper(I) chloride (CuCl, 99% extra pure), 1,1,7,7-pentamethyldiethylenetriamine (PMDETA, 99%), and 2-bromo-2-methylpropionyl bromide (BMPB, 98% pure) were purchased from Acros Organics. Acrylamide (AA, 40% solution in water), bisacrylamide (BisA, 2% solution in water), ammonium persulfate (APS, 98%), *N*,*N*,*N*,*N*-tetramethylethylenediamine (TEMED, 99%), hexadecane, acetic acid, and bind-silane were obtained from Sigma-Aldrich. Absolute ethanol and dichloromethane (DCM) were from Fischer Chemicals (Laboratory Grade). Ultrapure water (18.2 MΩ cm) was obtained from a Millipore Synergy system.

All reagents were used as received except NIPAM, which was recrystallized twice in *n*-hexane (Normapur, VWR) in order to remove the polymerization inhibitor present in the delivered bulk monomer.†

†As an alternative to recrystallization, the polymerization inhibitor, monomethyl ether hydroquinone, can be removed by preparing a solution of the as-received NIPAM monomer and passing it over a commercially available "inhibitor-remover" column.

Fibronectin from bovine plasma was obtained from Sigma before dilution in phosphate buffer saline solution (Sigma). Fibrinogen conjugated with Alexa 546 dye (Invitrogen) was used to visualise the micropattern.

12 mm-thick circular glass plates (50 mm in diameter) were purchased from Thorlabs (WG12012) with a specified flatness of $\lambda/10$.

Deep-UV patterning was performed using quartz-chromium photomasks (Delta Mask, Toppan, Selba Tech) and a UV/O_3 cleaner (model 342-220, Jelight).

Fluorescent carboxylated latex particles of 200 nm in diameter from ThermoFischer were loaded in the gels in order to track displacement fields in Traction Force Microscopy experiments.

Fluorescence, brightfield and traction force microscopy were done on a Leica SP8 confocal microscope equipped with an incubator allowing for CO_2 and humidity control and maintaining the temperature at 37 °C.

2.2 Grafting and patterning of polymer brushes

This first step of the protocol, illustrated on Fig. 1, is based on surface-initiated Atom Transfer Radical Polymerization (ATRP) and has been previously described in ref. 17. In contrast to our previous work, we use here thick glass plates as the substrates instead of coverslips. This ensures a good mechanical resistance of the molds to repeated transfers and sufficient flatness for large scale homogeneity of the patterns transferred to PAA gels.

(i) A glass substrate is first rinsed with ethanol, dried in a stream of nitrogen, and subsequently plasma-cleaned.

(ii) The substrate is then immersed, for 1 minute, in an aqueous solution of APTES of concentration 2×10^{-3} M that has been prepared and stirred for two hours before use (Fig. 1a).

(iii) After rinsing with water and drying, the sample is immersed, for 1 minute, in a solution of DCM (25 mL) containing TEA (1.25 mL) and BMPB (250 μL), followed by rinsing with DCM, ethanol and water (Fig. 1b and c).

(iv) After drying, the functionalized side of the substrate is put into close contact with a quartz-chromium photomask, using a few μL of hexadecane spread at the sample/mask interface in order to ensure tight contact. The substrate is irradiated with UV light ($\lambda \leq 185$ nm) through the photomask for about 2 minutes (Fig. 1d), then carefully rinsed with ethanol and dried. At this stage, the functional layer elaborated at step (ii) and (iii), which acts as a layer of initiating sites for the following polymerization step, has been selectively de-activated in the UV-irradiated regions.

(v) A solution of NIPAM (1 g), PMDETA (150 μL) and water (20 mL) was prepared in a flask, sealed with a rubber septum and bubbled with argon for 30 minutes before addition of CuCl (25 mg) and stirring. This solution is then poured onto the surface of the above-patterned substrate, polymerization is left to proceed for 2 to 5 minutes in the lab atmosphere, and the substrate is finally rinsed with water and dried (Fig. 1e). PNIPAM brushes grown under such conditions typically

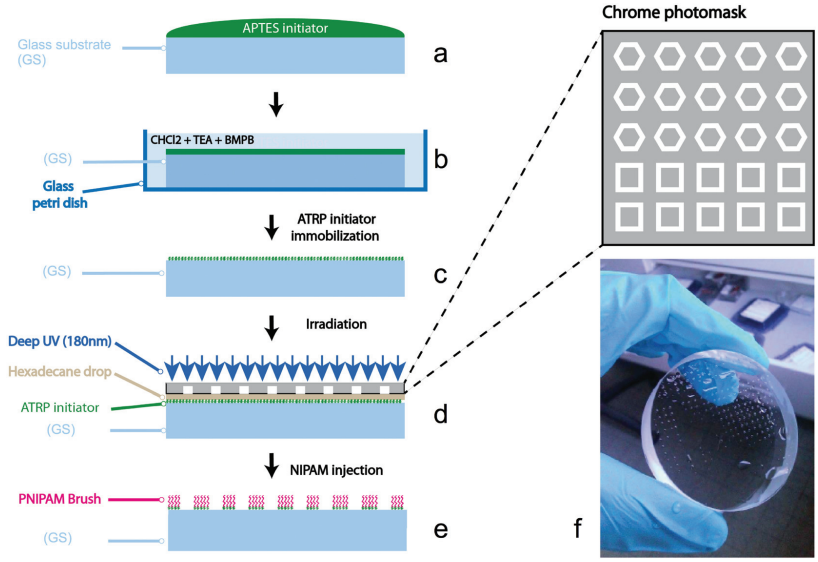

Fig. 1 Sketch of the various steps leading to patterned PNIPAM brushes grafted onto glass surfaces. We first create surface functionalization with ATRP initiator (a to c), then we proceed to deep-UV patterning of the initiator layer (d). After NIPAM injection, polymerization occurs leading to a patterned PNIPAM brush on the glass surface (e). This patterned PNIPAM brush, which displays the characteristic dewetting pattern shown in (f) after rinsing with water, will serve as a reusable template for subsequent polyacrylamide patterning.

display a dry thickness h_{dry} increasing from 50 to 100 nm for polymerization times going from 2 to 5 minutes, as measured by ellipsometry on oxidized silicon wafers that were functionalized in parallel to the glass substrates. Alternatively, this last polymerization step can be done using the so-called "activators regenerated by electron transfer" (ARGET) ATRP procedure,[18,19] which avoids protection of the copper catalyst from oxygen and can be fully performed in ambient air.

We have previously shown, from force measurements using the Surface Forces Apparatus[16,20] and from optical reflectometry characterization,[19] that the above-described functionalization scheme yields brushes having a grafting density of $\sigma \simeq 0.3$ chain per nm^2. From such a density, which is related to the brush dry thickness and the polymerization index N *via* $h_{dry} = Na^3\sigma$ (see *e.g.* ref. 20), we compute, using a monomer size of $a = 0.6$ nm,[19] a polymerization index N ranging from 770 to 1540 monomers per chain under the present conditions. Moreover, we have shown recently, using Atomic Force Microscopy (AFM), that our deep-UV patterning method allows us to obtain patterned brushes displaying geometric features with a spatial resolution of ~1 μm.

As a qualitative check for the success of the above-described procedure, rinsing of the brush-coated substrate with water should result in a characteristic dewetting pattern, where water droplets get pinned on the most hydrophilic regions of the surface and arrange in a periodic array, as shown on Fig. 1f.

In the following, we call "mold" the above-described glass substrate functionalized with a patterned PNIPAM brush.

2.3 Protein coating

Once a mold has been fabricated, its surface is coated with the proteins of interest as follows (see Fig. 2). The substrate is first cleaned with phosphate-buffered saline (PBS, pH 7.4). We then put a 100 μL drop‡ of protein solution composed of 20 μg mL^{-1} fibronectin and 5 μg mL^{-1} fibrinogen-Alexa§ in 10 mM Hepes (pH 8.5) (see Fig. 2A-1). Unless otherwise stated, experiments have been performed using such solution concentrations for coating. We have also investigated the effect of varying the concentrations by using fibronectin/fibrinogen solutions at 2/2, 20/20 and 100/100 μg mL^{-1}. In order to uniformly coat a well defined region of the mold, this drop is sandwiched between the patterned substrate and a glass coverslip (see Fig. 2A-2) bearing a homogeneous PNIPAM brush (elaborated as described in the previous section). Such a functionalized counter-surface is chosen so as to prevent protein adsorption onto it, hence reducing loss of proteins and maximizing the amount adsorbed on the brush-devoid regions of the mold. The solution is incubated for one hour at room

‡ This volume is used for a 20 × 20 mm glass coverslip and must be adapted to the coverslip size.

§ Fibrinogen-Alexa fluor 546 nm is employed here as a fluorescent marker used for pattern visualization and characterization by epifluorescence microscopy.

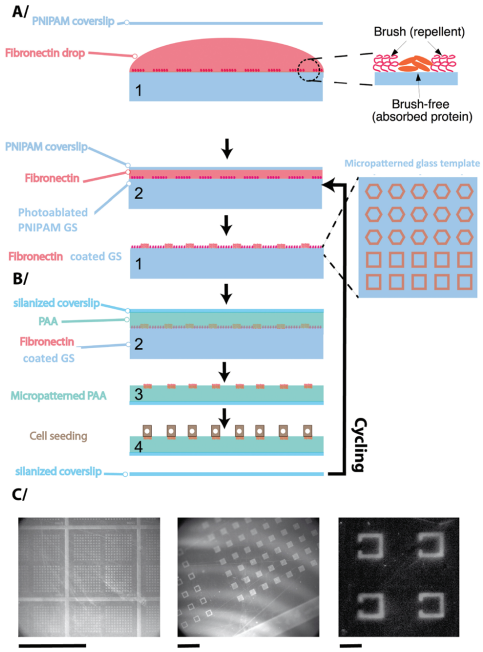

Fig. 2 Polyacrylamide patterning from PNIPAM glass template. (A) A drop of ECM protein (here fluorescent fibrinogen mixed with non fluorescent fibronectin) is squeezed in between the patterned PNIPAM glass surface and a previously treated PNIPAM coverslip to ensure an homogeneous and maximum transfer of proteins onto the glass template. (B) After rinsing the functionalized glass surface with PBS a drop of polyacrylamide is sandwiched between the patterned PNIPAM surface and a silanized glass coverslip. After 45 min polymerization, the silanized coverslip is detached from the glass surface while ECM protein are transferred onto the gel. (C) Fibronectin and fibrinogen coating on micropatterned Polyacrylamide at different magnifications. Scale bars are respectively 1.5 mm (left), 100 μm (middle), 30 μm (right).

temperature, protected from external light. Finally, the coated mold is washed twice in a PBS bath in order to remove unbound proteins.¶

2.4 Gel casting and protein transfer

Coating of the mold with proteins is immediately followed by gel casting, as described below (see Fig. 2).

A 20 mm diameter glass coverslip is first cleaned and silanized at room temperature by dipping during 5 min into a bind-silane solution composed of 161 μL acetic acid (10% aqueous solution), 5 mL of ethanol 100% and 18.5 μL of bind-silane. A solution containing 6.67% (v/v) acrylamide and 0.167% (v/v) bis-acrylamide is mixed with 1 μL of 10% (w/v) APS and 1 μL of TEMED. This yields PAA gels exhibiting an elastic modulus of $E \simeq 6$ kPa after curing, as measured by AFM.[4] A 40 μL drop of this solution is put directly on the mold.‖ The silanized coverslip is placed over the droplet, and the gel is left for curing at room temperature for 45 minutes (see Fig. 2B-2). The top coverslip, along with the crosslinked gel bound to it through the bind-silane layer, is then carefully peeled off the mold after immersion in water (see Fig. 2B-3). The gel is washed three times with PBS before seeding cells.

2.5 Cell plating

We have used Mouse Embryonic Fibroblasts (MEF, kindly provided by Dr Olivier Destaing, Institute for Advanced Biosciences, La Tronche, France) for our experiments. We first collect cells from their culture flask using trypsin or trypsin-EDTA (ethylenediaminetetraacetic acid). We then dilute and rinse the EDTA solution with pre-warmed culture medium and resuspend cells using a 1 mL micropipette in order to separate them well. A cell suspension, with 10^4 to 2×10^4 cells per mL,** is subsequently seeded on the gel surface, followed by gentle mixing in order to evenly distribute the cells over the surface. The gel-bearing coverslip is then placed inside an incubator at 37 °C under quiescent conditions. Finally, we wash unattached cells 30 minutes†† after seeding, using equilibrated pre-warmed culture medium, and let the remaining cells adhere and spread on the gel for 2 more hours at 37 °C before imaging (see Fig. 2B-4).

3 Results and discussion

3.1 Pattern transfer

As already shown in recent studies,[15,16] patterned polymer brushes elaborated using the grafting-from method are highly efficient substrates for protein patterning on hard surfaces. This efficiency stems from the high grafting densities that can be reached with grafting-from: according to theoretical studies of protein adsorption onto surfaces bearing brushes of neutral polymers, high-density brushes behave as superior protein-repellent layers owing to steric exclusion that prevents protein insertion within the polymer layer.[21] More specifically, theoretical predictions have been obtained for protein adsorption in the presence of PNIPAM brushes, which exhibit a hydrophilic to hydrophobic transition, associated to a marked change in conformation, across a Lower Critical Solution Temperature of 32 °C.[22,23] They show that protein-repellency is maintained and controlled by steric penalty even for hydrophobic and dehydrated PNIPAM brushes, provided that the brush grafting density is large enough[22] (typically $\sigma \geq 0.1$ chain per nm^2).

¶This coating procedure has been designed in order to use low solution volumes, requiring as little as possible of the protein of interest. However, for the sake of simplicity and if protein amount is not an issue, coating of the mold with protein can be done by directly immersing the substrate into a bulk solution.

‖The volume of the drop and the area of the silanized coverslip set the thickness of the gel (100 μm under the present conditions).
**This is to be adapted to the pattern density of the substrate.
††This may depend on the cell type.

This have been confirmed experimentally by various groups.[16,24] On this basis, our choice of patterned PNIPAM brushes in the present work has been motivated by the two following points: (i) they ensure that non-specific protein adsorption occurs only in the UV-exposed regions that are devoid of polymer, while the brush-bearing background remains protein-repellent (see sketch on Fig. 2A) irrespective of the polymer hydration state (hence irrespective of the temperature at which the protein coating is performed), and (ii) PNIPAM growth by surface-initiated ATRP is fast and rather tolerant to the presence of oxygen during the polymerization reaction, which simplifies the grafting procedure and sample handling. In order to investigate how the protein patterns thus obtained can be transferred to the surface of gels, we have used fluorescence imaging to observe and characterize the surface of PAA gels after they have been lifted off the mold.

On Fig. 2C, we show that protein patterns having well-defined micrometer-scale features are indeed present at the surface of the PAA gels, and are homogeneously distributed over large scales. Moreover, as illustrated in Fig. 3A, quantifying the fluorescence intensity across such patterns reveals a very good signal-to-noise ratio, which shows that proteins are well localized in the patterned regions, while the background surface of the gel is essentially devoid of them. To assess transfer homogeneity, we have measured the fluorescence intensity distribution over 50 contiguous patterns spanning a surface of 0.7×0.4 mm^2. Doing so, we compute a relative variation of intensity on the order of 20–25% (see Fig. 3B), which shows that pattern homogeneity at the gel surface is satisfactory.

In the spirit of the study reported in ref. 14, we have qualitatively investigated the effect of the lift-off step on protein transfer: we have checked that the peeling direction had no effect on the spatial homogeneity of the fluorescence intensity detected on the patterns. We did not observe any gel fracture or loss of integrity upon lift-off. Also, no significant difference was observed upon transfer of protein patterns using PAA gels of 5 or 40 kPa.

Moreover, we observe that the fluorescence intensity of the patterns at the gel surface, imaged under the same conditions for excitation and detection, increases with the protein concentration used for coating of the master mold, as illustrated in Fig. 4. This indicates that the amount of proteins transferred onto the gel surface can be controlled by adjusting the bulk concentration of the solution used at the coating step.

In order to estimate further the efficiency of protein transfer with our method, we have quantified and compared the fluorescence intensity measured across the patterns before and after the gel has been lifted off the mold. As shown in Fig. 5A, we observe only a slight decrease of fluorescence intensity upon lift-off, which suggests that a large fraction of the proteins adsorbed on the mold is transferred to the gel.

As in previously reported pattern transfer techniques,[2,11–14] our protocol is free of any chemical functionalization of the gel surface. The presence of proteins therefore most likely results from the fact that, upon curing and crosslinking of the pre-gel in contact with the patterned mold, proteins get physically embedded in the gel network, in the vicinity of its surface. This mechanism being *a priori* not dependent on the type of protein used, we anticipate that the method, tested here only with fibronectin/fibrinogen, should be applicable to other ECM proteins with only marginal modifications. As a rule of thumb, we expect that proteins should get efficiently embedded within the gels as long as their size is larger than the meshsize (ξ) of the PAA network forming the gel. This characteristic length scale can be estimated from the elastic

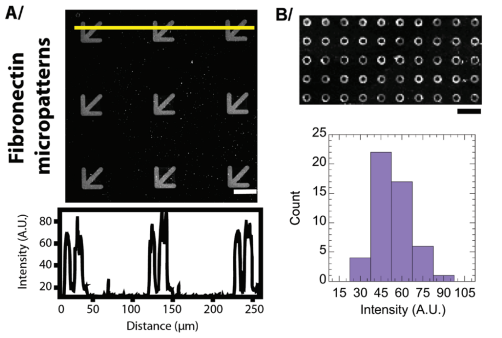

Fig. 3 (A) Linescan of fluorescence intensity along line (yellow) showing the homogeneity of fluorescence staining and reproducibility of micropattern shapes. Scale bar represents 30 μm. (B) Upper panel: Fluorescence image showing 50 adjacent micropatterns (scale bar: 100 μm). Lower panel: Histogram of intensity distribution over the 50 micropatterns shown above. Intensity distribution has a mean value of 55 and a standard deviation of 12.

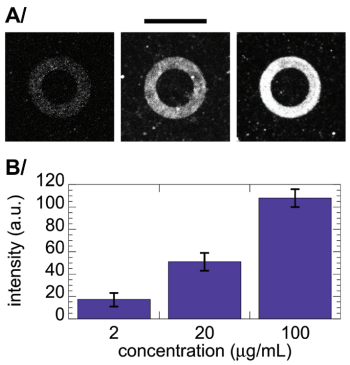

Fig. 4 (A) Images of patterns at the surface of gels obtained after coating of the PNIPAM mold with a solution containing 2 μg mL^{-1} (left), 20 μg mL^{-1} (middle), and 100 μg mL^{-1} (right) of fibronectin/fibrinogen. Scale bar: 30 μm. (B) Pattern intensity as a function of fibronectin/fibrinogen concentration. Average values and error bars (±1 standard deviation) correspond to measurements over 8 adjacent patterns on each gel.

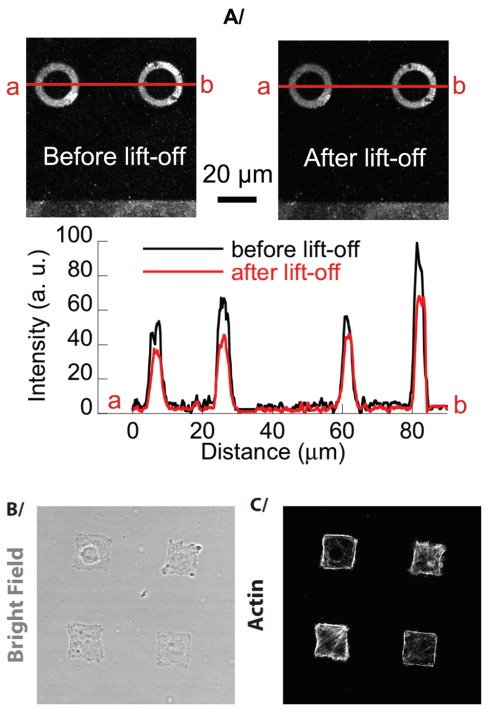

Fig. 5 (A) Upper panels: Fluorescence images of micro-patterns before (left) and after (right) the gel has been lifted off the glass template. Scale bar represents 20 μm. Lower panel: Linescan of fluorescence intensity (along the red line from a to b) before and after gel lift-off, showing the slight decrease in intensity observed upon transferring proteins from the mold to the gel. (B) MEF cells (phase contrast) plated on arrow shaped micropattern on Polyacrylamide and (C) their related actin immunofluorescent staining.

shear modulus of the gel ($G = E/3$ for incompressible materials such as hydrogels), which is related to the mesh size by $G \sim k_B T/\xi^3$, where k_B is the Boltzmann constant and T the temperature.[25] Taking $G \simeq 2$ kPa, we estimate ξ on the order of 10 nm. This suggests that bulky ECM proteins such as fibronectin, fibrinogen or laminins should easily be trapped within gels of shear moduli as low as a few kPa, whereas smaller globular proteins such as vitronectin might be immobilized only at the surface of gels having tighter meshsizes and moduli of a few tens of kPa.

Finally, we have evaluated the ability of such patterns to efficiently constrain cell adhesion. As illustrated in Fig. 5B and C, brightfield microscopy and fluorescence imaging of the actin skeleton of MEF seeded on the gel surface show that cell adhesion is indeed confined and controlled by the shape of the patterned region. This indicates that ECM proteins close to the gel surface are accessible to the cells, and that the bare PAA background surface exhibits intrinsically non-adhesive properties. We have obtained a similarly good cell confinement over the patterned gels with NIH 3T3 cells instead of MEF (data not shown).

3.2 Reusability and storage

One of the main advantage of our method over other transfer techniques is that one mold can nominally be reused several times, thanks to the robustness of the covalently bound polymer brush. This is an important improvement with respect to other patterning protocols that rely on the use of less robust and more weakly anchored polymer layers (typically poly(L-lysine)-*graft*-poly(ethylene glycol)) for pattern definition.[2]

We have assessed this feature by performing repeated coating/casting/lift-off using the same mold, and by monitoring the shapes of cells on the various generations of gel produced this way. Between each series of experiment, the mold has been simply cleaned by rinsing with milli-Q water, isopropanol 100% and dried in N_2 flow.

We have thus been able to reuse the same mold up to 20 times without noticing any significant loss of cell confinement, as illustrated in Fig. 6. A quantification of the average fluorescence intensity detected on individual patterns at different passages shows that the protein transfer efficiency is essentially unaffected when reusing the mold (see Fig. 6, lower panel). However, we notice that the spatial resolution of the patterns tends to decrease with passage number, and that the lateral size of the protein patterns, hence the size of the cell adhesive features, typically increase by 2 μm between the first and the twentieth use of the mold (see Fig. 6, middle and lower panels).

Our method therefore allows producing several tens of gels with only one microfabrication step. This greatly reduces the length and complexity of the procedure, compared to other

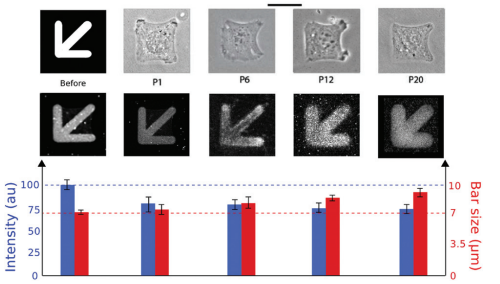

Fig. 6 Upper panel: Phase-contrast images of MEF cells confined by arrow-shaped patterns on the first (P1), sixth (P6), twelfth (P12) and twentieth (P20) gel elaborated with the same mold. Middle panel: Fluorescence images of protein patterns at the same passages. Scale bar: 30 μm. Lower panel: Blue bars (left scale) correspond to the average fluorescence intensity value on the individual patterns, and red bars (right scale) correspond to the width of the arrow arms, measured at the various passages (average and error bars measured over ten patterns at each passage).

established techniques, when batch production of gels having the same type of patterns is needed.

Another important feature of our method lies in the storage of the mold: owing to the high stability of chemically grafted PNIPAM brushes, the molds elaborated at the first step described in section 2.2 can be dried and stored at ambient conditions, and exhibit a shelf life of several months or more.

3.3 Coupling with traction force microscopy

The combination of gel patterning and traction force microscopy (TFM) is a highly powerful approach that has allowed shedding light onto the basic mechanisms that underly the couplings between cell shape and response.[3,12]

In this context, we have assessed the possibility to combine our patterning method with TFM. To this aim, PAA gels have been prepared and patterned as described above, with the only difference that pre-gels were loaded with dark-red fluorescent particles prior to casting, as described in previous works.[3] Confocal fluorescence images of the particles located near the gel surface, just beneath cells confined on micropatterns, were taken after 4 hours of spreading. Cells were then detached using trypsin-EDTA and reference images of the unstressed gel were taken at the positions of each previously imaged cells. By measuring the resultant displacement field of the beads, we then compute, using a previously described home-written Fourier Transform Traction Cytometry (FTTC) algorithm,[3,4] the stress field associated with the forces exerted by the cells on the substrate.

On Fig. 7A, we provide an example of a fluorescence image of the beads present at the surface of a gel bearing arrow-shaped patterns, obtained using the present method, along with the computed stress field. This shows that TFM can be straightforwardly performed using gels elaborated with our technique.

For the sake of completeness, we have also compared the TFM results obtained here (Fig. 7A) with data from a previous study, obtained on PAA gels exhibiting similar patterns and mechanical properties, which had been patterned using deep-UV photochemistry in order to bind proteins to the surface[3] (Fig. 7B). Such a comparison reveals the following important points:

(i) We observe, with the two patterning techniques, similar maps exhibiting stress concentrations at the vertices of the adhesion patterns, with stress levels in these regions reaching up to ~200 Pa in both cases. This validates quantitatively our method.

(ii) A noticeable difference lies in the fact that deep-UV photochemical protein coupling results in partial bleaching of the beads below the pattern (Fig. 7B, upper panel), while the present method allows maintaining the fluorescent particles fully intact over the whole surface of the gel.

A direct consequence of the latter point is that spatial resolution is improved upon computing stress fields. Indeed, as most of the cell-generated forces are exerted below the patterned regions, the higher bead contrast and density obtained in these regions with our patterning technique now improves the detection accuracy of our algorithm, which in turn increases the spatial resolution when computing the displacement field induced by cellular traction forces. In the particular case of the arrow-shaped micropattern, we are now able to spatially resolve, at one vertex of the arrow, two distinct zones of enhanced stresses that are related to the relative anchorage of two different sets of actin fibers coming from the non adhesive edges (we refer the reader to an upcoming ref. 26 for details regarding the description of this structure). Such an improved resolution is another important advantage of the patterning method described here.

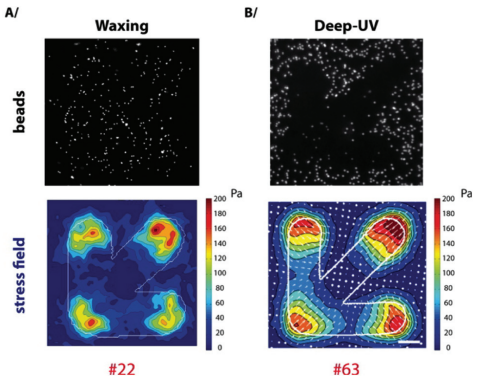

Fig. 7 Direct comparison of stress fields obtained with the same force reconstruction algorithm using 2 different PAA patterning methods. (A) Upper panel: Representative fluorescence image of beads obtained using the present "waxing" method based on transfer of proteins from the PNIPAM mold to the PAA gel. Lower panel: Associated stress map, obtained from averaging over 22 individual cells. (B) Upper panel: Image of beads after deep-UV patterning of the gel, showing that some beads are bleached below the arrow-shaped pattern. Lower panel: Stress field obtained from 63 cells. Scale bar: 6 μm.

4 Conclusion

We have reported a reliable, fast and cost-effective technique to design micropatterned hydrogels. Compared to the existing well-established templating techniques, the method we describe presents the following important features:

(i) Polymer brushes are elaborated from inexpensive chemicals and require only common chemistry facilities.

(ii) Brushes made of PNIPAM are of particular interest, for this polymer can be grown on glass surfaces *via* a robust and easy to implement protocol that does not require, for the present purpose, the high level of skills typical of surface-initiated ATRP procedures.

(iii) Micron-scale patterning of the brush is achieved in one single photo-deactivation step, without exposing the gel or the proteins of interest to deep-UV light.

(iv) Polymer chains being covalently bound to the substrate, such coatings show excellent usage and storage long-term

stability, and, most importantly, can be re-used for several experiments after being rinsed with common solvents.

The latter feature is a major improvement with respect to other patterning techniques, as it allows reducing greatly the number of steps required for microfabrication when many gels with similar patterns are to be produced for high resolution TFM studies.

Acknowledgements

We acknowledge financial support from the French Agence Nationale de la Recherche (ANR), under grant ANR-13-JS08-0002-01 (project SPOC).

References

1 M. Théry, V. Racine, M. Piel, A. Pépin, A. Dimitrov, Y. Chen, J. Sibarita and M. Bornens, *Proc. Natl. Acad. Sci. U. S. A.*, 2006, **103**, 19771–19776.
2 T. Vignaud, H. Ennomani and M. Théry, *Methods in Cell Biology*, Elsevier, 2014, vol. 120, ch. 6, pp. 93–116.
3 K. Mandal, I. Wang, E. Vitiello, L. A. C. Orellana and M. Balland, *Nat. Commun.*, 2014, **5**, 5749.
4 Q. Tseng, I. Wang, E. Duchemin-Pelletier, A. Azioune, N. Carpi, J. Gao, O. Filhol, M. Piel, M. Thery and M. Balland, *Lab Chip*, 2011, **11**, 2231–2240.
5 N. Wang, E. Ostuni, G. Whitesides and D. Ingber, *Cell Motil. Cytoskeleton*, 2002, **52**, 97–106.
6 T. Grevesse, M. Versaevel, G. Circelli, S. Desprez and S. Gabriele, *Lab Chip*, 2013, **13**, 777–780.
7 V. Damjanovic, B. Lagerholm and K. Jacobson, *BioTechniques*, 2005, **39**, 847–851.
8 A. Castaño, V. Hortigüela, A. Lagunas, C. Cortina, N. Montserrat, J. Samitier and E. Martinez, *RSC Adv.*, 2014, **4**, 29120.
9 J. J. Moon, M. S. Hahn, I. Kim, B. A. Nsiah and J. L. West, *Tissue Eng., Part A*, 2009, **15**, 579.
10 C. A. Goubko, S. Majumdar, A. Basak and X. Cao, *Biomed. Microdevices*, 2010, **12**, 555.
11 H. Yu, S. Xiong, C. Y. Tay, W. S. Leong and L. P. Tan, *Acta Biomater.*, 2012, **8**, 1267–1272.
12 A. D. Rape, W.-h. Guo and Y.-l. Wang, *Biomaterials*, 2011, **32**, 2043–2051.
13 S. R. Polio, K. E. Rothenberg, D. Stamenovic and M. L. Smith, *Acta Biomater.*, 2012, **8**, 82–88.
14 X. Tang, M. Y. Ali and M. T. A. Saif, *Soft Matter*, 2012, **8**, 7197–7206.
15 J. E. Gautrot, B. Trappmann, F. Oceguera-Yanez, J. Connely, X. He, F. M. Watt and W. T. S. Huck, *Biomaterials*, 2010, **31**, 5030–5041.
16 K. Mandal, M. Balland and L. Bureau, *PLoS One*, 2012, **7**, e37548.
17 L. Bureau and M. Balland, *Methods in Cell Biology*, Elsevier, 2014, vol. 120, ch. 9, pp. 145–154.
18 P. Shivapooja, L. K. Ista, H. E. Canavan and G. P. Lopez, *Biointerphases*, 2012, **7**, 32.
19 S. Varma, L. Bureau and D. Debarre, *Langmuir*, 2016, **32**, 3152.
20 I. B. Malham and L. Bureau, *Langmuir*, 2010, **26**, 4762–4768.
21 A. Halperin, *Langmuir*, 1999, **15**, 2525–2533.
22 A. Halperin and M. Kroeger, *Biomaterials*, 2012, **33**, 4975–4987.
23 A. Halperin and M. Kroeger, *Macromolecules*, 2011, **44**, 6986–7005.
24 C. Xue, B.-C. Choi, S. Choi, P. V. Braun and D. E. Leckband, *Adv. Funct. Mater.*, 2012, **22**, 2394–2401.
25 P. de Gennes, *Scaling concepts in polymer physics*, Cornell University Press, 1979.
26 R. De Mets, I. Wang, M. Balland, C. Oddou, P. Moreau, C. Albiges-Rizo, A. Delon and O. Destaing, Submitted to Cell Reports, 2016.

6.3. Study 4) Alkasalias et. al "RhoA knockout fibroblasts lose tumor-inhibitory capacity *in vitro* and promote tumor growth *in vivo*"

During my time at LiPhy, we collaborated with the group of Dr. Tatiana Pavlova from the Karolinska Institute in Stockholm, Sweden. Their project aimed at deciphering the molecular basis behind the loss of tumor inhibitory properties of cancer-associated fibroblasts, which promotes tumor growth. Their major target protein was RhoA, a signaling protein involved in cell contractility (Etienne-Manneville 2002). We assisted this project by performing static force measurements of control and RhoA knockdown fibroblasts. My contribution can be seen in **Figure 4a** of the scientific article, published in *Proceedings of the National Academy of Sciences* (*PNAS*) in 2017.

PNAS PLUS

RhoA knockout fibroblasts lose tumor-inhibitory capacity in vitro and promote tumor growth in vivo

Twana Alkasalias[a,b], Andrey Alexeyenko[a,c], Katharina Hennig[d], Frida Danielsson[c], Robert Jan Lebbink[e], Matthew Fielden[f], S. Pauliina Turunen[a], Kaisa Lehti[a,g], Vladimir Kashuba[a,h], Harsha S. Madapura[a], Benedek Bozoky[a], Emma Lundberg[i], Martial Balland[d], Hayrettin Guvén[a], George Klein[a,1], Annica K. B. Gad[j,1,2], and Tatiana Pavlova[a,1,2]

[a]Department of Microbiology, Tumour, and Cell Biology, Karolinska Institutet, 17177 Stockholm, Sweden; [b]Department of Biology, College of Science, Salahaddin University, 44002, Irbil, Kurdistan-Iraq; [c]National Bioinformatics Infrastructure Sweden, Science for Life Laboratory, Karolinska Institute, 17177 Stockholm, Sweden; [d]Laboratoire Interdisciplinaire de Physique, Université Joseph Fourier (Grenoble 1), 38402 Saint Martin d'Hères Cedex 9, France; [e]Department of Medical Microbiology, University Medical Centre Utrecht, 3584 CX Utrecht, The Netherlands; [f]Department of Applied Physics, Nanostructure Physics, Kungliga Tekniska Högskolan Royal Institute of Technology, Albanova University Center, 106 91 Stockholm, Sweden; [g]Research Programmes Unit, Genome-Scale Biology, University of Helsinki, Finnish Cancer Institute, F1-00014 Helsinki, Finland; [h]Department of Molecular Oncogenetics, Institute of Molecular Biology and Genetics, National Academy of Sciences of Ukraine, 01004 Kiev, Ukraine; [i]Cell Profiling Facility, Science for Life Laboratory, Kungliga Tekniska Högskolan Royal Institute of Technology, 17177 Stockholm, Sweden; and [j]Science for Life Laboratory, Division of Translational Medicine and Chemical Biology, Department of Medical Biochemistry and Biophysics, Karolinska Institutet, 17177 Stockholm, Sweden

Contributed by George Klein, January 6, 2017 (sent for review August 17, 2016); reviewed by Hakan Axelson and Peter H. Krammer)

Fibroblasts are a main player in the tumor-inhibitory microenvironment. Upon tumor initiation and progression, fibroblasts can lose their tumor-inhibitory capacity and promote tumor growth. The molecular mechanisms that underlie this switch have not been defined completely. Previously, we identified four proteins overexpressed in cancer-associated fibroblasts and linked to Rho GTPase signaling. Here, we show that knocking out the Ras homolog family member A (*RhoA*) gene in normal fibroblasts decreased their tumor-inhibitory capacity, as judged by neighbor suppression in vitro and accompanied by promotion of tumor growth in vivo. This also induced PC3 cancer cell motility and increased colony size in 2D cultures. RhoA knockout in fibroblasts induced vimentin intermediate filament reorganization, accompanied by reduced contractile force and increased stiffness of cells. There was also loss of wide F-actin stress fibers and large focal adhesions. In addition, we observed a significant loss of α-smooth muscle actin, which indicates a difference between RhoA knockout fibroblasts and classic cancer-associated fibroblasts. In 3D collagen matrix, RhoA knockout reduced fibroblast branching and meshwork formation and resulted in more compactly clustered tumor-cell colonies in coculture with PC3 cells, which might boost tumor stem-like properties. Coculturing RhoA knockout fibroblasts and PC3 cells induced expression of proinflammatory genes in both. Inflammatory mediators may induce tumor cell stemness. Network enrichment analysis of transcriptomic changes, however, revealed that the Rho signaling pathway per se was significantly triggered only after coculturing with tumor cells. Taken together, our findings in vivo and in vitro indicate that Rho signaling governs the inhibitory effects by fibroblasts on tumor-cell growth.

Rho GTPases | RhoA | cancer-associated fibroblasts | tumor-inhibitory capacity | cytoskeleton

The tumor microenvironment consists of various cells and extracellular matrix (ECM) proteins, which together form the tumor stroma. This stroma differs from normal tissue in that it is highly enriched in ECM proteins, which form fibrous networks that provide scaffolds for tumor-cell proliferation and migration. Defective organization and composition of the ECM can thus influence tumor growth and metastasis (1–4). The architecture of the stroma mainly depends on the composition of the ECM and the mechanical and biochemical functions of fibroblasts (5).

Fibroblasts can inhibit growth of cancer cells (6, 7). The ECM and soluble factors that are secreted upon fibroblast–tumor cell contact drive the fibroblast inhibitory effects (8). However, this inhibitory activity of fibroblasts can be lost, and even reversed, to provide an opposing tumor stimulatory activity during tumor development (9). In parallel, fibroblasts activate proinflammatory gene expression (10). These activatory fibroblasts are often referred to as cancer- or carcinoma-associated fibroblasts (CAFs), and they have been suggested to promote tumor growth and metastasis through remodeling of the ECM network and cytokine and chemokine secretion (11).

Small Rho GTPases control the shape and mechanical and adhesive properties of fibroblasts (12). Most notably, RhoA (Ras homolog family member A) has been shown to induce assembly of focal adhesions and F-actin stress fibers, and to control the shape and adhesive and contractile properties of fibroblasts, as well as their capacity to organize the ECM (13, 14). CAFs often express myofibroblast markers, such as α-smooth muscle actin (α-SMA). We recently identified 12 markers that are highly

Significance

In order for cancer to develop, normal tumor-inhibitory fibroblasts need to change into tumor-promoting, cancer-associated fibroblasts. We created Ras homolog family member A (*RhoA*) gene knockout fibroblasts and found that even though these cells lacked common markers of classic cancer-associated fibroblasts, they had lost their normal tumor-inhibitory capacity and induced tumor-cell migration and proliferation in vitro and tumor growth in vivo. *RhoA* knock-out cells also showed an altered cytoskeleton, reduced contractile force, and induced stiffness of the fibroblasts. *RhoA* knockout also induced a loss of α-smooth muscle actin and an activated proinflammatory state, which was reflected by interference with a number of Rho signaling cascades. Our data indicate that RhoA is a key regulator of the switch from tumor-inhibitory to tumor-promoting fibroblasts.

Author contributions: T.A., G.K., A.K.B.G., and T.P. designed research; T.A., K.H., F.D., R.J.L., S.P.T., V.K., H.S.M., H.G., A.K.B.G., and T.P. performed research; T.A., A.A., R.J.L., M.F., S.P.T., K.L., M.B., and T.P. contributed new reagents/analytic tools; T.A., A.A., K.H., F.D., M.F., S.P.T., K.L., V.K., B.B., E.L., G.K., A.K.B.G., and T.P. analyzed data; and T.A., A.A., S.P.T., K.L., H.G., G.K., A.K.B.G., and T.P. wrote the paper.

Reviewers: H.A., Lund University; and P.H.K., German Cancer Research Center.

The authors declare no conflict of interest.

Freely available online through the PNAS open access option.

Data deposition: The data reported in this paper have been deposited in the Gene Expression Omnibus (GEO) database, www.ncbi.nlm.nih.gov/geo (accession no. GSE83913).

[1]To whom correspondence may be addressed. Email: georg.klein@ki.se, Annica.Gad@ki.se, or tatiana.pavlova@ki.se.

[2]A.K.B.G. and T.P. contributed equally to this work.

This article contains supporting information online at www.pnas.org/lookup/suppl/doi:10.1073/pnas.1621161114/-/DCSupplemental.

expressed in cancer-associated stroma and not in normal stroma (15). Four of these markers, DLG1, ROCK2, ARHGAP31, and ARHGAP26, are linked to Rho GTPase signaling. In that study, we also identified the known CAF marker ACTA2 (encodes α-SMA), which is regulated by the Rho GTPase signaling pathway (16–19). This link to the Rho pathway prompted us to hypothesize that RhoA signaling in fibroblasts mediates their capacity to control tumor growth.

Recent findings have indicated that an actomyosin-based contractile force in fibroblasts is required for CAFs to remodel the ECM (20). The stiffness of the extracellular environment can activate RhoA in fibroblasts, which leads to increased expression of (the CAF marker) α-SMA and differentiation into myofibroblasts (16, 17, 19). In line with this, Calvo et al. have suggested that CAFs can increase the stiffness of the ECM to stimulate the formation of CAFs, which results in a feed-forward, self-reinforcing loop, through which CAFs can promote tumorigenesis (20).

Taken together, these observations suggested that tumor growth and invasion is shaped by cross-talk between mechanical and biochemical signaling, which is modulated by RhoA signaling in fibroblasts. Therefore, targeting this pathway in fibroblasts might influence their tumor-inhibition capacity.

Results

RhoA Is Required for the Tumor-Inhibitory Capacity of Fibroblasts in Vitro and in Vivo. To determine whether RhoA affects the tumor-regulatory capacity of fibroblasts, we ablated RhoA in Bj human telomerase reverse transcriptase (BjhTERT) fibroblasts. Endogenous RhoA expression in control fibroblasts and significant loss of *RhoA* gene and protein expression in RhoA knockout (KO) BjhTERT fibroblasts was confirmed by quantitative RT-PCR (qRT-PCR) ($P < 10^{-6}$) (Fig. 1*A* and Fig. S1*A*) and Western blotting (Fig. 1*B*).

To determine the regulatory capacity of these fibroblasts on tumor cells, proliferation of PC3 prostate cancer cells was measured in vitro in monocultures and in cocultures with either control or RhoA-KO fibroblasts. Consistent with previous reports (6), coculture with control fibroblasts dramatically decreased PC3 cell growth (Fig. 1*C*), whereas RhoA-KO fibroblasts showed significantly decreased inhibition of PC3 cell growth, compared with control fibroblasts ($P < 10^{-10}$) (Fig. 1*C* and Figs. S1*B* and S2).

We then asked whether this RhoA deficiency of fibroblasts can also regulate tumor-cell growth in vivo in SCID or SCID-beige mice. Here, 2×10^4 PC3 cells were injected subcutaneously alone and in combination with 1×10^6 of either control or RhoA-KO fibroblasts. Across three repeated experiments, this relatively low number of PC3 cells alone did not induce any detectable tumorigenic response in the 9 wk following their injection. Coinjection of control fibroblasts with PC3 cells resulted in the formation of one small tumor in one of the five mice in two of the three experiments (Fig. 1*D* and Fig. S3). However, all of the mice injected with PC3 cells plus RhoA-KO fibroblasts developed tumors (Fig. 1*D* and Fig. S3) across the three experiments. After prolonged initiation over the initial 6 to 7 wk, these subcutaneous tumors then grew extremely rapidly, reaching volumes of up to 1 cm^3 within the following 2 wk (Fig. 1*D*). These experiments demonstrate that fibroblasts that lack RhoA do not inhibit tumor-cell growth both in vitro and in vivo.

In the following sections, we report on our investigation into how the RhoA KO in these BjhTERT fibroblasts altered cell morphology and dynamics, gene expression, and the impact of RhoA KO on the signaling network.

RhoA-KO Fibroblasts Induce Tumor-Cell Motility and Proliferation. To study the mode of interaction of RhoA-KO fibroblasts with tumor cells, we examined the differences in the motility of PC3 mRFP cells (PC3 cells stably expressing monomeric red fluorescent protein) in coculture with control and RhoA-KO fibroblasts using total internal reflection fluorescence (TIRF) microscopy for live-cell time-lapse imaging. PC3 mRFP cell motility was recorded for 65 h, with these 65 (hourly) time points subdivided into five color-coded trajectories whereby each corresponded to 13 h of recording. Similar to their effect on PC3 cell proliferation in

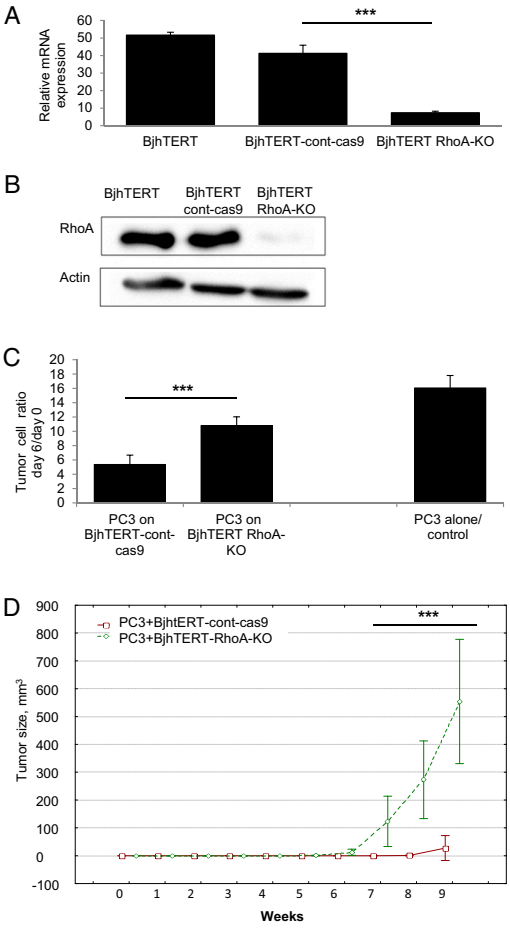

Fig. 1. Loss of RhoA in human fibroblasts reduces their tumor-inhibitory capacity in vitro and induces their tumor-stimulatory capacity in vivo. (*A*) qRT-PCR for RhoA expression in BjhTERT, BjhTERT–cont-cas9, and BjhTERT RhoA-KO fibroblasts. The *y* axis indicates the values of expression level of RhoA gene normalized to the *TBP* reference gene. The *x* axis shows the cDNA samples. Data are means with 0.95 confidence intervals. ***P = 0.00029 (one-way ANOVA with three levels). (*B*) Representative Western blots of BjhTERT, BjhTERT–cont-cas9 and BjhTERT RhoA-KO fibroblasts, for RhoA protein levels in total cell lysate (as indicated). Actin protein levels are shown as loading control. (*C*) Inhibitory capacity of BjhTERT–cont-cas9 and BjhTERT RhoA-KO fibroblasts as confluent monolayers (4-d-old) tested in coculture with PC3 mRFP prostate cancer cells. Data are proliferation ratios of PC3 mRFP cells after 6 d coculture with fibroblasts. ***$P < 10^{-10}$. (*D*) Tumor volumes in SCID mice injected with mixtures of PC3 mRFP cells with BjhTERT–cont-cas9 fibroblasts or BjhTERT RhoA-KO fibroblasts (as indicated). PC3 mRFP alone and with BjhTERT fibroblasts did not form tumors (not shown for clarity). Data are means of three independent experiments. ***$P < 10^{-10}$. See details and statistical analysis in Fig. S3.

vitro, the inhibitory effect of fibroblasts on cell motility of PC3 was significantly decreased upon knocking out the RhoA gene in fibroblasts ($P = 0.0037$) (Fig. 2 and Movies S1 and S2). Furthermore, in the RhoA-KO fibroblast cocultures, PC3 mRFP cells formed larger colonies than when cocultured with control fibroblasts, as measured by the distribution of the PC3 mRFP cells over a given area (Fig. S4 and Movies S3 and S4). Consistent with the contact-dependent neighbor suppression described by Alkasalias et al. (8), early contacts at the beginning of the cocultures between the fibroblasts and PC3 mRFP cells were essential to inhibit tumor-cell proliferation and motility. Remarkably, this inhibition was lost with the RhoA KO/deficiency of the RhoA-KO fibroblasts (Movies S5 and S6).

Altered Cytoskeleton and Adhesion Structures in RhoA-KO Fibroblasts Are Linked to Changes in Cellular Contractile Force and Stiffness. Control and RhoA-KO fibroblasts were examined under immunofluorescence microscopy, where the RhoA deficiency resulted in less regularly shaped cells compared with those of control fibroblasts (Fig. 3). Furthermore, RhoA-KO fibroblasts showed less formation of wide actin stress fibers and fewer distinct, dense, and large focal adhesions (Fig. 3*A*). RhoA-KO fibroblasts also showed significant reduction in α-SMA expression (Fig. S5). Furthermore, the structure of vimentin intermediate filaments in RhoA-KO cells appeared less organized, and in a more homogenous distribution of very thin and long filament extensions throughout the cell cytoplasm (Fig. 3*B*).

To determine whether this altered cytoskeleton structure of RhoA-KO fibroblasts was associated with changes in the mechanical properties of these cells, their contractile force and stiffness were measured using traction force and atomic force microscopy, respectively. Compared with control fibroblasts, RhoA-KO fibroblasts showed significantly reduced contractile forces ($P = 0.004$) (Fig. 4*A*). In contrast, the cell stiffness, here represented by the elastic modulus determined via indentation of the cells, was more homogenous and more evenly distributed for RhoA-KO fibroblasts than control fibroblasts (Fig. 4*B*). When the cell areas were analyzed in detail, RhoA-KO fibroblasts appeared significantly stiffer than control fibroblasts ($P = 0.0196$) (Fig. 4 *C* and *D*). RhoA-KO fibroblasts also showed lower numbers of very soft locations, compared with control fibroblasts (Fig. 4 *B* and *C*).

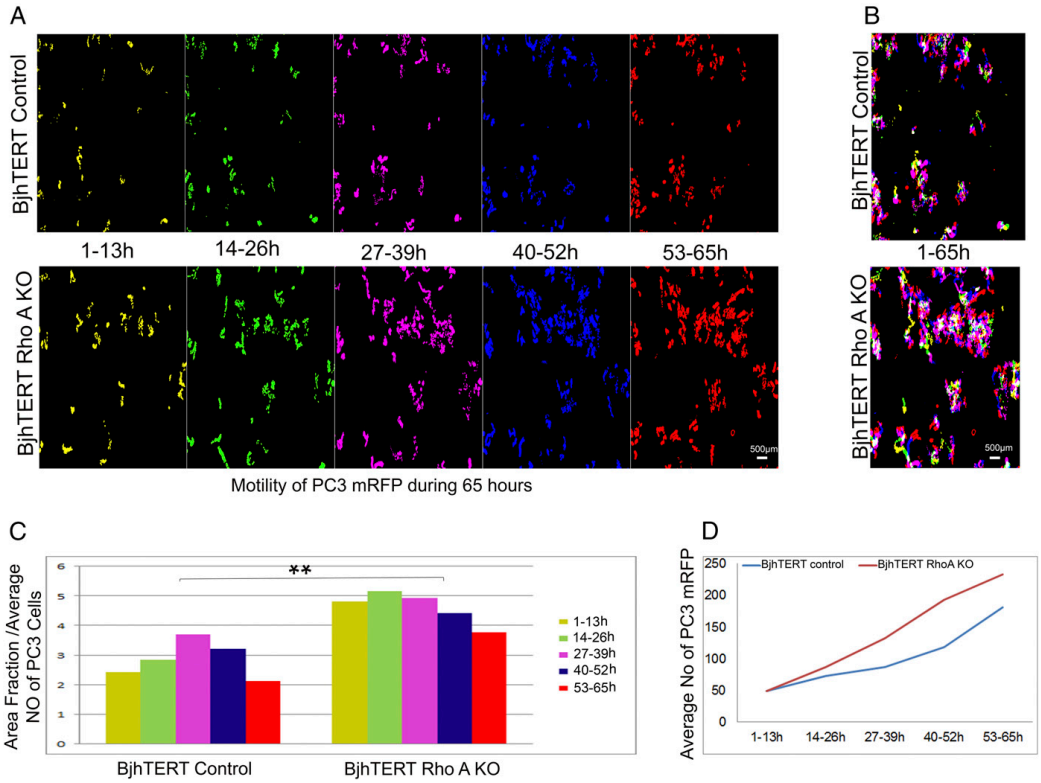

Fig. 2. RhoA-KO fibroblasts induce tumor-cell motility and proliferation. Live-cell TIRF microscopy imaging. (*A*) Trajectories of PC3 mRFP prostate cancer cells during 13-h intervals. Color-coded images show a 65-h time-point projection of the red-labeled tumor cells: yellow (1–13 h), green (14–26 h), magenta (27–39 h), blue (40–52 h), and red (53–65 h). (*B*) Maximum projection of all five color-coded images showing the total motility (full trajectories) of the PC3 mRFP tumor cells over the 65 h. (*C*) Kinetics of tumor-cell motility. Motility of tumor cells quantified by calculation of the areas of the cell trajectories, normalized for mean number of cells in each 13-h interval. $^{**}P = 0.0037$. (*D*) Mean number of PC3 mRFP cells that proliferated during each 13-h interval (of five time points). See also Movies S1 and S2.

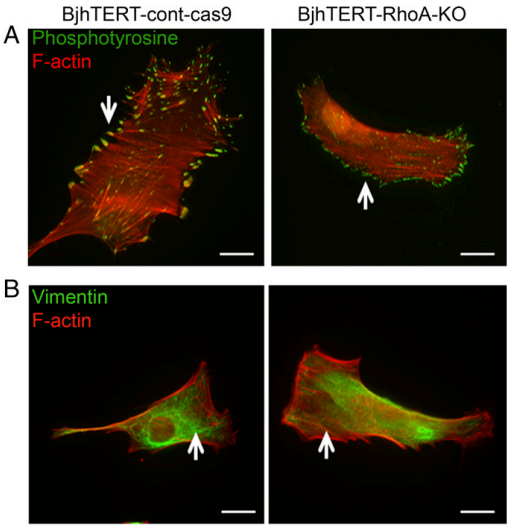

Fig. 3. RhoA-KO fibroblasts show altered cytoskeletal organization and cell-matrix adhesion. Representative images showing phosphotyrosine (pY) (green) (*A*), vimentin (*B*), and F-actin (red) (*A* and *B*) in the control and RhoA-KO fibroblasts (as indicated). Images are representative of at least three independent experiments. Arrows indicate large focal adhesions linked to stress fibers (*A*) and the spatial organization of the vimentin filaments (*B*). (Scale bars, 20 μm.)

Coculture of RhoA-KO Fibroblasts with Cancer Cells Activates Proinflammatory Genes and Rho-Related Pathway Activity. To identify factors that might mediate the tumor promoting effects of RhoA-KO fibroblasts, gene-expression analysis was performed for RhoA-KO fibroblasts and PC3 mRFP prostate cancer cells before coculturing and after 6 d of coculturing, using the Affymetrix Whole Transcript Assay platform and validation of selected genes using the qPCR technique on newly generated samples.

After coculture with PC3 mRFP cells, the RhoA-KO fibroblasts manifested higher expression levels of such proinflammatory signature genes as *IL-1A*, *IL-1B*, *IL-6*, *IL-8*, chemokine (C-C motif) ligand 2 (*CCL2*), and TNF-α–induced protein 2 (*TNFAIP2*) (Table S1) (10, 21). In contrast, in the control fibroblasts expression of genes for proinflammatory cytokines did not seem to change after the coculturing. In turn, the PC3 cells that were cocultured with RhoA-KO fibroblasts exhibited higher expression of certain genes of proinflammatory signature (*IL-6*, *IL-8*, and *CCL2*) (Table S2), compared with the PC3 cells cocultured with control fibroblasts.

To increase the power of our analysis, we further applied the network enrichment analysis (NEA) (22). Similarly to the gene-set enrichment analysis of differential expression (DE), NEA can summarize observations by raising them to the pathway level. However, it is more powerful than the former method because of considering network connections between differentially expressed and pathway genes, so that the latter may be identified even when their own expression is not changed (23).

Both the control and RhoA-KO fibroblasts were sampled before and after coculturing with the PC3 prostate cancer cells. Using Venn diagram sampling and NEA tools available at https://www.evinet.org, we created lists of genes that were differentially expressed between the control and RhoA-KO fibroblasts as measured before (Datasets S1 and S2) and after (Datasets S3 and S4), or both before and after (Datasets S5 and S6) coculturing them with the PC3 cells. Separating DE genes into up- and down-regulated fractions produced six gene lists in total. Unexpectedly, the "up" and "down" gene lists specifically before the coculturing (Fig. 5, UP_BEFORE, DOWN_BEFORE) did not manifest any significant network connections toward Rho signaling pathways. Remarkably though, the latter pathways appeared significantly connected to a set of 55 genes that were consistently up-regulated with the fibroblast and cancer cell coculturing (Fig. 5, UP_BOTH). Similarly, the Rho pathways were enriched in connections to the gene sets specifically up-regulated and down-regulated following the coculturing (Fig. 5, UP_AFTER, DOWN_AFTER). As an example, we looked at details of functional connections with the mDia-SRF pathway, which is known for its involvement in actin modifications and thus appeared potentially implicated in the consequences of our RhoA KO. At the gene-expression level, we observed that neither serum response factor (SRF) nor other relevant genes were altered because of the knockout. However, in network enrichment analysis this pathway functionally linked to the UP_BOTH, UP_AFTER, and DOWN_AFTER lists (Fig. 5). We could see that the most central, significantly linked gene was SRF itself, with a potential

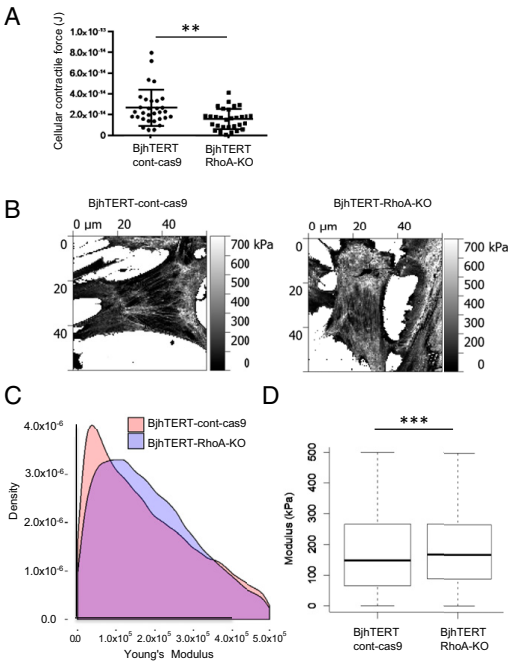

Fig. 4. Altered cellular contractile forces and cell stiffness of tumor-stimulatory fibroblasts. (*A*) Contractile forces of individual control (dots) and RhoA-KO (squares) fibroblasts. The *P* value indicates a difference of 0.004. $^{**}P > 0.01$. (*B*) Image showing the Young's modulus of the locations over the control (*Left*) and RhoA-KO (*Right*) fibroblasts. Lighter colors indicate higher modulus. (*C*) Density plot showing distribution of the measured stiffness for values of individual locations of measurement within the physiological range of 0 kPA to 75 kPa, for 33,505 data points from control fibroblasts, and 33,505 data points from RhoA-KO fibroblasts. (*D*) Boxplot showing distributions and median values of measured stiffness for values within the physiological range of 0 kPa to 75 kPa, including 33,505 data points for control fibroblasts, and 33,505 data points for RhoA-KO fibroblasts. Data for the RhoA-KO cells show significantly higher stiffness. $^{***}P < 2.2e\text{-}16$.

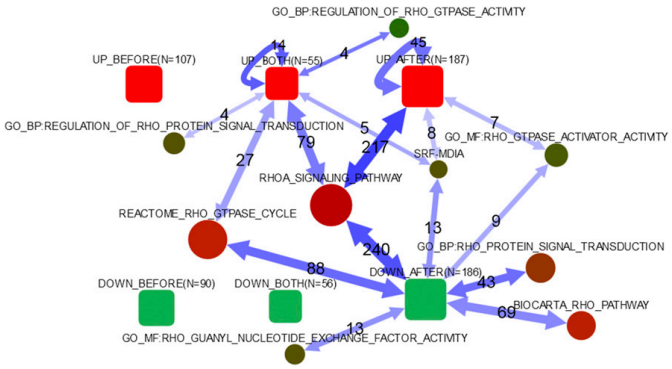

Fig. 5. Network enrichment of differentially expressed genes in pathways related to RhoA regulation. Global patterns in regard to pathways related to Rho signaling. Connectivity between DE lists and individual genes of the SRF–mDia pathway. Rounded boxes: lists of differentially expressed genes; AFTER, after coculturing; BEFORE, before coculturing; BOTH, both before and after coculturing; DOWN, down-regulation because of RhoA knock-out of ≥twofold; N, number of genes in list; UP, up-regulation due to RhoA KO of ≥ twofold. Circles: pathways; the size reflects the number of member genes, the color indicates the relative activity in the global network (total number of links). Double-headed arrows summarize individual gene–gene connections (in either direction, and undirected ones) in the global network between any differentially expressed genes and any pathway members. Numeric labels give numbers of individual gene–gene network connections behind the arrows. Only arrows corresponding to significant network enrichment are shown (adjusted $P < 0.05$). The lists of the genes in each group are given in Datasets S1–S6. The data on the SRF–mDia pathway are shown as described previously (24, 25).

involvement of the other genes presented by Gopinath et al. (24) and Geneste et al. (25).

Our observations suggest that the Rho-related transcriptome changes caused by the RhoA KO emerged mainly during the coculturing with the tumor cells rather than preexisting in the fibroblasts before this procedure (i.e., in the PC3-naive fibroblasts).

RhoA-KO Fibroblasts Support a Growth Pattern of Compact Tumor Clusters and Cell Contacts in 3D Collagen Cocultures. To understand how the changes in the fibroblast Rho pathways, gene-expression programs, contact-dependent neighbor suppression, and cytoskeleton that were induced by the RhoA KO and coculturing in vitro relate to the increased PC3 tumorigenesis in vivo, we established a 3D coculture model of the BjhTERT fibroblasts and PC3 mRFP prostate cancer cells. Equal numbers of control (BjhTERT cont-cas9) and RhoA-KO fibroblasts alone or in combination with PC3 mRFP cells were embedded in the 3D collagen matrix and (co)cultured for 7 d. In the 3D monocultures, control fibroblasts formed dense cross-networks with branching and elongated sprouting. Consistent with the cytoskeletal changes in 2D cultures, for RhoA-KO fibroblast 3D monocultures, fluorescence imaging of filamentous actin revealed impaired stress fibers in conjunction with less sprouting, as a blunt-ended phenotype (Fig. 6*A*). In the cocultures for RhoA-KO fibroblasts, the PC3 mRFP cells grew in clusters surrounded by these fibroblasts, and showed compact positioning of their nuclei, whereas both PC3 cells and fibroblasts were more dispersed in the control fibroblast cocultures (Fig. 6*B*). To quantify this compactness versus dispersal of PC3 tumor cells in the fibroblast cocultures, we generated a "Clustering Index." PC3 cells cocultured with RhoA-KO fibroblasts had a significantly higher Clustering Index compared with PC3-cell and control-fibroblast cocultures (Fig. 6*C*). These results suggest that by driving actin-cytoskeleton–dependent fibroblast branching, RhoA signaling can support coincident dispersal of the cocultured tumor cells. Therefore, in the 3D microenvironment, RhoA ablation in fibroblasts can promote the delayed tumor growth by supporting tumor-cell survival and stem-like properties via cell–cell contacts, altered Rho pathways, and interactions with (or the close distance of) the fibroblasts with increasing chemokine production (i.e., by mechanical and biochemical mechanisms).

Discussion

Although interactions between a tumor and the stroma are regulated by various biochemical reactions, it is becoming increasingly clear that mechanical cues also have a significant role in these interactions (26). In the present study, we have shown that these RhoA-KO fibroblasts that are characterized by altered gene-expression profile, cytoskeleton, and mechanical properties can promote tumor growth, although they do not show common markers of CAFs.

Indeed, our experimental model was different from any other model that studied CAFs. Here, we show that normal inhibitory fibroblasts can be switched into a promoting subtype before they become CAFs by the classic definition. Our cells showed that RhoA ablation had an immediate "net effect" on the interaction between fibroblasts and cancer cells. In other words, this effect of fibroblasts apparently was not induced by the cells' coexistence and coevolution during extended time periods.

Here, we investigated the proliferation and migration of the metastatic PC3 prostate cancer cell line in cocultures with fibroblasts in vitro and in a subcutaneous tumor xenograft model in mice. A loss of the tumor-inhibitory capacity of these fibroblasts upon RhoA ablation was observed in these 2D systems and in the xenograft tumors. Interestingly, in the presence of RhoA-KO fibroblasts in the 3D collagen system, the PC3 tumor cells formed colonies that were prominently compact clusters with closely positioned nuclei. This might be the underlying cause of the growth of the tumor xenografts in this study, whereby the tumor cells coinjected with RhoA-KO fibroblasts started to grow after a long lag-phase, to form subcutaneous tumors. We suggest that the cluster-like aggregation and ample homotypic cancer-cell contacts in the presence of RhoA-KO fibroblasts in this 3D system are linked to the tumor propagating and stem-like properties. Furthermore, in the in vivo xenograft model, low numbers of tumor cells were enough to initiate tumor growth when they were in the presence of RhoA-KO fibroblasts, with

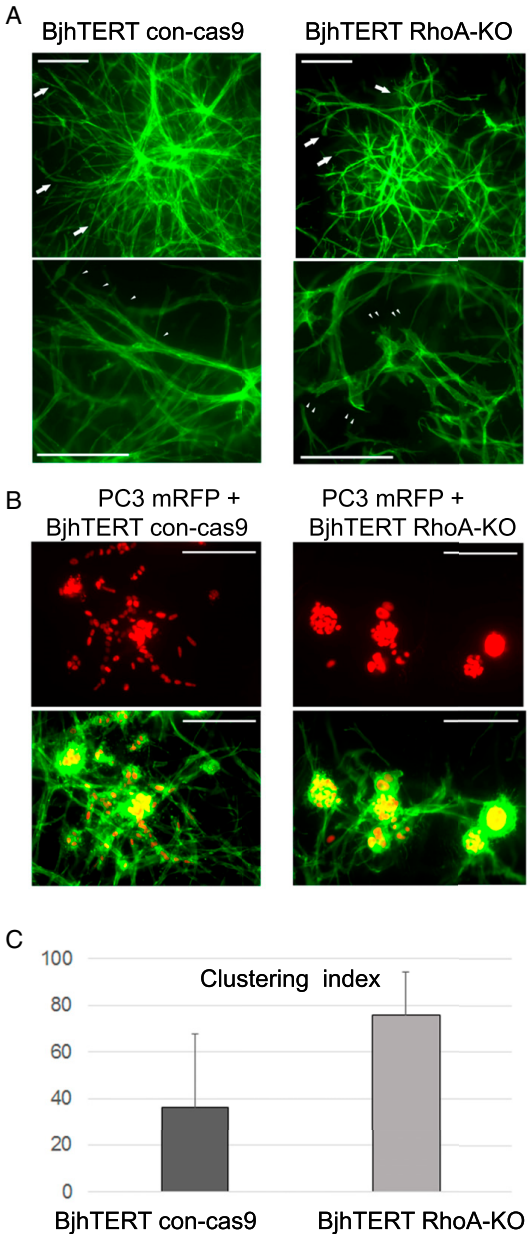

Fig. 6. Growth of PC3 tumor cells with RhoA-KO fibroblasts in 3D collagen. (*A*) Phenotypes of control (cont-cas9) and RhoA-KO BjhTERT fibroblasts cultured for 7 d in the 3D type I collagen matrix. Arrows indicate differences in sprouting ability between control and RhoA-KO fibroblasts. Higher magnifications and arrowheads indicate elongated sprouting in control compared with RhoA-KO fibroblasts with the blunt-ended phenotype. (*B*) To assess growth of PC3 tumor cells with RhoA-KO fibroblasts in 3D collagen, equal numbers of PC3mRFP cells and BjhTERT control or RhoA-KO fibroblasts were suspended as single cells into 3D collagen and cultured for 7 d. (*C*) Clustering Index calculated to quantify the spreading and compactness of growth of PC3 tumor spheres in coculture with RhoA-KO fibroblasts. For the Clustering Index, the number of sprouting growths was calculated (total n = 16 image fields from two independent repeats) and subtracted from a constant value: Clustering Index = [20 − (mean number of sprouting growths)] ×5. (Scale bars, 200 μm.)

the emergence of palpable tumors delayed, both of which are known hallmarks of tumor-propagating cells.

Our findings indicate that upon coculturing, the transcriptomes of both the RhoA-KO fibroblasts and the tumor cells are shaped by activation of the proinflammatory signature. It is known that inflammation promotes cancer growth and metastasis (27, 28). Thus, this RhoA KO might provide a link between inflammation and cancer via the induction of a proinflammatory environment. The observed increase of tumor-cell motility in the presence of the RhoA-KO fibroblasts is in line with previous observations that proinflammatory chemokines can promote tumor-cell migration (27). In addition, the increased PC3 cell motility appears to be because of the present finding that upon RhoA loss, these RhoA-KO fibroblasts lose their contact-dependent neighbor-suppression effects.

The observed RhoA-mediated orchestration of many different biochemical and physical factors makes RhoA a "master-regulator" of interactions between tumors and stroma (26). Cytoskeletal filaments in the cell can convert mechanical signals into biochemical signals via the mechano-sensitive proteins of the cell. In this way, the extracellular and intracellular mechanical properties of the cells can activate different downstream processes, such as cell migration, adhesion, gene transcription, and differentiation (29). Furthermore, these RhoA-KO tumor-promoting fibroblasts showed significant reduction in α-SMA expression. Such concordant down-regulation can be explained via the regulation of smooth muscle cell-specific promoter activity of the α-SMA gene through RhoA signaling (30).

We observed that the RhoA-KO fibroblasts showed increased homogeneous stiffness, with fewer soft locations, and decreased contractile forces. This is in line with the previous observations that RhoA is a key regulator of the mechanical properties of fibroblasts (31–33). These mechanical changes in the RhoA-KO fibroblasts were linked to the loss of wide stress fibers and large focal adhesions. De Wever et al. proposed that fibroblasts in the tumor microenvironment can behave as particularly motile units, which can invade the cancer-cell compartment (34), potentially because of the altered cytoskeleton of these cells (35). In line with the mechanical control of tumor growth by fibroblasts in the tumor microenvironment, Kumar and Weaver suggested that mechanical forces have a major role in the onset and progression of cancers (5). In addition, based on the literature in the field, Karagiannis et al. proposed a working model for how mechanical and adhesive properties of fibroblasts govern local cancer growth (36 and references therein). In their model, the fibroblasts in tumors show altered cell-matrix adhesion, increased migration, and changed mechanics, which might stimulate cancer cells to migrate toward stromal regions that are less dense, and thereby increase the size of a tumor. Moreover, cell-matrix stiffness has been shown to stimulate cytokinesis, which suggests that the increased stiffness of the surrounding fibroblasts can also stimulate the proliferation of cancer cells (37). These ideas are in line with our findings that these RhoA-KO tumor-promoting fibroblasts showed increased homogeneous stiffness and fewer soft locations, with altered cytoskeleton and cell-matrix adhesion.

Tumor cells go through many changes, both phenotypically and genetically, as they pass through the different stages of initiation, growth, invasion, colonization, and metastasis. This might be true for the fibroblasts in the tumor microenvironment

too. As we have shown here, the mere RhoA KO do not yet turn normal fibroblasts into full-scale CAFs, even though their phenotype shifts from inhibitory to noninhibitory and then into tumor-promoting cells. Thus, although not being classic CAFs, the fibroblasts acquired key properties that proved to be sufficient for promotion of tumor-cell growth.

The loss of α-SMA and reduction of contractile forces in these RhoA-KO fibroblasts was another difference from CAFs. Therefore, they might respond differently to certain signals, including RhoA signaling. Importantly, we found that knocking out RhoA in normal fibroblasts did not activate significant relations to the Rho signaling pathway until these fibroblasts met the tumor cells. This might be highly relevant in the context of tumor initiation and early development.

We have demonstrated that fibroblasts with ablated RhoA lose their normal inhibitory capacity in vitro, induce tumor growth in vivo and migration and proliferation of tumor cells in vitro, and support clustering of cocultured tumor cells in a 3D system. In the light of these results, RhoA appears to be an important regulator of the switch from tumor-inhibitory to tumor-promoting fibroblasts. The regulatory effects on tumor-cell growth must be imposed via a complex course of mechanical and biochemical reactions. An aspect here that remains elusive to the scope of the present study is how the loss of RhoA (which alters the mechanical and biochemical properties of normal stromal fibroblasts) can trigger a stem-like phenotype in these PC3 prostate cancer cells. Probably, increased level of proinflammatory genes plays role in inducing the expression of stemness-related properties of tumor cells (38, 39). We have demonstrated that loss of RhoA changed the cytoskeleton, the contractile forces and cell stiffness of the cells, induced a proinflammatory state, and interfered with Rho signaling cascades. However, further studies are needed to determine if the RhoA levels in stromal fibroblast govern the carcinoma aggressiveness and the clinical outcome.

Conclusions

Our findings suggest that RhoA controls the tumor-inhibitory capacity of fibroblasts through their mechanical properties and biochemical signaling. It also appears that a significant part of the RhoA-dependent signaling is activated by the presence of these tumor cells. A more detailed identification of the molecular mechanisms that underlie this intercellular control is a promising area for future studies.

Materials and Methods

RhoA CRISPR/Cas and Lentivirus System. We prepared lentiviral CRISPR/Cas9 vectors that coexpressed *Streptococcus pyogenes* Cas9, PuroR, and a human U6 promoter driving expression of anti-RhoA guideRNAs (40). The gene-specific regions of the guideRNA sequences were designed by the CRISPR design tool from the Zhang laboratory (crispr.mit.edu/), and their sequences were: RhoA_1, GAACTATGTGGCAGATATCG; RhoA_2, GACAGCCCTGATAGTTT; and RhoA_3, GCTGCCATCCGGAAGAAAC. The lentiviruses were generated using standard third-generation packaging vectors in 293T cells. In addition, we constructed an empty lentiviral control vector.

Established RhoA KO BjhTERT Fibroblast Line. We transduced three BjhTERT clones of different origin: BjhTERT (original), BjhTERT-C (crossy), and BjhTERT-W (whirly) (6), with the RhoA lentiviral CRISPR/Cas9 vector. A mixture of the three vectors (i.e., RhoA_1, RhoA_2, and RhoA_3) was used to transduce the fibroblasts in the presence of Polybrene. In parallel to the KO line, a negative control BjhTERT fibroblast line was generated using the empty lentiviral vector. The cells were selected with 2 μg/mL puromycin. A polyclonal line was collected and subcultured, and the status of RhoA at the protein level was evaluated using Western blotting.

RT-PCR Analysis. Quantitative real-time PCR protocol is described in *SI Materials and Methods*. qPCR data were analyzed using the reference genes TBP. Each reaction was repeated three times.

Ct values were determined for the internal control (glyceraldehyde-3-phosphate dehydrogenase or TATA-binding protein) and for the test genes at the same threshold level in the exponential phase of the PCR curves. Relative quantification [comparative Ct (ΔΔCt) method] was used to compare the expression level of the test genes with the internal control. Dissociation curve analysis was performed after every run to check the specificity of the reaction.

Western Blotting. Anti-RhoA antibody (Cat. no. sc-418; Santa Cruz Biotechnology) and anti–α-SMA antibody (Cat. no. M0851; Dako) were used. The protocol is described in *SI Materials and Methods*.

Tumor-Inhibitory Capacity Assay. Tumor-cell proliferation on fibroblast monolayers was analyzed in 384-well plates. Fibroblasts were plated in 100 μL cell-culture medium [IMDM; 10% (vol/vol) FBS, PSG] and cultured for 5 d, during which time they formed confluent monolayers. After the formation of full confluent monolayers, 80 μL medium was removed and 200 H2AmRFP-labeled PC3 prostate cancer cells (PC3 mRFP cells) were plated on top of the fibroblast monolayers in 80 μL cell-culture medium. The control wells contained 200 labeled tumor cells without the fibroblast monolayers.

Microscopy, Image Analysis, and Quantification. Immunofluorescence microscopy, automatic microscopy, and analysis of the tumor-cell numbers were carried out at the single-cell level using an automated microscope system, as previously described (6, 41, 42).

Coinjection of Tumor Cells and Fibroblasts in SCID and SCID-Beige Mice. A nontumorigenic number of PC3 prostate cancer cells (2×10^4 cells) (43, 44) were injected subcutaneously alone or when mixed with fibroblasts (1×10^6 cells) into 4-wk-old female SCID or SCID-beige mice (Taconik). Each mouse received one injection. The occurrence and growth of tumors were then analyzed up to 80-d postinjection. The procedures using the SCID and SCID-beige mice were approved by the North Stockholm Ethical Committee (Decision no. 192/14). Ten mice were used for the experiments. The mice were monitored for tumor growth twice a week, with the tumors measured using a caliper (mm^3).

TIRF Microscopy Live-Cell Motility Assay. Fibroblasts were seeded into six-well plates, with 70,000 BjhTERT control or BjhTERT RhoA-KO fibroblasts cultured in each well, for 18–24 h. Each fibroblast culture was cocultured with 5,000 PC3 mRFP prostate cancer cells, with the coculture then kept in the incubator for another 24 h. The next day, each well was washed and supplemented with fresh medium. The plates were then relocated to the TIRF microscope incubation chamber, at constant 37 °C and under 5% (vol/vol) CO_2. The ZEN2 Software was used to design the experiment and guided the complete microscopic unit automatically. The time-lapse imaging was recorded for 65 h, with a 1-h interval per capture. A field of 25 images (5 × 5) that covered a total area of 4.118 × 3.085 mm^2 was captured using the 10× objective lens.

Three-Dimensional Growth Assays. Collagen matrix was prepared by dissolving rat-tail collagen I (Sigma-Aldrich) in 0.3% acetic acid, with this neutralized with NaOH and diluted to a final concentration of 2.25 mg/mL in MEM on ice (45). Single-cell suspensions of 5,000 H2AmRFP-plasmid expressing PC-3 cells and 5,000 control or RhoA-KO fibroblasts were prepared in IMDM supplemented with 10% (vol/vol) FBS, GlutaMAX (Gibco), and 100 U/mL penicillin-streptomycin. The cells were rapidly mixed with collagen gels and casted in 48-well plates (Nunclon Delta Surface, Thermo Scientific). The cultures were incubated in an incubator at 37 °C and 5% (vol/vol) CO_2 for 7 d and fixed with 4% (vol/vol) PFA for 1 h at room temperature. Three-dimensional matrices were stained with phalloidin-Alexa488 to analyze PC-3 sphere growth and mounted into Vectashield reagent for imaging with a Zeiss AxioImager.Z2 upright epifluorescence microscope. *Z*-stacks were imaged with the 10× objective (EC Plan Neofluar, NA 0.3) using a digital camera (Hamamatsu Orca Flash 4.0 LT). Images were processed with ZEN 2 pro software (Zeiss) using extended depth-of-focus module (contrast function; *z*-stack alignment: highest; contrast length scale 7; smoothing 11; reconstruction 0.15) for sharply extracting *z*-stacks for image quantification using the ImageJ software. The growth of the PC3 tumor cell spheres was analyzed and the Clustering Index was calculated to quantify the nonspreading, compact growth of the PC3 tumor spheres in coculture with RhoA-KO fibroblasts. For the Clustering Index, the level of sprouting was calculated (total $n = 16$ image fields, from two independent repeats) and subtracted from a constant value: Clustering Index = [20 − (mean number of sprouting growths)] ×5.

Atomic Force Microscopy. Atomic force microscopy imaging was performed using a JPK Nanowizard 3 system installed on an inverted optical microscope (Nikon TE-1). The system was fitted with a Petri dish heater that held the cell-culture

dishes in a 37 °C. Advanced QI Mode provided the possibility to rapidly collect maps of approach-retract cycles (force curves) across the samples, from which mechanical maps were constructed (46). Atomic force microscopy has a lateral range of 100 μm and a vertical range of 15 μm, which is easily sufficient to characterize the cells used in this study. A standard contact mode cantilever (Bruker MLCT-E; nominal spring constant, 0.1 nm^{-1}; resonance frequency, 50 kHz; tip radius, 20 nm) was calibrated in air before the measurements, by first measuring the deflection sensitivity (nm/V) against a stiff polystyrene substrate, and then fitting the fundamental resonance peak in the thermal noise spectrum to determine the spring constant (47). This relatively stiff cantilever was chosen to minimize the effects of bulk hydrodynamic drag, while being soft enough to register differences in force and provide sufficiently large indentations (hundreds of nanometers) that the cytoskeleton controlled the stiffness. The cell dish was placed in the Petri dish heater, and the head placed over it. Before acquiring images, the deflection sensitivity was measured against a bare Petri dish with medium. Image resolution was 128 × 128 pixels. Approach and retract distances were set to 1.5 μm, and the speed was set to 50 μm s^{-1}. At this speed and resolution, the acquisition time was around 20 min per image.

Each interaction can be considered as an indentation experiment from which the effective Young's modulus can be extracted (JPK Data Processing software). The approach curve was first corrected for baseline position and slope, and converted to force versus separation. The Hertz model was then performed using square pyramidal indenter geometry, with an average edge angle of 25°. A batch process was used to fit the 128 × 128 indentation plots after optimizing the fitting parameters on a representative selection of the data. Apart from the Young's modulus, the contact position was also determined via this fitting procedure (i.e., the height at which the fit to the cantilever deflection deviated from zero).

Further image handling was performed in Gwyddion (gwyddion.net). Modulus histograms for each image were prepared using 246 bins. Graphs were prepared in Origin (OriginLab). There was a large variation between cells, and one image of each cell shows the qualitative difference in stiffness distribution over the cell (Fig. S6).

Traction Force Microscopy. Traction force microscopy calculations were performed as previously described (48). A description may also be found in *SI Materials and Methods*.

Affymetrix Microarrays. Four-day-old fibroblast monolayers were cocultured with the PC3 mRFP prostate tumor cells, plated at a ratio of 1:30 according to the number of plated fibroblasts. After 6 d of coculturing, the cells were sorted by fluorescence-activated cell sorting. The total RNA was isolated from monocultured and cocultured cells using kits. Then, 150 ng total RNA was used for the transcriptomic analysis.

Array hybridization, washing, staining, and scanning were performed using the Affymetrix WT Plus labeling and hyb to the HG 2.1 ST Array plate. Summary, normalization, and background correction were performed in Affymetrix Expression Console (v1.3.1) using the robust multiarray average method. The GEO accession number for the Affymetrix data is GSE83913 and available at www.ncbi.nlm.nih.gov/geo/query/acc.cgi?acc=GSE83913.

Differential Expression Analysis. We compared expression in the following contrasts of our interest: (*i*) BjhTERT before confrontation (control) vs. BjhTERT before confrontation (knock-out); (*ii*) BjhTERT after confrontation (control) vs. BjhTERT after confrontation (knock-out); and (*iii*) PC3 after confrontation (control) vs. PC3 after confrontation (knock-out).

To increase confidence, we calculated fold-change values by using both the wild-type control and the empty vector control as substitutes for biological replicates.

For the NEA, we selected genes with twofold change in either direction the "up" and "down" lists were treated separately. Fold-change values were calculated as arithmetic differences between the log-transformed Affymetrix expression values obtained at the processing steps described in section "Affymetrix microarrays" above.

Network Enrichment Analysis. As there were not enough replicated samples for a detailed differentially expressed analysis at the level of the individual genes, we used a new method of NEA (22) that estimates pathway enrichment in differentially expressed gene lists in a more robust manner (49) compared with both single-gene differential expression and the state-of-the-art gene-set enrichment analysis (50).

NEA evaluates the network connectivity between experimentally defined gene sets and some previously known or hypothesized gene sets with a clearly defined function. The individual connections are edges (functional links) in the global network between any of the genes of the former and latter gene sets. As even spurious connections between random gene sets can be found in a dense network, the significance of each pattern is evaluated using a special algorithm (22, 23).

The three components required for the network enrichment analysis were provided as follows: (*i*) experimental gene sets that were created as differentially expressed gene lists by comparing mRNA expression in KO cells with that in both of the controls, before and after coculturing with the cancer cells; (*ii*) functional genes sets (pathways of Gene Ontology terms); and (*iii*) a global network of physical interactions and other functional coupling between genes and proteins that was created from a multifaceted data integration of high-throughput and curated resources, as described in ref. 51. The current version included 19,027 genes (mapped to HUGO gene symbols) with 947,000 links that connected them.

ACKNOWLEDGMENTS. This study was supported by grants from the Swedish Research Council and the Swedish Cancer Society. Bioinformatics support from National Bioinformatics Infrastructure Sweden is gratefully acknowledged. A.K.B.G. was supported by the Syskonen Svenssons Foundation and Ollie and Elof Ericssons Foundation. T.P., V.K., and H.G. were supported by fellowships by a matching grant jointly awarded by the Concern Foundation, Los Angeles, and the Cancer Research Institute, New York. A.A. was supported by Emil och Wera Cornells Stiftelse. R.J.L. was supported by the Dutch Cancer Society Grant UU 2012-5667.

1. Donjacour AA, Cunha GR (1991) Stromal regulation of epithelial function. *Cancer Treat Res* 53:335–364.
2. Kenny PA, Bissell MJ (2003) Tumor reversion: Correction of malignant behavior by microenvironmental cues. *Int J Cancer* 107(5):688–695.
3. Mintz B, Illmensee K (1975) Normal genetically mosaic mice produced from malignant teratocarcinoma cells. *Proc Natl Acad Sci USA* 72(9):3585–3589.
4. Rønnov-Jessen L, Petersen OW, Bissell MJ (1996) Cellular changes involved in conversion of normal to malignant breast: Importance of the stromal reaction. *Physiol Rev* 76(1):69–125.
5. Kumar S, Weaver VM (2009) Mechanics, malignancy, and metastasis: The force journey of a tumor cell. *Cancer Metastasis Rev* 28(1-2):113–127.
6. Flaberg E, et al. (2012) The architecture of fibroblast monolayers of different origin differentially influences tumor cell growth. *Int J Cancer* 131(10):2274–2283.
7. Stoker MG, Shearer M, O'Neill C (1966) Growth inhibition of polyoma-transformed cells by contact with static normal fibroblasts. *J Cell Sci* 1(3):297–310.
8. Alkasalias T, et al. (2014) Inhibition of tumor cell proliferation and motility by fibroblasts is both contact and soluble factor dependent. *Proc Natl Acad Sci USA* 111(48):17188–17193.
9. Olumi AF, et al. (1999) Carcinoma-associated fibroblasts direct tumor progression of initiated human prostatic epithelium. *Cancer Res* 59(19):5002–5011.
10. Raz Y, Erez N (2013) An inflammatory vicious cycle: Fibroblasts and immune cell recruitment in cancer. *Exp Cell Res* 319(11):1596–1603.
11. Kalluri R, Zeisberg M (2006) Fibroblasts in cancer. *Nat Rev Cancer* 6(5):392–401.
12. Mogilner A, Keren K (2009) The shape of motile cells. *Curr Biol* 19(17):R762–R771.
13. Arthur WT, Noren NK, Burridge K (2002) Regulation of Rho family GTPases by cell-cell and cell-matrix adhesion. *Biol Res* 35(2):239–246.
14. Lessey EC, Guilluy C, Burridge K (2012) From mechanical force to RhoA activation. *Biochemistry* 51(38):7420–7432.
15. Bozoky B, et al. (2013) Novel signatures of cancer-associated fibroblasts. *Int J Cancer* 133(2):286–293.
16. Zhou Y, et al. (2013) Inhibition of mechanosensitive signaling in myofibroblasts ameliorates experimental pulmonary fibrosis. *J Clin Invest* 123(3):1096–1108.
17. Zhao XH, et al. (2007) Force activates smooth muscle alpha-actin promoter activity through the Rho signaling pathway. *J Cell Sci* 120(Pt 10):1801–1809.
18. Mullin BH, Mamotte C, Prince RL, Wilson SG (2014) Influence of ARHGEF3 and RHOA knockdown on ACTA2 and other genes in osteoblasts and osteoclasts. *PLoS One* 9(5): e98116.
19. Huang X, et al. (2012) Matrix stiffness-induced myofibroblast differentiation is mediated by intrinsic mechanotransduction. *Am J Respir Cell Mol Biol* 47(3):340–348.
20. Calvo F, et al. (2013) Mechanotransduction and YAP-dependent matrix remodelling is required for the generation and maintenance of cancer-associated fibroblasts. *Nat Cell Biol* 15(6):637–646.
21. Mookherjee N, et al. (2006) Modulation of the TLR-mediated inflammatory response by the endogenous human host defense peptide LL-37. *J Immunol* 176(4):2455–2464.
22. Alexeyenko A, et al. (2012) Network enrichment analysis: Extension of gene-set enrichment analysis to gene networks. *BMC Bioinformatics* 13:226.
23. Alexeyenko A, et al. (2015) Confrontation of fibroblasts with cancer cells in vitro: Gene network analysis of transcriptome changes and differential capacity to inhibit tumor growth. *J Exp Clin Cancer Res* 34:62.
24. Gopinath SD, Narumiya S, Dhawan J (2007) The RhoA effector mDiaphanous regulates MyoD expression and cell cycle progression via SRF-dependent and SRF-independent pathways. *J Cell Sci* 120(Pt 17):3086–3098.

25. Geneste O, Copeland JW, Treisman R (2002) LIM kinase and Diaphanous cooperate to regulate serum response factor and actin dynamics. *J Cell Biol* 157(5):831–838.
26. Stachowiak MR, et al. (2014) A mechanical-biochemical feedback loop regulates remodeling in the actin cytoskeleton. *Proc Natl Acad Sci USA* 111(49):17528–17533.
27. Sun Y, et al. (2015) Pro-inflammatory cytokine IL-1β up-regulates CXC chemokine receptor 4 via Notch and ERK signaling pathways in tongue squamous cell carcinoma. *PLoS One* 10(7):e0132677.
28. Erez N, Truitt M, Olson P, Arron ST, Hanahan D (2010) Cancer-associated fibroblasts are activated in incipient neoplasia to orchestrate tumor-promoting inflammation in an NF-kappaB-dependent manner. *Cancer Cell* 17(2):135–147.
29. Hoffman BD, Grashoff C, Schwartz MA (2011) Dynamic molecular processes mediate cellular mechanotransduction. *Nature* 475(7356):316–323.
30. Mack CP, Somlyo AV, Hautmann M, Somlyo AP, Owens GK (2001) Smooth muscle differentiation marker gene expression is regulated by RhoA-mediated actin polymerization. *J Biol Chem* 276(1):341–347.
31. Chrzanowska-Wodnicka M, Burridge K (1996) Rho-stimulated contractility drives the formation of stress fibers and focal adhesions. *J Cell Biol* 133(6):1403–1415.
32. Gad AKB, et al. (2012) Rho GTPases link cellular contractile force to the density and distribution of nanoscale adhesions. *FASEB J* 26(6):2374–2382.
33. Jatho A, et al. (2015) RhoA ambivalently controls prominent myofibroblast characteritics by involving distinct signaling routes. *PLoS One* 10(10):e0137519.
34. De Wever O, Demetter P, Mareel M, Bracke M (2008) Stromal myofibroblasts are drivers of invasive cancer growth. *Int J Cancer* 123(10):2229–2238.
35. De Wever O, et al. (2004) Critical role of N-cadherin in myofibroblast invasion and migration in vitro stimulated by colon-cancer-cell-derived TGF-beta or wounding. *J Cell Sci* 117(Pt 20):4691–4703.
36. Karagiannis GS, et al. (2012) Cancer-associated fibroblasts drive the progression of metastasis through both paracrine and mechanical pressure on cancer tissue. *Mol Cancer Res* 10(11):1403–1418.
37. Sambandamoorthy S, et al. (2015) Matrix compliance and the regulation of cytokinesis. *Biol Open* 4(7):885–892.
38. Avnet S, et al. (November 26, 2016) Cancer-associated mesenchymal stroma fosters the stemness of osteosarcoma cells in response to intratumoral acidosis via NF-κB acivation. *Int J Cancer*, 10.1002/ijc.30540.
39. Chang TS, et al. (2016) Inflammation promotes expression of stemness-related properties in HBV-related hepatocellular carcinoma. *PLoS One* 11(2):e0149897.
40. van de Weijer ML, et al. (2014) A high-coverage shRNA screen identifies TMEM129 as an E3 ligase involved in ER-associated protein degradation. *Nat Commun* 5:3832.
41. Flaberg E, et al. (2011) High-throughput live-cell imaging reveals differential inhibition of tumor cell proliferation by human fibroblasts. *Int J Cancer* 128(12): 2793–2802.
42. Rathje L-SZ, et al. (2015) Oncogenes induce a vimentin filament collapse mediated by HDAC6 that is linked to cell stiffness. *Proc Natl Acad Sci USA* 111(4):1515–1520.
43. Nemeth JA, et al. (1999) Severe combined immunodeficient-hu model of human prostate cancer metastasis to human bone. *Cancer Res* 59(8):1987–1993.
44. Wang M, Stearns ME (1991) Isolation and characterization of PC-3 human prostatic tumor sublines which preferentially metastasize to select organs in S.C.I.D. mice. *Differentiation* 48(2):115–125.
45. Sugiyama N, et al. (2010) Fibroblast growth factor receptor 4 regulates tumor invasion by coupling fibroblast growth factor signaling to extracellular matrix degradation. *Cancer Res* 70(20):7851–7861.
46. Hutter JL, Bechhoefer J (1993) Calibration of atomic-force microscope tips. *Rev Sci Instrum* 64(7):1868–1873, and erratum (1993) 64(11):3342.
47. Chopinet L, Formosa C, Rols MP, Duval RE, Dague E (2013) Imaging living cells surface and quantifying its properties at high resolution using AFM in QI™ mode. *Micron* 48: 26–33.
48. Tseng Q, et al. (2011) A new micropatterning method of soft substrates reveals that different tumorigenic signals can promote or reduce cell contraction levels. *Lab Chip* 11(13):2231–2240.
49. Jeggari A, Alexeyenko A (2017) NEArender: An R package for functional interpretation of 'omics' data via network enrichment analysis. *BMC Bioinformatics*, in press.
50. Bayerlová M, et al. (2015) Comparative study on gene set and pathway topology-based enrichment methods. *BMC Bioinformatics* 16:334.
51. Alexeyenko A, Sonnhammer ELL (2009) Global networks of functional coupling in eukaryotes from comprehensive data integration. *Genome Res* 19(6): 1107–1116.

6.4. List of references

Akhmanova, A. and Steinmetz, M.O. „Tracking the ends: a dynamic protein network controls the fate of microtubule tips.“ *Nature reviews Molecular cell biology* 9, Nr. 4 (2008): 309.

Alkasalias, T., Alexeyenko, A., Hennig, K., Danielsson, F., Lebbink, R.J., Fielden, M., Turunen, S.P., Lehti, K., Kashuba, V., Madapura, H.S. and Bozoky, B. „RhoA knockout fibroblasts lose tumor-inhibitory capacity in vitro and promote tumor growth in vivo.“ *Proceedings of the National Academy of Sciences*, 2017: 201621161.

Anderson, P.W. „More is different.“ *Science* 177, Nr. 4047 (1972): 393-396.

Aubry, D., Gupta, M., Ladoux, B. and Allena, R. „Mechanical link between durotaxis, cell polarity and anisotropy during cell migration.“ *Physical Biology* 12, Nr. 2 (2015): 026008.

Auffret, M., Ravano, V.L., Rossi, G.M., Hankov, N., Petersen, M.F. and Petersen, C.C.,. „Optogenetic stimulation of cortex to map evoked whisker movements in awake head-restrained mice.“ *Neuroscience* 368 (2018): 199-213.

Aumeier, C., Schaedel, L., Gaillard, J., John, K., Blanchoin, L. and Théry, M. „Self-repair promotes microtubule rescue.“ *Nature cell biology* 18, Nr. 10 (2016): 1054.

Barnhart, E., Lee, K.C., Allen, G.M., Theriot, J.A. and Mogilner, A. „Balance between cell-substrate adhesion and myosin contraction determines the frequency of motility initiation in fish keratocytes.“ *Proceedings of the National Academy of Sciences* 112, Nr. 16 (2015): 5045-5050.

Barnhart, E.L., Lee, K.C., Keren, K., Mogilner, A. and Theriot, J.A. „An Adhesion-Dependent Switch between Mechanisms That Determine Motile Cell Shape.“ *PLoS biology* 9, Nr. 5 (2011): e1001059.

Beadle, C., Assanah, M.C., Monzo, P., Vallee, R., Rosenfeld, S.S. and Canoll, P. „The role of myosin II in glioma invasion of the brain.“ *Molecular biology of the cell* 19, Nr. 8 (2008): 3357-3368.

Bergert, M., Erzberger, A., Desai, R.A., Aspalter, I.M., Oates, A.C., Charras, G., Salbreux, G. and Paluch, E.K. „Force transmission during adhesion-independent migration.“ *Nature cell biology* 17, Nr. 4 (2015): 524-529.

Blanchoin, L., Boujemaa-Paterski, R., Sykes, C. and Plastino, J. „Actin dynamics, architecture, and mechanics in cell motility.“ *Physiological reviews* 94, Nr. 1 (2014): 235-263.

Budday, S., Nay, R., de Rooij, R., Steinmann, P., Wyrobek, T., Ovaert, T.C. and Kuhl, E. „Mechanical properties of gray and white matter brain tissue by indentation.“ *Journal of the mechanical behavior of biomedical materials* 46 (2015): 318-330.

Bugaj, L.J., Choksi, A.T., Mesuda, C.K., Kane, R.S. and Schaffer, D.V. „optogenetic protein clustering and signaling activation in mammalian cells.“ 10, Nr. 3 (2013): 249.

Burkel, B., Morris, B.A., Ponik, S.M., Riching, K.M., Eliceiri, K.W. and Keely, P.J. „Preparation of 3D Collagen Gels and Microchannels for the Study of 3D Interactions In Vivo." *Journal of visualized experiments: JoVE*, Nr. 111 (2016).

Burnette, D.T., Shao, L., Ott, C., Pasapera, A.M., Fischer, R.S., Baird, M.A., Der Loughian, C., Delanoe-Ayari, H., Paszek, M.J., Davidson, M.W. and Betzig, E.104. „A contractile and counterbalancing adhesion system controls the 3D shape of crawling cells." *Journal of Cell Biology*, 2014: jcb-201311104.

Burton, K. and Taylor, D.L. „Traction forces of cytokinesis measured with optically modified elastic substrata." (Nature) 385, Nr. 6615 (1997): 450.

Butler, J.P., Tolic-Nørrelykke, I.M., Fabry, B. and Fredberg, J.J. „Traction fields, moments, and strain energy that cells exert on their surroundings." *American Journal of Physiology-Cell Physiology* 282, Nr. 3 (2002): C595-C605.

Caballero, D. and Goetz, J.G. „Foreword: Physics of cell migration." *Cell adhesion & migration* 9, Nr. 5 (2015): 325.

Calero-Cuenca, F.J., Janota, C.S. and Gomes, E.R. „Dealing with the nucleus during cell migration." *Current opinion in cell biology* 50 (2018): 35-41.

Campellone, K.G. and Welch, M.D. „A nucleator arms race: cellular control of actin assembly." *Nature reviews Molecular cell biology* 11, Nr. 4 (2010): 237.

Case, L.B. and Waterman, C.M. „Integration of actin dynamics and cell adhesion by a three-dimensional, mechanosensitive molecular clutch." (Nature Cell Biology) 17, Nr. 8 (2015): 955.

Chen, C.S. „Mechanotransduction – a field pulling together?" *Journal of cell science* 121, Nr. 20 (2008): 3285-3292.

Chung, B.M., Rotty, J.D. and Coulombe, P.A. „Networking galore: intermediate filaments and cell migration." *Current opinion in cell biology* 25, Nr. 5 (2013): 600-612.

Ciobanasu, C., Faivre, B. and Le Clainche, C. „Actin dynamics associated with focal adhesions." *International journal of cell biology* 2012 (2012).

Coppola, S., Carnevale, I., Danen, E.H., Peters, G.J., Schmidt, T., Assaraf, Y.G. and Giovannetti, E. „A mechanopharmacology approach to overcome chemoresistance in pancreatic cancer." *Drug Resistance Updates* 31 (2017): 43-51.

Cramer, L.P. „Forming the cell rear first: breaking cell symmetry to trigger directed cell migration." *Nature Cell Biology* 12, Nr. 7 (2010): 628.

Cuddapah, V.A., Robel, S., Watkins, S. and Sontheimer, H. „A neurocentric perspective on glioma invasion." *Nature Reviews Neuroscience* 15, Nr. 7 (2014): 455-465.

Dandy, W.E. „Removal of right cerebral hemisphere for certain tumors with hemiplegia: Preliminary report." *Journal of the American Medical Association,* 90, Nr. 11 (1928): 23-825.

Demuth, T. and Berens, M.E. „Molecular mechanisms of glioma cell migration and invasion." *Journal of neuro-oncology* 70, Nr. 2 (2004): 217-228.

Di Lullo, G.A., Sweeney, S.M., Körkkö, J., Ala-Kokko, L. and San Antonio, J.D. „Mapping the ligand-binding sites and disease-associated mutations on the most abundant protein in the human, type I collagen." *Journal of Biological Chemistry* 277, Nr. 6 (2002): 4223-4231.

Diz-Muñoz, A., Romanczuk, P., Yu, W., Bergert, M., Ivanovitch, K., Salbreux, G., Heisenberg, C.P. and Paluch, E.K. „Steering cell migration by alternating blebs and actin-rich protrusions. ." *BMC biology* 14, Nr. 1 (2016): 74.

Doyle, A. D., Wang, F. W., Matsumoto, K., & Yamada, K. M. „One-dimensional topography underlies three-dimensional fibrillar cell migration." *The Journal of cell biology* 184, Nr. 4 (2009): 481-490.

Doyle, A.D. „Generation of 3D collagen gels with controlled, diverse architectures." *Current protocols in cell biology*, 2016: 10-20.

Doyle, A.D., Kutys, M.L., Conti, M.A., Matsumoto, K., Adelstein, R.S. and Yamada, K.M. „Micro-environmental control of cell migration–myosin IIA is required for efficient migration in fibrillar environments through control of cell adhesion dynamics." *Journal of Cell Science* 125, Nr. 9 (2012): 2244-2256.

Duncan, J.S. and Tisi, J. „MRI in the diagnosis and management of epileptomas." *Epilepsia* 54, Nr. s9 (2013): 40-43.

Dunn, G.P., Rinne, M.L., Wykosky, J., Genovese, G., Quayle, S.N., Dunn, I.F., Agarwalla, P.K., Chheda, M.G., Campos, B., Wang, A. and Brennan, C. „Emerging insights into the molecular and cellular basis of glioblastoma." *Genes & development* 26, Nr. 8 (2012): 756-784.

Etienne-Manneville, S. and Hall, A. „RhoGTPases in cell biology." *Nature* 420, Nr. 6916 (2002): 629.

Etienne-Manneville, Sandrine. „Cdc42 - the centre of polarity." *Journal of cell science* 117, Nr. 8 (2004): 1291-1300.

Even-Ram, S. and Yamada, K.M. „Cell migration in 3D matrix." *Current opinion in cell biology* 17, Nr. 5 (2005): 524-532.

Eyckmans, J., Boudou, T., Yu, X. and Chen, C.S. „A hitchhiker's guide to mechanobiology." *Developmental cell* 21, Nr. 1 (2011): 35-47.

Farin, A., Suzuki, S.O., Weiker, M., Goldman, J.E., Bruce, J.N. and Canoll, P. „Transplanted glioma cells migrate and proliferate on host brain vasculature: a dynamic analysis." *Glia* 53, Nr. 8 (2006): 799-808.

Feynman, R.P., Leighton, R.B. and Sands, M. „The Feynman lectures on physics." No. 53 FEY (1971).

Fiedler, J., Brill, C., Blum, W.F. and Brenner, R.E. „IGF-I and IGF-II stimulate directed cell migration of bone-marrow-derived human mesenchymal progenitor cells." *Biochemical and biophysical research communications* 345, Nr. 3 (2006): 1177-1183.

Fletcher, D.A. and Mullins, R.D. „Cell mechanics and the cytoskeleton. .“ *Nature* 463, Nr. 7280 (2010): 485.

Frantz, C., Stewart, K.M. and Weaver, V.M. „The extracellular matrix at a glance.“ *Journal of Cell Science* 123, Nr. 24 (2010): 4195-4200.

Friedl, P. and Gilmour, D. „Collective cell migration in morphogenesis, regeneration and cancer.“ *Nature reviews Molecular cell biology* 10, Nr. 7 (2009): 445.

Friedl, P. and Wolf, K. „Plasticity of cell migration: a multiscale tuning model.“ *The Journal of cell biology*, 2009: jcb-200909003.

Gardel, M.L., Sabass, B., Ji, L., Danuser, G., Schwarz, U.S. and Waterman, C.M. „Traction stress in focal adhesions correlates biphasically with actin retrograde flow speed.“ *Journal of Cell Biology* 183, Nr. 6 (2008): 999-1005.

Gardel, M.L., Schneider, I.C., Aratyn-Schaus, Y. and Waterman, C.M. „Mechanical integration of actin and adhesion dynamics in cell migration.“ *Annual review of cell and developmental biology* 26 (2010): 315-333.

Gardner, M.K., Zanic, M. and Howard, J. „Microtubule catastrophe and rescue.“ *Current opinion in cell biology,* 25, Nr. 1 (2013): 14-22.

Genz, H. „Symmetry and symmetry breaking in nature.“ *Interdisciplinary Science Reviews* 24, Nr. 2 (1999): 129-138.

Griveau, A., Seano, G., Shelton, S.J., Kupp, R., Jahangiri, A., Obernier, K., Krishnan, S., Lindberg, O.R., Yuen, T.J., Tien, A.C. and Sabo, J.K. „A glial signature and Wnt7 signaling regulate glioma-vascular interactions and tumor microenvironment .“ *Cancer cell* 33, Nr. 5 (2018): 874-889.

Grobben, B., De Deyn, P. and Slegers, H. „Rat C6 glioma as experimental model system for the study of glioblastoma growth and invasion.“ *Cell and tissue research* 310, Nr. 3 (2002): 257-270.

Gross, D.J. „The role of symmetry in fundamental physics.“ *Proceedings of the National Academy of Sciences* 93, Nr. 25 (1996): 14256-14259.

Guck, J., Lautenschläger, F., Paschke, S. and Beil, M. „Critical review: cellular mechanobiology and amoeboid migration. .“ *Integrative biology* 2, Nr. 11-12 (2010): 575-583.

Guetta-Terrier, C., Monzo, P., Zhu, J., Long, H., Venkatraman, L., Zhou, Y., Wang, P., Chew, S.Y., Mogilner, A., Ladoux, B. and Gauthier, N.C. „Protrusive waves guide 3D cell migration along nanofibers.“ *Journal of Cell Biology* 211, Nr. 3 (2015): 683-701.

Gundersen, G.G. and Bulinski, J.C. „Selective stabilization of microtubules oriented toward the direction of cell migration.“ *Proceedings of the National Academy of Sciences* 85, Nr. 16 (1988): 5946-5950.

Guo, L., Degenstein, L., Dowling, J., Yu, Q.C., Wollmann, R., Perman, B. and Fuchs, E. „Gene targeting of BPAG1: abnormalities in mechanical strength and cell migration in stratified epithelia and neurologic degeneration.“ *Cell* 81, Nr. 2 (1995): 233-243.

Gupton, S.L. and Waterman-Storer, C.M. „Spatiotemporal feedback between actomyosin and focal-adhesion systems optimizes rapid cell migration." *Cell* 125, Nr. 7 (2006): 1361-1374.

Han, S.J., Rodriguez, M.L., Al-Rekabi, Z. and Sniadecki, N.J. „Spatial and temporal coordination of traction forces in one-dimensional cell migration." *Cell adhesion & migration* 10, Nr. 5 (2016): 529-539.

Harris, A.K., Wild, P. and Stopak, D. „Silicone rubber substrata: a new wrinkle in the study of cell locomotion." *Science* 208, Nr. 4440 (1980): 177-179.

Hawkins, R.J., Piel, M., Faure-Andre, G., Lennon-Dumenil, A.M., Joanny, J.F., Prost, J. and Voituriez, R. „Pushing off the walls: a mechanism of cell motility in confinement." *Physical review letters* 102, Nr. 5 (2009): 058103.

Hegemann, P. and Möglich, A. „Channelrhodopsin engineering and exploration of new optogenetic tools." *Nature methods* 8, Nr. 1 (2011): 39.

Hirata, E., Yukinaga, H., Kamioka, Y., Arakawa, Y., Miyamoto, S., Okada, T., Sahai, E. and Matsuda, M. „In vivo fluorescence resonance energy transfer imaging reveals differential activation of Rho-family GTPases in glioblastoma cell invasion." *Journal of Cell Science*, 2012: jcs-089995.

Hotulainen, P. and Lappalainen, P. „Stress fibers are generated by two distinct actin assembly mechanisms in motile cells." *The Journal of Cell Biology* 173, Nr. 3 (2006): 383-394.

Huber, F., Boire, A., Lopez, M.P. and Koenderink, G.H. „Cytoskeletal crosstalk: when three different personalities team up." *Current opinion in cell biology* 32 (2015): 39-47.

Huttenlocher, A. and Horwitz, A.R. „Integrins in cell migration." *Cold Spring Harbor perspectives in biology* 3, Nr. 9 (2011): a005074.

Iden, S. and Collard, J.G. „Crosstalk between small GTPases and polarity proteins in cell polarization." *Nature reviews Molecular cell biology* 9, Nr. 11 (2008): 846.

Isogai, T., Van Der Kammen, R. and Innocenti, M. „SMIFH2 has effects on Formins and p53 that perturb the cell cytoskeleton." *Scientific reports* 5 (2015): 9802.

Jiang, J., Zhang, Z.H., Yuan, X.B. and Poo, M.M. „Spatiotemporal dynamics of traction forces show three contraction centers in migratory neurons." *Journal of Cell Biology* 209, Nr. 5 (2015): 759-774.

Jones, T.R., Ruoslahti, E., Schold, S.C. and Bigner, D.D. „Fibronectin and glial fibrillary acidic protein expression in normal human brain and anaplastic human gliomas." *Cancer research,* 42, Nr. 1 (1982): 168-177.

Justus, C.R., Leffler, N., Ruiz-Echevarria, M. and Yang, L.V. „In vitro cell migration and invasion assays." *Journal of visualized experiments: JoVE* 88 (2014).

Kennedy, M.J., Hughes, R.M., Peteya, L.A., Schwartz, J.W., Ehlers, M.D. and Tucker, C.L. „Rapid blue-light–mediated induction of protein interactions in living cells." *Nature methods* 7, Nr. 12 (2010): 973.

Kovács, M., Tóth, J., Hetényi, C., Málnási-Csizmadia, A. and Sellers, J.R. „Mechanism of blebbistatin inhibition of myosin II." *Journal of Biological Chemistry* 279, Nr. 34 (2004): 35557-35563.

Krause, M. and Gautreau, A. „Steering cell migration: lamellipodium dynamics and the regulation of directional persistence." *Nature reviews Molecular cell biology* 15, Nr. 9 (2014): 577.

Lämmermann, T. and Sixt, M. „Mechanical modes of 'amoeboid' cell migration." *Current opinion in cell biology* 21, Nr. 5 (2009): 636-644.

Ladoux, B. and Mège, R.M. „Mechanobiology of collective cell behaviours." *Nature Reviews Molecular Cell Biology* 18, Nr. 12 (2017): 743.

Ladoux, B., Mège, R.M. and Trepat, X. „Front–Rear Polarization by Mechanical Cues: From Single Cells to Tissues." *Trends in cell biology* 26, Nr. 6 (2016): 420-433.

Lauffenburger, D. A., & Horwitz, A. F. „Cell migration: a physically integrated molecular process." *Cell* 84, Nr. 3 (1996): 359-369.

Lawson, C.D. and Ridley, A.J. „Rho GTPase signaling complexes in cell migration and invasion." *Journal Cell Biology* 217, Nr. 2 (2018): 447-457.

Leal-Egaña, A., Letort, G., Martiel, J.L., Christ, A., Vignaud, T., Roelants, C., Filhol, O. and Théry, M. „The size-speed-force relationship governs migratory cell response to tumorigenic factors." 28, Nr. 12 (2017): 1612-1621.

Leduc, C. and Etienne-Manneville, S. „Intermediate filaments in cell migration and invasion: the unusual suspects." *Current opinion in cell biology,* 32 (2015): 102-112.

Legant, W.R., Choi, C.K., Miller, J.S., Shao, L., Gao, L., Betzig, E. and Chen, C.S. „Multidimensional traction force microscopy reveals out-of-plane rotational moments about focal adhesions." *Proceedings of the National Academy of Sciences* 110, Nr. 3 (2013): 881-886.

Lenz, M., Thoresen, T., Gardel, M.L. and Dinner, A.R. „Contractile units in disordered actomyosin bundles arise from F-actin buckling." *Physical review letters* 108, Nr. 23 (2012): 238107.

Leung, E., Xue, A., Wang, Y., Rougerie, P., Sharma, V.P., Eddy, R., Cox, D. and Condeelis, J. „Blood vessel endothelium-directed tumor cell streaming in breast tumors requires the HGF/C-Met signaling pathway." *Oncogene* 36, Nr. 19 (2017): 2680.

Levental, K.R., Yu, H., Kass, L., Lakins, J.N., Egeblad, M., Erler, J.T., Fong, S.F., Csiszar, K., Giaccia, A., Weninger, W. and Yamauchi, M. „Matrix crosslinking forces tumor progression by enhancing integrin signaling." *Cell* 139, Nr. 5 (2009): 891-906.

Li, L., He, Y., Zhao, M. and Jiang, J. „Collective cell migration: Implications for wound healing and cancer invasion." *Burns & trauma* 1, Nr. 1 (2013): 21.

Li, R. and Bowerman, B. „Symmetry breaking in biology." *Cold Spring Harbor perspectives in biology* 2, Nr. 3 (2010): a003475.

Li, R. and Gundersen, G.G. „Beyond polymer polarity: how the cytoskeleton builds a polarized cell." *Nature reviews Molecular cell biology* 9, Nr. 11 (2008): 860.

Lim, M., Xia, Y., Bettegowda, C. and Weller, M. „Current state of immunotherapy for glioblastoma." *Nature Reviews Clinical Oncology*, 2018: 1.

Limouze, J., Straight, A.F., Mitchison, T. and Sellers, J.R. „Specificity of blebbistatin, an inhibitor of myosin II." *Journal of Muscle Research & Cell Motility* 25, Nr. 4-5 (2004): 337-341.

Liu, Y.J., Le Berre, M., Lautenschlaeger, F., Maiuri, P., Callan-Jones, A., Heuzé, M., Takaki, T., Voituriez, R. and Piel, M. „Confinement and low adhesion induce fast amoeboid migration of slow mesenchymal cells." *Cell* 160, Nr. 4 (2015): 659-672.

Lo, C.M., Wang, H.B., Dembo, M. and Wang, Y.L. „Cell Movement Is Guided by the Rigidity of the Substrate." *Biophysical journal* 79, Nr. 1 (2000): 144-152.

Lomakin, A. J., Lee, K. C., Han, S. J., Bui, D. A., Davidson, M., Mogilner, A., & Danuser, G. „Competition for actin between two distinct F-actin networks defines a bistable switch for cell polarization." *Nature Cell Biology* 17, Nr. 11 (2015): 1435.

Lombardi, M.L., Jaalouk, D.E., Shanahan, C.M., Burke, B., Roux, K.J. and Lammerding, J. „The interaction between nesprins and sun proteins at the nuclear envelope is critical for force transmission between the nucleus and cytoskeleton." *Journal of Biological Chemistry* 286, Nr. 30 (2011): 26743-26753.

Loschke, F., Seltmann, K., Bouameur, J.E. and Magin, T.M. „Regulation of keratin network organization." *Current opinion in cell biology* 32 (2015): 56-64.

Louis, D.N., Perry, A., Reifenberger, G., Von Deimling, A., Figarella-Branger, D., Cavenee, W.K., Ohgaki, H., Wiestler, O.D., Kleihues, P. and Ellison, D.W. „The 2016 World Health Organization Classification of Tumors of the Central Nervous System: a summary." *Acta neuropathologica* 131, Nr. 6 (2016): 803-820.

Mabeta, P. „PF573, 228 inhibits vascular tumor cell growth, migration as well as angiogenesis, induces apoptosis and abrogates PRAS40 and S6RP phosphorylation." *Acta Pharmaceutica* 66, Nr. 3 (2016): 399-410.

Maiuri, P., Rupprecht, J.F., Wieser, S., Ruprecht, V., Bénichou, O., Carpi, N., Coppey, M., De Beco, S., Gov, N., Heisenberg, C.P. and Crespo, C.L. „Actin flows mediate a universal coupling between cell speed and cell persistence." *Cell* 161, Nr. 2 (2015): 374-386.

Maiuri, P., Terriac, E., Paul-Gilloteaux, P., Vignaud, T., McNally, K., Onuffer, J., Thorn, K., Nguyen, P.A., Georgoulia, N., Soong, D. and Jayo, A. „The first world cell race." *Current Biology* 22, Nr. 17 (2012): 673-R675.

Mandal, K. „Role of ECM Physical Properties on Force Distribution and Cell Internal Organization." (École doctorale physique (Grenoble)) 2012.

Mandal, K., Wang, I., Vitiello, E., Orellana, L.A.C. and Balland, M. „Cell dipole behaviour revealed by ECM sub-cellular geometry." *Nature communications* 5 (2014): 5749.

Martiel, J.L., Leal, A., Kurzawa, L., Balland, M., Wang, I., Vignaud, T., Tseng, Q. and Théry, M. „Measurement of cell traction forces with ImageJ." *In Methods in cell biology* (Academic Press) 125 (2015): 269-287.

McKenzie, A.J., Hicks, S.R., Svec, K.V., Naughton, H., Edmunds, Z.L. and Howe, A.K. „The mechanical microenvironment regulates ovarian cancer cell morphology, migration, and spheroid disaggregation." *Scientific reports* 8, Nr. 1 (2018): 7228.

McMahon, A., Supatto, W., Fraser, S.E. and Stathopoulos, A. „Dynamic analyses of Drosophila gastrulation provide insights into collective cell migration." *Science* 322, Nr. 5907 (2008): 546-1550.

Meijering, E., Dzyubachyk, O. and Smal, I. „Methods for cell and particle tracking." *In Methods in enzymology* (Academic Press) 504 (2012): 183-200.

Melchers, F., Rolink, A.G. and Schaniel, C. „The role of chemokines in regulating cell migration during humoral immune responses." *Cell* 99, Nr. 4 (1999): 351-354.

Milloud, R., Destaing, O., de Mets, R., Bourrin-Reynard, I., Oddou, C., Delon, A., Wang, I., Albigès-Rizo, C. and Balland, M. „αvβ3 Integrins negatively regulate cellular forces by phosphorylation of its distal NPXY site." *Biology of the Cell* 109, Nr. 3 (2017): 127-137.

Mimori-Kiyosue, Y. „Shaping microtubules into diverse patterns: molecular connections for setting up both ends." *Cytoskeleton* 68, Nr. 11 (2011): 603-618.

Mitchison, T. and Kirschner, M. „Dynamic instability of microtubule growth." *Nature* 312, Nr. 5991 (1984): 237.

Montgomery, K.L., Yeh, A.J., Ho, J.S., Tsao, V., Iyer, S.M., Grosenick, L., Ferenczi, E.A., Tanabe, Y., Deisseroth, K., Delp, S.L. and Poon, A.S. „Wirelessly powered, fully internal optogenetics for brain, spinal and peripheral circuits in mice." *Nature methods* 12, Nr. 10 (2015): 969-974.

Monzo, P., Chong, Y.K., Guetta-Terrier, C., Krishnasamy, A., Sathe, S.R., Yim, E.K., Ng, W.H., Ang, B.T., Tang, C., Ladoux, B. and Gauthier, N.C. „Mechanical confinement triggers glioma linear migration dependent on formin FHOD3." *Molecular biology of the cell* 27, Nr. 8 (2016): 1246-1261.

Monzo, P., Chong, Y.K., Hennig, K., Ghisleni, A., Li, Q., Lim, S.W., Sandanaraj, E., Ng, W.H., Kon, N., Maiuri, P., Balland, M., Sheetz, M.P., Tang, C. and Gauthier, N.C. „The formin FMN1 promotes directional changes of invasive hGPC by increasing cell cytoskeleton's cohesion and traction forces on laminin linear substrate." *currently in preparation*, 2018.

Murrell, M., Oakes, P.W., Lenz, M. and Gardel, M.L. „Forcing cells into shape: the mechanics of actomyosin contractility." *Nature Reviews Molecular Cell Biology* 16, Nr. 8 (2015): 486.

O'Neill, P.R., Kalyanaraman, V. and Gautam, N. „Subcellular optogenetic activation of Cdc42 controls local and distal signaling to drive immune cell migration." *Molecular biology of the cell* 27, Nr. 9 (2016): 1442-1450.

Omary, M.B., Ku, N.O., Tao, G.Z., Toivola, D.M. and Liao, J. „'Heads and tails' of intermediate filament phosphorylation: multiple sites and functional insights." *Trends in biochemical sciences* 31, Nr. 7 (2006): 383-394.

Paňková, K., Rösel, D., Novotný, M. and Brábek, J. „The molecular mechanisms of transition between mesenchymal and amoeboid invasiveness in tumor cells." *Cellular and molecular life sciences,* 67, Nr. 1 (2010): 63-71.

Pathak, A. and Kumar, S. „Biophysical regulation of tumor cell invasion: moving beyond matrix stiffness." *Integrative Biology* 3, Nr. 4 (2011): 267-278.

Peron, S., and Svoboda, K. „From cudgel to scalpel: toward precise neural control with optogenetics." *Nature Methods* 8 (2011): 30-34.

Pierschbacher, M.D. and Ruoslahti, E. „Cell attachment activity of fibronectin can be duplicated by small synthetic fragments of the molecule." *Nature* 309, Nr. 5963 (1984): 30-33.

Polacheck, W.J. and Chen, C.S. „Measuring cell-generated forces: a guide to the available tools." *Nature methods* 13, Nr. 5 (2016): 415.

Ponti, A., Machacek, M., Gupton, S.L., Waterman-Storer, C.M. and Danuser, G. „Two distinct actin networks drive the protrusion of migrating cells." *Science* 305, Nr. 5691 (2004): 1782-1786.

Pudasaini, A., El-Arab, K.K. and Zoltowski, B.D. „LOV-based optogenetic devices: light-driven modules to impart photoregulated control of cellular signaling. ." *Frontiers in molecular biosciences* 2 (2015): 18.

Raab, M., Gentili, M., de Belly, H., Thiam, H.R., Vargas, P., Jimenez, A.J., Lautenschlaeger, F., Voituriez, R., Lennon-Duménil, A.M., Manel, N. and Piel, M. „ESCRT III repairs nuclear envelope ruptures during cell migration to limit DNA damage and cell death." *Science*, 2016: aad7611.

Raftopoulou, M. and Hall, A. „Cell migration: Rho GTPases lead the way." *Developmental biology* 265, Nr. 1 (2004): 23-32.

Raines, E.W. „The extracellular matrix can regulate vascular cell migration, proliferation, and survival: relationships to vascular disease." *International journal of experimental pathology* 81, Nr. 3 (2000): 173-182.

Ray, S.J., Franki, S.N., Pierce, R.H., Dimitrova, S., Koteliansky, V., Sprague, A.G., Doherty, P.C., de Fougerolles, A.R. and Topham, D.J. „The collagen binding α1β1 integrin VLA-1 regulates CD8 T cell-mediated immune protection against heterologous influenza infection." *Immunity* 20, Nr. 2 (2004): 167-179.

Reifenberger, G., Wirsching, H.G., Knobbe-Thomsen, C.B. and Weller, M. „Advances in the molecular genetics of gliomas—implications for classification and therapy." *Nature Reviews Clinical Oncology* 14, Nr. 7 (2017): 434.

Reig, G., Pulgar, E. and Concha, M.L. „Cell migration: from tissue culture to embryos." *Development* 141, Nr. 10 (2014): 1999-2013.

Renkawitz, J. and Sixt, M. "Mechanisms of force generation and force transmission during interstitial leukocyte migration." *EMBO reports* 11, no. 10 (2010): 744-750.

Renkawitz, J., Schumann, K., Weber, M., Lämmermann, T., Pflicke, H., Piel, M., Polleux, J., Spatz, J.P. and Sixt, M. „Adaptive force transmission in amoeboid cell migration.“ *Nature cell biology* 11, Nr. 12 (2009): 1438.

Revenu, C., Athman, R., Robine, S. and Louvard, D. „The co-workers of actin filaments: from cell structures to signals.“ *Nature reviews Molecular cell biology* 5, Nr. 8 (2004): 635.

Ridley, A.J. „Rho GTPase signalling in cell migration.“ *Current opinion in cell biology* 36 (2015): 103-112.

Ridley, A.J., Schwartz, M.A., Burridge, K., Firtel, R.A., Ginsberg, M.H., Borisy, G., Parsons, J.T. and Horwitz, A.R. „Cell migration: integrating signals from front to back.“ *Science* 302, Nr. 5651 (2003): 1704-1709.

Roberts, B.J., Pashaj, A., Johnson, K.R. and Wahl III, J.K. „Desmosome dynamics in migrating epithelial cells requires the actin cytoskeleton.“ *Experimental cell research* 317, Nr. 20 (2011): 2814-2822.

Sabass, B., Gardel, M.L., Waterman, C.M. and Schwarz, U.S., . ,. „High resolution traction force microscopy based on experimental and computational advances.“ *Biophysical journal* 94, Nr. 1 (2008): 207-220.

Schuster, S.L., Segerer, F.J., Gegenfurtner, F.A., Kick, K., Schreiber, C., Albert, M., Vollmar, A.M., Rädler, J.O. and Zahler, S. „Contractility as a global regulator of cellular morphology, velocity, and directionality in low-adhesive fibrillary micro-environments.“ *Biomaterials* 102 (2016): 137-147.

Shattil, S.J., Kim, C. and Ginsberg, M.H. „The final steps of integrin activation: the end game.“ *Nature reviews Molecular cell biology,* 11, Nr. 4 (2010): 288.

Slack-Davis, J.K., Martin, K.H., Tilghman, R.W., Iwanicki, M., Ung, E.J., Autry, C., Luzzio, M.J., Cooper, B., Kath, J.C., Roberts, W.G. and Parsons, J.T. „Cellular characterization of a novel focal adhesion kinase inhibitor.“ *Journal of Biological Chemistry* 282, Nr. 20 (2007): 14845-14852.

Stitou, A. and Riethmuller, M.L. „Extension of PIV to super resolution using PTV.“ *Measurement Science and Technology* 12, Nr. 9 (2001): 1398.

Straight, A.F., Cheung, A., Limouze, J., Chen, I., Westwood, N.J., Sellers, J.R. and Mitchison, T.J. „Dissecting temporal and spatial control of cytokinesis with a myosin II Inhibitor.“ *Science* 299, Nr. 5613 (2003): 1743-1747.

Stupp, R., Mason, W.P., Van Den Bent, M.J., Weller, M., Fisher, B., Taphoorn, M.J., Belanger, K., Brandes, A.A., Marosi, C., Bogdahn, U. and Curschmann, J. „Radiotherapy plus concomitant and adjuvant temozolomide for glioblastoma.“ *New England Journal of Medicine,* 352, Nr. 10 (2005): 987-996.

Style, R.W., Boltyanskiy, R., German, G.K., Hyland, C., MacMinn, C.W., Mertz, A.F., Wilen, L.A., Xu, Y. and Dufresne, E.R. „Traction force microscopy in physics and biology." *Soft matter* 10, Nr. 23 (2014): 4047-4055.

Tanimoto, H. and Sano, M. „A simple force-motion relation for migrating cells revealed by multipole analysis of traction stress." *Biophysical Journal* 106, Nr. 1 (2014): 16-25.

Theocharis, A.D., Skandalis, S.S., Gialeli, C. and Karamanos, N.K. „Extracellular matrix structure." *Advanced drug delivery reviews* 97 (2016): 4-27.

Thiam, H.R., Vargas, P., Carpi, N., Crespo, C.L., Raab, M., Terriac, E., King, M.C., Jacobelli, J., Alberts, A.S., Stradal, T. and Lennon-Dumenil, A.M. „Perinuclear Arp2/3-driven actin polymerization enables nuclear deformation to facilitate cell migration through complex environments." *Nature communications* 7 (2016): 10997.

Titus, M.A. and Goodson, H.V. „An evolutionary perspective on cell migration: Digging for the roots of amoeboid motility." *Journal of Cell Biology* 216, Nr. 6 (2017): 1509-1511.

Toettcher, J.E., Voigt, C.A., Weiner, O.D. and Lim, W.A. „The promise of optogenetics in cell biology: interrogating molecular circuits in space and time." *Nature methods* 8, Nr. 1 (2011): 35.

Toyjanova, J., Bar-Kochba, E., López-Fagundo, C., Reichner, J., Hoffman-Kim, D. and Franck, C. „High resolution, large deformation 3D traction force microscopy." *PloS one* 9, Nr. 4 (2014): e90976.

Tse, J.R. and Engler, A.J. „Preparation of hydrogel substrates with tunable mechanical properties." *Current protocols in cell biology,*, 2010: 10-16.

Tseng, Q., Wang, I., Duchemin-Pelletier, E., Azioune, A., Carpi, N., Gao, J., Filhol, O., Piel, M., Théry, M. and Balland, M. „A new micropatterning method of soft substrates reveals that different tumorigenic signals can promote or reduce cell contraction levels." *Lab on a chip* 11, Nr. 13 (2011): 2231-2240.

Tyson, R.A., Zatulovskiy, E., Kay, R.R. and Bretschneider, T. „How blebs and pseudopods cooperate during chemotaxis." *Proceedings of the National Academy of Sciences* 111, Nr. 32 (2014): 11703-11708.

Ueland, T., Brixen, K., Mosekilde, L., Mosekilde, L., Flyvbjerg, A. and Bollerslev, J. „Age-related changes in cortical bone content of insulin-like growth factor binding protein (IGFBP)-3, IGFBP-5, osteoprotegerin, and calcium in postmenopausal osteoporosis: a cross-sectional study. ." *The journal of clinical endocrinology & metabolism* 88, Nr. 3 (2003): 1014-1018.

Ulrich, T.A., de Juan Pardo, E.M. and Kumar, S. „The Mechanical Rigidity of the Extracellular Matrix Regulates the Structure, Motility, and Proliferation of Glioma Cells." *Cancer research* 69, Nr. 10 (2009): 4167-4174.

Umans, R.A. and Sontheimer, H. „Combating malignant astrocytes: Strategies mitigating tumor invasion. ." *Neuroscience research.*, 2017.

Vale, R.D. „The molecular motor toolbox for intracellular transport." *Cell* 112, Nr. 4 (2003): 467-480.

Valon, L. „Contrôle Optogénétique de la Polarité Cellulaire." (Ecole normale supérieure-ENS PARIS) 2014.

Valon, L., Marín-Llauradó, A., Wyatt, T., Charras, G. and Trepat, X. „Optogenetic control of cellular forces and mechanotransduction." *Nature communications* 8 (2017): 14396.

van der Gucht, J. and Sykes, C., . „Physical model of cellular symmetry breaking. ." *Cold Spring Harbor perspectives in biology* 1, Nr. 1 (2009): a001909.

Vicente-Manzanares, M., Ma, X., Adelstein, R.S. and Horwitz, A.R. „Non-muscle myosin II takes centre stage in cell adhesion and migration." *Nature reviews Molecular cell biology* 10, Nr. 11 (2009): 778.

Vignaud, T., Ennomani, H. and Théry, M. „Polyacrylamide hydrogel micropatterning." *Methods in cell biology* (Academic Press) 120 (2014): 93-116.

Wagner, O.I., Rammensee, S., Korde, N., Wen, Q., Leterrier, J.F. and Janmey, P.A. „Softness, strength and self-repair in intermediate filament networks." *Experimental cell research* 313, Nr. 10 (2007): 2228-2235.

Wang, J.H. and Lin, J.S. „Cell traction force and measurement methods." *Biomechanics and modeling in mechanobiology* 6, Nr. 6 (2007): 361.

Webb, D.J., Parsons, J.T. and Horwitz, A.F. „Adhesion assembly, disassembly and turnover in migrating cells – over and over and over again." *Nature cell biology* 4, Nr. 4 (2002): E97.

Wedlich-Soldner, R. and Li, R. „Spontaneous cell polarization: undermining determinism." *Nature Cell Biology* 5, Nr. 4 (2003): 267.

Wehrle-Haller, B. and Imhof, B.A. „Actin, microtubules and focal adhesion dynamics during cell migration." *The international journal of biochemistry & cell biology* 35, Nr. 1 (2003): 39-50.

Wolpert, Lewis. „Cell polarity." *Royal Society*, 2013.

Wu, Y.I., Frey, D., Lungu, O.I., Jaehrig, A., Schlichting, I., Kuhlman, B. and Hahn, K.M. „A genetically encoded photoactivatable Rac controls the motility of living cells." *Nature* 461, Nr. 7260 (2009): 104.

Yadav, S., Puri, S. and Linstedt, A.D. „A primary role for Golgi positioning in directed secretion, cell polarity, and wound healing." *Molecular biology of the cell* 20, Nr. 6 (2009): 1728-1736.

Yadav, S., Puthenveedu, M.A. and Linstedt, A.D. „Golgin160 Recruits the Dynein Motor to Position the Golgi Apparatus." *Developmental cell* 23, Nr. 1 (2012): 153-165.

Yam, P.T., Wilson, C.A., Ji, L., Hebert, B., Barnhart, E.L., Dye, N.A., Wiseman, P.W., Danuser, G. and Theriot, J.A. „Actin–myosin network reorganization breaks symmetry at the cell rear to spontaneously initiate polarized cell motility." *Journal of Cell Biology* 178, Nr. 7 (2007): 1207-1221.

Yang, H.W., Collins, S.R. and Meyer, T. „Locally excitable Cdc42 signals steer cells during chemotaxis." (Nature Cell Biology) 18, Nr. 2 (2015): 191.

Yeung, T., Georges, P.C., Flanagan, L.A., Marg, B., Ortiz, M., Funaki, M., Zahir, N., Ming, W., Weaver, V. and Janmey, P.A. „Effects of Substrate Stiffness on Cell Morphology, Cytoskeletal Structure, and Adhesion." *Cytoskeleton* 60, Nr. 1 (2005): 24-34.

Zagzag, D., Amirnovin, R., Greco, M.A., Yee, H., Holash, J., Wiegand, S.J., Zabski, S., Yancopoulos, G.D. and Grumet, M. „Vascular apoptosis and involution in gliomas precede neovascularization: a novel concept for glioma growth and angiogenesis." *Laboratory investigation* 80, Nr. 6 (2000): 837.

Zahm, J.M., Kaplan, H., Hérard, A.L., Doriot, F., Pierrot, D., Somelette, P. and Puchelle, E. „Cell migration and proliferation during the in vitro wound repair of the respiratory epithelium." *Cell motility and the cytoskeleton* 37, Nr. 1 (1997): 33-43.

Zhang, C., Mejia, L.A., Huang, J., Valnegri, P., Bennett, E.J., Anckar, J., Jahani-Asl, A., Gallardo, G., Ikeuchi, Y., Yamada, T. and Rudnicki, M. „The X-linked intellectual disability protein PHF6 associates with the PAF1 complex and regulates neuronal migration in the mammalian brain." *Neuron* 78, Nr. 6 (2013): 986-993.

Zhang, J., Guo, W.H. and Wang, Y.L. „Microtubules stabilize cell polarity by localizing rear signals." *Proceedings of the National Academy of Sciences* 111, Nr. 46 (2014): 16383-16388.

Abstract

Directional cell motility during organism and tissue development, homeostasis and disease requires symmetry breaking. This process relies on the ability of single cells to establish a front-rear polarity, and can occur in absence of external cues. The initiation of migration has been attributed to the spontaneous polarization of cytoskeleton components, while the spatio-temporal evolution of cytoskeletal forces arising from continuous mechanical cell-substrate interaction has yet to be resolved. Here, we establish a one- dimensional microfabricated migration assay that mimics complex in vivo fibrillar environment while being compatible with high-resolution force measurements, quantitative microscopy, and optogenetics. Quantification of morphometric and mechanical parameters reveals a generic stick-slip behavior initiated by contractility-dependent stochastic detachment of adhesive contacts at one side of the cell, which is sufficient to drive directional cell motility in absence of pre-established cytoskeleton polarity or morphogen gradients. A theoretical model validates the crucial role of adhesion dynamics during spontaneous symmetry breaking, proposing that the examined phenomenon can emerge independently of a complex self-polarizing system.

Résumé

La motilité cellulaire directionnelle, qui intervient lors du développement de l'organisme et des tissus, du maintien de l'homéostasie et dans les pathologies, nécessite une rupture de symétrie. Ce processus repose sur la capacité des cellules individuelles à établir une polarité avant-arrière, et peut se produire en l'absence de signaux externes. L'initiation de la migration a été attribuée à la polarisation spontanée des composants du cytosquelette. Cependant, l'évolution spatio-temporelle des forces du cytosquelette résultant de l'interaction mécanique cellule-substrat continue n'est pas encore bien connue. Ici, nous avons développé un protocole expérimental pour étudier la migration utilisant des substrats microfabriqués qui, grâce à des motifs unidimensionnels, reproduisent l'environnement fibrillaire *in vivo* tout en étant compatibles avec les mesures de force à haute résolution, la microscopie quantitative et l'optogénétique. La quantification des paramètres morphométriques et mécaniques révèle un comportement de « stick-slip » générique initié par un détachement stochastique des contacts adhésifs d'un côté de la cellule. Ce processus dépend de la contractilité et s'avère suffisant pour déclencher la motilité cellulaire directionnelle en absence de polarité du cytosquelette préétablie ou de gradients morphogènes. Un modèle théorique valide le rôle crucial de la dynamique d'adhésion au cours de la rupture de symétrie spontanée, en montrant que le phénomène observé peut émerger indépendamment d'un système auto-polarisant complexe.